# MOLECULAR AND IMMUNOLOGICAL ADVANCES IN HEMATOLOGICAL MALIGNANCIES: VOLUME II

EDITED BY: Gurvinder Kaur and Ritu Gupta
PUBLISHED IN: Frontiers in Oncology

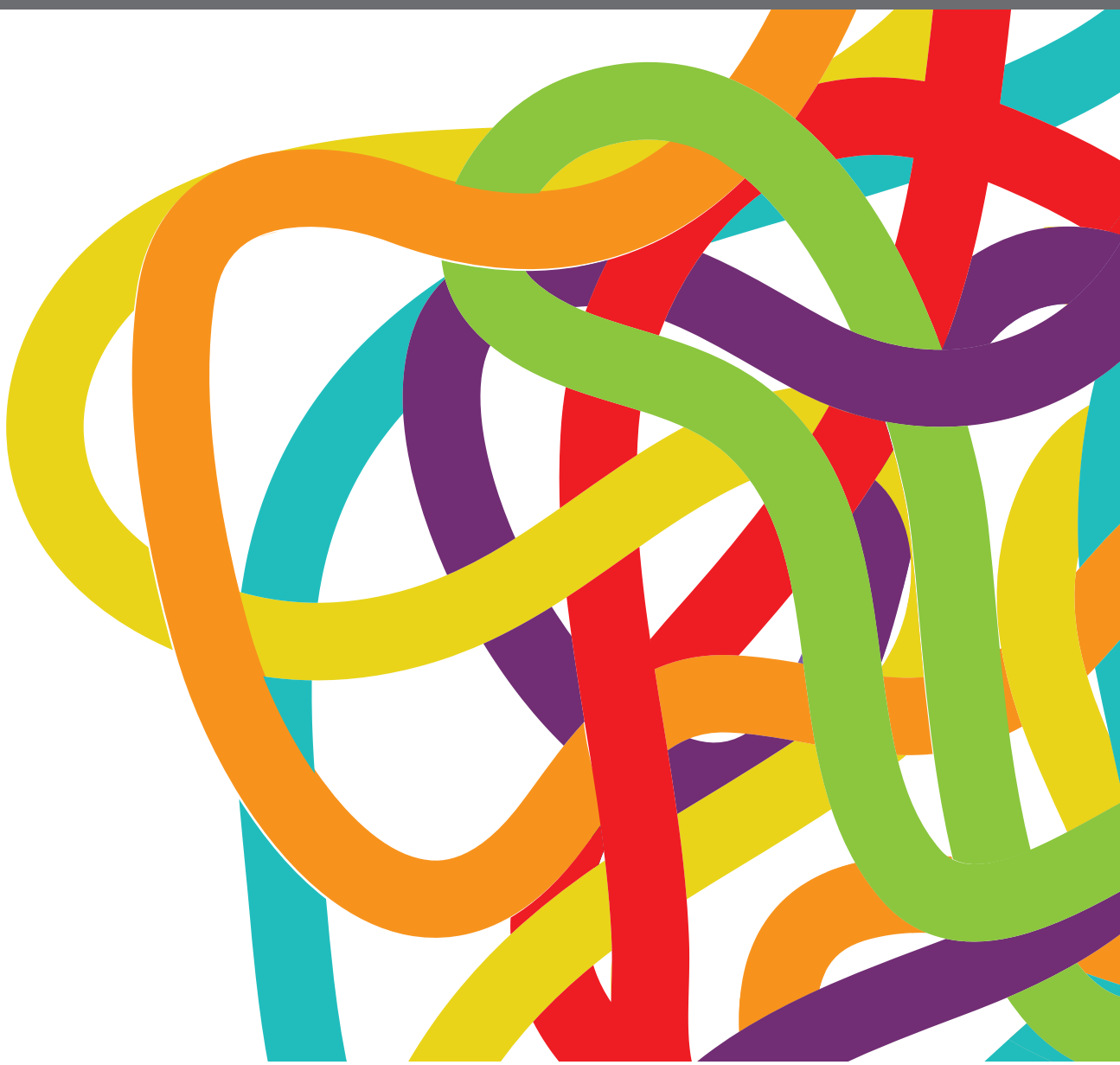

frontiers Research Topics

ISSN 1664-8714
ISBN 978-2-83250-167-2
DOI 10.3389/978-2-83250-167-2

## About Frontiers

Frontiers is more than just an open-access publisher of scholarly articles: it is a pioneering approach to the world of academia, radically improving the way scholarly research is managed. The grand vision of Frontiers is a world where all people have an equal opportunity to seek, share and generate knowledge. Frontiers provides immediate and permanent online open access to all its publications, but this alone is not enough to realize our grand goals.

## Frontiers Journal Series

The Frontiers Journal Series is a multi-tier and interdisciplinary set of open-access, online journals, promising a paradigm shift from the current review, selection and dissemination processes in academic publishing. All Frontiers journals are driven by researchers for researchers; therefore, they constitute a service to the scholarly community. At the same time, the Frontiers Journal Series operates on a revolutionary invention, the tiered publishing system, initially addressing specific communities of scholars, and gradually climbing up to broader public understanding, thus serving the interests of the lay society, too.

## Dedication to Quality

Each Frontiers article is a landmark of the highest quality, thanks to genuinely collaborative interactions between authors and review editors, who include some of the world's best academicians. Research must be certified by peers before entering a stream of knowledge that may eventually reach the public - and shape society; therefore, Frontiers only applies the most rigorous and unbiased reviews.
Frontiers revolutionizes research publishing by freely delivering the most outstanding research, evaluated with no bias from both the academic and social point of view. By applying the most advanced information technologies, Frontiers is catapulting scholarly publishing into a new generation.

## What are Frontiers Research Topics?

Frontiers Research Topics are very popular trademarks of the Frontiers Journals Series: they are collections of at least ten articles, all centered on a particular subject. With their unique mix of varied contributions from Original Research to Review Articles, Frontiers Research Topics unify the most influential researchers, the latest key findings and historical advances in a hot research area! Find out more on how to host your own Frontiers Research Topic or contribute to one as an author by contacting the Frontiers Editorial Office: frontiersin.org/about/contact

# MOLECULAR AND IMMUNOLOGICAL ADVANCES IN HEMATOLOGICAL MALIGNANCIES: VOLUME II

Topic Editors:
**Gurvinder Kaur,** All India Institute of Medical Sciences, India
**Ritu Gupta,** All India Institute of Medical Sciences, India

**Citation:** Kaur, G., Gupta, R., eds. (2022). Molecular and Immunological Advances in Hematological Malignancies: Volume II. Lausanne: Frontiers Media SA.
doi: 10.3389/978-2-83250-167-2

# Table of Contents

frontiers in Oncology

ORIGINAL RESEARCH
published: 27 May 2021
doi: 10.3389/fonc.2021.659201

# Prognostic Prediction of Cytogenetically Normal Acute Myeloid Leukemia Based on a Gene Expression Model

*Liu Yang*[1,2,3*], *Houyu Zhang*[1,4], *Xue Yang*[1,2,3], *Ting Lu*[1,2,3], *Shihui Ma*[1,2,3], *Hui Cheng*[1,2,3], *Kuangyu Yen*[1,2,3*] *and Tao Cheng*[1,2,3*]

[1] State Key Laboratory of Experimental Hematology, National Clinical Research Center for Blood Diseases, Institute of Hematology & Blood Diseases Hospital, Chinese Academy of Medical Sciences & Peking Union Medical College, Tianjin, China, [2] Department of Stem Cell and Regenerative Medicine, Peking Union Medical College, Tianjin, China, [3] Center for Stem Cell Medicine, Chinese Academy of Medical Sciences, Tianjin, China, [4] School of Biology and Biological Engineering, South China University of Technology, Guangzhou, China

OPEN ACCESS

**Edited by:**
Gurvinder Kaur,
All India Institute of Medical Sciences, India

**Reviewed by:**
Hussein A. Abbas,
MD Anderson Cancer Center, United States
Deepshi Thakral,
All India Institute of Medical Sciences, India

***Correspondence:**
Liu Yang
yangliu@ihcams.ac.cn
Kuangyu Yen
kuangyuyen@gmail.com
Tao Cheng
chengtao@ihcams.ac.cn

**Specialty section:**
This article was submitted to Hematologic Malignancies, a section of the journal Frontiers in Oncology

**Received:** 27 January 2021
**Accepted:** 26 March 2021
**Published:** 27 May 2021

**Citation:**
Yang L, Zhang H, Yang X, Lu T, Ma S, Cheng H, Yen K and Cheng T (2021) Prognostic Prediction of Cytogenetically Normal Acute Myeloid Leukemia Based on a Gene Expression Model. Front. Oncol. 11:659201. doi: 10.3389/fonc.2021.659201

Acute myeloid leukemia (AML) refers to a heterogeneous group of hematopoietic malignancies. The well-known European Leukemia Network (ELN) stratifies AML patients into three risk groups, based primarily on the detection of cytogenetic abnormalities. However, the prognosis of cytogenetically normal AML (CN-AML), which is the largest AML subset, can be hard to define. Moreover, the clinical outcomes associated with this subgroup are diverse. In this study, using transcriptome profiles collected from CN-AML patients in the BeatAML cohort, we constructed a robust prognostic Cox model named NEST (Nine-gEne SignaTure). The validity of NEST was confirmed in four external independent cohorts. Moreover, the risk score predicted by the NEST model remained an independent prognostic factor in multivariate analyses. Further analysis revealed that the NEST model was suitable for bone marrow mononuclear cell (BMMC) samples but not peripheral blood mononuclear cell (PBMC) samples, which indirectly indicated subtle differences between BMMCs and PBMCs. Our data demonstrated the robustness and accuracy of the NEST model and implied the importance of the immune dysfunction in the leukemogenesis that occurs in CN-AML, which shed new light on the further exploration of molecular mechanisms and treatment guidance for CN-AML.

**Keywords: cytogenetically normal acute myeloid leukemia, prognosis, biomarker, immune dysfunction, bone marrow**

## INTRODUCTION

Acute myeloid leukemia (AML) is a heterogeneous group of hematopoietic disorders with diverse clinical outcomes (1). The initial recognition of this heterogeneity depends primarily on morphology (2). The French-American-British (FAB) Cooperative Group developed a classification system based on morphologic and cytochemical characteristics, which classified

AML into eight subgroups (M0-M7) (3, 4). However, this classification provides limited prognostic guidance for AML patients (5).

Advances in sequencing technologies have contributed to an increased understanding of AML biology. Based on genetic abnormalities, the European Leukemia Network (ELN) risk stratification system classifies AML patients into three risk groups: favorable, intermediate, and adverse (**Table S1**) (6). The cytogenetic abnormalities associated with AML are recognized as being the most valuable prognostic factors (7). However, cytogenetically normal AML (CN-AML) represents the largest AML subset, comprising 45%–60% of all cases (8, 9). The prognosis of CN-AML must be assessed basing on genetic mutations alone due to the presentation of normal cytogenetic features (**Table S1**). In addition, the clinical outcomes of patients in this subgroup are also diverse and challenging to define (10).

According to the ELN recommendations, six genetic mutations have been demonstrated to be of prognostic significance among all AML patients, including mutations in *FLT3*, *NPM1*, *CEBPA*, *RUNX1*, *TP53*, and *ASXL1* (11). *NPM1* mutations occur at a high frequency, ranging from 25% to 35% of all AML patients and from 45.7% to 63.8% of all CN-AML patients (9). *FLT3* mutations were identified in approximately 20% of AML and 28%–34% of CN-AML patients (12). Aside from mutations in *NPM1* and *FLT3*, the mutation frequency of other genes in CN-AML is relatively low (6). Therefore, genetic mutations alone appear to be insufficient to provide a comprehensive prognostic assessment of CN-AML.

Genetic mutations can result in either the loss or gain of function and can subsequently influence the expression profiles of downstream genes. Given the diversity and uncertainty of prognoses among CN-AML patients, novel molecular markers may be discovered through the performance of transcriptome analyses that can be used to refine the risk stratification strategy for CN-AML patients. In recent decades, studies have identified that the expression of certain genes was correlated with poor prognosis in CN-AML (13–16). However, these studies have been associated with various limitations. For example, the identified prognostic factors have lacked consistency among different cohorts. And sample origins have been ignored when PBMCs and BMMCs were always mixed for analyses, whereas some studies have indicated that the proportions and properties differ between PBMCs and BMMCs (17, 18).

In this study, we integrated multiple transcriptome datasets [BeatAML (19), GSE71014 (20), GSE12417 (21), GSE6891 (22), TARGET-AML (23), and TCGA-LAML (11)] and identified nine prognostic markers in CN-AML BMMCs. We fitted a multivariate Cox proportional hazards model and developed a 9-gene model, named NEST (Nine-gEne SignaTure). The NEST model was able to provide a personalized prognostic value for risk assessment in CN-AML patients. Notably, our study suggested that the NEST model was applicable to BMMCs but not to PBMCs, which implied subtle differences between PBMCs and BMMCs in CN-AML patients. Our results pave the way for further explorations of the molecular mechanisms and prognostic markers associated with CN-AML.

# MATERIALS AND METHODS

## Data Source and Preprocessing

We downloaded gene expression profiles (raw count) and clinical information of *de novo* CN-AML patients from the BeatAML cohort (http://www.vizome.org/aml) as a training dataset. The cohort includes samples from both bone marrow and peripheral blood. On the one hand, bone marrow samples were derived from 105 patients with *de novo* CN-AML and 21 healthy donors. There were 33 samples in total derived from healthy donors. Among them, 19 samples were BMMCs, and the remaining 14 samples were $CD34^+$ bone marrow ($CD34^+$) cells. Notably, all $CD34^+$ cells were collected from three patients. $CD34^+$ sample from one patient was included in each sequencing batch (for a total of 12 times sequencing this control RNA). On the other hand, peripheral blood samples included 43 patients with *de novo* CN-AML in BeatAML. Moreover, to validate our model, we selected bone marrow data from four external validation datasets of CN-AML. Of these, GSE71014 (n = 104) (20), GSE12417 (n = 73) (21) and GSE6891 (n = 88) (22) were microarray datasets downloaded from the GEO database (http://www.ncbi.nlm.nih.gov/geo/), and TARGET-AML (23) were gene expression profiles (https://ocg.cancer.gov/programs/target). Apart from these datasets, we also download the TCGA-LAML (11) dataset obtained from the TCGA data portal (https://gdc-portal.nci.nih.gov/). The sample origin of the TCGA-LAML was PBMCs. Due to the different treatment regimens and favorable outcomes of AML-M3 patients, we excluded them from all cohorts. Ensemble IDs from the BeatAML dataset were converted to gene symbol with a GTF file (Homo_sapiens.GRCh37.75.gtf) downloaded from GENCODE (https://www.gencodegenes.org/). For microarray datasets, the median value was regarded as the gene's expression value for multiple probe sets corresponding to the same gene. The overall survival time and genetic mutation information were obtained from publications and the GEO database. No specific ethical approval is required for this study, as all datasets used were publicly available.

## Identification of Differentially Expressed Genes

The raw gene expression of the BeatAML dataset was normalized by the trimmed mean of M values (TMM) method with the "edgeR" package in the R platform (24). The voom method estimated the mean-variance relationship of the normalized data, generated a precision weight for each observation and entered the "limma" empirical Bayes analysis (25). Differences in gene expression with an adjusted P-value < 0.01 and absolute log2 fold change (log2FC) >= 2 were considered significant differences.

## Functional Enrichment Analysis

We used the "clusterProfiler" R package to perform Gene Ontology (GO) enrichment analysis (26). Moreover, DEGs were uploaded into the Ingenuity Pathway Analysis (IPA) system for core analysis (27). The ingenuity knowledge base (genes only) was selected as the reference set. IPA was performed

to identify the canonical pathways associated with common DEGs. P-value < 0.01 was set as the threshold value.

## Establishment of the Prognostic Cox Model

The gene expression data (raw count) were normalized with the TMM method. We got the normalized counts per million mapped reads (CPM) value. A log-based transformation (log (cpm+1)) value was used for subsequent survival analysis. Firstly, we used univariate Cox regression analysis and the log-rank test to detect prognosis-related DEGs. The cutoff value for univariate Cox analysis was 0.20, and the cutoff P-value for the log-rank test was 0.10. To ensure the biological significance of the identified DEGs, filtered genes whose highest expression value (log(cpm +1)) among CN-AML and healthy donors less than 1.0 were removed. Then, the BeatAML dataset was used as the training cohort to construct the prognostic Cox model. Least absolute shrinkage and selection operator (LASSO) analysis and stepwise algorithm were applied simultaneously to select the most significant prognostic gene from the identified prognosis −related DEGs. The optimal values of the penalty parameter λ were determined through ten folds cross-validation. The optimal tuning parameter λ was identified via the min criterion. A prognostic Cox model was established based on a linear combination of the gene expression level multiplied by a regression coefficient (β). The risk score of the model was calculated as follows: risk score = expression of $gene_1 \times \beta 1$ + expression of $gene_2 \times \beta 2$ + … expression of $gene_n \times \beta n$. We tested the proportional hazards assumption based on the scaled Schoenfeld residuals using the "survival" packages in the R platform.

## Validation of the Model

The risk score for each patient was calculated with constructed Cox model. Using the median of the risk score as the cutoff value, patients in each cohort were divided into high- and low-risk group. We applied a log-rank test to compare the overall survival difference between the high and low-risk group. Meanwhile, the time-dependent receiver operating characteristic (ROC) analysis was applied to calculate the area under the ROC curve (AUC) value at 1-, 2-, 3-years of the model. The AUC value of more than 0.5 indicates a non-random effect, and 1 indicating a perfect model (28). The GSE6891 included detailed genetic mutation information but no follow-up information. Therefore, these patients were classified into a favorable and adverse group assessed by ELN recommendations (6). The patient was defined to be favorable when FLT3-ITD is negative, and NPM1 is positive, or CEBPA double mutant is available. The patient was defined to be adverse if a sample has at least one of the following: (a) FLT3-ITD is positive and NPM1 is negative as well as CEBPA double mutant is not available. (b) EVI1 expression is positive. Risk scores were compared between two groups, and a Wilcoxon test $P < 0.05$ was considered statistically significant.

## Optimization of the Model With Three Independent Cohorts

Firstly, we enumerated all possible combinations of 12 genes included in the model. Specifically, we selected from 3 to 12 out of 12 genes to construct a new multivariate Cox model. We got 4017 combinations in total. Next, for each combination we constructed a new multivariate Cox model with selected genes in BeatAML. Then, for each combination, the new model was applied to predict risk scores for CN-AML patients in GSE12417, TARGET and BeatAML, respectively. We calculated the 1-, 2-, 3-years AUC value and the log-rank test's P-value in these cohorts. Combinations filtering was executed based on the following criteria: 1) the minimum value of 1-, 2-, 3-years AUC value should more than 0.60 (28); 2) the maximum AUC of 1-, 2-, 3-years AUC value should more than 0.70; 3) the P-values from a log-rank test should less than 0.05 (The cutoff for TARGET was 0.10). Subsequently, we got the combinations that passed our filtering criteria. Then, we used a min-max normalization to scale the original ROC. Each ROC value was replaced according to the following formula.

$$Normalized\ AUC_i = \frac{\mathrm{AUCi} - \mathrm{Min(AUC)}}{\mathrm{Max(AUC)} - \mathrm{Min(AUC)}}$$

We summed up all normalized AUC values in three independent cohorts in each combination and selected the combination with the largest AUC value. Finally, we constructed a new Cox model with the genes included in the combination with the largest AUC value.

## Comparison With Other Published Predictive Models for Prognostic Assessment

We screened publications from 2014 to 2020 on PubMed using the following keyword terms: ("CN-AML" OR "cytogenetical" OR "normal karyotype") AND ("TCGA" OR "GEO" OR "biomarker" OR "prognosis" OR "prognostic"). We got three published models in total. The detailed model formulas were as follow: 1) MPG6 score = (0.0492 * CD52) - (0.0018 * CD96) + (0.0131 * EMP1) + (0.2058 * TSPAN2) + (0.0234 * STAB1) - (0.3658 * MBTPS1) (13); 2) 3-genes model = (0.2016 * ROBO2) + (0.1274 * IL1R2) - (0.5365 * SCNN1B) (14); 3) 7-genes model = (0.71900 * CD34) + (0.61927 * MIR155HG) + (0.67258 * RHOC) + (0.66929 * SCRN1) + (0.65925 * F2RL1) + (0.65777 * FAM92A1) + (0.61491 * VWA8) (29). We applied these models to four BMMCs datasets, which included BeatAML, TARGET, GSE12417 and GSE71014, to compare the performance of these models comprehensively.

## Statistical Analysis

In our study, overall survival (OS) was defined as the time interval between the date of diagnosis and the date of death or lost to follow-up. We conducted univariate Cox analysis, and factors with P-value <0.10 were incorporated into a multivariate Cox analysis, which was used to construct a prognostic Cox model and to identify independent prognostic factors. All

statistical analyses were performed with the R 3.6.1 software (http://www.r-project.org/).

# RESULTS

## Clinical Information and Dataset Quality Control

We downloaded RNA-sequencing data and clinical information for *de novo* CN-AML patients from BeatAML (19), which included 105 BMMCs samples obtained from CN-AML patients (**Figure 1A**) and 33 samples from healthy donors (see *Methods*). The ages of the CN-AML patients ranged from 2 to 84 years, a large proportion of which were older than 40 years (88.57%). No significant difference in the sex composition was observed. According to the ELN recommendations, 30% of the patients in the BeatAML cohort had a good prognosis, 26% had an intermediate prognosis, and 31% had an adverse prognosis, which implied prognostic heterogeneity among the CN-AML population. The spectrum of genetic mutations in the BeatAML cohort was broad (**Figure 1B**), with 34.38% of the CN-AML patients harboring an *NPM1* mutation, which formed the largest subgroup, consistent with previous studies (6, 9, 30). Other common mutations included *DNMT3A* mutations (32.29%), *FLT3-TKD* mutations (28.12%), and *NRAS* mutations (15.62%). Among the 33 samples from healthy donors, 19 samples were BMMCs samples and 14 samples were bone marrow $CD34^+$ cells. All of $CD34^+$ cells were collected from three healthy donors. Notably, $CD34^+$ sample from a single donor was included in each sequencing batch, and this sample (Control_CD34) was sequenced 12 times in total. Control_CD34 served as a quality check against intergroup batch effects. Few batch effects were observed for the BeatAML dataset (**Figure 1C**). We chose the 105 BMMC samples from CN-AML patients and the 19 BMMC samples from healthy donors in the BeatAML cohort for use in further downstream analyses. The overall flowchart used for the bioinformatics analysis is shown in **Figure 1D**.

## Association Between CN-AML Pathogenesis and Immune Dysfunction

To identify differences in the BMMC transcriptomic profiles between CN-AML patients and healthy donors, we performed a differential gene expression analysis with edgeR, which resulted in the identification of 2,170 differential expressed genes (DEGs; **Table S2**), including 1,956 downregulated and 214 upregulated genes in CN-AML patients compared with healthy donors (**Figure 2A**). The identified DEGs included several known disease-linked genes, including cell cycle-related genes, HOX family genes (31), and *WT1* (32) (**Figure 2D**). To further explore the biological functions of the identified DEGs, we performed enrichment analyses. The IPA results suggested that the canonical Wnt/β-catenin pathway was activated in CN-AML, which agrees with previous reports (**Figure 2B**) (33, 34). Particularly, these identified DEGs were enriched in immune-related pathways, including primary immunodeficiency signaling, communications between innate and adaptive immune cells, and T cell receptor signaling. Furthermore, GO enrichment analysis revealed that the downregulated DEGs were primarily associated with the activation of immune cells, including neutrophils, leukocytes, and T cell (**Figure 2C**). We then examined the expression of several classical T cell and neutrophil activation-related genes in CN-AML (**Figure 2D**), which included *RAG2*, *IRF4* and *CD8*. The results revealed that these genes were significantly downregulated in CN-AML patients compared with healthy donors. These observations indicated that immune dysfunction was associated with CN-AML pathology.

## Prognostic Cox Model Construction

To identify DEGs related to CN-AML prognosis, we performed univariate Cox and Kaplan-Meier (KM) analyses (see *Materials and Methods*). After the initial screening from all DEGs, we identified 110 DEGs significantly associated with the clinical outcome (**Table S3**). The prognostic impacts on AML of several of the genes we identified have previously been validated in previous studies, such as *CD72* (35), *ALOX12* (36), *CD7* (37), and *BMP2* (38). Using these 110 prognosis-related DEGs, we performed LASSO regression and stepwise regression analysis to confirm whether any combination of these DEGs could be used to accurately predict prognosis (**Figures 3A, B**). We identified 12 genes, which we used to construct a prognostic multivariate Cox model (**Figure 3C**). Because the proportional hazards assumption is critical to the Cox regression (39), we tested this assumption for our model. The proportional hazard assumption is supported by the finding of a non-significant relationship between residuals and time (40). And our results suggested that the test was not significant for all 12 genes, and the global test was also not statistically significant (**Figure S1**). Therefore, we could assume that the model met the proportional hazards assumption.

To confirm the association between these 12 genes and the clinical outcomes of CN-AML, we performed KM analyses for all 12 genes using the BeatAML cohort. We noticed that 10 of the 12 genes were significantly associated with prognosis (log-rank test $P < 0.05$, **Figure S2**). We then assessed the performance of the model, primarily focusing on two indicators: the P-value of the KM analysis (log-rank test) was used to evaluate a model's ability to distinguish between patients with favorable and adverse prognoses, and the AUC value was used to evaluate the accuracy of the model. An AUC value above 0.5 indicates a non-random effect, with a value of 1 indicating a perfect model (28). In the KM analysis, low-risk patients had significantly improved overall survival (OS) compared with those in the high-risk group (log-rank test, $P < 0.05$, **Figure 3D**). The 1, 2, and 3-year AUC values for this model were 0.918, 0.973, and 0.915, respectively (**Figure 3E**). When we divided the CN-AML patients from the BeatAML cohort into favorable and adverse groups, based on ELN recommendations (6), the predicted risk score was able to clearly distinguish between the favorable and adverse groups (Wilcoxon test, $P < 0.01$, **Figure 3F**), which suggested that our model was generally consistent with clinical

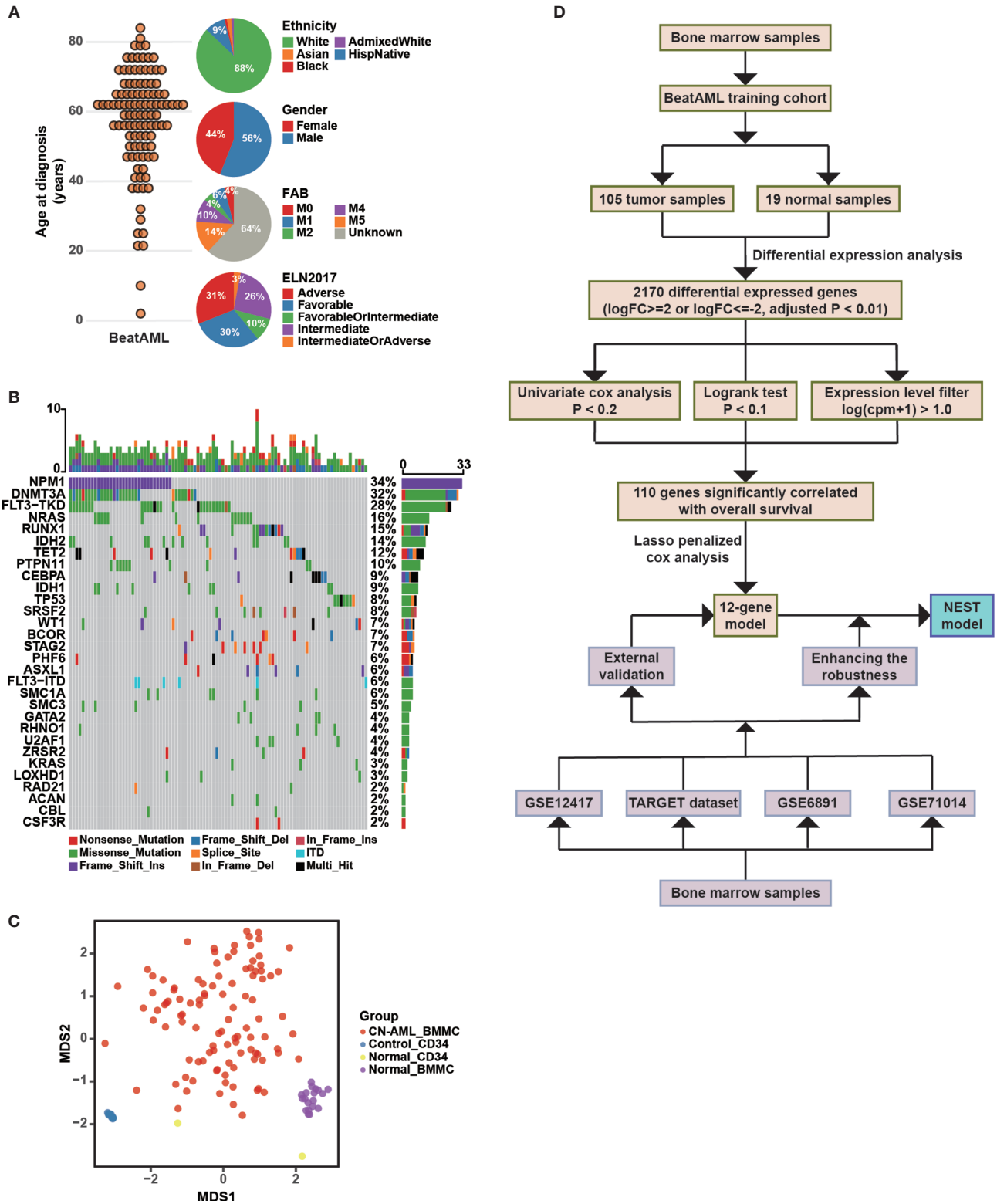


**FIGURE 1** | Clinical characteristics of CN-AML in the BeatAML cohort and analysis strategy. **(A)** The age distribution (left panel) and the clinical characteristics (right panel) of CN-AML patients in the BeatAML cohort. **(B)** Genetic mutation pattern in BeatAML CN-AML patients. **(C)** Multidimensional scaling (MDS) plot of all samples in the BeatAML dataset. **(D)** The overall flow chart of the bioinformatic analyses applied to this study.

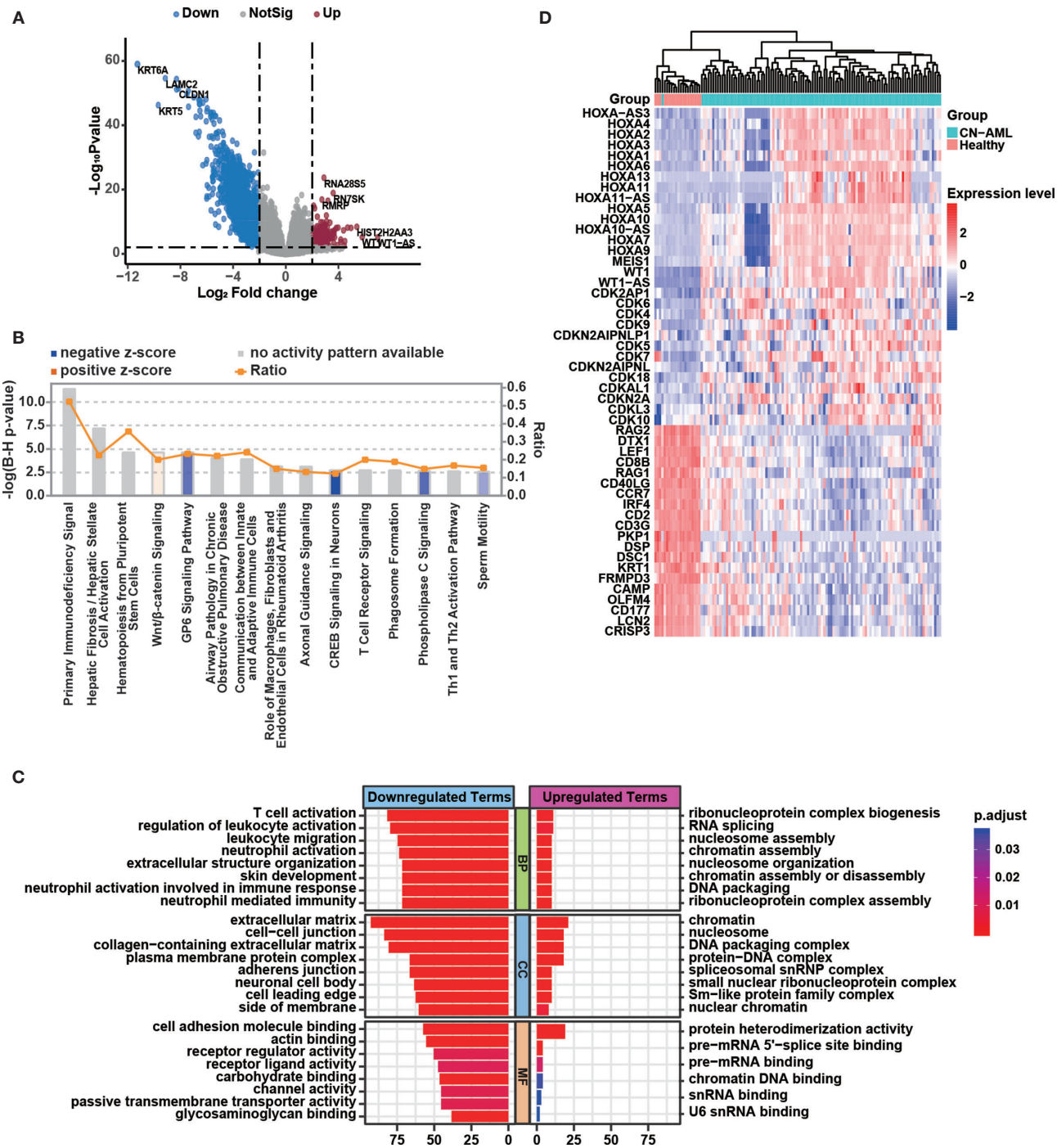


**FIGURE 2** | Immune dysfunction plays a vital role in CN-AML pathogenesis. **(A)** Volcano plot showing differentially expressed genes (DEGs) in bone marrow mononuclear cells (BMMCs) between CN-AML patients and healthy control. Upregulated genes in CN-AML are highlighted in red, and downregulated genes are highlighted in blue. **(B)** Canonical pathways enriched by Ingenuity Pathway Analysis (IPA) analysis. The orange bar indicates that the pathway in CN-AML is activated with a positive z-score. The blue bar indicates that the pathway is suppressed with a negative z-score. The gray bars indicate pathways for which no predictions can be made. **(C)** Enriched gene ontology (GO) terms for the upregulated and downregulated genes in CN-AML patients compared with healthy controls. **(D)** The expression of T cell and neutrophil activation-related genes and several well-known leukemia-related genes in CN-AML patients and healthy controls.

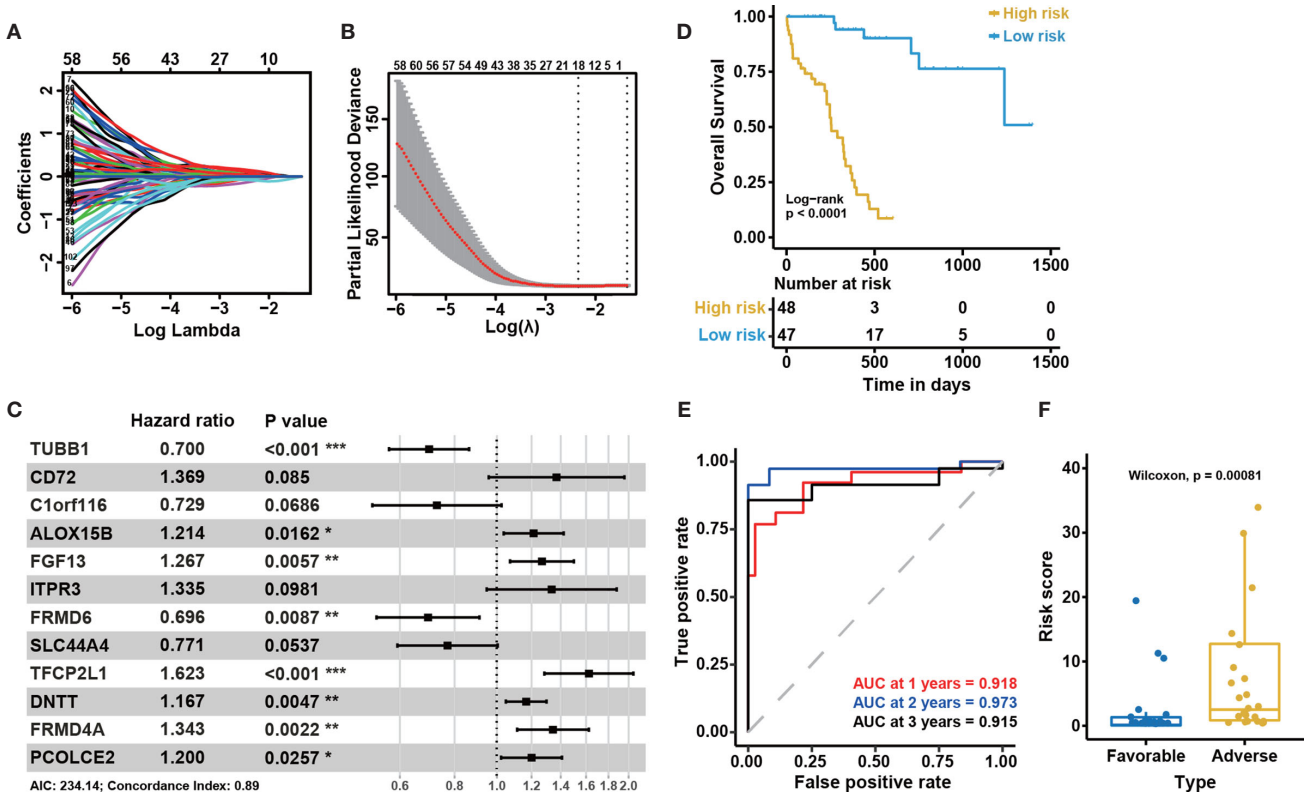


**FIGURE 3** | Construction of the 12-gene model and internal cohort validation. **(A)** LASSO coefficient profiles for the 110 prognosis-related differentially expressed genes. **(B)** Tenfold cross-validation for tuning parameter selection in the LASSO model. The solid vertical lines represent partial likelihood deviance ± standard error (SE) values. The dotted vertical lines are drawn at the optimal values according to the minimum criteria (left) and 1-SE criteria (right). **(C)** A forest plot showing the risk associated with gene expression for the genes included in the Cox model. Hazard ratio (HR) < 1 indicates that the gene is protective. Otherwise, it is a risk gene. P < 0.05 indicates that this gene is an independent prognostic factor (P-value significant codes: 0≤***<0.001≤**<0.01≤*<0.05). **(D)** Kaplan-Meier curves for overall survival based on the predicted risk score. The P-value for Kaplan-Meier curves is calculated by the log-rank test. **(E)** Time-dependent ROC curves for overall survival at 1, 2, and 3 years based on the 12-gene model. **(F)** The distribution of predicted risk scores in patients with favorable and adverse clinical outcomes, as assessed by European Leukemia Net (ELN) recommendations in the BeatAML cohort (n = 95).

guidelines. All of these results implied that the 12-gene model could reliably predict the prognosis of CN-AML patients.

## External Validation of the 12-Gene Model in Four Independent Cohorts

To further examine the performance of the 12-gene model, we applied the model to four external independent cohorts, including GSE12417 (n = 73), GSE71014 (n = 104), GSE6891 (n = 88), and TARGET (n = 26). The detailed demographic data for these cohorts are listed in **Table 1**. Similar to the outcome for the BeatAML cohort, the low-risk group had a significantly longer OS than the high-risk group for both the GSE12417 and GSE71014 cohorts (log-rank test, P < 0.05, **Figures 4A, B**). The AUC values at 1, 2, and 3 years for GSE12417 were 0.686, 0.709, and 0.685 (**Figure 4D**), and AUC values for GSE71014 were 0.599, 0.652, and 0.690 (**Figure 4E**). The AUC values for both the GSE12417 and GSE71014 cohorts approached 0.70, which suggested that the 12-gene model performed well in these two external independent cohorts. The survival analysis in the TARGET cohort indicated no significant difference between low- and high-risk groups (log-rank test, P > 0.05, **Figure 4C**). We speculated that the small cohort size and younger patients of the TARGET cohort contributed to this observation. Nevertheless, AUC values for the TARGET cohort at 1, 2, and 3 years were 0.521, 0.733, and 0.715, respectively (**Figure 4F**), which indicated that the model could be acceptable for the prediction of short-term clinical outcomes for pediatric patients. Moreover, we divided CN-AML patients from the GSE6891 cohort into favorable and adverse groups according to the ELN recommendations (see Methods). The predicted risk score was able to significantly distinguish favorable and adverse groups (Wilcoxon test P < 0.01, **Figure 4G**). The above results further validated the performance of the 12-genes model.

## Enhancing the Robustness of the 12-Gene Model

The 12 genes used in our model were determined by machine learning algorithms based only on the BeatAML cohort. Because we noted differences between the various cohorts, such as the age and sex distributions, we decided to optimize the model based on

**TABLE 1** | Clinical characteristics of patients from multiple cohorts.

| Characteristics | Bone marrow | | | | | Peripheral blood | |
|---|---|---|---|---|---|---|---|
| | BeatAML (n = 95) | GSE12417 (n = 73) | GSE71014 (n = 104) | GSE6891 (n = 88) | TARGET (n = 26) | BeatAML (n = 43) | TCGA (n = 60) |
| Age | | | | | | | |
| Median (yr) | 60 | 62 | NA | 46 | 13 | 62 | 56 |
| <60 yr | 47 (49.5%) | 31 (42.5%) | NA | 83 (94.3%) | 26 (100%) | 18 (41.9%) | 34 (56.7%) |
| >=60 yr | 48 (50.5%) | 42 (57.5%) | NA | 5 (5.7%) | 0 | 25 (58.1%) | 26 (43.3%) |
| Sex | | | | | | | |
| Male | 52 (54.7%) | NA | NA | 45 (51.2%) | 17 (65.4%) | 23 (53.5%) | 30 (50.0%) |
| Female | 43 (45.3%) | NA | NA | 43 (48.9%) | 9 (34.6%) | 20 (46.5%) | 30 (50.0%) |
| FAB | | | | | | | |
| M0 | 4 (4.2%) | 1 (1.4%) | NA | 0 | 0 | 0 | 3 (5.0%) |
| M1 | 5 (5.3%) | 21 (28.8%) | NA | 23 (26.1%) | 6 (23.1%) | 1 (2.3%) | 19 (31.7%) |
| M2 | 2 (2.1%) | 33 (45.21%) | NA | 12 (13.6%) | 7 (26.9%) | 1 (2.3%) | 17 (28.33%) |
| M4 | 11 (11.6%) | 9 (12.3%) | NA | 18 (20. 5%) | 6 (23.1%) | 1 (2.3%) | 11 (18.3%) |
| M5 | 15 (15.8%) | 6 (8.2%) | NA | 29 (33.0%) | 3 (11.5%) | 2 (4.7%) | 9 (15.0%) |
| M6 | 0 | 3 (4.1%) | NA | 2 (2.3%) | 0 | 0 | 0 |
| M7 | 0 | 0 | NA | 0 | 1 (3.9%) | 0 | 1 (1.7%) |
| Unknown | 58 (61.1%) | 0 | NA | 4 (4.6%) | 3 (11.5%) | 38 (88.4%) | 0 |
| OS state | | | | | | | |
| Alive | 56 (59.0%) | 31 (42.5%) | 68 (65.38%) | NA | 16 (61.5%) | 18 (41.9%) | 18 (30%) |
| Death | 39 (41.1%) | 42 (57.5%) | 36 (34.62%) | NA | 10 (38.5%) | 25 (58.1%) | 42 (70%) |

*OS, overall survival; NA, not available.*

multiple cohorts simultaneously to improve the robustness of the model. The median age of the TARGET cohort was 13 years, which was quite different from those of the other examined cohorts. The distribution of FAB subtypes in the TARGET cohort also differed significantly from those in the BeatAML and GSE12417 cohorts. Moreover, the detailed demographic information for the GSE71014 cohort was unknown (**Table 1**). Therefore, we selected the GSE12417, TARGET, and BeatAML datasets to optimize the model, whereas GSE71014 functioned as an external validation dataset (**Figure 5A**). Specifically, we enumerated all possible combinations of the 12 identified genes, resulting in 4,017 total combinations (**Figure 5B**). We set strict criteria to filter the candidate combinations (see *Methods*). After filtering, we obtained 20 candidate combinations. We then calculated a normalized AUC value to determine the optimal combination (see *Methods*), and we selected the combination highlighted by the red box, which presented with the largest normalized AUC value (**Figure 5C**). Finally, based on nine selected genes, we developed a new Cox model (**Figure 5D**). The nine-gene model met the global assumptions of proportional hazards (**Figure S3**). We termed this nine-gene model NEST (Nine-gEne SignaTure).

As shown in **Figures 6A, B**, the survival analysis inferred significant differences between the low- and high-risk group in the GSE12417 and BeatAML cohorts (log-rank test, $P < 0.05$). Although the log-rank test for the TARGET cohort was not significant, the performance of the NEST model was enhanced compared with that of the 12-gene model (**Figure 6C**). In addition, the AUC value for the BeatAML cohort slightly declined (**Figure 6D**), indicating no overfitting in the training data. The AUC value for NEST, when applied to GSE12417, appeared to be comparable to those obtained using the 12-gene model (**Figure 6E**). Notably, the AUC values for TARGET increased clearly (**Figure 6F**). According to the ELN recommendations, we divided the BeatAML cohort into favorable and adverse groups, and the predicted risk scores were able to significantly distinguish between these two groups (Wilcoxon test, $P < 0.01$, **Figure 7A**). These results indicated that the NEST model was more robust than the 12-gene model and performed well in both pediatric and adult CN-AML patients.

To further validate the generality of the NEST model, we used two additional external independent datasets, GSE71014 and GSE6891 (**Table 1**), to validate the model. The survival analysis showed significant differences between the low- and high-risk groups in the GSE71014 cohort (log-rank test, $P < 0.05$, **Figure 7B**). The AUC values for GSE71014 at 1, 2, and 3 years were 0.631, 0.697, and 0.744, respectively (**Figure 7C**), which was significantly

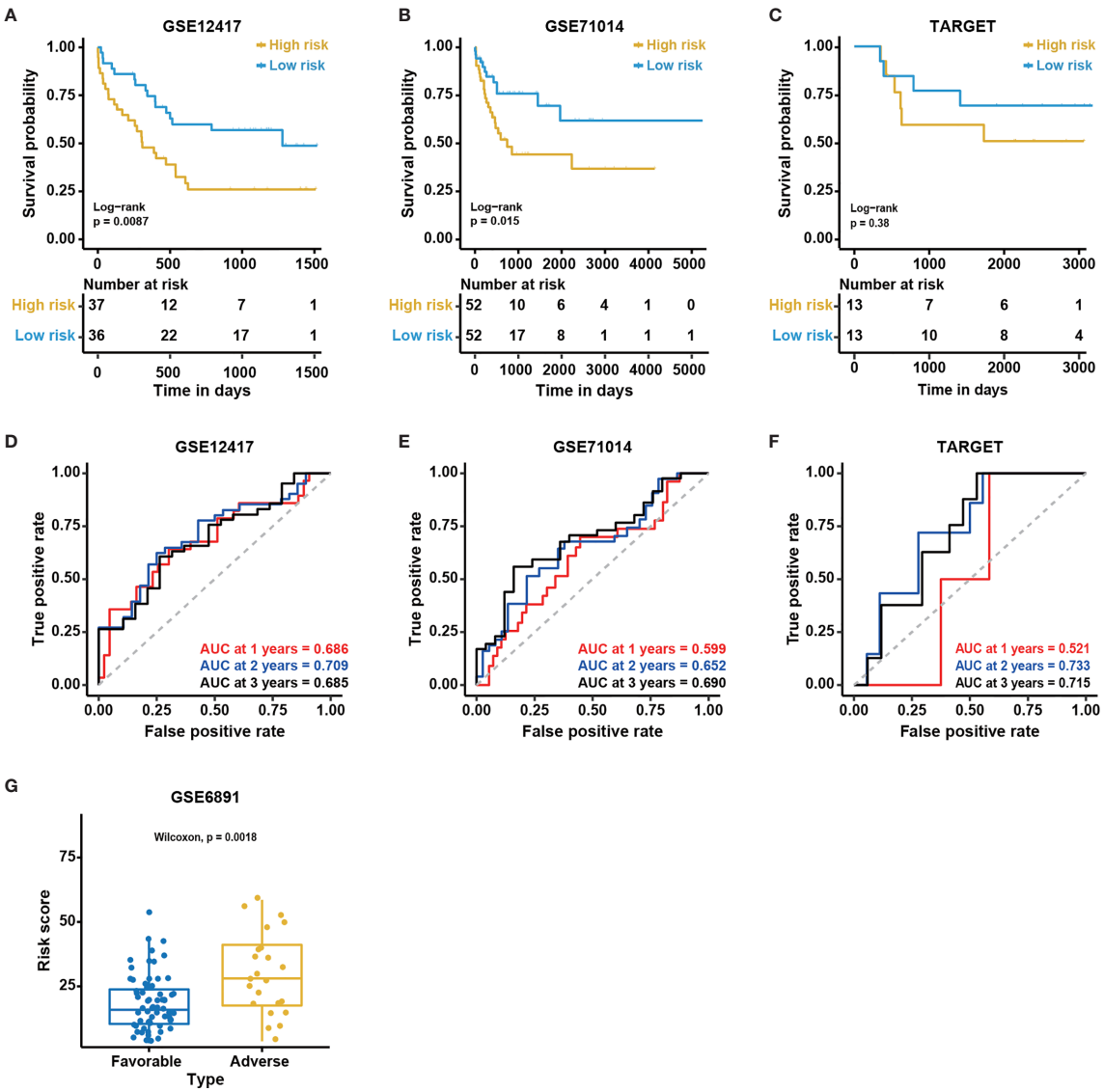


**FIGURE 4** | Validation of the 12-gene model in external cohorts. Kaplan-Meier curves for overall survival in different external independent cohorts, **(A)** GSE12417 (n = 73); **(B)** GSE71014 (n = 104); **(C)** TARGET (n = 26). The P-value for Kaplan-Meier curves is calculated by the log-rank test. Time-dependent ROC curves for overall survival at 1, 2 and 3 years in different external independent cohorts based on the 12-gene model, **(D)** GSE12417 (n = 73); **(E)** GSE71014 (n = 104); **(F)** TARGET (n = 26). **(G)** The distribution of predicted risk scores in patients with favorable and adverse clinical outcomes, assessed by European Leukemia Net (ELN) recommendations in GSE6891 (n = 88).

enhanced compared with the 12-gene model. Additionally, the results in GSE6891 showed a high level of agreement with the ELN recommendations (Wilcoxon test, $P < 0.01$, **Figure 7D**). Because not every CN-AML patient harbors genetic mutations with prognostic significance (**Figure 1**), these CN-AML patients cannot be assessed by ELN guidance. Importantly, we were able to apply our model to these patients using nine gene expression levels to evaluate their prognosis. The performance of the NEST model for CN-AML patients who could not be assessed by ELN guidance was outstanding. The survival analysis inferred significant differences between the low- and high-risk groups (log-rank test, $P < 0.05$, **Figure 7E**), and the AUC values at 1 and 2 years were 0.863 and 1.000, respectively (**Figure 7F**). Even using fewer genes, these results indicated that the NEST model was more robust and performed better than the 12-gene model and worked well for patients who could not be assessed by ELN clinical guidance.

## Comparison of the NEST Model With Published Predictive Models for Prognostic Assessment

To further evaluate the performance of the NEST model, we compared our NEST model with other CN-AML prognostic models that were published from 2014 to 2020. These models

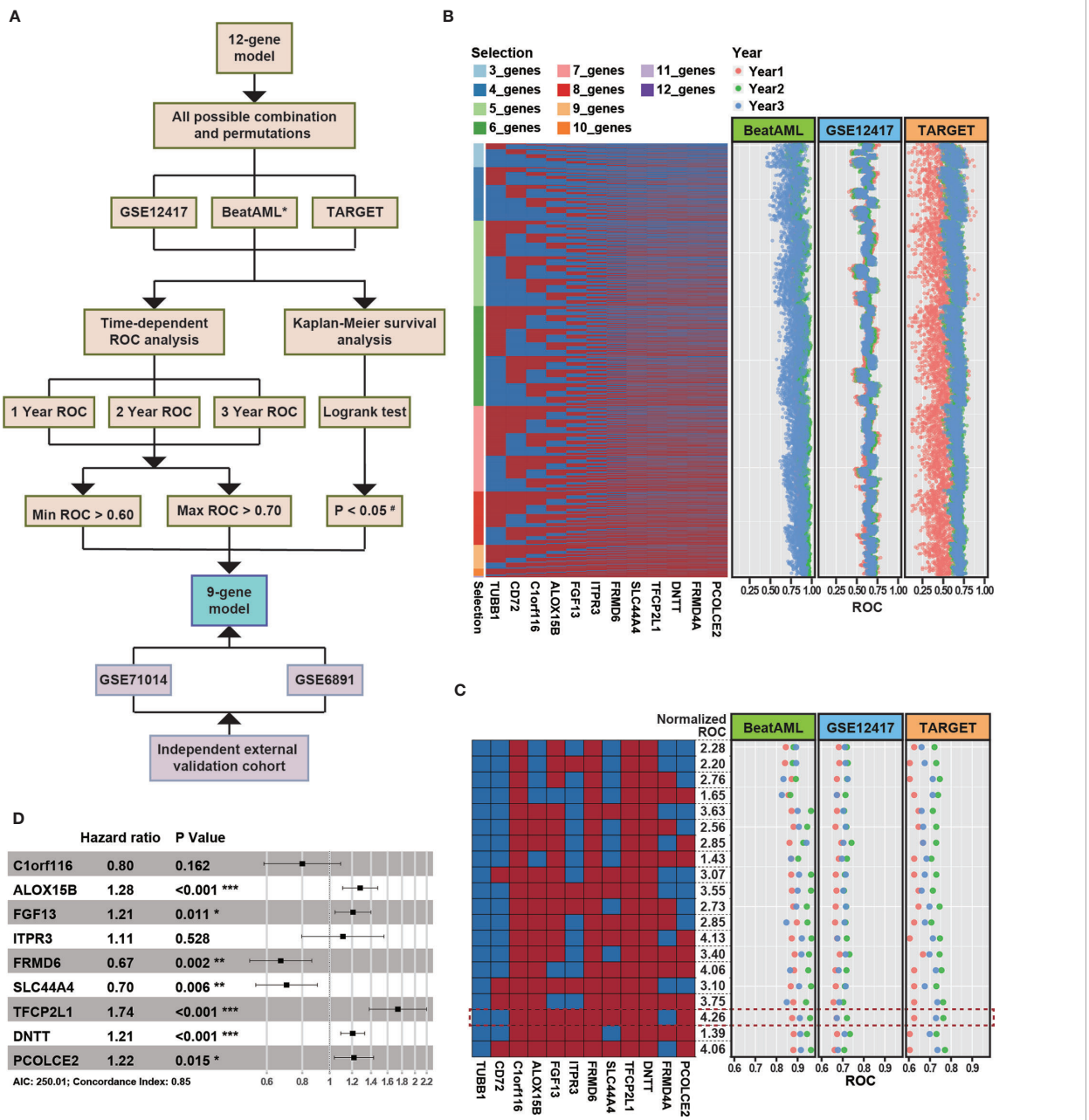


**FIGURE 5** | The strategy for enhancing the robustness of the model. **(A)** The overall flow chart for enhancing the robustness of the model. * indicates the cohort was used as a training dataset. The cutoff P-value for the log-rank test in the TARGET cohort was 0.10 (#). **(B)** The heatmap represents all combinations of 12 genes. Each column represents a gene, and each row represents a gene combination. In the heatmap, red rectangles denote selected genes, and blue rectangles denote unselected genes. The dot plot represents the area under the ROC curve (AUC) value for overall survival at 1 (red), 2 (green), and 3 years (blue) in various external independent cohorts based on the new model. **(C)** Combinations that passed the filtering criteria. The formula used to normalize the AUC can be found in Methods. The combinations highlighted with a red rectangle represent the combinate with the highest normalized AUC value. **(D)** A forest plot of the risk associated with the expression of each gene is included in the Cox model (P-value significant codes: 0≤***<0.001≤**<0.01≤*<0.05).

included the MPG6 model (13), the 3-gene model (14), and the 7-gene model (29). We obtained each model's formula from the corresponding literature (see *Methods*) and compared the performance using the BMMC datasets, including GSE12417, GSE71014, TARGET, and BeatAML. For these comparisons, we focused on two indicators: the P-value of the KM analysis (log-rank test), to evaluate each model's ability to distinguish between patients with favorable and adverse prognoses, and the AUC value of each model, to reflect the accuracy. The AUC value of more than 0.5 indicates a non-random effect, and 1 indicating a perfect model.

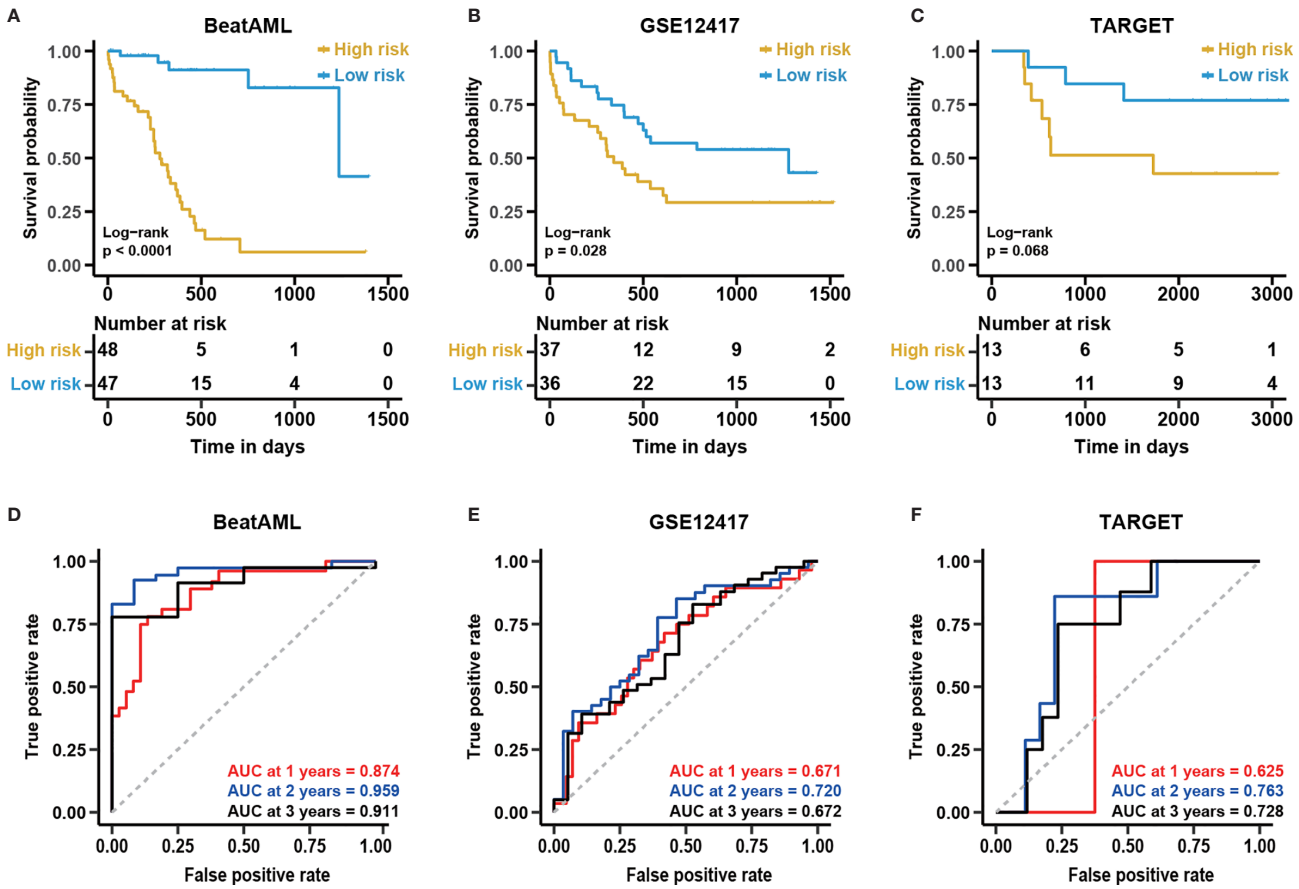


**FIGURE 6** | The enhanced performance of the NEST model in various cohorts. Kaplan-Meier curves for overall survival in different external independent cohorts, **(A)** BeatAML (n = 95); **(B)** GSE12417 (n = 73); **(C)** TARGET (n = 26). The P-value for the Kaplan-Meier curves was calculated by the log-rank test. Time-dependent ROC curves for overall survival at 1, 2, and 3 years in different external independent cohorts based on the 12-gene model, **(D)** BeatAML (n = 95); **(E)** GSE12417 (n = 73); **(F)** TARGET (n = 26).

The survival analysis showed that the risk score predicted by our model was significantly correlated with the survival of the patients in three out of four cohorts (log-rank test, $P < 0.05$, **Figure S4**). Although the P-value was higher than 0.05 for the TARGET cohort (log-rank test, $P = 0.068$), the difference between the high- and the low-risk group was clear. In contrast, other published predictive models could only distinguish between the low- and high-risk groups in at most two of the four cohorts (log-rank test, $P > 0.05$, **Figure S4**). The performance of the NEST model was stable in multiple cohorts, as reflected by the consistent high AUC values (**Table 2**). The MPG6 model exhibited excellent performance only for the TARGET cohort, which might suggest that this model is better suited for pediatric patients. The small size of the TARGET cohort may also account for this result. In the BeatAML and GSE12417 cohorts, the AUC values of the NEST model were consistently higher than those for the previously published models. At 1 year, although the AUC of the NEST model was lower than those for the MPG6 and 7-gene models for the GSE71014 cohort, the AUC values were higher than all models for the 2- and 3-year survival assessments. These results indicated that the performance of the NEST model was better and more robust than the performance of the other models across various cohorts.

## Independence of the Predicted Risk Score

Certain clinical characteristics and known genetic mutations could affect the prognosis of CN-AML patients; therefore, we next examined whether the risk score predicted by the NEST model could function as an independent prognostic factor that was not affected by other factors. First, we applied a univariate Cox analysis to common clinical factors and genetic mutations identified in the BeatAML cohort (**Table S4**). We found the NEST predicted risk score, age, *TP53* mutation, *ZRSR2* mutation, *TET2* mutation, *FLT3-ITD*, and *U2AF1* mutations were risk factors for a poor prognosis (**Figure 8A**), as reported by previous studies (6, 19, 41–44). In addition, the result suggested that *PTPN11* mutation was a protective factor for CN-AML, which appeared to contrast with previous reports (45). We believe that the low *PTPN11* mutation frequency among the

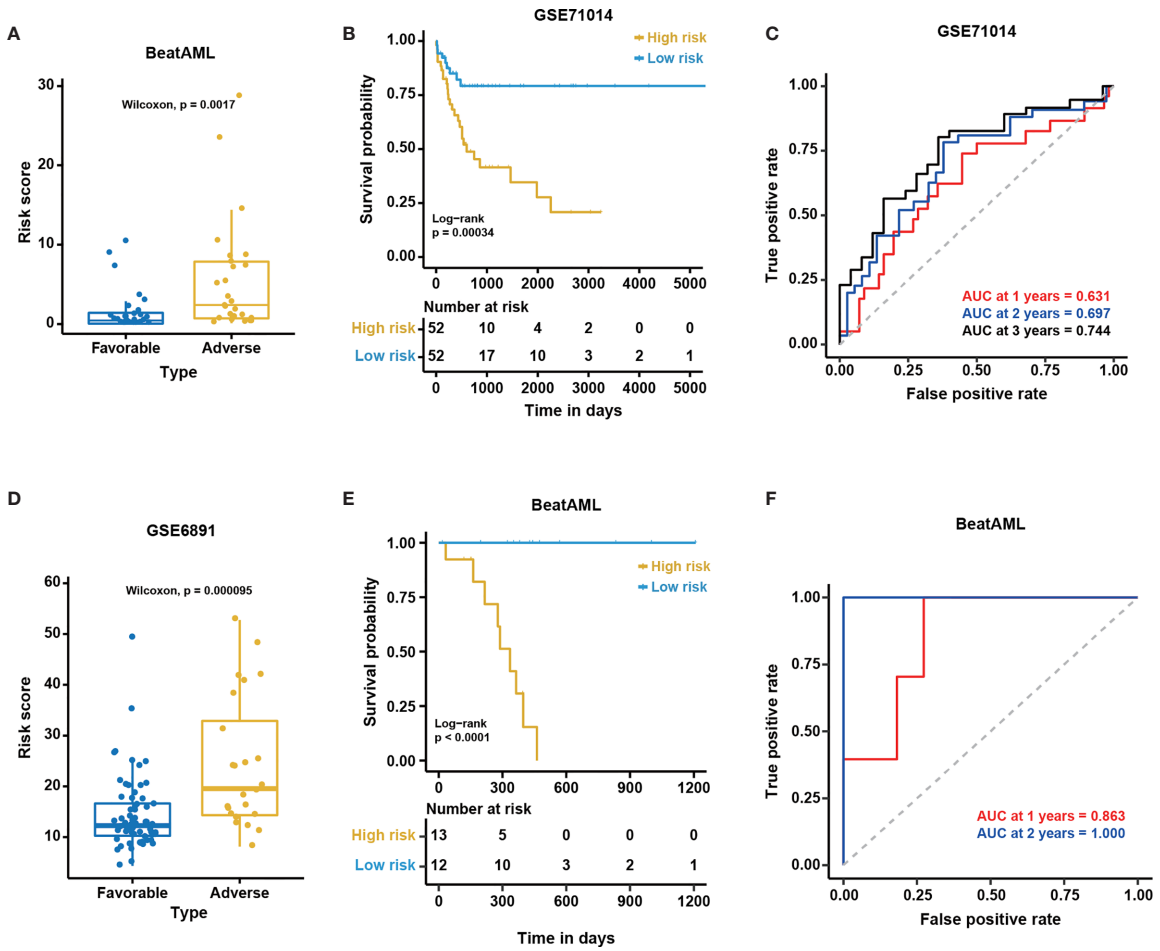


**FIGURE 7** | The excellent performance of the NEST model among external cohorts. The distribution of predicted risk scores among patients with favorable and adverse clinical outcomes as assessed by European Leukemia Net (ELN) recommendations in the **(A)** BeatAML and **(D)** GSE6891 cohorts. Kaplan-Meier curves for overall survival based on the predicted risk scores for individuals in the **(B)** GSE71014 (n = 104) and **(E)** BeatAML (n = 25) cohorts who were unable to be assessed by ELN. The P-value for Kaplan-Meier curves was calculated by the log-rank test. Time-dependent ROC curves for overall survival at 1, 2 and 3 years in **(C)** GSE71014 (n = 104) and **(F)** BeatAML (n = 25) patients who were unable to be assessed by ELN.

BeatAML cohort could explain this discrepancy. Secondly, we selected those factors with P-values less than 0.1 in the univariate Cox analysis for inclusion in the multivariate Cox analysis. The result indicated that *ZRSR2* mutation was an independent risk factor (**Figure 8B**), which agreed with previous reports (42–44). Notably, the NEST predicted risk score was also an independent risk factor for poor clinical outcomes, which was not affected by age or the presence of other gene mutations. These results suggested that the NEST predicted risk score could serve as an independent prognostic factor in CN-AML.

## Applicability of the Model

Our reported results demonstrated the good results of the model among BMMC datasets. For clinical convenience, we next examined whether our model could apply to PBMC datasets. We selected the PBMC data (n = 43) from the BeatAML dataset. Meanwhile, we downloaded the TCGA-LAML (n = 151) from the TCGA data portal (https://gdc-portal.nci.nih.gov/), which is also a PBMC dataset. We selected CN-AML (n = 60) from the TCGA-LAML. Time-dependent ROC and KM analyses were applied to both datasets. No difference between the low- and high-risk groups was observed for either cohort (log-rank test, P > 0.05, **Figures 8C, D**). The AUC values were also not acceptable for these cohorts (**Figures 8E, F**). The above results illustrated that our model was only suitable for BMMCs, not for PBMCs, which implied subtle differences between PBMCs and BMMCs.

To further verify the differences between BMMCs and PBMCs in CN-AML patients, we first adjusted for confounding variables, including the percentage of blasts and tissue sources in the multivariate Cox analysis. We obtained the percentage of blasts in BMMCs and PBMCs from clinical records to perform the test. Moreover, we calculated risk scores for patients with the BMMC and PBMC samples. To correct for the effects of blast percentages and tissue sources, we included the risk scores and the percentages of blasts in the multivariate Cox analysis. The results suggested that the risk score predicted by

**TABLE 2** | The AUC values of the ROC analyses in various cohorts using different predictive models.

| | | 3-gene model | MPG6 model | 7-gene model | NEST model |
|---|---|---|---|---|---|
| BeatAML | Year1 | 0.665 | 0.633 | 0.638 | 0.874 |
| | Year2 | 0.578 | 0.602 | 0.742 | 0.959 |
| | Year3 | 0.528 | 0.425 | 0.662 | 0.911 |
| GSE12417 | Year1 | 0.551 | 0.563 | NA | 0.671 |
| | Year2 | 0.605 | 0.566 | NA | 0.720 |
| | Year3 | 0.592 | 0.601 | NA | 0.672 |
| TARGET | Year1 | 0.667 | 0.729 | 0.771 | 0.625 |
| | Year2 | 0.505 | 0.795 | 0.554 | 0.763 |
| | Year3 | 0.535 | 0.765 | 0.498 | 0.728 |
| GSE71014 | Year1 | 0.628 | 0.698 | 0.712 | 0.631 |
| | Year2 | 0.636 | 0.674 | 0.680 | 0.697 |
| | Year3 | 0.595 | 0.680 | 0.742 | 0.744 |

*NA, not available.*

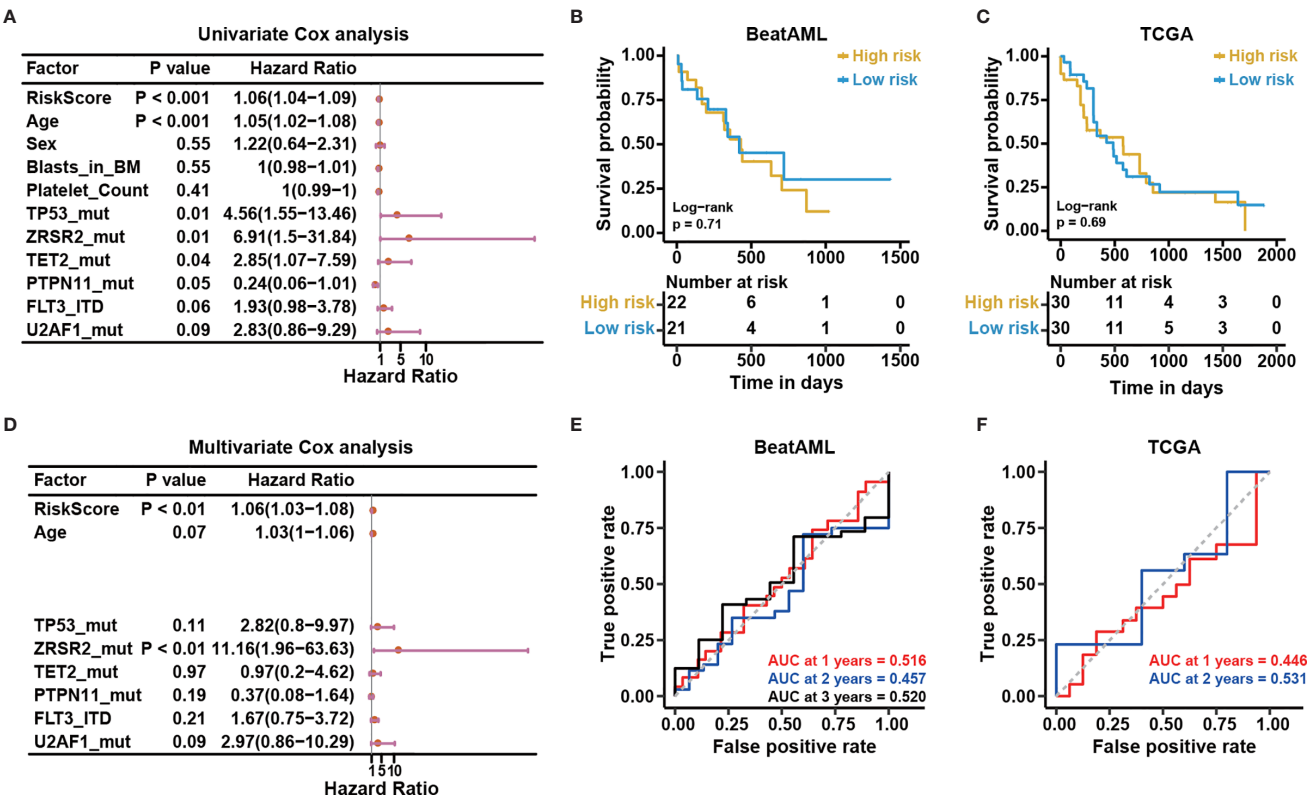


**FIGURE 8** | The risk score predicted based on bone marrow mononuclear cells is an independent risk factor. **(A)** Univariable Cox regression analysis of the relationship between the predicted risk score and common clinical outcomes. **(B)** Multivariable Cox regression analysis of the relationship between the significant factors in univariable Cox regression analysis (P < 0.10) and clinical outcomes. Kaplan-Meier curves for overall survival based on the predicted risk scores in the **(C)** BeatAML and **(E)** TCGA cohorts. The P-value for Kaplan-Meier curves was calculated by the log-rank test. Time-dependent ROC curves for overall survival at 1, 2, and 3 years in the **(D)** BeatAML and **(F)** TCGA cohorts.

our model was independent of the percentages of blasts and tissue sources (**Figure S5A**, P<0.01), indicating our previous results were driven primarily by the model rather than differences in the percentages of blasts and tissue sources. Furthermore, we found that the PBMC samples were more likely to cluster separately from the BMMC samples during unsupervised clustering when including all genes. As shown in **Figure S5B**, we divided all samples into three groups, named A, B, and C. To test the statistical significance of PBMC sample enrichment in these three groups, we performed a hypergeometric test. The results indicated that PBMC samples were not significantly enriched in group A (P = 0.907) and group

B (P = 0.987). Notably, PBMC samples were significantly enriched in group C (P = 0.004). The unsupervised clustering results implied that PBMC samples were more likely to cluster separately from BMMC samples, which might account for the differences in the model application between these two populations.

## DISCUSSION

Although specific genetic mutations have been associated with prognosis in CN-AML patients (6, 11, 46), the specific relationships between aberrant gene expression and clinical outcomes in CN-AML remain largely unknown. Novel biomarkers uncovered from transcriptome analysis that can provide prognosis assessment and potential targets for precision therapy strategies in CN-AML are urgently necessary. In this study, we integrated multiple cohorts to construct a multivariate Cox model, which we named the NEST model, to refine the risk stratification strategy in CN-AML patients.

The NEST model exhibited excellent robustness in five independent cohorts. The predictive capability of the NEST model for survival outcomes was validated by examining AUC values, which were greater than 0.70 in all cohorts (**Table 2**). Moreover, we also discovered that among CN-AML patients who could not be assessed by ELN recommendations, the performance of the NEST model remained outstanding (**Figures 7E, F**). However, the survival analysis of the NEST model in the TARGET cohort indicated no significant difference between the low- and high-risk group (log-rank test, P > 0.05, **Figure 6**). We believe that the small size of the TARGET cohort (n = 26) may explain this lack of significance. However, compared with the 12-gene model, the significance of the survival analysis and the AUC values were enhanced obviously by NEST for the TARGET cohort, which suggested that the NEST model was not only suitable for adult CN-AML patients but was also suitable for pediatric patients. Furthermore, the risk score predicted by the NEST model could function as an independent risk factor for CN-AML survival that was not affected by common clinical factors and genetic mutations (**Figure 8B**). Some limitations remain in this study that should be considered. In addition to the limited sizes of the CN-AML cohorts used to establish the NEST model, we only validated the NEST model on two external cohorts. Thus, the performance of the NEST model should be validated in further prospective studies to guide clinicians in the assessment of prognostic outcomes among CN-AML patients.

Despite these limitations, our NEST model showed more robust performance than three other models, which were published from 2014 to 2020, when tested in four independent cohorts (**Figure S5** and **Table 2**), which showed stable performance for both the survival and ROC analyses. In addition, our results revealed that the NEST model was only suitable for BMMCs, and could not be applied to PBMCs in CN-AML, indicating the existence of variability between BMMCs and PBMCs, which were not due to differences in the percentages of blasts (**Figure S5A**). The results of the unsupervised clustering further supported our conclusion (**Figure S5B**). Previous studies have provided insufficient evidence to support a lack of significant differences between BM and PB samples (21, 47, 48). Metzeler et al. (21) cited two pieces of literature (47, 48) to support the applicability of their model to both PB and BM samples. In the first cited study, Bullinger et al. (48) found that the expression profiles of three paired samples of PB and BM obtained from three patients were positively correlated according to unsupervised hierarchical cluster analysis. However, this result was not significant (n = 3), and this result could be interpreted as the patient heterogeneity was more significant than tissue source heterogeneity. In the second cited study, Sakhinia et al. (47) reported no significant differences in expression between BM and PB for 15 AML indicator genes. However, not only was the number of tested genes limited (n = 15) but also 5 of the 15 tested genes, representing one-third of the tested pool, showed significant differences. These findings argue against the interpretations represented by their conclusion. Moreover, differences have been found in the cell cycle phases between blasts from BM and PB (49–51), and recent studies have also indicated an increase in $CD3^+CD56^+$ T cells in the PB but not the BM of AML patients (52). Therefore, we believe that subtle differences do exist between PBMCs and BMMCs in CN-AML, and future studies should consider the sample origins more strictly.

Except for *ALOX15B* and *SLC44A4*, all of the genes included in our NEST model have previously been associated with leukemia [*FGF13* (53) and *DNTT* (54)] or other cancer types [*C1orf116* (55), *FRMD6* (56), *TFCP2L1* (57), *ITPR3* (58), and *PCOLCE2* (59)]. Princy et al. (55) found that *C1orf116* was associated with the epithelial to mesenchymal transition (EMT), which could represent a critical early event that occurs during tumor metastasis in multiple cancers. Furthermore, they demonstrated that the decreased expression of *C1orf116* was associated with poor prognosis in lung and prostate cancer patients, which is consistent with our results in CN-AML. *DNTT* has been reported to play important functional roles in VDJ recombination and T cell receptor (TCR) (60) and B cell receptor (BCR) (61) signaling, which might indicate an association between immune dysfunction and CN-AML pathogenesis. *FRMD6* has been associated with clinical outcomes in prostate cancer (56). Interestingly, *FRMD6* also plays a vital role in the Hippo pathway, which was originally identified as an evolutionarily conserved signaling pathway that controls organ size. An increasing amount of recent evidence has connected this pathway to the regulation of innate and adaptive immune responses (62–64). In addition, *TFCP2L1* has been reported to serve as a protective factor in clear cell renal cell carcinoma (57). However, our study suggested that *TFCP2L1* serves as a risk factor in CN-AML patients (**Figure 5D**), which could be explained by differences between tissue types. Notably, *TFCP2L1* has also been found to play an important role in stem cells as a component of a complicated transcriptional network that includes other key transcription factors, such as *Nanog*, *Oct4*, and *Sox2*, and maintains the pluripotency of mouse

embryonic stem cells (mESCs) (65). Moreover, *TFCP2L1* is a downstream target of the leukemia inhibitory factor (LIF)/signal transducer and activator of transcription (STAT3) pathway, which mediates self-renewal (66). As a result, *TFCP2L1* might represent a potential target for anti-leukemogenic drug design.

Current dogma holds a "2-hit" model for leukemogenesis, which suggests that the development of AML is associated with dual dysfunction in cell proliferation and hematopoietic differentiation. Class I mutations, such as *FLT3-ITD* and *N-* or *K-RAS* mutations, confer a proliferative advantage to cells. Class II mutations serve primarily to block hematopoietic differentiation. As a result, aberrations in several canonical pathways associated with cell proliferation and differentiation, such as the STAT5, RAS/MAPK, PI3K/AKT, Notch, and Wnt pathways, have been associated with leukemogenesis (67). Given the particularity of cytogenetics in CN-AML, the specific leukemogenesis for CN-AML remains unclear. The current "2-hit" model only interprets the observed alterations that occur in blast cells. According to the NEST model, several immune cell-related genes may also be associated with CN-AML pathogenesis. In addition to *DNTT* and *FRMD6*, *ALOX15B* is constitutively expressed in human monocyte-derived macrophages. Although the function of *ALOX15B* in macrophages remains unclear (68), these immune-related genes suggest that immune dysfunction might also play a vital role in the pathogenesis of CN-AML. To summarize, we speculate that the development of CN-AML might be related to the dysfunction of immune cells in the BM microenvironment, which broadens our understand of the "2-hit" leukemogenesis model. However, more evidence remains necessary to confirm this idea in future studies.

In conclusion, this study identified nine prognosis-related genes in CN-AML and constructed an accurate and robust predictive Cox regression model that is suitable for BMMCs. The predicted risk score could serve as a powerful prognostic indicator, independent of other risk factors. Furthermore, our results shed new light on the pathogenesis of CN-AML and a new potential therapeutic target.

## DATA AVAILABILITY STATEMENT

The original contributions presented in the study are included in the article/**Supplementary Material**. Further inquiries can be directed to the corresponding authors.

## AUTHOR CONTRIBUTIONS

LY collected and analyzed the data and wrote the manuscript. LY and HZ interpreted the results. XY and TL edited the paper and revised the manuscript. SM, HC, KY, and TC revised the manuscript critically. KY and TC performed a final approval of the version to be published. All authors have read and approved the manuscript. All authors contributed to the article and approved the submitted version.

## FUNDING

This work was supported by grants from the Ministry of Science and Technology of China [2020YFE0203000], the National Natural Science Foundation of China [81890990, 81861148029].

## ACKNOWLEDGMENTS

The authors would like to thank their lab members and collaborators for their contribution to the work.

## SUPPLEMENTARY MATERIAL

The Supplementary Material for this article can be found online at: https://www.frontiersin.org/articles/10.3389/fonc.2021.659201/full#supplementary-material

## REFERENCES

1. Lowenberg B, van Putten WL, Touw IP, Delwel R, Santini V. Autonomous proliferation of leukemic cells in vitro as a determinant of prognosis in adult acute myeloid leukemia. *N Engl J Med* (1993) 328(9):614–9. doi: 10.1056/NEJM199303043280904
2. Walter RB, Othus M, Burnett AK, Lowenberg B, Kantarjian HM, Ossenkoppele GJ, et al. Significance of FAB subclassification of "acute myeloid leukemia, NOS" in the 2008 WHO classification: analysis of 5848 newly diagnosed patients. *Blood* (2013) 121(13):2424–31. doi: 10.1182/blood-2012-10-462440
3. Bennett JM, Catovsky D, Daniel MT, Flandrin G, Galton DA, Gralnick HR, et al. Proposed revised criteria for the classification of acute myeloid leukemia. A report of the French-American-British Cooperative Group. *Ann Intern Med* (1985) 103(4):620–5. doi: 10.7326/0003-4819-103-4-620
4. Bennett JM, Catovsky D, Daniel MT, Flandrin G, Galton DA, Gralnick HR, et al. Proposals for the classification of the acute leukaemias. French-American-British (FAB) co-operative group. *Br J Haematol* (1976) 33 (4):451–8. doi: 10.1111/j.1365-2141.1976.tb03563.x
5. Haferlach T, Schoch C, Loffler H, Gassmann W, Kern W, Schnittger S, et al. Morphologic dysplasia in de novo acute myeloid leukemia (AML) is related to unfavorable cytogenetics but has no independent prognostic relevance under the conditions of intensive induction therapy: results of a multiparameter analysis from the German AML Cooperative Group studies. *J Clin Oncol* (2003) 21(2):256–65. doi: 10.1200/JCO.2003.08.005
6. Dohner H, Estey E, Grimwade D, Amadori S, Appelbaum FR, Buchner T, et al. Diagnosis and management of AML in adults: 2017 ELN recommendations from an international expert panel. *Blood* (2017) 129 (4):424–47. doi: 10.1182/blood-2016-08-733196
7. Grimwade D, Walker H, Oliver F, Wheatley K, Harrison C, Harrison G, et al. The importance of diagnostic cytogenetics on outcome in AML: analysis of 1,612 patients entered into the MRC AML 10 trial. The Medical Research Council Adult and Children's Leukaemia Working Parties. *Blood* (1998) 92 (7):2322–33. doi: 10.1182/blood.V92.7.2322.2322_2322_2333
8. Mrozek K, Heinonen K, Bloomfield CD. Clinical importance of cytogenetics in acute myeloid leukaemia. *Best Pract Res Clin Haematol* (2001) 14(1):19–47. doi: 10.1053/beha.2000.0114
9. Falini B, Nicoletti I, Martelli MF, Mecucci C. Acute myeloid leukemia carrying cytoplasmic/mutated nucleophosmin (NPMc+ AML): biologic and clinical features. *Blood* (2007) 109(3):874–85. doi: 10.1182/blood-2006-07-012252
10. Mrozek K, Marcucci G, Paschka P, Whitman SP, Bloomfield CD. Clinical relevance of mutations and gene-expression changes in adult acute myeloid

leukemia with normal cytogenetics: are we ready for a prognostically prioritized molecular classification? *Blood* (2007) 109(2):431–48. doi: 10.1182/blood-2006-06-001149
11. Cancer Genome Atlas Research N., Ley TJ, Miller C, Ding L, Raphael BJ, Mungall AJ, et al. Genomic and epigenomic landscapes of adult de novo acute myeloid leukemia. *N Engl J Med* (2013) 368(22):2059–74. doi: 10.1056/NEJMoa1301689
12. Meyer SC, Levine RL. Translational implications of somatic genomics in acute myeloid leukaemia. *Lancet Oncol* (2014) 15(9):e382–394. doi: 10.1016/S1470-2045(14)70008-7
13. Lin SY, Miao YR, Hu FF, Hu H, Zhang Q, Li Q, et al. A 6-Membrane Protein Gene score for prognostic prediction of cytogenetically normal acute myeloid leukemia in multiple cohorts. *J Cancer* (2020) 11(1):251–9. doi: 10.7150/jca.35382
14. Yin X, Huang H, Huang S, Xu A, Fan F, Luo S, et al. A Novel Scoring System for Risk Assessment of Elderly Patients With Cytogenetically Normal Acute Myeloid Leukemia Based on Expression of Three AQP1 DNA Methylation-Associated Genes. *Front Oncol* (2020) 10:566:566. doi: 10.3389/fonc.2020.00566
15. Lin SY, Hu FF, Miao YR, Hu H, Lei Q, Zhang Q, et al. Identification of STAB1 in Multiple Datasets as a Prognostic Factor for Cytogenetically Normal AML: Mechanism and Drug Indications. *Mol Ther Nucleic Acids* (2019) 18:476–84. doi: 10.1016/j.omtn.2019.09.014
16. Cao L, Zhang W, Liu X, Yang P, Wang J, Hu K, et al. The Prognostic Significance of PDE7B in Cytogenetically Normal Acute Myeloid Leukemia. *Sci Rep* (2019) 9(1):16991. doi: 10.1038/s41598-019-53563-x
17. Capiod JC, Tournois C, Vitry F, Sevestre MA, Daliphard S, Reix T, et al. Characterization and comparison of bone marrow and peripheral blood mononuclear cells used for cellular therapy in critical leg ischaemia: towards a new cellular product. *Vox Sang* (2009) 96(3):256–65. doi: 10.1111/j.1423-0410.2008.01138.x
18. Cuende N, Rico L, Herrera C. Concise review: bone marrow mononuclear cells for the treatment of ischemic syndromes: medicinal product or cell transplantation? *Stem Cells Transl Med* (2012) 1(5):403–8. doi: 10.5966/sctm.2011-0064
19. Tyner JW, Tognon CE, Bottomly D, Wilmot B, Kurtz SE, Savage SL, et al. Functional genomic landscape of acute myeloid leukaemia. *Nature* (2018) 562 (7728):526–31. doi: 10.1038/s41586-018-0623-z
20. Chuang MK, Chiu YC, Chou WC, Hou HA, Tseng MH, Kuo YY, et al. An mRNA expression signature for prognostication in de novo acute myeloid leukemia patients with normal karyotype. *Oncotarget* (2015) 6(36):39098–110. doi: 10.18632/oncotarget.5390
21. Metzeler KH, Hummel M, Bloomfield CD, Spiekermann K, Braess J, Sauerland MC, et al. An 86-probe-set gene-expression signature predicts survival in cytogenetically normal acute myeloid leukemia. *Blood* (2008) 112 (10):4193–201. doi: 10.1182/blood-2008-02-134411
22. Verhaak RG, Wouters BJ, Erpelinck CA, Abbas S, Beverloo HB, Lugthart S, et al. Prediction of molecular subtypes in acute myeloid leukemia based on gene expression profiling. *Haematologica* (2009) 94(1):131–4. doi: 10.3324/haematol.13299
23. Bolouri H, Farrar JE, Triche TJr, Ries RE, Lim EL, Alonzo TA, et al. The molecular landscape of pediatric acute myeloid leukemia reveals recurrent structural alterations and age-specific mutational interactions. *Nat Med* (2018) 24(1):103–12. doi: 10.1038/nm.4439
24. Law CW, Alhamdoosh M, Su S, Dong X, Tian L, Smyth GK, et al. RNA-seq analysis is easy as 1-2-3 with limma, Glimma and edgeR. *F1000Res* (2016) 5:1408. doi: 10.12688/f1000research.9005.3
25. Law CW, Chen Y, Shi W, Smyth GK. voom: Precision weights unlock linear model analysis tools for RNA-seq read counts. *Genome Biol* (2014) 15(2):R29. doi: 10.1186/gb-2014-15-2-r29
26. Yu G, Wang LG, Han Y, He QY. clusterProfiler: an R package for comparing biological themes among gene clusters. *OMICS* (2012) 16(5):284–7. doi: 10.1089/omi.2011.0118
27. Kramer A, Green J, Pollard JJr, Tugendreich S. Causal analysis approaches in Ingenuity Pathway Analysis. *Bioinformatics* (2014) 30(4):523–30. doi: 10.1093/bioinformatics/btt703
28. Mandrekar JN. Receiver operating characteristic curve in diagnostic test assessment. *J Thorac Oncol* (2010) 5(9):1315–6. doi: 10.1097/JTO.0b013e3181ec173d
29. Marcucci G, Yan P, Maharry K, Frankhouser D, Nicolet D, Metzeler KH, et al. Epigenetics meets genetics in acute myeloid leukemia: clinical impact of a novel seven-gene score. *J Clin Oncol* (2014) 32(6):548–56. doi: 10.1200/JCO.2013.50.6337
30. Papaemmanuil E, Gerstung M, Bullinger L, Gaidzik VI, Paschka P, Roberts ND, et al. Genomic Classification and Prognosis in Acute Myeloid Leukemia. *N Engl J Med* (2016) 374(23):2209–21. doi: 10.1056/NEJMoa1516192
31. Alharbi RA, Pettengell R, Pandha HS, Morgan R. The role of HOX genes in normal hematopoiesis and acute leukemia. *Leukemia* (2013) 27(5):1000–8. doi: 10.1038/leu.2012.356
32. Karakas T, Miething CC, Maurer U, Weidmann E, Ackermann H, Hoelzer D, et al. The coexpression of the apoptosis-related genes bcl-2 and wt1 in predicting survival in adult acute myeloid leukemia. *Leukemia* (2002) 16 (5):846–54. doi: 10.1038/sj.leu.2402434
33. Wang Y, Krivtsov AV, Sinha AU, North TE, Goessling W, Feng Z, et al. The Wnt/beta-catenin pathway is required for the development of leukemia stem cells in AML. *Science* (2010) 327(5973):1650–3. doi: 10.1126/science.1186624
34. Stoddart A, Wang J, Hu C, Fernald AA, Davis EM, Cheng JX, et al. Inhibition of WNT signaling in the bone marrow niche prevents the development of MDS in the Apc(del/+) MDS mouse model. *Blood* (2017) 129(22):2959–70. doi: 10.1182/blood-2016-08-736454
35. Kataoka TR, Kumanogoh A, Hirata M, Moriyoshi K, Ueshima C, Kawahara M, et al. CD72 regulates the growth of KIT-mutated leukemia cell line Kasumi-1. *Sci Rep* (2013) 3:2861. doi: 10.1038/srep02861
36. Ohgami RS, Ma L, Ren L, Weinberg OK, Seetharam M, Gotlib JR, et al. DNA methylation analysis of ALOX12 and GSTM1 in acute myeloid leukaemia identifies prognostically significant groups. *Br J Haematol* (2012) 159(2):182–90. doi: 10.1111/bjh.12029
37. Rohrs S, Scherr M, Romani J, Zaborski M, Drexler HG, Quentmeier H. CD7 in acute myeloid leukemia: correlation with loss of wild-type CEBPA, consequence of epigenetic regulation. *J Hematol Oncol* (2010) 3:15. doi: 10.1186/1756-8722-3-15
38. Doron B, Abdelhamed S, Butler JT, Hashmi SK, Horton TM, Kurre P. Transmissible ER stress reconfigures the AML bone marrow compartment. *Leukemia* (2019) 33(4):918–30. doi: 10.1038/s41375-018-0254-2
39. Alexander BM, Schoenfeld JD, Trippa L. Hazards of Hazard Ratios - Deviations from Model Assumptions in Immunotherapy. *N Engl J Med* (2018) 378(12):1158–9. doi: 10.1056/NEJMc1716612
40. O'Quigley J, Xu R, Stare J. Explained randomness in proportional hazards models. *Stat Med* (2005) 24(3):479–89. doi: 10.1002/sim.1946
41. Coombs CC, Tallman MS, Levine RL. Molecular therapy for acute myeloid leukaemia. *Nat Rev Clin Oncol* (2016) 13(5):305–18. doi: 10.1038/nrclinonc.2015.210
42. Wang M, Yang C, Zhang L, Schaar DG. Molecular Mutations and Their Cooccurrences in Cytogenetically Normal Acute Myeloid Leukemia. *Stem Cells Int* (2017) 2017:6962379. doi: 10.1155/2017/6962379
43. Santamaria CM, Chillon MC, Garcia-Sanz R, Perez C, Caballero MD, Ramos F, et al. Molecular stratification model for prognosis in cytogenetically normal acute myeloid leukemia. *Blood* (2009) 114(1):148–52. doi: 10.1182/blood-2008-11-187724
44. Bejar R. Splicing Factor Mutations in Cancer. *Adv Exp Med Biol* (2016) 907:215–28. doi: 10.1007/978-3-319-29073-7_9
45. Alfayez M, Issa GC, Patel KP, Wang F, Wang X, Short NJ, et al. The Clinical impact of PTPN11 mutations in adults with acute myeloid leukemia. *Leukemia* (2020) 35(3):691–700. doi: 10.1038/s41375-020-0920-z
46. Zhou J, Chng WJ. Identification and targeting leukemia stem cells: The path to the cure for acute myeloid leukemia. *World J Stem Cells* (2014) 6(4):473–84. doi: 10.4252/wjsc.v6.i4.473
47. Sakhinia E, Farahangpour M, Tholouli E, Liu Yin JA, Hoyland JA, Byers RJ. Comparison of gene-expression profiles in parallel bone marrow and peripheral blood samples in acute myeloid leukaemia by real-time polymerase chain reaction. *J Clin Pathol* (2006) 59(10):1059–65. doi: 10.1136/jcp.2005.031161
48. Bullinger L, Dohner K, Bair E, Frohling S, Schlenk RF, Tibshirani R, et al. Use of gene-expression profiling to identify prognostic subclasses in adult acute myeloid leukemia. *N Engl J Med* (2004) 350(16):1605–16. doi: 10.1056/NEJMoa031046
49. Vidriales MB, Orfao A, Lopez-Berges MC, Gonzalez M, Lopez-Macedo A, Ciudad J, et al. Prognostic value of S-phase cells in AML patients. *Br J Haematol* (1995) 89(2):342–8. doi: 10.1111/j.1365-2141.1995.tb03310.x

50. Hiddemann W, Buchner T, Andreeff M, Wormann B, Melamed MR, Clarkson BD. Cell kinetics in acute leukemia: a critical reevaluation based on new data. *Cancer* (1982) 50(2):250–8. doi: 10.1002/1097-0142(19820715)50:2<250::aid-cncr2820500215>3.0.co;2-4
51. Sellar RS, Fraser L, Khwaja A, Gale RE, Marafioti T, Akarca A, et al. Cell cycle status in AML blast cells from peripheral blood, bone marrow aspirates and trephines and implications for biological studies and treatment. *Br J Haematol* (2016) 174(2):275–9. doi: 10.1111/bjh.14055
52. Le Dieu R, Taussig DC, Ramsay AG, Mitter R, Miraki-Moud F, Fatah R, et al. Peripheral blood T cells in acute myeloid leukemia (AML) patients at diagnosis have abnormal phenotype and genotype and form defective immune synapses with AML blasts. *Blood* (2009) 114(18):3909–16. doi: 10.1182/blood-2009-02-206946
53. Gutierrez NC, Lopez-Perez R, Hernandez JM, Isidro I, Gonzalez B, Delgado M, et al. Gene expression profile reveals deregulation of genes with relevant functions in the different subclasses of acute myeloid leukemia. *Leukemia* (2005) 19(3):402–9. doi: 10.1038/sj.leu.2403625
54. Mendler JH, Maharry K, Radmacher MD, Mrozek K, Becker H, Metzeler KH, et al. RUNX1 mutations are associated with poor outcome in younger and older patients with cytogenetically normal acute myeloid leukemia and with distinct gene and MicroRNA expression signatures. *J Clin Oncol* (2012) 30 (25):3109–18. doi: 10.1200/JCO.2011.40.6652
55. Parsana P, Amend SR, Hernandez J, Pienta KJ, Battle A. Identifying global expression patterns and key regulators in epithelial to mesenchymal transition through multi-study integration. *BMC Cancer* (2017) 17(1):447. doi: 10.1186/s12885-017-3413-3
56. Haldrup J, Strand SH, Cieza-Borrella C, Jakobsson ME, Riedel M, Norgaard M, et al. FRMD6 has tumor suppressor functions in prostate cancer. *Oncogene* (2020) 40(4):763–76. doi: 10.1038/s41388-020-01548-w
57. Tun HW, Marlow LA, von Roemeling CA, Cooper SJ, Kreinest P, Wu K, et al. Pathway signature and cellular differentiation in clear cell renal cell carcinoma. *PloS One* (2010) 5(5):e10696. doi: 10.1371/journal.pone.0010696
58. Wu Y, Liu Z, Tang D, Liu H, Luo S, Stinchcombe TE, et al. Potentially functional variants of HBEGF and ITPR3 in GnRH signaling pathway genes predict survival of non-small cell lung cancer patients. *Transl Res* (2021) S1931–5244(20)30320-0. doi: 10.1016/j.trsl.2020.12.009
59. Harvie MN, Sims AH, Pegington M, Spence K, Mitchell A, Vaughan AA, et al. Intermittent energy restriction induces changes in breast gene expression and systemic metabolism. *Breast Cancer Res* (2016) 18(1):57. doi: 10.1186/s13058-016-0714-4
60. Patil P, Cieslak A, Bernhart SH, Toprak UH, Wagener R, Lopez C, et al. Reconstruction of rearranged T-cell receptor loci by whole genome and transcriptome sequencing gives insights into the initial steps of T-cell prolymphocytic leukemia. *Genes Chromosomes Cancer* (2020) 59(4):261–7. doi: 10.1002/gcc.22821
61. Hunter ZR, Xu L, Yang G, Tsakmaklis N, Vos JM, Liu X, et al. Transcriptome sequencing reveals a profile that corresponds to genomic variants in Waldenstrom macroglobulinemia. *Blood* (2016) 128(6):827–38. doi: 10.1182/blood-2016-03-708263
62. Yamauchi T, Moroishi T. Hippo Pathway in Mammalian Adaptive Immune System. *Cells* (2019) 8(5):398. doi: 10.3390/cells8050398
63. Wang X, Ha T, Liu L, Hu Y, Kao R, Kalbfleisch J, et al. TLR3 Mediates Repair and Regeneration of Damaged Neonatal Heart through Glycolysis Dependent YAP1 Regulated miR-152 Expression. *Cell Death Differ* (2018) 25(5):966–82. doi: 10.1038/s41418-017-0036-9
64. Taha Z, Janse van Rensburg HJ, Yang X. The Hippo Pathway: Immunity and Cancer. *Cancers (Basel)* (2018) 10(4):94. doi: 10.3390/cancers10040094
65. Kim J, Orkin SH. Embryonic stem cell-specific signatures in cancer: insights into genomic regulatory networks and implications for medicine. *Genome Med* (2011) 3(11):75. doi: 10.1186/gm291
66. Onishi K, Zandstra PW. LIF signaling in stem cells and development. *Development* (2015) 142(13):2230–6. doi: 10.1242/dev.117598
67. Gilliland DG, Griffin JD. The roles of FLT3 in hematopoiesis and leukemia. *Blood* (2002) 100(5):1532–42. doi: 10.1182/blood-2002-02-0492
68. Snodgrass RG, Brune B. Regulation and Functions of 15-Lipoxygenases in Human Macrophages. *Front Pharmacol* (2019) 10:719. doi: 10.3389/fphar.2019.00719


**Conflict of Interest:** The authors declare that the research was conducted in the absence of any commercial or financial relationships that could be construed as a potential conflict of interest.

frontiers in Oncology

ORIGINAL RESEARCH
published: 01 June 2021
doi: 10.3389/fonc.2021.682436

# A Novel Mechanism of Action of Histone Deacetylase Inhibitor Chidamide: Enhancing the Chemotaxis Function of Circulating PD-1(+) Cells From Patients With PTCL

*Chong Wei[1], Shaoxuan Hu[2], Mingjie Luo[3], Chong Chen[4], Wei Wang[1], Wei Zhang[1] and Daobin Zhou[1]**

*[1] Department of Hematology, Peking Union Medical College Hospital, Chinese Academy of Medical Sciences & Peking Union Medical College, Beijing, China, [2] Key Laboratory of Carcinogenesis and Translational Research (Ministry of Education), Department of Lymphoma, Peking University Cancer Hospital & Institute, Beijing, China, [3] Department of General Surgery, Peking Union Medical College Hospital, Chinese Academy of Medical Sciences & Peking Union Medical College, Beijing, China, [4] Department of Immunology, Institute of Basic Medical Sciences, Chinese Academy of Medical Sciences; School of Basic Medicine, Peking Union Medical College, Beijing, China*

OPEN ACCESS

**Edited by:**
*Gurvinder Kaur, All India Institute of Medical Sciences, India*

**Reviewed by:**
*Tijana Martinov, Fred Hutchinson Cancer Research Center, United States*
*Xiaoxia Hu, Ruijin Hospital, China*

***Correspondence:**
*Daobin Zhou*
*zhoudb@pumch.cn*

**Specialty section:**
*This article was submitted to Hematologic Malignancies, a section of the journal Frontiers in Oncology*

**Received:** *18 March 2021*
**Accepted:** *06 May 2021*
**Published:** *01 June 2021*

**Citation:**
*Wei C, Hu S, Luo M, Chen C, Wang W, Zhang W and Zhou D (2021) A Novel Mechanism of Action of Histone Deacetylase Inhibitor Chidamide: Enhancing the Chemotaxis Function of Circulating PD-1(+) Cells From Patients With PTCL. Front. Oncol. 11:682436. doi: 10.3389/fonc.2021.682436*

**Background:** Peripheral T-cell lymphomas (PTCLs) are a heterogeneous group of neoplasms characterized by a poor prognosis. Histone deacetylase (HDAC) inhibitors have emerged as novel therapeutic agents for PTCLs. In this study, we aimed to explore the immunomodulatory effect of the HDAC inhibitor chidamide on circulating PD-1(+) cells from patients with PTCL, as well as its correlation with treatment response.

**Methods:** We enrolled newly diagnosed patients with PTCLs treated with a combination of chidamide and chemotherapy. Gene expression profile analysis was performed on peripheral blood PD-1(+) cells, both at baseline and at the end of treatment. A list of differentially expressed genes (DEGs) was identified. Gene Ontology (GO) and Kyoto Encyclopedia of Genes and Genomes (KEGG) pathway analyses were performed to annotate the biological implications of the DEGs. A gene concept network was constructed to identify the key DEGs for further PCR verification.

**Results:** A total of 302 DEGs were identified in the complete remission (CR) group, including 162 upregulated and 140 downregulated genes. In contrast, only 12 DEGs were identified in the non-CR group. GO analysis revealed that these upregulated DEGs were mainly involved in chemokine activity, cell chemotaxis, and cellular response to interleukin-1 and interferon-γ. Furthermore, KEGG pathway analysis showed that these DEGs were enriched in cytokine-cytokine receptor interaction and chemokine signaling pathways. The innate immune signaling pathways, including the Toll-like and NOD-like receptor signaling pathways, were also influenced. The gene concept network revealed that the key upregulated genes belonged to the C-C chemokine family.

**Conclusion:** Our results showed that chidamide treatment notably enhanced the expression of genes associated with chemokine activity and chemotaxis function of circulating PD-1(+) cells. By recruiting immune cells and improving the innate immune function of PD-1(+) cells, chidamide may reshape the tumor microenvironment to an anti-tumor phenotype and synergize with checkpoint inhibitors.

**Keywords: peripheral T-cell lymphoma, chidamide, innate immune, chemotaxis, programmed cell death-1**

## INTRODUCTION

Peripheral T-cell lymphomas (PTCLs) are a heterogeneous group of mature T-cell and natural killer (NK) - cell neoplasms, characterized by aggressive clinical behavior and poor prognosis (1, 2). Given the unsatisfactory outcomes of patients with PTCLs upon receiving conventional anthracycline-based chemotherapies, there is a need for novel targeted therapies and immunotherapies. In recent years, histone deacetylase (HDAC) inhibitors have emerged as novel therapeutic agents against PTCLs. The anti-tumor effects of HDAC inhibitors are commonly known as inducing apoptosis and cell cycle arrest (3). Beyond the direct anti-tumor effect, recent advances show that HDAC inhibitors are also involved in the immune-mediated anti-tumor effect (4–6). However, the mechanism is still not clear.

Programmed cell death protein 1 (PD-1), expressed on immune cells, and its ligand PD ligand 1 (PD-L1), expressed on tumor cells, are crucial regulators of the tumor immunosurveillance system (7). The binding of PD-1 to PD-L1 results in suppression of the host immune response and escape of tumor cells from immune surveillance. Previously, we found that the innate immunity of circulating PD-1(+) cells from patients with PTCLs was compromised compared with healthy controls (8). Furthermore, our *in vitro* study revealed that the class I HDAC inhibitor chidamide enhances IFN-γ production and restores the cytotoxic activity of PD-1(+) cells from patients with PTCL, indicating that chidamide may exert its immunomodulatory effect by regulating the function of PD-1(+) cells (8).

Here, we explored the impact of chidamide as an immune regulator on circulating PD-1(+) cells and its correlation with treatment response. Gene expression profile (GEP) analysis was performed on peripheral blood PD-1(+) cells from patients with PTCL, both at baseline and end of first-line treatment. Differentially expressed genes (DEGs) were identified and their biological implications were investigated. The findings described in this study demonstrate a novel mechanism by which HDAC inhibitors regulate PD-1(+) cells and highlight the potential of HDAC inhibitors to synergize with immunotherapies.

## MATERIALS AND METHODS

### Patients and Treatment

Nine patients who were newly diagnosed with PTCL and treated in Peking Union Medical College Hospital (PUMCH) were enrolled in this study. Histological findings were consistent with PTCLs, according to the World Health Organization (WHO) classification. Histologic subtypes included peripheral T-cell lymphoma, not otherwise specified (PTCL, NOS), anaplastic large cell lymphoma, ALK-negative (ALCL, ALK-), and angioimmunoblastic T-cell lymphoma (AITL).

All patients received a combination of chidamide with cyclophosphamide, epirubicin, vindesine, prednisone, and etoposide (CHOEP) regimen as first-line chemotherapy. The regimen of CHOEP chemotherapy were as follows: cyclophosphamide (750 mg/m$^2$ intravenously on day 1), epirubicin (70 mg/m$^2$ intravenously on day 1), vindesine (4 mg intravenously on day 1), prednisone (100 mg/d orally on days 1–5), and etoposide (100 mg intravenously on days 1-3). Chidamide 20mg twice weekly was started on day 1 of the first cycle of CHOEP therapy and administered continuously.

Treatment responses were assessed according to the 2014 Lugano classification criteria and classified as complete remission (CR), partial remission (PR), stable disease (SD), and progressive disease (PD) (9). Patients were divided according to the treatment response into CR and non-CR groups (including patients with PR, SD, and PD response). The study was approved by the institutional review board of PUMCH. All participants provided written informed consent.

### Isolation of PD-1(+) Cells

Blood samples were collected both at baseline and at the end of first-line treatment. Flow cytometry analysis was performed to ensure that there were no tumor cells in the peripheral blood. Peripheral blood mononuclear cells (PBMCs) were isolated from blood samples using the Ficoll-Hypaque density centrifugation method. Approximately $10^6$–$10^8$ PBMCs were harvested from 25 mL of peripheral blood. Flow cytometry analysis was performed on PBMCs to evaluate the components of PD-1(+) cells. The cells were labelled with anti-PD-1-PE, anti-CD4-APC, anti-CD8-FITC, anti-CD56-PE, and anti-CD14-APC antibodies.

PD-1(+) cells were isolated from PBMCs using the magnetic-activated cell sorting (MACS) method according to the manufacturer's instructions (Miltenyi Biotech, Germany). Briefly, PBMCs were first incubated with 20 μL anti-CD279-PE antibodies (Miltenyi Biotech, Germany; 130-117-384) at 4°C for 20 min. After washing and centrifugation, the cells were incubated with anti-PE microbeads (Miltenyi Biotech, Germany; 130-048-801). The labeled cell suspension was then filled into the reservoir of a large-volume separation column (Miltenyi Biotech, Germany) placed in a magnetic field.

After removing the column from the magnetic field, PD-1(+) cells were eluted by flushing the column with PBS buffer. The collected PD-1(+) cell suspension was counted and prepared for mRNA extraction.

## Construction of mRNA Library and Sequencing

Total RNA was extracted from the collected PD-1(+) cells using TRIzol reagent (Invitrogen, Carlsbad, CA, USA, 15596018). A NanoDrop 2000 (Thermo Scientific, USA) was used to verify the purity of the RNA. The quality of RNA was measured using the Qubit RNA Assay Kit in Qubit 2.0 Fluorometer (Life Technologies, USA). The sequencing library of each RNA sample was prepared using an Ion Total RNA-Seq Kit v2 (Life Technologies, USA) according to the manufacturer's instructions. Emulsion PCR was performed using the cDNA library as template. RNA-sequencing (RNA-Seq) was conducted by NovelBio Bio-Pharm Technology Co. Ltd (Shanghai, China) using an ABI Ion Proton (Life Technologies, USA) instrument.

## Gene Expression Data Analysis

Differentially expressed genes (DEGs), between pre-treatment and post-treatment conditions and between CR and non-CR group at baseline, were filtered using the EBseq algorithm. Genes with an absolute fold change (FC) of > 1.5, or < 0.667, and false discovery rate (FDR) < 0.05, were considered significant DEGs. Average linkage hierarchical clustering was performed, and heatmaps were generated.

## Gene Ontology (GO) and Kyoto Encyclopedia of Genes and Genomes (KEGG) Pathway Analyses

GO analysis was performed to annotate the biological functions of the DEGs, including three GO categories: biological process (BP), cellular component (CC), and molecular function (MF). GO annotations were downloaded from the NCBI (http://www.ncbi.nlm.nih.gov), Gene Ontology (http://www.geneontology.org), and UniProt (http://www.uniprot.org). Pathway annotation of DEGs was performed using the KEGG database. Fisher's exact test was used to identify the significantly influenced GO categories and KEGG pathways. Statistical significance was set at $P < 0.05$. The gene concept network was constructed using cluster Profiler for enriched GO biological pathways with statistical significance ($P < 0.05$) (10).

# RESULTS

## Patient Characteristics

Nine newly diagnosed patients with PTCL, administered chidamide combined with CHOEP regimen as first-line chemotherapy, were included in this study. The CR group included 5 patients and the non-CR group included 4 patients (3 PR and 1 PD). The baseline characteristics of patients in the 2 groups are listed in **Table 1**. The median age at diagnosis was 45 (range, 27–71) years, and the male: female ratio was 4:5.

**TABLE 1** | Clinical characteristics of the patients in the 2 groups.

| Characteristic | CR group (n = 5) | Non-CR group (n = 4) |
|---|---|---|
| Age, years | | |
| Median (range) | 42 (27-58) | 55 (22-71) |
| Sex, male | 2 | 2 |
| Ann Arbor stage III/IV | 3 | 3 |
| ECOG performance status>1 | 2 | 1 |
| IPI score>2 | 1 | 1 |
| Histologic subtypes | | |
| PTCL, NOS | 1 | 1 |
| AITL | 2 | 2 |
| ALK- ALCL | 2 | 1 |

*ECOG, Eastern Cooperative Oncology Group; IPI, International Prognostic Index; PTCL, NOS, peripheral T-cell lymphoma; not otherwise specified; AITL, angioimmunoblastic T-cell lymphoma; ALK- ALCL, anaplastic large cell lymphoma, ALK negative.*

Histologic subtypes included peripheral PTCL, NOS (n = 2), ALK-ALCL (n = 3), and AITL (n = 4). Most patients were in clinical stages III–IV (6/9, 66.7%). The proportion of high-intermediate or high-risk patients, based on the International Prognostic Index (IPI) score, was 2/9 (22.2%).

## Components of PD-1(+) Cells

Flow cytometry analysis was performed on PBMCs to evaluate the components of PD-1(+) cells in 3 patients. **Figure 1** shows the flow cytometry result of one patient. The average proportion of PD-1 (+) cells in PBMCs was 18.8%. The average proportion of CD4+, CD8+, CD56+, and CD14+ cells in the PD-1(+) cell subset were 13.3%, 80.9%, 3.2%, and 3.1%, which indicated the proportion of CD4+ T-cells, CD8+ T-cells, NK cells, and monocytes, respectively.

## DEGs Between the Pre-Treatment and Post-Treatment Conditions

The gene expression profiles of peripheral blood PD-1(+) cells were compared between the pre-treatment and post-treatment conditions. With a criterion of FDR < 0.05 and $|\log_2 FC| \geq 0.58$, a total of 302 DEGs were identified in the CR group, including 162 up-regulated and 140 down-regulated genes (**Figure 2A**). Contrastingly, only 12 DEGs were identified in the non-CR group, including 9 up-regulated and 3 down-regulated genes.

To test whether these DEGs, identified in the CR group, were consistently expressed between the CR and non-CR groups, hierarchical clustering heat maps were generated using the expression levels of the 302 DEGs. These genes were only differentially expressed between pre-treatment and post-treatment conditions in the CR group (**Figure 2B**).

## GO and KEGG Pathway Analyses of DEGs Between the Pre-Treatment and Post-Treatment Conditions

To further investigate the potential functional mechanisms, the 302 DEGs identified in the CR group were subjected to GO analysis. The top 15 significant GO terms for the 162 upregulated DEGs in the BP and MF categories are shown in **Figures 3A, B**. GO annotation and significance analysis revealed that these DEGs were mainly involved in chemokine activity, cell

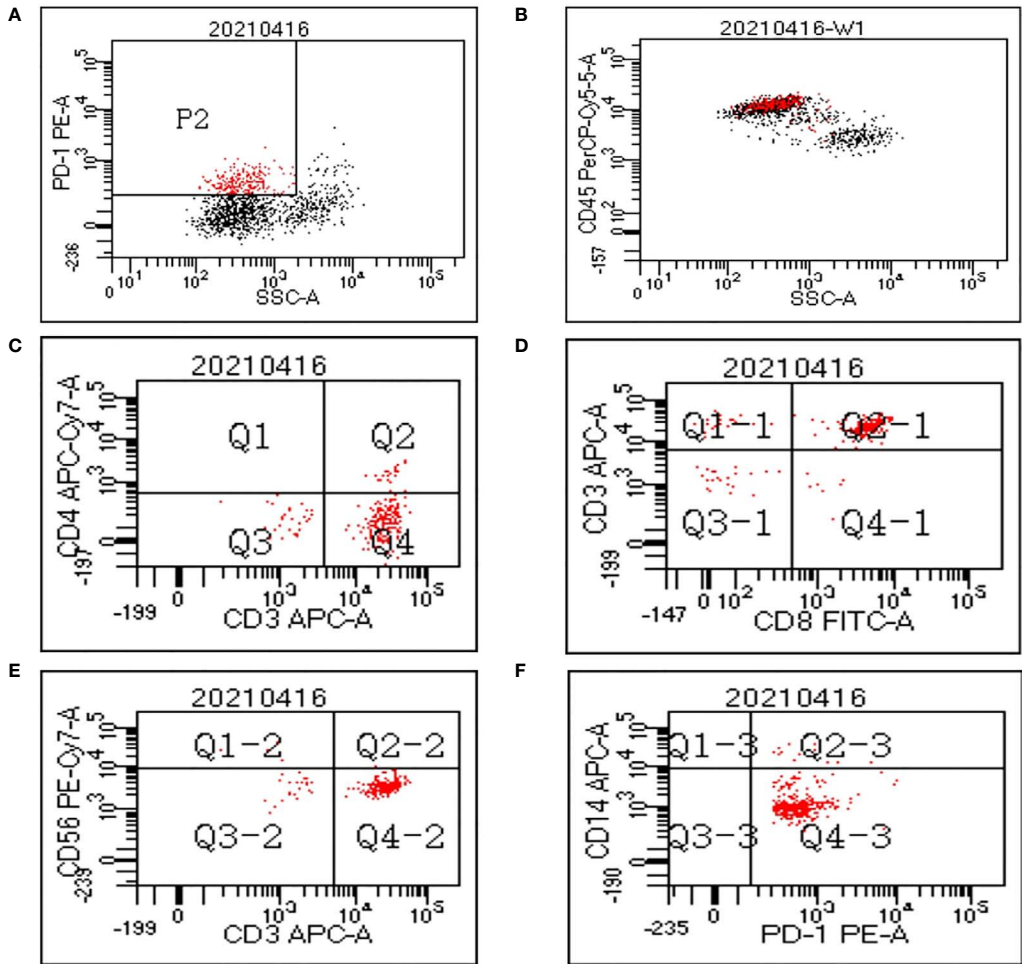


**FIGURE 1** | Flow cytometry data of peripheral blood mononuclear cells (PBMCs). **(A)** In the cytogram of side scatter (SSC) versus PD-1, the population P2 refers to the PD-1(+) cells which were colored red. **(B)** The PD-1(+) cells mainly fall in the cluster of lymphocytes in the cytogram of SSC versus CD45. A gate was set to show only the cells in P2 population on the cytogram of CD4 versus CD3 **(C)**, CD8 versus CD3 **(D)**, CD56 versus CD3 **(E)**, and CD14 versus PD-1 **(F)**.

chemotaxis (including monocyte, neutrophil, and lymphocyte chemotaxis), cellular response to interleukin-1 (IL-1) and interferon-gamma (IFN-γ).

Pathway annotation of the DEGs was performed using the KEGG database. The top 15 significant KEGG pathways for the 162 upregulated DEGs are shown in **Figure 3C**. Furthermore, pathway analyses also revealed that these DEGs were mainly involved in cytokine-cytokine receptor interactions and chemokine signaling pathways. The innate immune signaling pathways, including Toll-like receptor and NOD-like receptor signaling pathways, were also influenced.

To further explore the interaction of these DEGs and identify key DEGs for further PCR verification, a gene concept network was established based on the top 15 significant GO terms in the BP category. The key up-regulated genes located in the center of the network belonged to the C-C chemokine family, including CCL2, CCL3L1, CCL4, CCL7, CCL8, and CCL20 (**Figure 3D**). The products of these genes recruit monocytes, neutrophils, memory T cells, and dendritic cells (11, 12).

## GO and KEGG Pathway Analyses of DEGs Between CR and Non-CR Group at Baseline

The gene expression profiles of peripheral blood PD-1(+) cells were also compared between the CR and non-CR group at baseline level. A total of 470 DEGs were identified, including 115 up-regulated and 355 down-regulated genes (**Figure 4A**). The 470 DEGs were further subjected to GO analysis. The top 15 significant GO terms in the BP and MF categories are shown in **Figures 4B, C**. GO annotation revealed that these DEGs were mainly involved in humoral immune response, including complement activation and immunoglobulin mediated immune response, which were all down-regulated in the CR group.

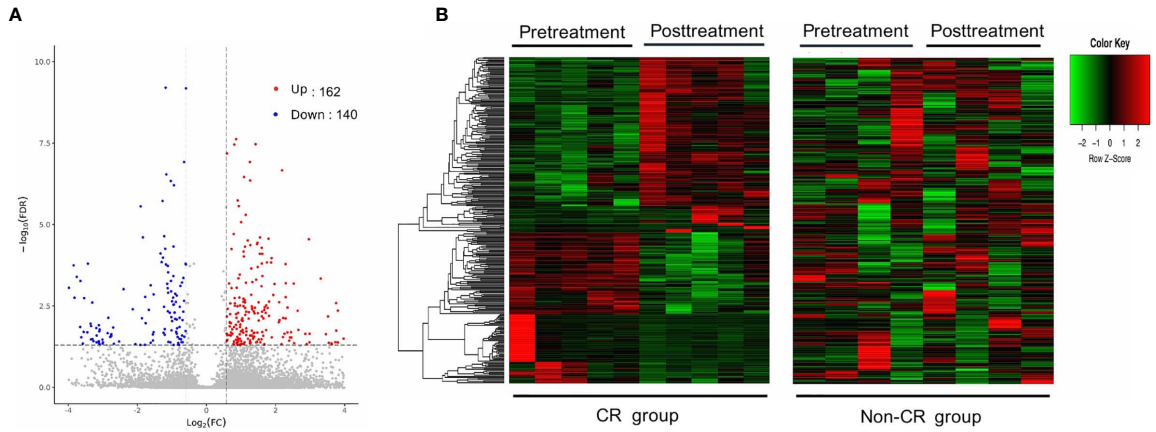


**FIGURE 2** | Differentially expressed genes (DEGs) between pre-treatment and post-treatment conditions. **(A)** Volcano plot of DEGs between pre-and post-treatment conditions in the CR group. Significantly up-regulated genes are marked in light red and downregulated ones are marked in blue. **(B)** Hierarchical clustering heatmap. Heatmaps were generated using the expression levels of the 302 DEGs identified in the CR group. The abscissa indicates different samples, and the ordinate indicates different gene probes. These genes were only differentially expressed in the CR group (left), but not in the non-CR group (right).

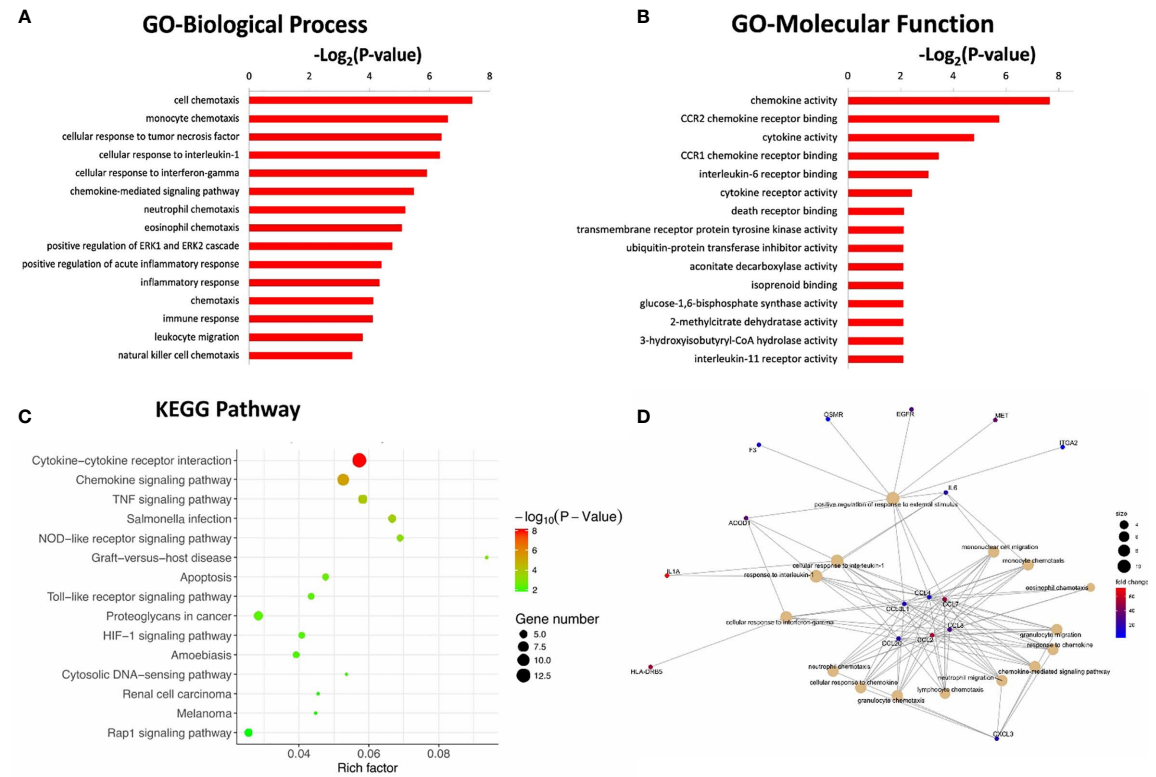


**FIGURE 3** | The top 15 significant GO terms for the 162 up-regulated DEGs in the categories of biological process **(A)**, molecular function **(B)**. **(C)** The bubble chart of the top 15 significant KEGG pathways. The number of genes related to each pathway is indicated by different sizes and fold change by different colors. **(D)** Gene concept network of the top 15 GO terms. The number of genes related to each term is indicated by different sizes and fold change by different colors.

## DISCUSSION

PTCLs account for 25–30% of non-Hodgkin's lymphomas (NHLs) in China, significantly higher than that of western countries (13). Contrasting the progress made in the treatment of B-cell NHLs, the management of patients with PTCL is disappointing, with no major progress made over the past decade. Conventional anthracycline-based regimens remain the

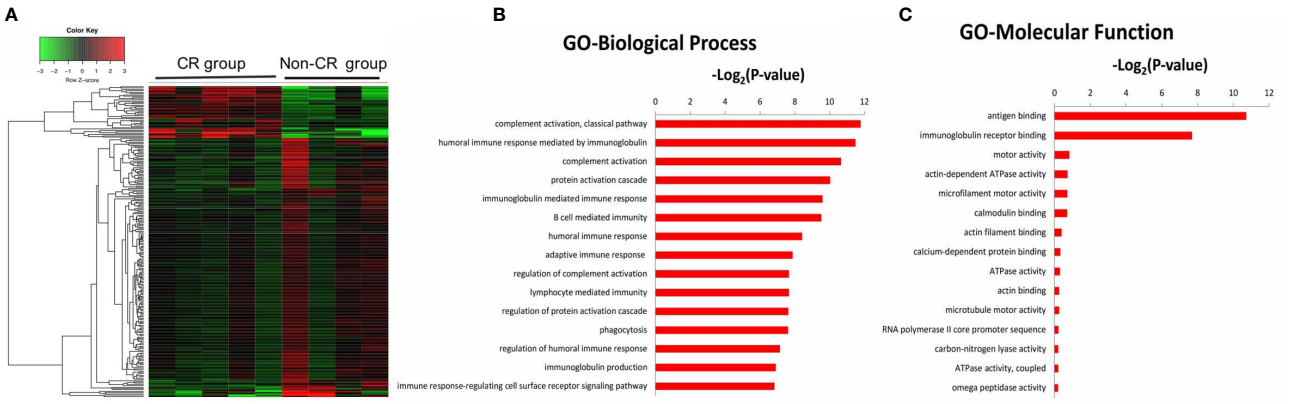


**FIGURE 4** | **(A)** Hierarchical clustering heatmap of DEGs between the CR and non-CR group at baseline level. The top 15 significant GO terms for the 470 DEGs in the categories of biological process **(B)**, molecular function **(C)**.

frontline regimen for patients newly diagnosed with PTCL. However, except for ALK-positive ALCL, most types of PTCLs exhibit a poor long-term survival of 30–40% (2).

In recent years, new agents, including HDAC and checkpoint inhibitors, have shown some promise for the treatment of PTCLs. At present, the available HDAC inhibitors worldwide include vorinostat, romidepsin, belinostat, and chidamide, an innovative class I HDAC inhibitor, independently developed in China (14). The overall response rates (ORRs) of HDAC inhibitors for patients with relapsed or refractory PTCLs were around 25–39% (15–17). The clinical benefit of PD-1 inhibitors for patients with PTCLs is also being investigated in several clinical trials, with an ORR of approximately 33–40% for patients with relapsed or refractory PTCL (18, 19). A significant limitation of these new agents is the relatively low response rate as monotherapy. Therefore, the combination of such new agents with conventional chemotherapies can potentially be an effective approach, in response to the search for improved treatments for patients with PTCL.

HDAC inhibitors prevent the removal of acetyl groups by HDAC and maintain accessible conformation of chromatin, resulting in increased transcriptional activity of anti-tumor genes (20). In recent studies, HDAC inhibitors have also been shown to have an immune-mediated anti-tumor effect. Both *in vitro* and *in vivo* studies have evaluated the novel role of HDAC inhibitors in manipulating the immune landscape and the potential ability to augment the response to immunotherapy. Guerriero et al. found that the HDAC inhibitor TMP195 promotes macrophage differentiation toward an anti-tumor phenotype in mouse models of breast cancer (4). Zheng et al. found that the HDAC inhibitor romidepsin enhances T cell chemokine expression and promoted T cell infiltration in mouse models of lung cancer, resulting in a strongly augmented response to PD-1 inhibitor (5). Kim et al. found that HDAC inhibitor CG-745 induces prolonged cytotoxic T cell activation and suppresses M2 macrophage polarization, promoting the effect of PD-1 blockade in mouse models of hepatocellular cancer (6).

Despite the relatively widespread use of HDAC inhibitors in PTCLs, their exact role in the immune system of patients with PTCL remains poorly understood. Our results showed that chidamide treatment notably enhanced the expression of genes associated with chemokine activity and chemotaxis function of circulating PD-1(+) cells, which might promote the recruitment of lymphocytes, monocytes, neutrophils, and dendritic cells. These innate immune cells are major components of the tumor microenvironment. In addition, KEGG pathway analysis revealed that the expression of genes involved in the innate immune signaling pathways of PD-1(+) cells was up-regulated after chidamide treatment. By regulating the innate immune cell trafficking and improving the innate immune function of circulating PD-1(+) cells, chidamide may reshape the tumor microenvironment to an anti-tumor phenotype. This may be an attractive approach to anti-tumor immunotherapy.

As suggested by previous studies, insufficient tumor-infiltrating CD8+ T cells and T-cell exhaustion are recognized as major resistance mechanisms to checkpoint inhibitors (21, 22). During the exhausting state of T-cells, cytokine expression is impaired, including interleukin-2, TNF-α, and IFN-γ. Our study found that genes associated with lymphocyte chemotaxis, TNF signaling pathway, and cellular response to IFN-γ were up-regulated after chidamide treatment. By recruiting lymphocytes to the tumor microenvironment and enhancing reinvigoration of exhausted CD8+ T-cells, chidamide treatment may "prime" the host immune response and synergize with checkpoint inhibitors. Pairing chidamide with PD-1 blockade may offer potential benefits in the treatment of patients with PTCLs. Notably, several clinical trials employing this combination approach are now underway. In a multicenter phase Ib/II trial conducted in China, the ORR of chidamide combined with PD-1 inhibitor (sintilimab) for relapsed/refractory extranodal NK/T - cell lymphoma was 58.3%, which was better than either single drug (23).

The up-regulated expression of genes associated with chemotaxis and innate immunity of PD-1(+) cells was only observed in patients in the CR group. Contrastingly, no significant changes were

observed in the gene expression of PD-1(+) cells of patients in the non-CR group. This indicated that treatment failure may be partially due to failure of immune reconstitution in patients with PTCLs. When comparing the gene expression of PD-1(+) cells between the CR and non-CR group at baseline level, we found that genes associated with humoral immune response, including complement activation and immunoglobulin mediated immune response, were up-regulated in the non-CR group. The differences of baseline gene expression may be part of the reason for the differences of treatment response. However, based on the current research, it is difficult to explain how these differences of gene expression are related to the efficacy of HDAC inhibitor treatment.

The limitations of this study need to be acknowledged. First, the set of PD-1(+) cells is complex and comprises the following: CD8+ T-cells, CD4+ T-cells, NK cells, and monocytes. Additional studies are required to determine the specific roles of each of these cell types. In future studies, we will perform flow cytometry sorting and single-cell sequencing. Second, our results require verification *via* PCR analysis. In *vitro* cell experiments using transwell assays can also be performed to evaluate the chemotactic function of PD-1(+) cells. Additionally, the synergistic effect of chidamide and PD-1 inhibitors could be further assessed *via* animal experiments. expression pattern may not be related to the type of disease.

In conclusion, we report here for the first time that chidamide treatment enhanced the expression of genes associated with chemokine activity and chemotaxis function of circulating PD-1(+) cells from patients with PTCLs. This novel mechanism of action of chidamide may provide a rationale for therapeutic strategies that combine chidamide with PD-1 inhibitors for patients with PTCLs.

## DATA AVAILABILITY STATEMENT

The data presented in the study are deposited in the GEO repository, the accession number is GSE174537.

## ETHICS STATEMENT

The studies involving human participants were reviewed and approved by Peking Union Medical College Hospital review board. The patients/participants provided their written informed consent to participate in this study.

## AUTHOR CONTRIBUTIONS

CW and SH designed the study. CW, SH, and ML performed the experiment. ML and CC analyzed all the data. WW and WZ helped perform the analysis with constructive discussions. CW wrote the main manuscript. DZ reviewed and revised the manuscript. All authors contributed to the article and approved the submitted version.

## FUNDING

National Natural Science Foundation of China (NSFC) (No.81970188).

CAMS Innovation Fund for Medical Sciences (CIFMS) (No. 2016-12M-1-001).

Natural Science Foundation of Beijing Municipality (No. 7202154).

## SUPPLEMENTARY MATERIAL

The Supplementary Material for this article can be found online at: https://www.frontiersin.org/articles/10.3389/fonc.2021.682436/full#supplementary-material

**Supplementary Table 1 |** Differentially expressed genes of the CR group.

**Supplementary Table 2 |** Differentially expressed genes of the non-CR group.

**Supplementary Data Sheet 1 |** Differentially expressed genes of one patient who received CHOEP treatment alone.

**Supplementary Figure 1 |** PNG: GO enrichment analysis of DEGs in the CR group.

**Supplementary Figure 2 |** PNG: KEGG enrichment analysis of DEGs in the CR group.

## REFERENCES

1. Vose J, Armitage J, Weisenburger D. International Peripheral T-Cell and Natural Killer/T-Cell Lymphoma Study: Pathology Findings and Clinical Outcomes. *J Clin Oncol* (2008) 26(25):4124–30. doi: 10.1200/JCO.2008.16.4558
2. Liu W, Ji X, Song Y, Wang X, Zheng W, Lin N, et al. Improving Survival of 3760 Patients With Lymphoma: Experience of an Academic Center Over Two Decades. *Cancer Med* (2020) 9(11):3765–74. doi: 10.1002/cam4.3037
3. Yuan XG, Huang YR, Yu T, Jiang HW, Xu Y, Zhao XY. Chidamide, a Histone Deacetylase Inhibitor, Induces Growth Arrest and Apoptosis in Multiple Myeloma Cells in a Caspase-Dependent Manner. *Oncol Lett* (2019) 18 (1):411–9. doi: 10.3892/ol.2019.10301
4. Guerriero JL, Sotayo A, Ponichtera HE, Castrillon JA, Pourzia AL, Schad S, et al. Class IIa HDAC Inhibition Reduces Breast Tumours and Metastases Through Anti-Tumour Macrophages. *Nature* (2017) 543(7645):428–32. doi: 10.1038/nature21409
5. Zheng H, Zhao W, Yan C, Watson CC, Massengill M, Xie M, et al. HDAC Inhibitors Enhance T-Cell Chemokine Expression and Augment Response to PD-1 Immunotherapy in Lung Adenocarcinoma. *Clin Cancer Res* (2016) 22 (16):4119–32. doi: 10.1158/1078-0432.CCR-15-2584
6. Kim YD, Park SM, Ha HC, Lee AR, Won H, Cha H, et al. HDAC Inhibitor, CG-745, Enhances the Anti-Cancer Effect of Anti-PD-1 Immune Checkpoint Inhibitor by Modulation of the Immune Microenvironment. *J Cancer* (2020) 11(14):4059–72. doi: 10.7150/jca.44622
7. Gong J, Chehrazi-Raffle A, Reddi S, Salgia R. Development of PD-1 and PD-L1 Inhibitors as a Form of Cancer Immunotherapy: A Comprehensive Review of Registration Trials and Future Considerations. *J Immunother Cancer* (2018) 6(1):8. doi: 10.1186/s40425-018-0316-z
8. Zhang W, Shen H, Zhang Y, Wang W, Hu S, Zou D, et al. Circulating PD-1 (+) Cells may Participate in Immune Evasion in Peripheral T-Cell Lymphoma and Chidamide Enhance the Antitumor Activity of PD-1 (+) Cells. *Cancer Med* (2019) 8(5):2104–13. doi: 10.1002/cam4.2097

9. Cheson BD, Fisher RI, Barrington SF, Cavalli F, Schwartz LH, Zucca E, et al. Recommendations for Initial Evaluation, Staging, and Response Assessment of Hodgkin and Non-Hodgkin Lymphoma: The Lugano Classification. *J Clin Oncol* (2014) 32(27):3059–68. doi: 10.1200/JCO.2013.54.8800
10. Yu G, Wang LG, Han Y, He QY. clusterProfiler: An R Package for Comparing Biological Themes Among Gene Clusters. *OMICS* (2012) 16(5):284–7. doi: 10.1089/omi.2011.0118
11. Xu LL, Warren MK, Rose WL, Gong W, Wang JM. Human Recombinant Monocyte Chemotactic Protein and Other C-C Chemokines Bind and Induce Directional Migration of Dendritic Cells In Vitro. *J Leukoc Biol* (1996) 60 (3):365–71. doi: 10.1002/jlb.60.3.365
12. Mollica Poeta V, Massara M, Capucetti A, Bonecchi R. Chemokines and Chemokine Receptors: New Targets for Cancer Immunotherapy. *Front Immunol* (2019) 10:379. doi: 10.3389/fimmu.2019.00379
13. Sun J, Yang Q, Lu Z, He M, Gao L, Zhu M, et al. Distribution of Lymphoid Neoplasms in China: Analysis of 4,638 Cases According to the World Health Organization Classification. *Am J Clin Pathol* (2012) 138(3):429–34. doi: 10.1309/AJCP7YLTQPUSDQ5C
14. Lu X, Ning Z, Li Z, Cao H, Wang X. Development of Chidamide for Peripheral T-Cell Lymphoma, the First Orphan Drug Approved in China. *Intractable Rare Dis Res* (2016) 5(3):185–91. doi: 10.5582/irdr.2016.01024
15. Piekarz RL, Frye R, Prince HM, Kirschbaum MH, Zain J, Allen SL, et al. Phase 2 Trial of Romidepsin in Patients With Peripheral T-Cell Lymphoma. *Blood* (2011) 117(22):5827–34. doi: 10.1182/blood-2010-10-312603
16. O'Connor OA, Horwitz S, Masszi T, Hoof AV, Brown P, Doorduijn J, et al. Belinostat in Patients With Relapsed or Refractory Peripheral T-Cell Lymphoma: Results of the Pivotal Phase II Belief (CLN-19) Study. *J Clin Oncol* (2015) 33(23):2492–9. doi: 10.1200/JCO.2014.59.2782
17. Shi Y, Dong M, Hong X, Zhang W, Feng J, Zhu J, et al. Results From a Multicenter, Open-Label, Pivotal Phase II Study of Chidamide in Relapsed or Refractory Peripheral T-Cell Lymphoma. *Ann Oncol* (2015) 26(8):1766–71. doi: 10.1093/annonc/mdv237
18. Lesokhin AM, Ansell SM, Armand P, Scott EC, Halwani A, Gutierrez M, et al. Nivolumab in Patients With Relapsed or Refractory Hematologic Malignancy: Preliminary Results of a Phase Ib Study. *J Clin Oncol* (2016) 34(23):2698–704. doi: 10.1200/JCO.2015.65.9789
19. Barta SK, Zain J, MacFarlane AW4th, Smith SM, Ruan J, Fung HC, et al. Phase II Study of the PD-1 Inhibitor Pembrolizumab for the Treatment of Relapsed or Refractory Mature T-Cell Lymphoma. *Clin Lymphoma Myeloma Leuk* (2019) 19(6):356–64.e3. doi: 10.1016/j.clml.2019.03.022
20. Greer CB, Tanaka Y, Kim YJ, Xie P, Zhang MQ, Park IH, et al. Histone Deacetylases Positively Regulate Transcription Through the Elongation Machinery. *Cell Rep* (2015) 13(7):1444–55. doi: 10.1016/j.celrep.2015.10.013
21. Nowicki TS, Hu-Lieskovan S, Ribas A. Mechanisms of Resistance to PD-1 and PD-L1 Blockade. *Cancer J* (2018) 24(1):47–53. doi: 10.1097/PPO.0000000000000303
22. Ghoneim HE, Fan Y, Moustaki A, Abdelsamed HA, Dash P, Dogra P, et al. De Novo Epigenetic Programs Inhibit PD-1 Blockade-Mediated T Cell Rejuvenation. *Cell* (2017) 170(1):142–57. doi: 10.1016/j.cell.2017.06.007
23. Gao Y, Huang HQ, Wang XX, Bai B, Zhang LL, Xiao Y, et al. Anti-PD-1 Antibody (Sintilimab) Plus Histone Deacetylase Inhibitor (Chidamide) for the Treatment of Refractory or Relapsed Extranodal Natural Killer/T Cell Lymphoma, Nasal Type (R/r-ENKTL): Preliminary Results From a Prospective, Multicenter, Single-Arm, Phase Ib/II Trial (SCENT). Blood (2020) 136(Supplement 1):39–40. doi: 10.1182/blood-2020-134665


**Conflict of Interest:** The authors declare that the research was conducted in the absence of any commercial or financial relationships that could be construed as a potential conflict of interest.

frontiers in Oncology

ORIGINAL RESEARCH
published: 14 June 2021
doi: 10.3389/fonc.2021.691064

# An Analysis of Cardiac Disorders Associated With Chimeric Antigen Receptor T Cell Therapy in 126 Patients: A Single-Centre Retrospective Study

*Kunming Qi[1,2,3†], Zhiling Yan[1,2,3†], Hai Cheng[1,2,3†], Wei Chen[1,2,3], Ying Wang[1,2,3], Xue Wang[1,2,3], Jiang Cao[1,2,3], Huanxin Zhang[1,2,3], Wei Sang[1,2,3], Feng Zhu[1,2,3], Haiying Sun[1,2,3], Depeng Li[1,2,3], Qingyun Wu[1,2,3], Jianlin Qiao[1,2,3], Chunling Fu[1,2,3], Lingyu Zeng[1,2,3], Zhenyu Li[1,2,3*], Junnian Zheng[4*] and Kailin Xu[1,2,3*]*

[1] Blood Diseases Institute, Affiliated Hospital of Xuzhou Medical University, Xuzhou Medical University, Xuzhou, China, [2] Department of Hematology, Affiliated Hospital of Xuzhou Medical University, Xuzhou, China, [3] Key Laboratory of Bone Marrow Stem Cell, Jiangsu Province, Xuzhou, China, [4] Cancer Institute, Xuzhou Medical University, Xuzhou, China

**Introduction:** Chimeric antigen receptor T (CAR-T) cells are effective in treating hematological malignancies. However, in patients receiving CAR-T therapy, data characterizing cardiac disorders are limited.

**Methods:** 126 patients with hematologic malignancies receiving CAR-T cell therapy were analyzed to determine the impact of CAR-T therapy on occurrence of cardiac disorders, including heart failure, arrhythmias, myocardial infarction, which were defined by the Common Terminology Criteria for Adverse Events (CTCAE). Parameters related to cardiac disorders were detected including myocardial enzyme, NT-proBNP and ejection fraction (EF). Cardiovascular (CV) events included decompensated heart failure (HF), clinically significant arrhythmias and CV death.

**Results:** The median age of patients was 56 years (6 to 72 years). 58% patients were male, 62% had multiple myeloma, 20% had lymphoma and 18% had ALL. 33 (26%) patients had cardiac disorders, most of which were grade 1-2. 13 patients (10%) were observed with cardiac disorders grade 3-5, which comprised 5(4%) patients with new-onset HF, 2 (2%) patients with new-onset arrhythmias, 4 (3%) patients with the acute coronary syndrome, 1(1%) patient with myocardial infarction and 1(1%) patient with left ventricular systolic dysfunction. There were 9 CV events (7%) including 6 decompensated heart failure, 1 clinically significant arrhythmias and 2 CV deaths. Among the 33 patients with cardiac disorders, the patients with cardiac disorders CTCAE grade 3-5 had higher grade CRS (grade ≥ 3) than those with cardiac disorders CTCAE grade ≤ 2 ($P$ <0.001). More patients with cardiac disorders CTCAE grade 3-5 were observed in the cohort who did not receive corticosteroids and/or tocilizumab therapy timely comparing with those who received corticosteroids and/or tocilizumab therapy timely ($P$ =0.0004).

OPEN ACCESS

***Edited by:***
*Gurvinder Kaur, All India Institute of Medical Sciences, India*

***Reviewed by:***
*Narendranath Epperla, The Ohio State University, United States*
*Kitsada Wudhikarn, Mayo Clinic, United States*

****Correspondence:***
*Kailin Xu*
*lihmd@163.com*
*Junnian Zheng*
*jnzheng@xzmc.edu.cn*
*Zhenyu Li*
*lizhenyumd@163.com*

*[†]These authors have contributed equally to this work*

***Specialty section:***
*This article was submitted to Hematologic Malignancies, a section of the journal Frontiers in Oncology*

***Received:*** *05 April 2021*
***Accepted:*** *26 May 2021*
***Published:*** *14 June 2021*

***Citation:***
*Qi K, Yan Z, Cheng H, Chen W, Wang Y, Wang X, Cao J, Zhang H, Sang W, Zhu F, Sun H, Li D, Wu Q, Qiao J, Fu C, Zeng L, Li Z, Zheng J and Xu K (2021) An Analysis of Cardiac Disorders Associated With Chimeric Antigen Receptor T Cell Therapy in 126 Patients: A Single-Centre Retrospective Study. Front. Oncol. 11:691064. doi: 10.3389/fonc.2021.691064*

**Conclusions:** Cardiac disorders CAR-T cell therapy were common and associated with occurrence of CRS. However, most cases were mild. For patients with CRS grade 3-5, timely administration of corticosteroids and/or tocilizumab can effectively prevent the occurrence and progression of cardiac disorders.

**Keywords: CAR-T cell therapy, cardiac disorders, CRS, corticosteroids, tocilizumab**

## INTRODUCTION

Chimeric antigen receptor (CAR)-T cell therapy has sparked a wave of optimism in relapsed/refractory hematologic malignancies. CAR-T cells targeting new tumor antigens would emerge in the near future. Some side effects were observed after CAR-T cell therapies with cytokine releasing syndrome (CRS) as the most common one, presenting as fever, hypotension, hypoxia, and capillary leakage. Neurotoxicity and coagulation dysfunction have also been reported (1–4). These side effects were intensively studied, however, other side effects such as cardiac disorders might be underestimated. Case report has shown some cases of cardiac disorders (5). Thus, a comprehensive study is needed to evaluate occurrence of cardiac disorders after CAR-T cell therapy.

Here, we performed a comprehensive analysis of the incidence, dynamic changes and outcomes of cardiac disorders defined by CTCAE in 126 patients with relapsed/refractory (R/R) hematologic malignancies after receiving CAR-T cell therapy. The correlation between cardiac disorders and CRS was also analyzed.

## SUBJECT AND METHODS

### Study Design and Patient Selection

The study cohort was derived from the patients receiving CAR-T at Affiliated Hospital of Xuzhou Medical University between January 1, 2019, and November 20, 2020; 126 patients were included. (China) (Clinical Trials: NCT02782351, NCT03207178, ChiCTR-OIC-17011272). All patients were followed-up until a fixed calendar date (i.e., January 31, 2021). Clinical events were extracted by detailed chart review. For the patients who died during the follow-up, the last follow-up date was the date of death. This was a retrospective study conducted according to the Declaration of Helsinki's principles with approval by the Ethics Committee of the Affiliated Hospital of Xuzhou Medical University. Informed consents were obtained from all patients.

### CAR-T Cell Manufacturing and Infusion

The humanized single-chain variable fragment (scFv) sequence specific for CD19 was derived from clone FMC63 as previously described (6) and the anti-CD20, anti-CD22 and anti-BCMA scFv was derived from a murine anti-human CD20, CD22 and BCMA monoclonal antibody. The scFv sequence for CD19, CD20 and BCMA were inserted in tandem with the human CD8 transmembrane, CD8 hinge, 4-1BB costimulatory domain, CD3z intracellular regions, and T2A-EGFRt sequence. The scFv sequence for CD22 was inserted in tandem with the human CD8 transmembrane, CD8 hinge, CD28 costimulatory domain, CD3z intracellular regions, and T2A-EGFRt sequence. CARs targeting CD19, CD20, CD22 and BCMA were synthesized and subcloned into lentivirus expression vector Lenti-EF1a-puro and stably expressed in CD3-positive T cells after transfection of lentiviral vector.

Peripheral blood mononuclear cells were obtained from patients by leukapheresis as previously described (3). Most patients received lymphodepletion chemotherapy with the FC regimens included both fludarabine (750 mg/m$^2$, day-5) and cyclophosphamide (30 mg/m$^2$/d, days -5~2). On day 0, patients with MM received CD19 CAR-T cell and BCMA CAR-T cell infusion at the median dose $2 \times 10^6$ cells/kg ($1.4 - 4 \times 10^6$ cells/kg), patients with B-NHL received CD19 CAR-T cell and CD22 CAR-T cell infusion at the median dose $2 \times 10^6$ cells/kg ($0.8\text{-}6 \times 10^6$ cells/kg) and patients with ALL received a single dose of CD19 CAR-T cell infusion at the median dose $1 \times 10^6$ cells/kg ($0.8\text{-}2 \times 10^6$ cells/kg) respectively.

### Collection of Clinical and Laboratory Data

Peripheral blood was collected before lymphodepletion, on day -3 or day -1, and at approximately 1~3, 4~6, 7~10, 11~13, 14~16, 17~20, 21-24, 25~30, 31-40, 41-50 days after CAR-T cell infusion for analysis of complete blood counts, hepatic function, renal function, hs-cTnT, NT-proBNP, cytokine including IL-6, Ferritin, CRP, IL-8, IFN-γ and IL-10. The morphological characteristics of bone marrow were evaluated on day 0, 14 and 28 respectively. Minimal residual disease was detected by flow cytometry. If the patient did not die, the CAR-T cells were followed up for at least 90 days.

### Cardiac Disorders Diagnosis and CRS Grading

Cardiac disorders was defined according to Common Terminology Criteria for Adverse Events (CTCAE; version 4.03) (7). According to the hs-cTnT assay, the lower limit of detection is 3 ng/L for the 99th percentile is 14 ng/L according to the manufacturer. The diagnosis of myocardial infarction required a rise and/or fall of hs-cTnT with at least one value above the 99th percentile upper reference limit, with the symptoms of ischaemia or development electrocardiogram (8). NT-proBNP elevation of patients ≤ 50 years old, patients > 50 years old and patients with baseline glomerular filtration rate (GFR) < 60ml/min were defined > 450 pg/ml, > 900 pg/ml and >1200 pg/ml respectively. A reduction in left ventricular ejection fraction (LVEF) was defined as a reducing at least ten

percentage points, less than 50%. Cardiovascular events included decompensated HF, clinically significant arrhythmias and CV death (9). CRS was graded according to consensus criteria proposed by Lee et al. (10). All results were reviewed and confirmed by the research team without considering other variables. The onset of CRS was defined as the first appearance of a fever after CAR-T therapy, excluding other factors for fever. The time to corticosteroid or tocilizumab administration was defined as the time from the onset of CRS to the administration of corticosteroid or tocilizumab. This article reports cardiac disorders presenting within 50 days after the first CAR-T cell infusion.

## Statistical Analysis

Descriptive statistics (median/interquartile range [IQR], count, and percentage) are reported for key variables. Continuous data were compared using unpaired Student's *t*-tests and categorical data were compared using the chi-square or the Fisher exact test. The factors associated with cardiac disorders were explored using ordinal regression with cardiac disorders CTCAE frequency as the dependent variable and baseline glomerular filtration rate, sex, age, diagnosis, underlying disease (including diabetes, hypertension, etc) and CRS as independent variables. The Wilcoxon test was adopted for continuous variables between 2 groups, and the Kruskal-Wallis test was for multiple groups. The Spearman correlation test was used for correlation analysis. Statistical significance was defined using a 2-tailed *p*-value < 0.05. Statistical analyses were performed using IBM SPSS for Windows 25.0 software (SPSS, Inc., Chicago, IL).

# RESULTS

## Patients' Baseline Characteristics

Baseline demographics and clinical characteristics of the 126 patients with R/R hematologic malignancies receiving lymphodepletion chemotherapy and CAR-T cell therapy, are shown in **Table 1**. In the entire cohort, the median age was 56 years (range, 6 to 72 years), including 73(58%) males and 53(42%) females. The most of patients were multiple myeloma (MM) ($n$ = 78, 62%), followed by non-Hodgkin's lymphoma (NHL) ($n$ = 25, 20%) and acute lymphoblastic leukemia (ALL) ($n$=23, 18%). In the MM cohort, 13 patients (86%) had low baseline glomerular filtration rate (< 60ml/min) and 44(57%) patients bone marrow plasma cells were ≥10%. In the NHL cohort, 21 patients (84%) were Ann Arbor stage III~IV. The percentage of bone marrow blasts was ≥20% in 13 (57%) patients with ALL. Before the CAR-T cell therapy, 120 (95%) patients received lymphodepletion chemotherapy of FC regimen, and 6 (5%) received non-FC regimen, including 2 with fludarabine alone, 1 with cyclophosphamide alone and 3 without regimen (**Table 1**).

## Factors Associated With Subsequent Cardiac Disorders

Within 50 days of CAR-T cell infusion, cardiac disorders of any grade were more frequent in female patients ($P$ = 0.012), the patients with low baseline glomerular filtration rate (< 60ml/min) ($P$ < 0.0001) and the patients with CRS ($P$ < 0.0001) by univariate analyses (**Table 1**). The patient's age, diagnosis, ECOG, the number of plasma cells in bone marrow of MM patients, Charlson Comorbidity Index and hypertension were not associated with cardiac disorders by univariate analyses. The baseline of hs-cTnT, NT-proBNP, Ann Arbor stage of NHL, ALL patients with a high tumor burden (blasts ≥20% in bone marrow), lymphodepletion regimens and underlying diseases (including diabetes, coronary artery disease, chronic heart failure and atrial fibrillation) were no statistical significance. Multivariable analysis showed that after CAR-T cell therapy, the patients with low baseline glomerular filtration rate (< 60ml/min) and CRS were associated with an increased risk of cardiac disorders ($P$ = 0.031, $P$ < 0.0001 perspective) (**Table 1**).

## Cardiac Disorders and CRS After CAR-T Cell Immunotherapy

Of 126 patients treated with lymphodepletion chemotherapy and CAR-T cell infusion, 33(26%) patients (25 MM patients, 3 NHL patients, 5 ALL patients) had cardiac disorders as defined by the Common Terminology Criteria for Adverse Events (CTCAE). There were 10 patients (8%) with CTCAE grade 1, 10 patients (8%) with CTCAE grade 2, 8 patients (6%) with CTCAE grade 3, 2 patients (2%) with CTCAE grade 4 and 3 patients (2%) with CTCAE grade 5. In MM cohort, cardiac disorders CTCAE 1, CTCAE 2, CTCAE 3, CTCAE 4 and CTCAE 5 were 9, 7, 6, 2 and 1 patients. In NHL cohort, cardiac disorders CTCAE 1, CTCAE 2, CTCAE 3, CTCAE 4 and CTCAE 5 were 1, 1, 1, 0 and 0 patients respectively. In ALL cohort, cardiac disorders CTCAE 1, CTCAE 2, CTCAE 3, CTCAE 4 and CTCAE 5 were 0, 2, 1, 1, 1 patients respectively (**Figure 1**).

CRS was found in all 33 patients (26%) with cardiac disorders. Among 20 (16%) patients with cardiac disorders CTCAE grade 1-2, there were 12 patients with CRS grade 1-2 and 8 patients with CRS grade 3-5. Among 13 (10%) patients with cardiac disorders CTCAE grade 3-5, all patients had severe CRS (grade 3-5) (**Figure 1**).

Of 13 patients (10%) with cardiac disorders grade 3-5, 5(4%) patients had new-onset HF, 2 (2%) patients had new-onset arrhythmias, 4 (3%) patients had the acute coronary syndrome, 1(1%) patient had myocardial infarction and 1(1%) patient had left ventricular systolic dysfunction. There were 9 CV events (7%) with a median onset time of 5 days (IQR: 3 to 9 days) among all cardiac disorder patients. The CV events included 6 decompensated heart failures, 1 clinically significant arrhythmias and 2 CV deaths (**Table 2**).

## Severe Cardiac disorders Are More Frequent in Patients With Severe CRS

The patients who developed CTCAE grade ≥3 cardiac disorders had more severe CRS (p < 0.001, **Tables 1**, **3**). The occurrence time of CRS grade 3-5 was earlier than that of cardiac disorders CTCAE grade 1-2 and 3-5. The median onset time of CRS grade 3-5 and cardiac disorders CTCAE grade 3-5 was 3 days (IQR: 1 to 7 days) and 8 days (IQR: 4 to 9 days) ($P$ = 0.0054)

**TABLE 1** | Baseline characteristics and factors associated with cardiac disorders.

| Cardiac disorders CTCAE grade | | Grade 0[a] | Grade 1-2[a] | Grade 3-5[a] | Total | Univariate[b] | Multivariable[c] |
|---|---|---|---|---|---|---|---|
| Overall, n (%) | | 93 (74) | 20 (16) | 13 (10) | 126(100) | | |
| Age, n (%) | <40 years | 19 (83) | 1 (4) | 3 (13) | 23 | 0.413 | |
| | 40–60 years | 48 (75) | 10 (16) | 6 (9) | 64 | | |
| | >60 years | 26 (67) | 9 (23) | 4 (10) | 39 | | |
| Sex, n (%) | Male | 55 (75) | 15 (21) | 3 (4) | 73 | 0.012 | 0.116 |
| | Female | 38 (72) | 5 (9) | 10 (19) | 53 | | |
| Diagnosis | MM[d] | 53 (68) | 16 (20) | 9 (12) | 78 | 0.274 | |
| n (%) | NHL[e] | 22 (88) | 2 (8) | 1 (4) | 25 | | |
| | ALL[f] | 18 (78) | 2 (9) | 3 (13) | 23 | | |
| ECOG | 0 | 62 (77) | 11(14) | 7 (9) | 80 | 0.461 | |
| | 1-2 | 31(67) | 9 (20) | 6 (13) | 46 | | |
| Primary refractory[g] | | 6 (60) | 2 (20) | 2 (20) | 10 | 0.805 | |
| Prior lines of therapy | 2-4 | 38 (73) | 9 (17) | 5 (10) | 52 | | |
| | >4 | 49 (77) | 9 (14) | 6 (9) | 64 | | |
| Baseline | ≤14ng/L | 93 (75) | 19 (15) | 12 (10) | 124 | – | |
| hs-cTnT | >14ng/L | 0 (0) | 1 (50) | 1 (50) | 2 | | |
| Baseline | Normal | 92 (78) | 17 (14) | 9 (8) | 118 | – | |
| NT-proBNP | Increased[h] | 1 (12) | 3 (38) | 4 (50) | 8 | | |
| Baseline | <60ml/min | 4 (29) | 4 (29) | 6 (42) | 14 | <0.0001 | 0.031 |
| Glomerular | ≥60ml/min | 89 (80) | 16 (14) | 7 (6) | 112 | | |
| Filtration rate | | | | | | | |
| BM plasma | <10% | 25 (74) | 7 (20) | 2 (6) | 34 | 0.378 | |
| cells of MM | ≥10% | 28 (64) | 9 (20) | 7 (16) | 44 | | |
| Ann Arbor | I-II | 4 (100) | 0 (0) | 0 (0) | 4 | – | |
| stage of NHL | III-IV | 18 (86) | 2 (9) | 1 (5) | 21 | | |
| BM Blast | <20% | 10 (100) | 0 (0) | 0 (0) | 10 | – | |
| of ALL | ≥20% | 8 (62) | 2 (15) | 3 (23) | 13 | | |
| Lymphodepletion | FC | 88(73) | 20 (17) | 12 (10) | 120 | – | |
| Regimen[i], n(%) | Non-FC | 5 (83) | 0 (0) | 1(17) | 6 | | |
| CAR-T | 0.8-2 | 66 (72) | 15 (16) | 11 (12) | 92 | 0.57 | |
| Cell Dose | 3-6 | 27 (79) | 5 (15) | 2 (6) | 34 | | |
| Charlson | ≦2 | 30 (77) | 4 (10) | 5 (13) | 39 | 0.386 | |
| Comorbidity | 2-4 | 49 (75) | 12 (19) | 4 (6) | 65 | | |
| Index[j] | >4 | 14 (64) | 4 (18) | 4 (18) | 22 | | |
| Diabetes | Yes | 3 (33) | 4 (45) | 2 (22) | 9 | – | |
| | No | 90 (77) | 16 (14) | 11 (9) | 17 | | |
| Hypertension | Yes | 15 (65) | 6 (26) | 2 (9) | 23 | 0.333 | |
| | No | 78 (76) | 14 (14) | 11 (10) | 3 | | |
| Coronary artery | Yes | 1 (100) | 0 (0) | 0 (0) | 1 | – | |
| Disease | No | 92 (74) | 20 (16) | 13 (10) | 125 | | |
| Chronic Heart | Yes | 0 (0) | 0 (0) | 2 (100) | 2 | – | |
| Failure | No | 93 (75) | 20 (16) | 11 (9) | 124 | | |
| Atrial fibrillation | Yes | 0 (0) | 0 (0) | 1 (100) | 1 | – | |
| | No | 93 (74) | 20 (16) | 12 (10) | 125 | | |
| CRS[k], n (%) | Grade 0 | 23 (100) | 0 (0) | 0 (0) | 23 | <0.0001 | <0.0001 |
| | Grade 1-2 | 69(85) | 12 (15) | 0 (0) | 81 | | |
| | Grade 3-5 | 1 (5) | 8 (36) | 13 (59) | 22 | | |

[a]*Percentages are shown in parentheses.*
[b]*Two-sided P values calculated based on the Mann-Whitney test for continuous variables and based on chi-square or the Fisher exact test for categorical variables.*
[c]*Ordinal regression models were performed to assess the impact of baseline factors on the occurrence of cardiac disorders.*
[d]*multiple myeloma.*
[e]*non-Hodgkin's lymphoma.*
[f]*acute lymphoblastic leukemia.*
[g]*Refractory was defined as disease progression on or within 60 days after the last dose of the most recent drug given in each drug class.*
[h]*NT-proBNP elevation of patients ≤ 50 years old, patients > 50 years old and patients with baseline glomerular filtration rate < 60ml/min were defined > 450 pg/ml, > 900 pg/ml and >1200 pg/ml respectively.*
[i]*FC regimens included both fludarabine (750 mg/m$^2$, day-5) and cyclophosphamide (30 mg/m$^2$/d, days -5～-2).*
[j]*Charlson Comorbidity Index was scored according to consensus criteria proposed by Charlson M et al. (11) (**Supplementary Table 1**).*
[k]*cytokine release syndrome.*

(**Table 4**). Earlier onset of CRS after CAR-T therapy was associated with a higher risk of subsequent developing severe cardiac disorders. The severity of cardiac disorders was related to the higher peak concentrations of hs-cTnT, NT-proBNP, ferritin, C-reactive protein (CRP) and multiple cytokines, including IL-6, IL-8, IFN-γ and IL-10 (**Figure 2**).

After further analysis of the correlation between the levels of hs-cTnT, NT-proBNP and cytokines in patients with the grade

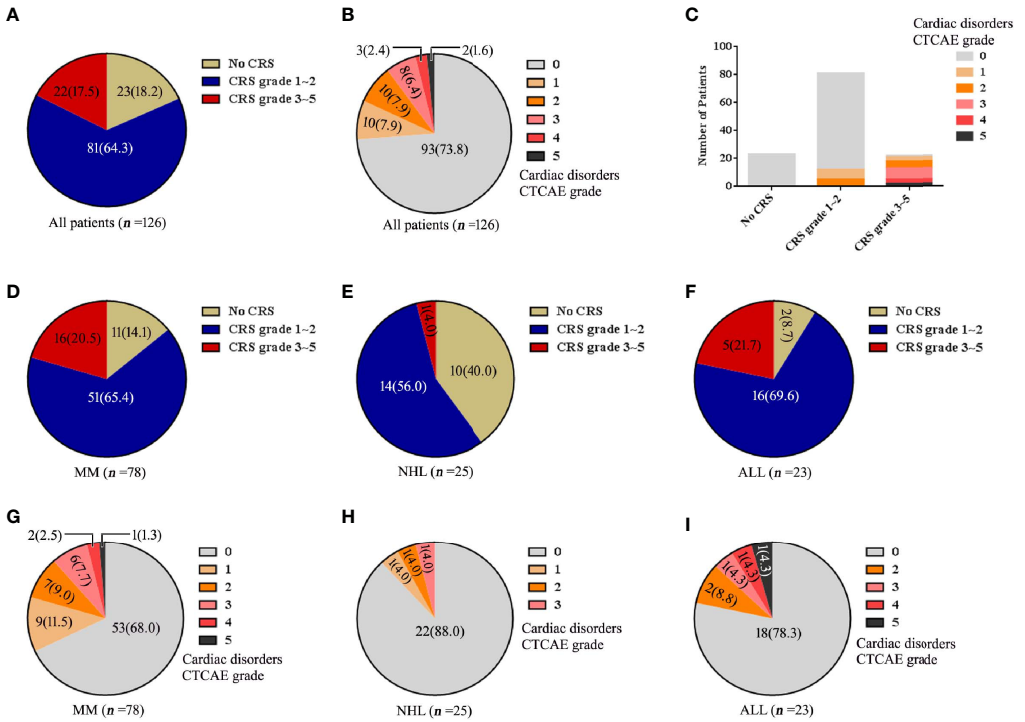


**FIGURE 1** | The changes of CRS, cardiac disorders CTCAE before and after CAR-T cell infusion. **(A)** Numbers of patients with each CRS. **(B)** Numbers of patients with each cardiac disorders grade. **(C)** Numbers of patients with each grade of cardiac disorders and CRS. The numbers of patients with each CRS grade are shown for each disease of **(D)** MM, **(E)** NHL and **(F)** ALL. Cardiac disorders CTCAE for each disease of **(G)** MM, **(H)** NHL and **(I)** ALL. Percentage is shown in parentheses.

**TABLE 2** | 33 (26%) patients in the entire cohort of 126 had cardiac disorders.

| Cardiac disorders CTCAE | Grade 1[a] | Grade 2[a] | Grade 3[a] | Grade 4[a] | Grade 5[a] | Total[a] |
|---|---|---|---|---|---|---|
| Heart failure[b] | 7 (6) | 3 (2) | 3 (2) | 2 (2) | 0 (0) | 15 (12) |
| New Arrhythmia[c] | 3 (2) | 2 (2) | 1 (1) | 0 (0) | 1( 1) | 7 (6) |
| Acute coronary syndrome | – | 5 (4) | 4 (3) | 0 (0) | 0 (0) | 9 (7) |
| Myocardial disease[d] | 0 (0) | 0 (0) | 0 (0) | 0 (0) | 1 (1) | 1 (1) |
| Left ventricular systolic dysfunction | – | – | 0 (0) | 1 (1) | 0 (0) | 1 (1) |
| New Valve disease[e] | 0 (0) | 0 (0) | 0 (0) | 0 (0) | 0 (0) | 0 (0) |
| Pericardial disease[f] | 0 (0) | 0 (0) | 0 (0) | 0 (0) | 0 (0) | 0 (0) |
| Cardiac arrest | 0 (0) | 0 (0) | 0 (0) | 0 (0) | 0 (0) | 0 (0) |

[a]*Percentage is shown in parentheses.*

[b]*New onset of heart failure, including left ventricular failure and right ventricular dysfunction.*

[c]*Asystole, Atrial fibrillation, Atrial flutter, Atrioventricular block complete, Atrioventricular block first degree, Mobitz (type) II atrioventricular block, Mobitz type I, Paroxysmal atrial tachycardia, sick sinus syndrome, Sinus bradycardia, Sinus tachycardia, Supraventricular tachycardia, Ventricular arrhythmia, Ventricular fibrillation and Ventricular tachycardia.*

[d]*Myocardial infarction, Myocarditis and Restrictive cardiomyopathy.*

[e]*Tricuspid valve disease, Pulmonary valve disease, Mitral valve disease and Aortic valve disease.*

[f]*Constrictive pericarditis, Pericardial effusion, Pericardial tamponade and Pericarditis.*

3-5 cardiac disorders CTCAE ($n$ =13), we found that the values of hs-cTnT were positively correlated with the levels of serum IL-6, Ferritin, IFN-γ (**Figures 3A, B, E**). The values of NT-proBNP were positively correlated with the levels of serum IL-6, Ferritin, IFN-γ and IL-10 (**Figures 3G, H, K, L**).

## Treatment of Cardiac Disorders and CRS

In 10 patients with cardiac disorders CTCAE grade 1, which were asymptomatic or mild, no intervention was needed. In 10 patients with CTCAE grade 2, 3 patients with HF were given torasemide and the other patients were only given symptomatic treatment. In cardiac disorders CTCAE grade≥3 cohort, all patients required an intervention that included the administration of diuretic, amiodarone, cedilanid and/or IV metoprolol and/or vasopressors and oxygen supplementation. Some patients were typically transferred to the intensive care unit for further management. After treatment, 2 (2%) patients died, among which one patient died of malignant arrhythmia and

**TABLE 3 |** Cardiac disorders CTCAE grade and CRS grade.

| Cardiac disorders CTCAE | CRS grade[a] 1-2 | CRS grade[a] 3-5 | Total[a] | *P* |
|---|---|---|---|---|
| Heart failure[b] | | | | 0.044 |
| Grade 1-2 | 6 (5) | 4 (3) | 10( 8) | |
| Grade 3-5 | 0 (0) | 5 (4) | 5 (4) | |
| New Arrhythmias[c] | | | | 0.047 |
| Grade 1-2 | 5 (4) | 0 (0) | 5 (4) | |
| Grade 3-5 | 0 (0) | 2 (2) | 2 (2) | |
| Acute coronary syndrome | | | | 1 |
| Grade 1-2 | 1 (1) | 4 (3) | 5 (4) | |
| Grade 3-5 | 0 (0) | 4 (3) | 4 (3) | |
| Myocardial disease[d] | | | | 1 |
| Grade 1-2 | 0 (0) | 0 (0) | 0 (0) | |
| Grade 3-5 | 0 (0) | 1 (1) | 1 (1) | |
| Left ventricular systolic dysfunction | | | | – |
| Grade 1-2 | – | – | – | |
| Grade 3-5 | 0 (0) | 1 (1) | 1 (1) | |
| New Valve diseases[e] | | | | – |
| Grade 1-2 | 0 (0) | 0 (0) | 0(0) | |
| Grade 3-5 | 0 (0) | 0 (0) | 0 (0) | |
| Pericardial diseases[f] | | | | – |
| Grade 1-2 | 0 (0) | 0 (0) | 0 (0) | |
| Grade 3-5 | 0 0) | 0 (0) | 0 (0) | |
| Cardiac arrest | | | | – |
| Grade 1-2 | – | – | – | |
| Grade 3-5 | 0 (0) | 0 (0) | 0(0) | |
| Total | | | | 0.0005 |
| Grade 1-2 | 12 (10) | 8 (6) | 20 (16) | |
| Grade 3-5 | 0 (0) | 13 (10) | 13 (10) | |

[a]*Percentage is shown in parentheses. P-value was tested by the Chi-Square test.*
[b,c,d,e] *and* [f] *are the same as in* ***Table 2***.

**TABLE 4 |** The temporal relation between cardiac disorders CTCAE and severe CRS.

| | Cardiac disorders CTCAE | | CRS |
|---|---|---|---|
| | Grade 1-2 | Grade 3-5 | Grade 3-5 |
| Onset time (day) | | | |
| Median | 9 | 8 | 3* |
| IQR | 4-11 | 4-9 | 1-7 |
| Range | 3-25 | 2-23 | 1-10 |
| Maximum time (day)[a] | | | |
| Median | 11 | 14 | 12 |
| IQR | 7-15.75 | 8.5-17 | 8-15.25 |
| Range | 4-30 | 6-31 | 5-30 |
| Duration time (day)[b] | | | |
| Median | 6 | 12* | 13*** |
| IQR | 3-9 | 8-21.5 | 9-24 |
| Range | 2-20 | 2-25 | 5-34 |
| Recovery time (day)[c] | | | |
| Median | 13 | 20* | 19* |
| IQR | 11-19 | 17-29 | 16.25-27.75 |
| Range | 6-45 | 8-31 | 7-37 |

[a]*The time required from the onset time to the peak (day).*
[b]*The time from the onset to recovery (day).*
[c]*The time from the beginning of CAR-T cell infusion to return to normal (day).*
**P < 0.05, *** P < 0.001.*

another died of myocardial infarction. However, 31 of 33 patients (94%) recovered. The arrhythmia and HF disappeared quickly after treatment. NT proBNP and hs TnT returned to normal baseline levels within one month after treatment.

**Tables 5** and **6** shows the treatments in patients with CRS ($n$ = 103) and cardiac disorders. In cohort 1, patients were given corticosteroids and/or tocilizumab therapy within 24 hours after the onset of CRS and in cohort 2 patients were not given corticosteroids and/or tocilizumab therapy within 24 hours or received corticosteroids and/or tocilizumab therapy more than 24 hours after the onset of CRS. Among the 51 patients with CRS grade 1 and 30 patients with CRS grade 2, there was no difference in the incidence of cardiac disorders between cohort 1 and cohort 2 ($P$ = 0.1336, 0.3742). While among the 22 patients with grade 3-5, 2 of 8 patients (25%) in cohort 1 developed cardiac disorders, which was lower than 11 of 14 patients (79%) in cohort 2 ($P$ = 0.0260). In 33 patients with cardiac disorders, compared with 11 of 15 patients (73%) developed cardiac disorders (CTCAE Grade 3-5) in cohort 2, there were fewer patients in cohort 1, with only 2 of 18 patients (11%) progressed to cardiac disorders (CTCAE grade 3-5) ($P$ = 0.0004) (**Tables 5**, **6**).

# DISCUSSION

## Early Detection of Severe Cardiac Disorders Is Necessary

CRS is one of the most common side effects in CAR-T cell therapy (12–14). Other toxicities including neurotoxicity and

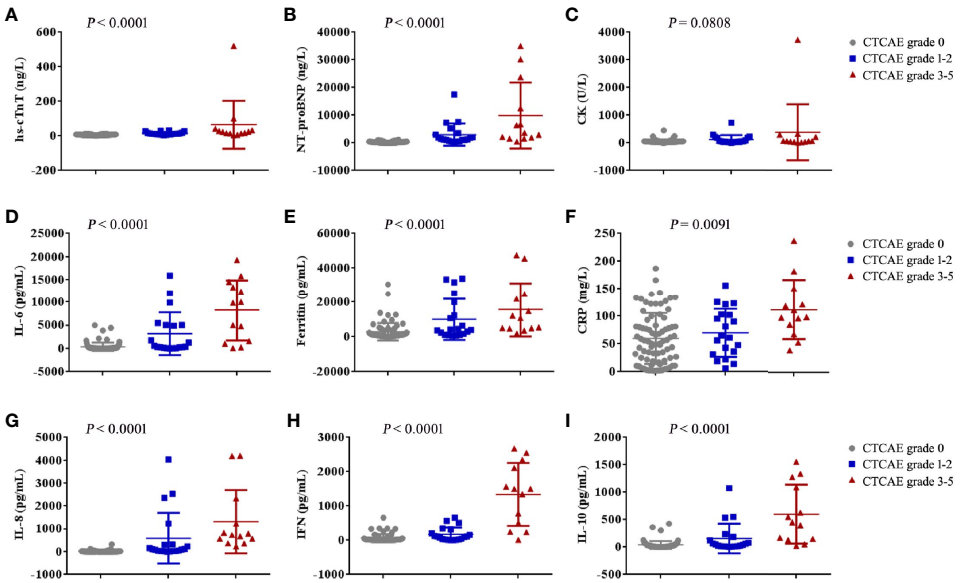


**FIGURE 2** | The maximum values of myocardial enzyme parameters, NT-proBNP and cytokines in patients with cardiac disorders CTCAE grade 0, 1-2 and 3-5 after CAR-T cell infusion. The maximum hs-cTnT **(A)**, maximum NT-proBNP **(B)**, maximum CK **(C)**, maximum IL-6 **(D)**, maximum Ferritin **(E)**, maximum CRP **(F)**, maximum IL-8 **(G)**, maximum IFN-γ **(H)** and maximum IL-10 **(I)** in the first 30 days after CAR-T cell infusion are shown in patients who had cardiac disorders CTCAE grade 0 (n = 80), cardiac disorders CTCAE grade 1-2 (n = 20) and cardiac disorders CTCAE grade 3-5 (n =13). Each point represents data from a single patient. The median and IQR are shown. Two-sided P values were determined using the Kruskal-Wallis test.

coagulation dysfunction were also reported (2–4). However, there have been very few reports of cardiac disorders after CAR-T. Cardiac disorders had different manifestations, of which the most common was HF (12%), followed by acute coronary syndrome (7%) and arrhythmia (6%), and the least was myocardial infarction (1%). The diagnosis of CAR-T cell-related cardiac disorders required the appearance of new symptoms or signs of HF, arrhythmia or myocardial infarction. Although most cardiac disorders are mild and temporary, some patients developed severe cardiac disorders, which may be life-threatening in the form of malignant arrhythmias, myocardial infarction, and decompensated HF. Early diagnosis and treatment of CAR-T-related cardiac disorders is an important step to reduce the mortality after CAR-T cell therapy. Serial testing of myocardial enzymes, especially hs-cTnT and NT-proBNP, is very necessary for early detection of cardiac disorders. Alvi RM (9) reported that an elevated troponin occurred in 29 of 53 tested patients (54%) and was associated with an increased risk for a CV event. In our study, 9 and 12 of 13 patients with cardiac disorders (CTCAE grade 3-5) had elevated hs-cTnT and NT-proBNP, with the median peak value 23.60 ng/L (IQR: 14.00 to 37.52 ng/L) and 3657 pg/ml (IQR: 1724 to 18186 pg/ml) respectively, suggesting that continuous testing of hs-cTnT and NT-proBNP may be of use for identifying high-risk patients with cardiac disorders after CAR-T. Shalabi H also found out troponin and proBNP may help to earlier identify those patients at highest risk of severe cardiac systolic dysfunction (15).

## Risk Factors Associated With Cardiac Disorders CTCAE

Some study had demonstrate that ≈10% of patients develop cardiomyopathy in the context of high-grade CRS after CAR-T cell therapy (16). In our study, baseline factors, including patients with CRS and low baseline GFR levels were associated with an increased risk of subsequent cardiac disorders by multivariable analysis. According to univariate and multivariable analysis, patients with baseline GFR < 60ml/min were more likely to have cardiac disorders than that with baseline GFR ≥ 60ml/min. Lefebvre B also found that baseline creatinine and CRS grade 3 or 4 were independently associated with major adverse cardiovascular events (17). However, after CAR-T treatment, if the treatment were effective, many patients' renal function would be improved with creatinine and glomerular filtration rate (GFR) returning to normal, which is consistent with our previous published paper (18). Alvi RM showed that troponin elevation was associated with CRS, but not with CAR-T type, cancer type, therapies before CAR-T, race or age (9). The Baseline of NT-proBNP was higher in patients with renal dysfunction, which was prone to heart failure (19). In our study, the baseline of hs-cTnT and NT-proBNP were no statistical significance.

## CRS Was Closely Related to Cardiac Disorders, or Cardiac Disorders Was a Part of CRS

There was a graded relationship between CRS and cardiac disorders. After CAR-T treatment, fever is the most common

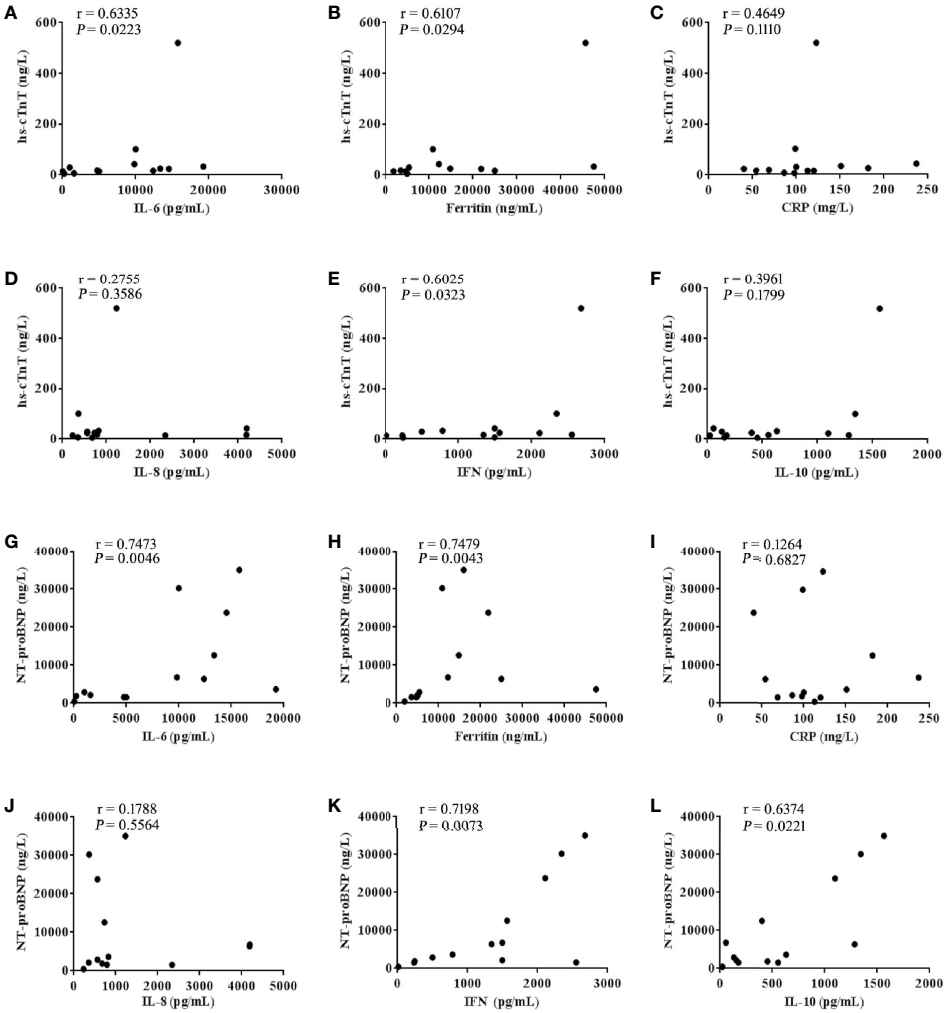


**FIGURE 3** | hs-cTnT and NT-proBNP were closely correlated to cytokine levels in patients with CTCAE grade 3-5 (n = 13). The correlation of hs-cTnT concentration with serum **(A)** IL-6, **(B)** Ferritin, **(C)** CRP, **(D)** IL-8, **(E)** IFN-γ and **(F)** IL-10. The correlation of NT-proBNP concentration with serum **(G)** IL-6, **(H)** Ferritin, **(I)** CRP, **(J)** IL-8, **(K)** IFN-γ and **(L)** IL-10. Each point represents data from a single patient; r values were determined using the spearman correlation test.

**TABLE 5** | The relationship between CRS grade 1-2, cardiac disorders and intervention therapy.

| Cardiac disorders CTCAE | Grade 0 | Grade 1-2 | Total | *P* |
|---|---|---|---|---|
| CRS grade 1 | 47 (92) | 4 (8) | 51 (100) | |
| Cohort 1[a] | 26 (87) | 4 (13) | 30 | 0.1336 |
| Cohort 2[b] | 21 (100) | 0 (0) | 21 | |
| CRS grade 2 | 22 (73) | 8 (27) | 30 (100) | |
| Cohort 1[a] | 14 (67) | 7 (33) | 21 | 0.3742 |
| Cohort 2[b] | 8 (89) | 1 (11) | 9 | |

*Data were described as n (%). P-value was tested by the Chi-Square test.*

[a]*Patients were given corticosteroids and/or tocilizumab therapy within 24 hours after the onset of CRS.*

[b]*Patients were not given corticosteroids and/or tocilizumab therapy within 24 hours or received corticosteroids and/or tocilizumab therapy more than 24 hours after the onset of CRS.*

sign of CRS (2). In our study, 100% of patients with CAR-T-related cardiac disorders had CRS. Patients who developed cardiac disorders CTCAE grade ≥3 were more frequently observed in the severe CRS (grade ≥3) cohort (**Tables 1**, **3**) and no severe CRS (grade ≥3) was found in patients without cardiac disorders, which indicated that there was a close and graded relationship between the development of CRS and cardiac disorders. We found the occurrence time of CRS grade 3-5 was earlier than that of cardiac disorders grade 3-5, and the median onset time of CRS grade 3-5 and cardiac disorders CTCAE grade 3-5 was 3 days (IQR: 1 to 7 days) and 8 days (IQR: 4 to 9 days) (**Table 4**), suggesting that CRS may cause cardiac disorders. Some studies have found that CRS after CAR-T therapy was related to hepatic dysfunction, coagulation abnormality and neurotoxicity (20–22). Our study indicated that CRS was

**TABLE 6** | The relationship between CRS grade 3-5, cardiac disorders and intervention therapy.

| Cardiac disorders CTCAE | Grade 0-2 | Grade 3-5 | Total | *P* |
|---|---|---|---|---|
| CRS grade 3-5 | 9 (41) | 13 (59) | 22 (100) | |
| Cohort 1[a] | 6 (75) | 2 (25) | 8 | 0.026 |
| Cohort 2[b] | 3 (21) | 11 (79) | 14 | |
| Cardiac disorders | | | | |
| CTCAE | 20 (61) | 13 (39) | 33 (100) | |
| Cohort 1[a] | 16 (89) | 2 (11) | 18 | 0.0004 |
| Cohort 2[b] | 4 (27) | 11 (73) | 15 | |

*Data were described as n (%). P-value was tested by the Chi-Square test.*

[a]*Patients were given corticosteroids and/or tocilizumab therapy within 24 hours after the onset of CRS.*

[b]*Patients were not given corticosteroids and/or tocilizumab therapy within 24 hours or received corticosteroids and/or tocilizumab therapy more than 24 hours after the onset of CRS.*

closely related to cardiac disorders, or cardiac disorders was a part of CRS.

## The Pathogenesis of Cardiac Disorders May Be Related to the Injury of Endothelial by a Large Number of Cytokines

Endothelial dysfunction and hypercoagulability are considered to be the main factors of CAR-T toxicity. Indeed, the biomarkers of endothelial cell activation, such as angiopoietin 2, the angiopoietin-2 to angiopetin-1 ratio and von Willebrand Factor (VWF) were higher in patients with neurotoxicity (grade ≥4) (2). Similarly, it should be noted that endothelial dysfunction is considered an early event in the pathophysiology of cardiovascular disease (23). In our study, after CAR-T therapy, cytokines such as IL-6, IFN-γ which can cause endothelial injury, were significantly increased in patients with severe cardiac disorders. We also observed that patients with earlier peak concentrations of IL-6, IFN-γ had a higher grade of cardiac disorders, suggesting that the rising rate of serum cytokine concentration as well as the peak concentration, may be determinants of the severity of cardiac disorders. IL-6, Ferritin and CRP are the most frequently detected cytokines in CRS (24, 25). After further analysis of the correlation between the levels of myocardial enzyme parameters and cytokines in patients with cardiac disorders (grade ≥3), we found the values of both hs-cTnT and NT-proBNP were positively correlated with the levels of serum IL-6, Ferritin and IFN-γ (**Figure 3**). Like IL-6, IFN-γ is a proinflammatory cytokine involved in the biological process of inducing macrophages to secrete tumor necrosis factor (TNF-α) and stimulating macrophages to release reactive oxygen species (26, 27). Thus, we speculate that besides targeting IL-6, targeting IFN-γ may be a novel strategy for managing CRS or cardiac disorders that are caused by CAR-T, although this theory requires further investigation.

## The Onset Time of CRS and Administration Time of Corticosteroids/ Tocilizumab Were Associated With Severity of CRS and Cardiac Disorders

Among the 103 patients with CRS administered different treatments, we found that there was no difference in the incidence of cardiac disorders of patients with CRS grade 1-2 between cohort 1 and cohort 2. However, patients with CRS grade 3-5 in cohort 2 were more likely to develop cardiac disorders than those in cohort 1. In other words, when severe CRS (grade 3-5) occurs, prompt treatment (given corticosteroids and/or tocilizumab therapy within 24 hours) could reduce the incidence of cardiac disorders (**Tables 5**, **6**).

Tocilizumab, an antagonistic IL-6R mAb, effectively ameliorates fever and hypotension in most patients developed severe CRS after CAR-T cell (28). Our study found that in addition to IL-6, other cytokines such as IFN-γ, CRP, ferritin, IL-8 and IL-10 were significantly increased in the occurrence of cardiac disorders. Corticosteroids may be a double-edged sword in the management of immunomodulation and inflammatory response. Its pharmacological mechanisms involve reducing inflammatory cytokines production, leukocyte infiltration and phagocytosis at the onset of inflammation (29, 30). Besides, the corticosteroid can interfere with the interaction between proinflammatory factors (31, 32). Although corticosteroids may cause injury to the infused CAR-T cell and reduce the curative effect, previous studies and our results show that corticosteroids are still very important for the treatment of cytokine storm-related diseases as hemophagocytic syndrome and CRS (33–35). Our study suggested that timely administration of corticosteroids and/or tocilizumab at the early stage of CRS grade 3-5 may relieve syndromes and delay cardiac disorders progression.

## Study Limitations

These data are obtained retrospectively. As with all retrospective studies, there may be missing data at some points after CAR-T infusion. For example, some patients with CRS grade 1-2 had mild symptoms, and sometimes may miss cytokine assay. Meanwhile, because the hs-cTnT and NT-proBNP assay in our study was often based on clinical suspicion of cardiac injury (not a protocol driven study as expected), with no symptoms of heart failure, acute coronary syndrome, some patients were not given hs-cTnT or NT-proBNP assay and color doppler echocardiography examination. Therefore, the value of hs-cTnT or NT-proBNP at some time points were missed. In addition, some patients undergo cardiac MRI or ECT examinations at designated locations after developing severe cardiac disorders. This part of the data was also unavailable and without a cardiac biopsy, the exact mechanism of cardiac disorders cannot be determined.

## CONCLUSION

In summary, cardiac disorders were common events after CAR-T cell therapy closelyassociated with CRS. However, the most cardiac disorders were mild. Patients who developed cardiac disorders CTCAE grade ≥3 had more severe CRS (≥3 grade). The values of hs-cTnT were positively correlated with the levels of serum IL-6, Ferritin, IFN-γ. The values of NT-proBNP were positively correlated with the levels of serum IL-6, Ferritin, IFN-γ and IL-10. The onset time of CRS and administration time of corticosteroids/tocilizumab were associated with severity of CRS and cardiac disorders.

## DATA AVAILABILITY STATEMENT

The raw data supporting the conclusions of this article will be made available by the authors, without undue reservation.

## ETHICS STATEMENT

The studies involving human participants were reviewed and approved by The Ethics Committee of the Xuzhou Medical University. Written informed consent to participate in this study was provided by the participants' legal guardian/next of kin.

## AUTHOR CONTRIBUTIONS

KQ, ZY, and HC designed the research, analyzed the data and drafted the paper. WC, YW, XW, JC, HZ, WS, FZ, HS, and DL were mainly responsible for data collection and analysis. QW, JQ, CF, and LZ were primarily responsible for statistical analysis. KX, ZL, and JZ contributed to study design and revised the manuscript. All authors contributed to the article and approved the submitted version.

## FUNDING

This work was supported by the National Natural Science Foundation of China (81871263, 81930005, 82070127), Natural Science Foundation of Jiangsu Province (BK2020022348), and the Postgraduate Research & Practice Innovation Program of Jiangsu (KYCX19-2229).

## SUPPLEMENTARY MATERIAL

The Supplementary Material for this article can be found online at: https://www.frontiersin.org/articles/10.3389/fonc.2021.691064/full#supplementary-material

## REFERENCES

1. Lee DW, Santomasso BD, Locke FL, Ghobadi A, Turtle CJ, Brudno JN, et al. ASTCT Consensus Grading for Cytokine Release Syndrome and Neurologic Toxicity Associated With Immune Effector Cells. *Biol Blood Marrow Transplant* (2019) 25:625–38. doi: 10.1016/j.bbmt.2018.12.758
2. Gust J, Hay KA, Hanafi LA, Li D, Myerson D, Gonzalez-Cuyar LF, et al. Endothelial Activation and Blood-Brain Barrier Disruption in Neurotoxicity After Adoptive Immunotherapy With CD19 CAR-T Cells. *Cancer Discov* (2017) 7:1404–19. doi: 10.1158/2159-8290.CD-17-0698
3. Wang Y, Qi K, Cheng H, Cao J, Shi M, Qiao J, et al. Coagulation Disorders After Chimeric Antigen Receptor T Cell Therapy: Analysis of 100 Patients With Relapsed and Refractory Hematologic Malignancies. *Biol Blood Marrow Transplant* (2020) 26:865–75. doi: 10.1016/j.bbmt.2019.11.027
4. Neelapu SS, Tummala S, Kebriaei P, Wierda W, Gutierrez C, Locke FL, et al. Chimeric Antigen Receptor T-Cell Therapy - Assessment and Management of Toxicities. *Nat Rev Clin Oncol* (2018) 15:47–62. doi: 10.1038/nrclinonc.2017.148
5. Brudno JN, Kochenderfer JN. Toxicities of Chimeric Antigen Receptor T Cells: Recognition and Management. *Blood* (2016) 30:3321–30:127. doi: 10.1182/blood-2016-04-703751
6. Cao J, Wang G, Cheng H, Chen W, Qi K, Sang W, et al. Potent Anti-Leukemia Activities of Humanized CD19-Targeted Chimeric Antigen Receptor T (CAR-T) Cells in Patients With Relapsed/Refractory Acute Lymphoblastic Leukemia. *Am J Hematol* (2018) 93:851–8. doi: 10.1002/ajh.25108
7. US Department of Health and Human Services. *Common Terminology Criteria for Adverse Events (CTCAE) version 4.03* [National Institutes of Health Web site]. (2010). Available at: http://evs.nci.nih.gov/ftp1/CTCAE/CTCAE_4.03_2010-06-14_QuickReference_5x7.pdf.
8. Thygesen K, Alpert JS, Jaffe AS, Simoons ML, Chaitman BR, White HD, et al. Third Universal Definition of Myocardial Infarction. *Eur Heart J* (2012) 33:2551–67. doi: 10.1093/eurheartj/ehs184
9. Alvi RM, Frigault MJ, Fradley MG, Jain MD, Mahmood SS, Awadalla M, et al. Cardiovascular Events Among Adults Treated With Chimeric Antigen Receptor T-Cells (CAR-T). *J Am Coll Cardiol* (2019) 24:3099–108:74. doi: 10.1016/j.jacc.2019.10.038
10. Lee DW, Gardner R, Porter DL, Louis CU, Ahmed N, Jensen M, et al. Current Concepts in the Diagnosis and Management of Cytokine Release Syndrome. *Blood* (2014) 10:188–95:124. doi: 10.1182/blood-2014-05-552729
11. Charlson M, Pompei P, Ales KL, MacKenzie CR. A New Method of Classifying Prognostic Comorbidity in Longitudinal Studies: Development and Validation. *J Chronic Dis* (1987) 40:373–83. doi: 10.1016/0021-9681(87)90171-8
12. Giavridis T, van der Stegen SJC, Eyquem J, Hamieh M, Piersigilli A, Sadelain M. CAR-T Cell-Induced Cytokine Release Syndrome Is Mediated by Macrophages and Abated by IL-1 Blockade. *Nat Med* (2018) 24:731–8. doi: 10.1038/s41591-018-0041-7
13. Gardner RA, Finney O, Annesley C, Brakke H, Summers C, Leger K, et al. Intent to Treat Leukemia Remission by CD19CAR T Cells of Defined Formulation and Dose in Children and Young Adults. *Blood* (2017) 129:3322–31. doi: 10.1182/blood-2017-02-769208
14. Maude SL, Frey N, Shaw PA, Aplenc R, Barrett DM, Bunin NJ, et al. Chimeric Antigen Receptor T Cells for Sustained Remissions in Leukemia. *N Engl J Med* (2014) 371:1507–17. doi: 10.1056/NEJMoa1407222
15. Shalabi H, Sachdev V, Kulshreshtha A, Cohen JW, Yates B, Rosing DR, et al. Impact of Cytokine Release Syndrome on Cardiac Function Following CD19 CAR-T Cell Therapy in Children and Young Adults With Hematological Malignancies. *J Immunother Cancer* (2020) 8:e001159. doi: 10.1136/jitc-2020-001159
16. Ganatra S, Redd R, Hayek SS, Parikh R, Azam T, Yanik GA, et al. Chimeric Antigen Receptor T-Cell Therapy-Associated Cardiomyopathy in Patients With Refractory or Relapsed Non-Hodgkin Lymphoma. *Circulation* (2020) 142:1687–90. doi: 10.1161/CIRCULATIONAHA.120.048100
17. Lefebvre B, Kang Y, Smith AM, Frey NV, Carver JR, Scherrer-Crosbie M. Cardiovascular Effects of CAR T Cell Therapy: A Retrospective Study. *JACC CardioOncol* (2020) 2:193–203. doi: 10.1016/j.jaccao.2020.04.012
18. Li H, Yin L, Wang Y, Wang X, Shi M, Cao J, et al. Safety and Efficacy of Chimeric Antigen Receptor T-Cell Therapy in Relapsed/Refractory Multiple Myeloma With Renal Impairment. *Bone Marrow Transplant* (2020) 55:2215–8. doi: 10.1038/s41409-020-0930-5
19. Hogenhuis J, Voors AA, Jaarsma T, Hoes AW, Hillege HL, Kragten JA, et al. Anaemia and Renal Dysfunction are Independently Associated With BNP and

NT-proBNP Levels in Patients With Heart Failure. *Eur J Heart Fail* (2007) 9:787–94. doi: 10.1016/j.ejheart.2007.04.001
20. Locke FL, Neelapu SS, Bartlett NL, Siddiqi T, Chavez JC, Hosing CM, et al. Phase 1 Results of ZUMA-1: A Multicenter Study of KTE-C19 Anti-CD19 CAR T Cell Therapy in Refractory Aggressive Lymphoma. *Mol Ther* (2017) 25:285–95. doi: 10.1016/j.ymthe.2016.10.020
21. Cohen AD, Garfall AL, Stadtmauer EA, Melenhorst JJ, Lacey SF, Lancaster E. B Cell Maturation Antigen-Specific CAR T Cells are Clinically Active in Multiple Myeloma. *J Clin Invest* (2019) 129:2210–21. doi: 10.1172/JCI126397
22. Jiang H, Liu L, Guo T, Wu Y, Ai L, Deng J, et al. Improving the Safety of CAR-T Cell Therapy by Controlling CRS-Related Coagulopathy. *Ann Hematol* (2019) 98:1721–32. doi: 10.1007/s00277-019-03685-z
23. Gkaliagkousi E, Gavriilaki E, Triantafyllou A, Douma S. Clinical Significance of Endothelial Dysfunction in Essential Hypertension. *Curr Hypertens Rep* (2015) 17:85. doi: 10.1007/s11906-015-0596-3
24. Nagle SJ, Murphree C, Raess PW, Schachter L, Chen A, Hayes-Lattin B. Prolonged Hematologic Toxicity Following Treatment With Chimeric Antigen Receptor T Cells in Patients With Hematologic. *Am J Hematol* (2021) 96:455–61. doi: 10.1002/ajh.26113
25. Winkler U, Jensen M, Manzke O, Schulz H, Diehl V, Engert A. Cytokine-Release Syndrome in Patients With B-Cell Chronic Lymphocytic Leukemia and High Lymphocyte Counts After Treatment With an Anti-CD20 Monoclonal Antibody (Rituximab, IDEC-C2B8). *Blood* (1999) 94:2217–24. doi: 10.1182/blood.V94.7.2217.419k02_2217_2224
26. Damoulis PD, Hauschka PV. Nitric Oxide Acts in Conjunction With Proinflammatory Cytokines to Promote Cell Death in Osteoblasts. *J Bone Miner Res* (1997) 12:412–22. doi: 10.1359/jbmr.1997.12.3.412
27. Saini NK, Sinha R, Singh P, Sharma M, Pathak R, Rathor N, et al. Mce4A Protein of Mycobacterium Tuberculosis Induces Pro Inflammatory Cytokine Response Leading to Macrophage Apoptosis in a TNF-Alpha Dependent Manner. *Microb Pathog* (2016) 100:43–50. doi: 10.1016/j.micpath.2016.08.038
28. Gardner RA, Ceppi F, Rivers J, Annesley C, Summers C, Taraseviciute A, et al. Preemptive Mitigation of CD19 CAR T-Cell Cytokine Release Syndrome Without Attenuation of Antileukemic Efficacy. *Blood* (2019) 134:2149–58. doi: 10.1182/blood.2019001463
29. Urwyler SA, Blum CA, Coslovsky M, Mueller B, Schuetz P, Christ-Crain M. Cytokines and Cortisol - Predictors of Treatment Response to Corticosteroids in Community-Acquired Pneumonia? *J Intern Med* (2019) 286:75–87. doi: 10.1111/joim.12891
30. Ouisse LH, Remy S, Lafoux A, Larcher T, Tesson L, Chenouard V, et al. Immunophenotype of a Rat Model of Duchenne's Disease and Demonstration of Improved Muscle Strength After Anti-CD45RC Antibody Treatment. *Front Immunol* (2019) 10:2131. doi: 10.3389/fimmu.2019.02131
31. Turner MJ, Dauletbaev N, Lands LC, Hanrahan JW. The Phosphodiesterase Inhibitor Ensifentrine Reduces Production of Proinflammatory Mediators in Well Differentiated Bronchial Epithelial Cells by Inhibiting PDE4. *J Pharmacol Exp Ther* (2020) 375:414–29. doi: 10.1124/jpet.120.000080
32. Löwenberg M, Stahn C, Hommes DW, Buttgereit F. Novel Insights Into Mechanisms of Glucocorticoid Action and the Development of New Glucocorticoid Receptor Ligands. *Steroids* (2008) 73:1025–9. doi: 10.1016/j.steroids.2007.12.002
33. Rivière S, Galicier L, Coppo P, Marzac C, Aumont C, Lambotte O, et al. Reactive Hemophagocytic Syndrome in Adults: A Retrospective Analysis of 162 Patients. *Am J Med* (2014) 127:1118–25. doi: 10.1016/j.amjmed.2014.04.034
34. Li F, Yang Y, Jin F, Dehoedt C, Rao J, Zhou Y, et al. Clinical Characteristics and Prognostic Factors of Adult Hemophagocytic Syndrome Patients: A Retrospective Study of Increasing Awareness of a Disease From a Single-Center in China. *Orphanet J Rare Dis* (2015) 10:20. doi: 10.1186/s13023-015-0224-y
35. Davila ML, Riviere I, Wang X, Bartido S, Park J, Curran K, et al. Efficacy and Toxicity Management of 19-28z CAR T Cell Therapy in B Cell Acute Lymphoblastic Leukemia. *Sci Transl Med* (2014) 6:224ra25. doi: 10.1126/scitranslmed.3008226

**Conflict of Interest:** The authors declare that the research was conducted in the absence of any commercial or financial relationships that could be construed as a potential conflict of interest.

frontiers in Oncology

BRIEF RESEARCH REPORT
published: 22 July 2021
doi: 10.3389/fonc.2021.690218

# A Recurrent Cryptic *MED14-HOXA9* Rearrangement in an Adult Patient With Mixed-Phenotype Acute Leukemia, T/myeloid, NOS

*Qian Wang[1†], Ling Zhang[1†], Ming-qing Zhu[1†], Zhao Zeng[1], Bao-zhi Fang[2], Jun-dan Xie[1], Jin-lan Pan[1], Chun-xiao Wu[1], Ni Wu[1], Ri Zhang[1*], Su-ning Chen[1,3*] and Hai-ping Dai[1,3*]*

*[1] National Clinical Research Center for Hematologic Diseases, Jiangsu Institute of Hematology, The First Affiliated Hospital of Soochow University, Suzhou, China, [2] Department of Hematology, The Affiliated Suzhou Hospital of Nanjing Medical University (Main part of Suzhou Municipal Hospital), Suzhou, China, [3] Institute of Blood and Marrow Transplantation, Collaborative Innovation Center of Hematology, Soochow University, Suzhou, China*

To define the fusion genes in T/myeloid mixed-phenotype acute leukemia (T/M MPAL), we performed transcriptome sequencing of diagnostic bone marrow samples from 20 adult patients. Our analysis identified a second instance of a recurrent *MED14-HOXA9* chimeric gene resulting from the in-frame fusion of exon 23 of *MED14* and exon 1 of *HOXA9*, the first in an adult patient. The *MED14-HOXA9* fusion gene was detected in both the diagnostic and relapsed blasts with reverse transcription-polymerase chain reaction and Sanger sequencing. The patient received combined conventional chemotherapy but suffered relapse at 11 months and died of disease progression one year after the initial diagnosis. Our data suggest that *MED14-HOXA9* is a cryptic recurrent aberration in T/M MPAL, which might indicate an aggressive clinical course and inferior outcome after conventional chemotherapy. Further studies will be carried out to reveal the effects of the *MED14-HOXA9* fusion on the differentiation and proliferation of leukemia stem cells, as well as suitable treatment strategies for this emerging entity.

**Keywords: mixed-phenotype acute leukemia, *MED14-HOXA9*, fusion gene, *PTPN11*, *NOTCH1***

OPEN ACCESS

***Edited by:***
*Gurvinder Kaur,*
*All India Institute of Medical Sciences, India*

***Reviewed by:***
*Michael Diamantidis,*
*University Hospital of Larissa, Greece*
*Laura N. Eadie,*
*South Australian Research and Development Institute, Australia*

***Correspondence:**
*Ri Zhang*
*zhangri_sz@163.com*
*Su-ning Chen*
*chensuning@sina.com*
*Hai-ping Dai*
*daihaiping8@126.com*

*[†]These authors have contributed equally to this work*

***Specialty section:***
*This article was submitted to Hematologic Malignancies, a section of the journal Frontiers in Oncology*

***Received:*** *02 April 2021*
***Accepted:*** *07 July 2021*
***Published:*** *22 July 2021*

***Citation:***
*Wang Q, Zhang L, Zhu M-q, Zeng Z, Fang B-z, Xie J-d, Pan J-l, Wu C-x, Wu N, Zhang R, Chen S-n and Dai H-p (2021) A Recurrent Cryptic MED14-HOXA9 Rearrangement in an Adult Patient With Mixed-Phenotype Acute Leukemia, T/myeloid, NOS. Front. Oncol. 11:690218. doi: 10.3389/fonc.2021.690218*

## INTRODUCTION

T/myeloid mixed-phenotype acute leukemia (T/M MPAL) is a rare malignancy responsible for approximately 1% of all leukemia cases and is characterized by leukemic blasts presenting both T lineage and myeloid markers (1). Only a few patients with T/M MPAL have been identified with recurrent genetic aberrations, such as the t(9;22)(q34.1;q11.2)/*BCR-ABL1* and t(v;11q23.3)/*KMT2A* rearrangements (2). Most T/M MPAL cases carry nonspecific clonal chromosomal abnormalities, lack uniform treatment strategies and carry unfavorable prognoses (3, 4). Using next-generation and transcriptome sequencing, Takahashi and Alexander et al. elucidated the genetic and epigenetic heterogeneity of MPAL in a case series (5, 6), but only a few of the patients had T/M MPAL. For a better understanding of the genomic landscape of T/M MPAL, we performed transcriptome sequencing of diagnostic blasts from 20 adult patients with normal karyotype or karyotype

failure and, thereby, detected a cryptic cytogenetic aberration involving chromosomes X and 7 effecting the novel occurrence of a chimeric fusion *MED14-HOXA9* in an adult patient.

# MATERIALS AND METHODS

## Patient Characteristics

From March 2008 to November 2019, a total of 37 T/M MPAL patients were enrolled. Their median age was 45 years-old (range 17-84 years), comprising 22 males and 15 females. The study was approved by the Ethics Committee of the First Affiliated Hospital of Soochow University in accordance with the Declaration of Helsinki. Written informed consents were obtained from all patients.

## R-Banding Karyotype Analysis

Bone marrow (BM) samples were taken at diagnosis. Mononuclear cells were harvested, R-banded according to the routine institutional protocols and 20 metaphases were analyzed for each sample if possible. Chromosomal abnormalities were described according to the International System for Human Cytogenomic Nomenclature (ISCN, 2016) (7).

## RNA Sequencing and RT-PCR

Total RNA from BM samples taken at diagnosis was extracted using a RNeasy Mini Kit (QIAgen, Hilden, Germany). RNA sequencing libraries were prepared using 20-100 ng total RNA of BM samples with the TruSeq RNA library preparation kit v2 (Illumina, CA, USA). Paired-end sequencing with a read length of 150bp was performed on Illumina NovaSeq platforms to at least 12G raw data per sample according to the manufacturer's protocol. Read pairs were aligned to human reference genome (hg38) using the Spliced Transcripts Alignment to a Reference (STAR, version 2.5) (8). The FusionCatcher software was used to find fusion genes. SNVs/indels were analyzed by following the GATK best practices for variant calling on RNA sequencing. The forward and reverse primer sequences used for detection of the *MED14-HOXA9* fusion by reverse transcription-polymerase chain reaction (RT-PCR) were 5'-AAGGTCTGTAAATGAGG ACG-3' and 5'-TCGTCTTTTGCTCGGTCTT-3', respectively.

# RESULTS

After R-banding, 17 patients (17/37, 45.9%) evidenced abnormal karyotypes, 17 tested normal (17/37, 45.9%), and 3 failed analysis. RNA sequencing was performed on the 20 patients with normal karyotypes or who failed karyotype analysis. In 19 patients, RNA sequencing failed to detect any clinically relevant fusion genes. In one patient with a normal karyotype, however, the *MED14-HOXA9* fusion transcript was detected using RNA sequencing: accordingly, exon 23 of *MED14* was fused in frame with exon 1 of *HOXA9* (**Figure 1A** and **Supplementary Table 1**), which was further confirmed with RT-PCR and Sanger sequencing (**Figures 1B, C**). Moreover, the *MED14-HOXA9* fusion was also detected in the blasts at relapse with RT-PCR (**Figure 1D**). The 1153 amino acids encoded by the *MED14-HOXA9* fusion transcript cover the entire Med14 and homeobox domains of *MED14* and *HOXA9*, respectively (**Figure 1E**). Though fusion genes are frequently resulted from balanced chromosome translocations, results of RNA sequencing and RT-PCR revealed no reciprocal *HOXA9-MED14* fusion transcripts in this patient (data not shown).

The affected patient was a 37-year-old male referred to our hospital in June 2016 because of mild fever. Physical examination revealed enlarged lymph nodes of the right neck, without hepatomegaly or splenomegaly. Complete blood cell counts showed a white blood cell count of $11.09\times10^9$/L, hemoglobin of 10.9 g/dL and a platelet count of $84\times10^9$/L (**Supplementary Table 2**). Differentiation analysis of white blood cells showed 59% blasts. BM aspirates revealed 71% blasts, which were variable in cell and nucleolus size and negative for peroxidase staining (**Figure 2A**). The blasts were positive for myeloid markers, including CD13 (97.8%), CD15 (68.9%), CD117 (63.2%) and weak expression of MPO (36.1%), as well as the T lineage markers cCD3 (46.1%) and TdT (23.0%) by flow cytometry (**Figure 2B** and **Supplementary Figure 1A**). No fusion genes were detected using a multiplex RT-PCR panel covering 43 fusion genes commonly seen in acute leukemia (**Supplementary Table 3**). Cytogenetic analysis of the BM indicated a normal karyotype. Next generation sequencing (NGS) was not feasible due to sample non-availability. *CREBBP-p.Pro583Ser, EED-p.Arg216Ter, NOTCH1-p.Val1578_Leu1579del* and *PTPN11-p.Ser506Leu* were detected by RNA sequencing (**Supplementary Table 4**). Accordingly, a diagnosis of T/M MPAL, NOS was made according to revised WHO 2016 criteria (2).

After induction chemotherapy, consisting of idarubicin, vinorelbine and prednisone, the patient achieved complete remission, which was maintained during the subsequent 5 cycles of consolidation chemotherapy. He refused allogenic stem cell transplantation due to concerns regarding transplantation-related mortality. Unfortunately, relapse occurred 11 months after diagnosis when he presented with high fever and general soreness. At relapse, the complete blood cell count showed a white blood cell count of $16.04\times10^9$/L, a hemoglobin level of 12.5 g/dL, and a platelet count of $61\times10^9$/L, with 26% blasts in the peripheral blood. Morphology analysis revealed 72.5% blasts in the BM (**Figure 2D**). Flow cytometry showed that the blasts were positive for CD7 (99.7%), CD13 (67.0%), CD33 (99.9%) and CD34 (93.9%), had weak expression of both MPO (35.7%) and cCD3 (4.2%) (**Figure 2C** and **Supplementary Figure 1B**), confirming the diagnosis of relapse. Cytogenetic analysis of the BM at relapse showed a karyotype of 46,XY,add(1)(p36),del(9)(q12q31),del (12)(q23q24)[16]/46,idem,add (8)(q24)[2]/46,XY[2] (**Figure 2E**). NGS of the relapse BM samples using a targeted 222-gene panel revealed mutations, including *CREBBP-p.Pro583Ser*, *EED-p.Arg216Ter*, *NOTCH1-p.Val1578Glu*, *PTPN11-p.Ser506Leu*, *ZNF292-p.Asp829fs* and *ZNF292-p.Met1243fs* (**Supplementary Tables 4, 5**). The patient failed to respond to the initial induction chemotherapy regimen (idarubicin, vinorelbine, prednisone) combined with cyclophosphamide. He was also refractory to another chemotherapy regimen comprising homoharringtonine and cytarabine. The patient died of pulmonary infection at 34 days after relapse. Timeline is shown in **Supplementary Figure 2**.

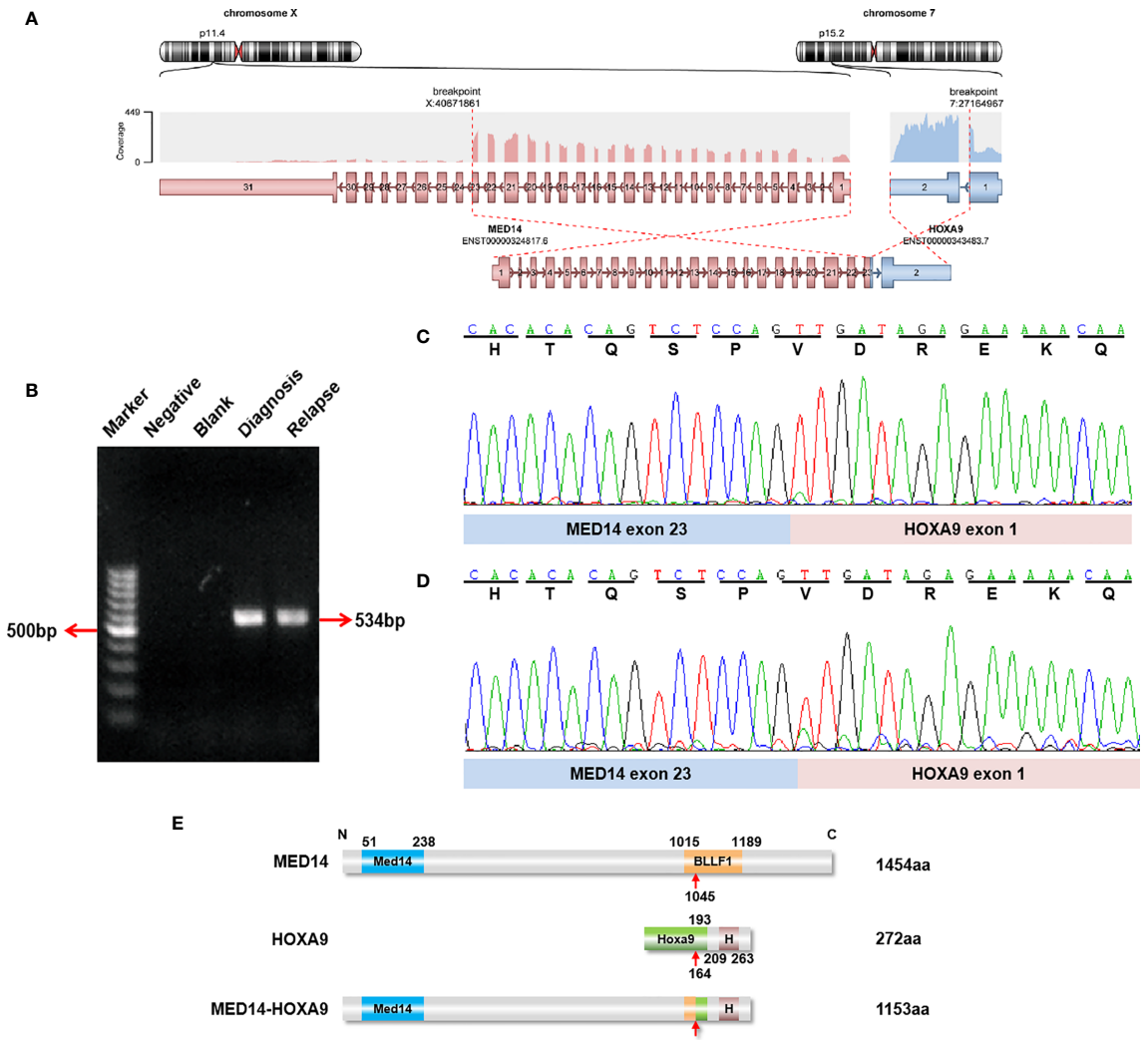


**FIGURE 1** | Identification of recurrent *MED14-HOXA9* fusion transcripts. **(A)** RNA sequencing analysis revealed one breakpoint in exon 23 of the *MED14* gene and one breakpoint in exon 1 of the *HOXA9* gene. **(B)** A product of 534 bp was detected by RT-PCR in samples taken at diagnosis and relapse. Marker: GeneRuler 100 bp DNA ladder; negative control (with cDNA sample with the JIH-5 cell line); blank control (without cDNA template). **(C, D)** Sequence alignment of the amplified product revealed breakpoints between exon 23 of *MED14* and exon 1 of *HOXA9* at diagnosis **(C)** and relapse **(D)**. **(E)** Schematic diagram of the *MED14* and *HOXA9* proteins and the *MED14-HOXA9* fusion protein. The breakpoint is indicated by a red arrow. Med14, Mediator complex subunit *MED14*; BLLF1, Herpes virus major outer envelope glycoprotein (BLLF1); HoxA9, HoxA9 activation region; H, Homeobox domain.

## DISCUSSION

T/M MPAL has both of myeloid and T lineage features immunophenotypically. Some studies applied NGS on the sorted blasts by flowcytometry to unravel the driver molecular lesions of T/M MPAL in the literature. The study of Xiao et al. showed that *PHF6* mutations were present in all blast compartments regardless of lineage differentiation, implicating that *PHF6* was an early mutation in T/M MPAL pathogenesis (9). Alexander et al. reported that biallelic *WT1* alterations were common in T/M MPAL (5). Because of the low incidence of T/M MPAL, these findings should be confirmed in larger scale studies using flowcytometry, NGS and single cell RNA sequencing. In this study, we performed RNA sequencing on diagnostic BM samples from 20 adult patients in order to explore the genomic landscape of T/M MPAL.

Here, we present the first case of *MED14-HOXA9* fusion to be reported in an adult T/M MPAL patient, confirming this fusion to be a rare but recurrent abnormality in T/M MPAL. *MED14* and *HOXA9* locate in chromosomes X and 7, respectively. Because there were no visible signs of abnormality in chromosomes X and 7 both at diagnosis and at relapse, we suggest that the *MED14-HOXA9* fusion resulted from a cryptic chromosomal rearrangement involving Xp11.4 and 7p15. *MED14-HOXA9* was detected in both the diagnostic and relapsed BM samples, therefore we believe that it might be one

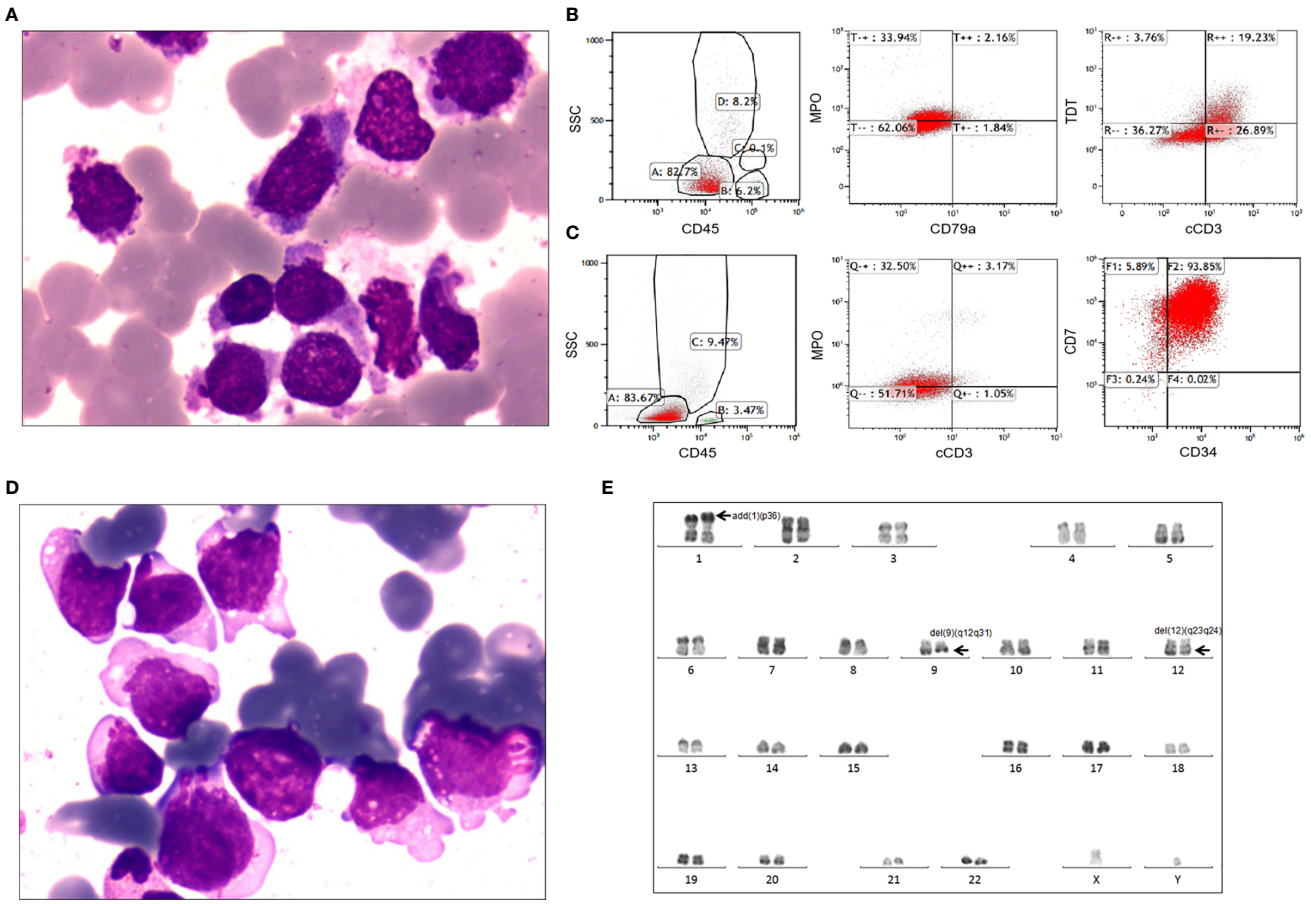


**FIGURE 2** | Laboratory characteristics of the adult patient with T/M MPAL with the *MED14-HOXA9* fusion. **(A)** Bone marrow aspirate at diagnosis. Morphological analysis showed hypercellular marrow with increased blasts variable in both cell and nucleolus sizes and negative for POX staining. (Wright's staining ×1,000). **(B)** Immunophenotyping of bone marrow cells at diagnosis. Flow cytometric analyses of leukemic cells revealed that the blast cells were positive for TDT, cCD3 and weak positive for myeloperoxidase (MPO), but negative for cCD79a. **(C)** Immunophenotyping of bone marrow cells at relapse. The blast cells were positive for CD34 and CD7 and weakly positive for MPO and cCD3. **(D)** Bone marrow aspirate at relapse. Morphological analysis showed 72.5% blasts in the bone marrow smear. (Wright's staining ×1,000). **(E)** Karyotype analysis at relapse. R-banding analysis using the bone marrow sample revealed a karyotype of 46,XY,add(1)(p36),del(9)(q12q31),del(12)(q23q24)[16]/46,idem,add(8)(q24)[2]/46,XY[2].

of the driver mutations responsible for leukemogenesis in this case. Because the patient presented with a normal karyotype at diagnosis but had acquired additional abnormalities at relapse, we reason that the structural aberrations involving chromosomes 1, 8, 9 and 12 observed at relapse were secondary to *MED14-HOXA9*, whether randomly occurring or contributory to disease progression.

*HOXA9*, located on chromosome 7p15, encodes a homeobox domain-containing and DNA-binding transcription factor, which plays an important role in regulating morphogenesis, differentiation and expansion of hematopoietic stem cells (10, 11). *HOXA9* is overexpressed in more than 50% of acute myeloid leukemia (AML) cases and is associated with poor prognoses (12, 13). A variety of upstream genetic alterations, such as *MLL* translocations, *NUP98* fusions, *NPM1* mutations and translocations involving *HOXA9* itself, have been demonstrated to cause overexpression of *HOXA9* (14). *HOXA9* reportedly forms translocations with 5 partner genes in myeloid malignancies: *ANGPT1*, *GATA2* and *NIPBL* in pediatric acute megakaryoblastic leukemia (15, 16); *NUP98* mostly in patients with AML and occasionally in patients with chronic myelogenous leukemia (CML) in blast crisis (17–19); and *MSI2* in a patient with CML in the accelerated phase (20). Other rearrangement partners of *HOXA9* have been reported in lymphoid malignancies, such as *TRB* in T cell acute lymphoblastic leukemia (T-ALL) patients (21) and *MED12* in a pediatric patient with B cell acute lymphoblastic leukemia (B-ALL) (22) (**Supplementary Table 6**). This report adds a new case, with a novel *HOXA9* rearrangement in T/M MPAL.

In previously reported *HOXA9*-related fusions, all *HOXA9* homeodomains were retained. *HOXA9-ANGPT1* apart, all other reported fusions comprise the N-terminus of the partner gene

and exon 1 of *HOXA9* (located in the C-terminus). In this *MED14-HOXA9* case, the breakpoint also occurred in exon 1 of *HOXA9*, and the *HOXA9* segment was identical to that reported in other fusions, which indicates that the homeodomain of *HOXA9* is essential for leukemogenesis. *HOXA9* was shown to be upregulated by upstream fusions such as *NUP98-HOXA9*, which inhibits the differentiation of hematopoietic stem cells and increases the self-renewal of hematopoietic stem or progenitor cells (23). Collectively, these findings support the view that *HOXA9* is also aberrantly activated by the *MED14-HOXA9* fusion, which may play critical roles in the leukemogenesis of T/M MPAL.

MED14, mediator (MED) complex 14, plays an important role in coactivating RNA polymerase II (Pol II)-mediated transcription (24). In the *MED14-HOXA9* fusion gene, the main transcriptional domain of *MED14* was retained, which suggests an important role in *MED14*-mediated transactivation of *HOXA9* in this fusion. *MSI2*, another fusion partner of *HOXA9*, is also a putative RNA-binding protein. Thus, the *MED14-HOXA9* fusion adds another fusion gene in human leukemia encoding proteins with RNA-binding properties. A further MED-family gene, *MED12*, forms a fusion gene with *HOXA9* in B-ALL (22, 25). Mechanisms underlying the diversity of cellular settings with different *HOXA9* translocations might be attributable to the functions of the various translocation partners.

*MED14-HOXA9* fusion has been previously reported in a pediatric patient with T/M MPAL (5). Both the previously reported pediatric patient and the patient in this case were males diagnosed with T/M MPAL, had *PTPN11* mutations, relapsed with complex karyotypes, failed ALL chemotherapy and had short overall survivals (**Supplementary Table 7**). These shared characteristics indicate that patients with *MED14-HOXA9* fusion may: 1) be accompanied by *PTPN11* mutation serving as a critical alteration; and 2) follow an aggressive clinical course and confer an inferior outcome after conventional chemotherapy. Different *NOTCH1* mutations were detected in both diagnostic (p.Val1578_Leu1579del) and relapsed (p.Val1578Glu) BM samples, which both locate in the same hotspot in the heterodimerization domain of *NOTCH1* (**Supplementary Table 4** and **Supplementary Figure 3**). The different *NOTCH1* mutations at different disease timepoints suggest outgrowth of an alternate leukaemic clone carrying the missense mutation potentially due to some selective growth advantage or in response to therapy. Taken together, we speculated that in addition to the *MED14-HOXA9* fusion gene, mutations in *PTPN11* and *NOTCH1* co-operate and could be important for disease pathogenesis and potentially targeted treatments.

In summary, we report the first case of *MED14-HOXA9* in an adult T/M MPAL patient accompanied by precise clinical data, and confirm the presence of *MED14-HOXA9* fusion gene in both diagnostic and relapsed BM samples. Further studies will be carried out to reveal the mechanisms underlying the effects of the *MED14-HOXA9* fusion on the differentiation and proliferation of leukemia stem cells, as well as suitable treatment strategies for this rare disease.

## DATA AVAILABILITY STATEMENT

The data generated by RNA-seq (raw FASTQ files) have been deposited to NCBI Sequence Read Archive (SRA) and have been assigned a BioProject accession number PRJNA726744.

## ETHICS STATEMENT

The studies involving human participants were reviewed and approved by the Ethics Committee of the First Affiliated Hospital of Soochow University. Written informed consent to participate in this study was provided by the participants' legal guardian/next of kin. Written informed consent was obtained from the individual(s), and minor(s)' legal guardian/next of kin, for the publication of any potentially identifiable images or data included in this article.

## AUTHOR CONTRIBUTIONS

QW, LZ and M-qZ analyzed the clinical data and wrote the manuscript. ZZ and J-dX performed molecular studies and analyses. B-zF and NW performed the analysis of bone marrow smear and flow cytometry data. J-lP and C-xW performed karyotype analyses. RZ, S-nC and H-pD conceived and organized the work, and were major contributors in writing the manuscript. All authors contributed to the article and approved the submitted version.

## FUNDING

This study was supported by grant from the National Key R&D Program of China (2019YFA0111000), the National Natural Science Foundation of China (81000222, 81200370, 81700140, 81873449, 81970142, 81900130, 81970136, 82000132), the Natural Science Foundation of the Jiangsu Higher Education Institution of China (18KJA320005), the Natural Science Foundation of Jiangsu Province (BK20190180), China Postdoctoral Science Foundation (2018M632372), the Priority Academic Program Development of Jiangsu Higher Education Institution, Translational Research Grant of NCRCH (2020WSB11, 2020WSB13).

## ACKNOWLEDGMENTS

All the samples were from Jiangsu Biobank of Clinical Resources.

## SUPPLEMENTARY MATERIAL

The Supplementary Material for this article can be found online at: https://www.frontiersin.org/articles/10.3389/fonc.2021.690218/full#supplementary-material

**Supplementary Figure 1 |** Immunophenotyping of bone marrow cells at diagnosis **(A)** and at relapse **(B)**, respectively.

**Supplementary Figure 2 |** Timeline of the treatment regimens and responses. I, idarubicin; V, vinorelbine; P, prednisone; C, cyclophosphamide; H, homoharringtonine; A, cytarabine.

**Supplementary Figure 3 |** Gene mutations and karyotype results in newly diagnostic and relapsed samples.

**Supplementary Table 1 |** The result of RNA sequencing for MED14-HOXA9 fusion gene.

**Supplementary Table 2 |** Clinical characteristics of the patient at diagnosis and at the time of relapse.

**Supplementary Table 3 |** Detection of 43 fusion genes by a multiplex RT-PCR panel.

**Supplementary Table 4 |** Gene mutations detected by NGS and RNA sequencing.

**Supplementary Table 5 |** Detection of 222 genes by a NGS panel.

**Supplementary Table 6 |** Reported cases of HOXA9 gene rearrangements in AML, ALL, CML, and MPAL.

**Supplementary Table 7 |** Clinical characteristics of two patients with the MED14-HOXA9 fusion gene.

## REFERENCES


1. Weinberg OK, Arber DA. Mixed-Phenotype Acute Leukemia: Historical Overview and a New Definition. *Leukemia* (2010) 24:1844–51. doi: 10.1038/leu.2010.202
2. Arber DA, Orazi A, Hasserjian R, Thiele J, Borowitz MJ, Le Beau MM, et al. The 2016 Revision to the World Health Organization Classification of Myeloid Neoplasms and Acute Leukemia. *Blood* (2016) 127:2391–405. doi: 10.1182/blood-2016-03-643544
3. Matutes E, Pickl WF, Van't Veer M, Morilla R, Swansbury J, Strobl H, et al. Mixed-Phenotype Acute Leukemia: Clinical and Laboratory Features and Outcome in 100 Patients Defined According to the WHO 2008 Classification. *Blood* (2011) 117:3163–71. doi: 10.1182/blood-2010-10-314682
4. Maruffi M, Sposto R, Oberley MJ, Kysh L, Orgel E. Therapy for Children and Adults With Mixed Phenotype Acute Leukemia: A Systematic Review and Meta-Analysis. *Leukemia* (2018) 32:1515–28. doi: 10.1038/s41375-018-0058-4
5. Alexander TB, Gu Z, Iacobucci I, Dickerson K, Choi JK, Xu B, et al. The Genetic Basis and Cell of Origin of Mixed Phenotype Acute Leukaemia. *Nature* (2018) 562:373–9. doi: 10.1038/s41586-018-0436-0
6. Takahashi K, Wang F, Morita K, Yan Y, Hu P, Zhao P, et al. Integrative Genomic Analysis of Adult Mixed Phenotype Acute Leukemia Delineates Lineage Associated Molecular Subtypes. *Nat Commun* (2018) 9:2670. doi: 10.1038/s41467-018-04924-z
7. McGowan-Jordan J, Simons A, Schmid R eds. *An International System for Human Cytogenomic Nomenclature*. S. Karger, Basel (2016). [Reprint of Cytogenet and Genome Res 149(1–2)]
8. Dobin A, Davis CA, Schlesinger F, Drenkow J, Zaleski C, Jha S, et al. STAR: Ultrafast Universal RNA-Seq Aligner. *Bioinformatics* (2013) 29:15–21. doi: 10.1093/bioinformatics/bts635
9. Xiao W, Bharadwaj M, Levine M, Farnhoud N, Pastore F, Getta BM, et al. PHF6 and DNMT3A Mutations are Enriched in Distinct Subgroups of Mixed Phenotype Acute Leukemia With T-Lineage Differentiation. *Blood Adv* (2018) 2:3526–39. doi: 10.1182/bloodadvances.2018023531
10. Abramovich C, Pineault N, Ohta H, Humphries RK. Hox Genes: From Leukemia to Hematopoietic Stem Cell Expansion. *Ann N Y Acad Sci* (2005) 1044:109–16. doi: 10.1196/annals.1349.014
11. Ferrell CM, Dorsam ST, Ohta H, Humphries RK, Derynck MK, Haqq C, et al. Activation of Stem-Cell Specific Genes by HOXA9 and HOXA10 Homeodomain Proteins in CD34+ Human Cord Blood Cells. *Stem Cells* (2005) 23:644–55. doi: 10.1634/stemcells.2004-0198
12. Collins CT, Hess JL. Role of HOXA9 in Leukemia: Dysregulation, Cofactors and Essential Targets. *Oncogene* (2016) 35:1090–8. doi: 10.1038/onc.2015.174
13. Lambert M, Alioui M, Jambon S, Depauw S, Van Seuningen I, David-Cordonnier MH. Direct and Indirect Targeting of HOXA9 Transcription Factor in Acute Myeloid Leukemia. *Cancers* (2019) 11:837. doi: 10.3390/cancers11060837
14. De Braekeleer E, Douet-Guilbert N, Basinko A, Le Bris MJ, Morel F, De Braekeleer M. Hox Gene Dysregulation in Acute Myeloid Leukemia. *Future Oncol* (2014) 10:475–95. doi: 10.2217/fon.13.195
15. Gruber TA, Larson Gedman A, Zhang J, Koss CS, Marada S, Ta HQ, et al. An Inv(16)(p13.3q24.3)-Encoded CBFA2T3-GLIS2 Fusion Protein Defines an Aggressive Subtype of Pediatric Acute Megakaryoblastic Leukemia. *Cancer Cell* (2012) 22:683–97. doi: 10.1016/j.ccr.2012.10.007
16. De Rooij JD, Branstetter C, Ma J, Li Y, Walsh MP, Cheng J, et al. Pediatric non-Down Syndrome Acute Megakaryoblastic Leukemia Is Characterized by Distinct Genomic Subsets With Varying Outcomes. *Nat Genet* (2017) 49:451–6. doi: 10.1038/ng.3772
17. Ahuja HG, Popplewell L, Tcheurekdjian L, Slovak ML. NUP98 Gene Rearrangements and the Clonal Evolution of Chronic Myelogenous Leukemia. *Genes Chromosomes Cancer* (2001) 30:410–5. doi: 10.1002/1098-2264(2001)9999:9999<::aid-gcc1108>3.0.co;2-9
18. Yamamoto K, Nakamura Y, Saito K, Furusawa S. Expression of the NUP98/HOXA9 Fusion Transcript in the Blast Crisis of Philadelphia Chromosome-Positive Chronic Myelogenous Leukaemia With T (7,11)(P15;P15). *Br J Haematol* (2000) 109:423–6. doi: 10.1046/j.1365-2141.2000.02003.x
19. Borrow J, Shearman AM, Stanton VPJr., Becher R, Collins T, Williams AJ, et al. The T (7,11(P15;P15) Translocation in Acute Myeloid Leukaemia Fuses the Genes for Nucleoporin NUP98 and Class I Homeoprotein HOXA9. *Nat Genet* (1996) 12:159–67. doi: 10.1038/ng0296-159
20. Barbouti A, Höglund M, Johansson B, Lassen C, Nilsson PG, Hagemeijer A, et al. A Novel Gene, MSI2, Encoding a Putative RNA-Binding Protein Is Recurrently Rearranged at Disease Progression of Chronic Myeloid Leukemia and Forms a Fusion Gene With HOXA9 as a Result of the Cryptic T (7,17) (P15;Q23). *Cancer Res* (2003) 63:1202–6.
21. Le Noir S, Ben Abdelali R, Lelorch M, Bergeron J, Sungalee S, Payet-Bornet D, et al. Extensive Molecular Mapping of Tcrα/δ- and Tcrβ-Involved Chromosomal Translocations Reveals Distinct Mechanisms of Oncogene Activation in T-ALL. *Blood* (2012) 120:3298–309. doi: 10.1182/blood-2012-04-425488
22. Lilljebjörn H, Henningsson R, Hyrenius-Wittsten A, Olsson L, Orsmark-Pietras C, von Palffy S, et al. Identification of ETV6-RUNX1-Like and DUX4-Rearranged Subtypes in Paediatric B-Cell Precursor Acute Lymphoblastic Leukaemia. *Nat Commun* (2016) 7:11790. doi: 10.1038/ncomms11790
23. Gough SM, Slape CI, Aplan PD. NUP98 Gene Fusions and Hematopoietic Malignancies: Common Themes and New Biologic Insights. *Blood* (2011) 118:6247–57. doi: 10.1182/blood-2011-07-328880
24. Cevher MA, Shi Y, Li D, Chait BT, Malik S, Roeder RG. Reconstitution of Active Human Core Mediator Complex Reveals a Critical Role of the MED14 Subunit. *Nat Struct Mol Biol* (2014) 21:1028–34. doi: 10.1038/nsmb.2914
25. Gu Z, Churchman M, Roberts K, Li Y, Liu Y, Harvey RC, et al. Genomic Analyses Identify Recurrent MEF2D Fusions in Acute Lymphoblastic Leukaemia. *Nat Commun* (2016) 7:13331. doi: 10.1038/ncomms13331


**Conflict of Interest:** The authors declare that the research was conducted in the absence of any commercial or financial relationships that could be construed as a potential conflict of interest.

frontiers in Oncology

SYSTEMATIC REVIEW
published: 09 September 2021
doi: 10.3389/fonc.2021.683263

# The Addition of Sirolimus to GVHD Prophylaxis After Allogeneic Hematopoietic Stem Cell Transplantation: A Meta-Analysis of Efficacy and Safety

*Xiaoli Chen[1], Hengrui Sun[1], Kaniel Cassady[2†], Shijie Yang[1], Ting Chen[1], Li Wang[1], Hongju Yan[1], Xi Zhang[1*] and Yimei Feng[1*]*

[1] Medical Center of Hematology, The Xinqiao Hospital of Third Military Medical University, Chongqing, China,
[2] Irell and Manella Graduate School of Biological Sciences of City of Hope, Duarte, CA, United States

OPEN ACCESS

**Edited by:**
Gurvinder Kaur,
All India Institute of Medical Sciences, India

**Reviewed by:**
Alejandro Majlis,
Las Condes Clinic, Chile
Shigeo Fuji,
Osaka International Cancer Institute, Japan

***Correspondence:**
Xi Zhang
zhangxxi@sina.com
Yimei Feng
yimeifeng@163.com

**†Present address:**
Kaniel Cassady,
Department of Hematology and Translational Sciences, Regeneron Pharmaceuticals, Tarrytown, NY, United States

**Specialty section:**
This article was submitted to Hematologic Malignancies, a section of the journal Frontiers in Oncology

**Received:** 20 March 2021
**Accepted:** 23 August 2021
**Published:** 09 September 2021

**Citation:**
Chen X, Sun H, Cassady K, Yang S, Chen T, Wang L, Yan H, Zhang X and Feng Y (2021) The Addition of Sirolimus to GVHD Prophylaxis After Allogeneic Hematopoietic Stem Cell Transplantation: A Meta-Analysis of Efficacy and Safety. Front. Oncol. 11:683263. doi: 10.3389/fonc.2021.683263

**Objective:** The objective of this study was to evaluate the safety and efficacy of sirolimus (SRL) in the prevention of graft-*versus*-host disease (GVHD) in recipients following allogeneic hematopoietic stem cell transplantation (allo-HSCT).

**Methods:** Randomized controlled trials (RCTs) evaluating the safety and efficacy of SRL-based prophylaxis regimens in patients receiving allo-HSCT were obtained from PubMed, Embase, and the Cochrane database. Following specific inclusion and exclusion criteria, studies were selected and screened by two independent reviewers who subsequently extracted the study data. The Cochrane risk bias evaluation tool was used for quality evaluation, and RevMan 5.3 software was used for statistical analysis comparing the effects of SRL-based and non–SRL-based regimens on acute GVHD, chronic GVHD, overall survival (OS), relapse rate, non-relapse mortality (NRM), thrombotic microangiopathy (TMA), and veno-occlusive disease (VOD).

**Results:** Seven studies were included in this meta-analysis, with a total sample size of 1,673 cases, including 778 cases of patients receiving SRL-based regimens and 895 cases in which patients received non-SRL-based regimens. Our data revealed that SRL containing prophylaxis can effectively reduce the incidence of grade II–IV acute GVHD (RR = 0.75, 95% CI: 0.68~0.82, $p < 0.0001$). SRL-based prophylaxis was not associated with an improvement of grade III–IV acute GVHD (RR = 0.78, 95% CI: 0.59~1.03, $p = 0.08$), chronic GVHD ($p = 0.89$), OS ($p = 0.98$), and relapse rate ($p = 0.16$). Despite its immunosuppressant effects, SRL-based regimens did not increase bacterial ($p = 0.68$), fungal ($p = 0.70$), or CMV ($p = 0.10$) infections. However, patients receiving SRL-based regimens had increased TMA ($p < 0.00001$) and VOD ($p < 0.00001$).

**Conclusions:** This meta-analysis indicates that addition of sirolimus is an effective alternative prophylaxis strategy for II–IV aGVHD but may cause endothelial cell injury and result in secondary TMA or VOD events.

**Keywords: sirolimus, GVHD, HSCT, prophylaxis, TMA**

# INTRODUCTION

Allogeneic hematopoietic stem cell transplantation (allo-HSCT) is currently one of the most effective means to cure hematological malignancies. However, high incidence of graft *versus* host disease (GVHD) after transplantation results in high non-recurrence of transplantation-related death. The incidence of acute GVHD (aGVHD) is about 40%–75% and is an important factor affecting the overall efficacy of HSCT (1). In addition, chronic GVHD (cGVHD) has become the main cause of late non-relapse mortality (NRM) after HSCT, which also seriously affects the efficacy of transplantation and the quality of patient life. Currently, GVHD prophylaxis regimens among transplant centers are not uniform and mainly include calcineurin inhibitor (CNI), sirolimus (SRL), and posttransplantation cyclophosphamide (PT-Cy)-based regimens.

Our study focuses on the role of SRL in GVHD. SRL is an mTOR inhibitor, possessing antifungal, immunosuppressive, and antitumor properties (2). SRL can inhibit the proliferation and activation of T cells, reduce the release of pro-inflammatory cytokines, and modulate $CD4^+CD25^+$ regulatory T (Treg) cells, making it a widely used therapeutic candidate in benign and malignant hematological diseases (3). Accumulating evidence suggests that SRL may play a role in the prevention and treatment of GVHD after HSCT (4). However, some studies have reported that SRL-based regimens did not decrease the incidence of aGVHD (5, 6). Moreover, some have reported that SRL-based prophylaxis was associated with high incidence of thrombotic microangiopathy (TMA) (7). On the other hand, another group reported that the combination of tacrolimus (TAC)/SRL did not pose a higher risk of TMA (8). Therefore, to better understand the efficacy and safety of SRL-based regimens and their impact on GVHD, we performed a meta-analysis of SRL-based GVHD prophylaxis in patients after allo-HSCT.

# MATERIALS AND METHODS

## Search Strategy

A literature search was conducted to identify randomized controlled trials (RCTs) evaluating the efficacy of SRL-based prophylaxis in patients after allo-HSCT. The search was conducted through August 2020 in PubMed, Cochrane Library, Embase, and Web of Science. The search terms included "sirolimus," "rapamycin," "graft *versus* host disease" and "GVHD." The search language was restricted to English.

## Inclusion and Exclusion Criteria

Inclusion criteria: the RCT study must include an SRL-based group and a non-SRL-based prophylaxis group. RCTs included patients with hematological malignancies that have received allo-HSCT. The meta-analysis did not exclude studies or patients based on age, gender, source of donor, and level of radiotherapy and chemotherapy before transplantation. Primary outcomes included the incidence of aGVHD and cGVHD. The secondary outcomes included TMA, VOD, and overall survival (OS).

Exclusion criteria are non-RCTs, such as retrospective studies, conference articles, animal experiments, and review articles.

## Data Extraction

All data, including the first author of the studies, published year, country of origin, period of enrollment, sample size, median follow-up duration, SRL-based regimens, non-SRL-based regimens, and trial outcomes, were extracted by two independent researchers. Any discrepancies were resolved by discussion and/or consultations with a third independent researcher.

## Methodologic Quality Evaluation

### Statistical Analysis

The risk ratio (RR) and 95% confidence interval (CI) were used to analyze extracted dichotomous outcomes. Heterogeneity was assessed using the $I^2$ statistic. An $I^2$ value of greater than 50% and a p value less than 0.10 indicated significant heterogeneity (9). Sensitivity and subgroup analyses were performed to identify and reduce heterogeneity. Meta-analyses were conducted using random effects, regardless of the existence or non-existence of heterogeneity.

# RESULTS

## Study Selection and Characteristics

In total, 644 potentially relevant records were identified in database records using the selected search terms **(Figure 1)**. After a thorough screening of the remaining 569 titles and abstracts, 535 non-relevant studies were excluded. The full texts of the remaining 34 studies were assessed, leading to the elimination of 27 studies that did not meet the eligibility criteria. Subsequently, the remaining seven studies were included in our meta-analysis. Characteristics of the studies included in this analysis are listed in **Tables 1**, **2**. Totally, seven studies were included ranging from 74 to 707 patients. In five of these studies, the prophylactic regimen was CNI + methotrexate (MTX) *vs.* CNI + MTX + SRL (10–14). In two studies, CNI + mycophenolate mofetil (MMF) was compared with CNI + MMF + SRL (15, 16) for GVHD prophylaxis.

## Risk-of-Bias Assessment

The quality evaluation of the included studies was performed according to the Cochrane handbook. The risk-of-bias assessment was performed to address six aspects: random sequence generation, allocation concealment, blinding of participants and personnel, blinding of outcome assessment, incomplete outcome data, and selective reporting. In the selection bias assessment, three papers described the use of computer-generated random sequences, one paper randomized according to age and donor type, and the other three papers did not mention their grouping method. Seven studies did not mention their method for allocation concealment, while one mentioned the method of blinding data extraction. Seven studies were all low risk on other bias assessment **(Figure 2)**.

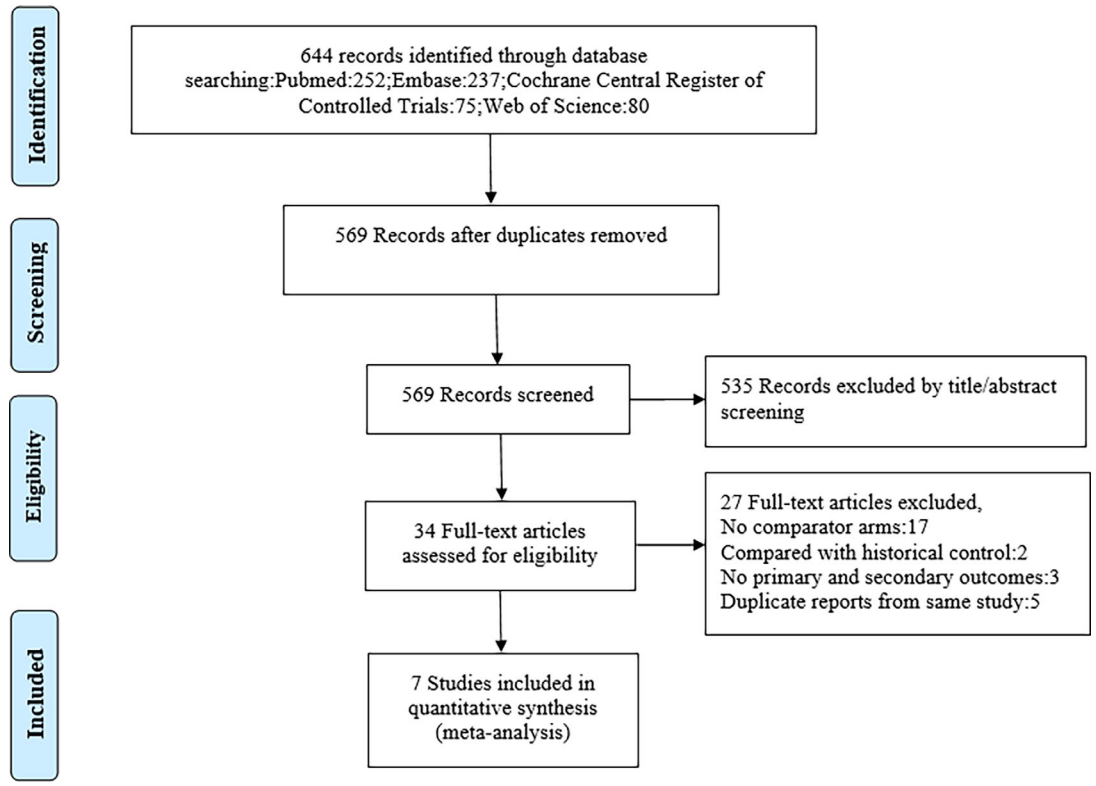


**FIGURE 1** | Flow diagram of this study.

**TABLE 1** | Characteristics of the included RCTs, comparing the SRL-based and non–SRL-based groups.

| First author and year | Disease | Age (SRL group) | Sample size SRL/non-SRL | Donors | Conditioning regimen |
|---|---|---|---|---|---|
| Armand 2016 (10) | Lymphoma, except Burkitt lymphoma. | 57 (23–70) | 66/73 | HLA-matched related donors or MUD. | RIC regimen |
| Pulsipher 2014 (11) | High-risk ALL in CR | NA (1–21) | 73/70 | HLA-matched siblings, HLA-matched related or unrelated donors, or single cord blood unit with 4–6/6 matched. | Myeloablative regimen (TBI followed by thiotepa or etoposide and CY) |
| Cutler 2014 (12) | Acute leukemia in remission, MDS, or CML. | 45 (19–59) | 151/153 | HLA-matched sibling. | Myeloablative regimen (TBI in combination with either CY or etoposide) |
| Khimani 2017 (13) | AML, MDS, CML, ALL, CLL, sAA, MM, and lymphoma | 52 (19–74) | 293/414 | HLA-matched sibling<br>HLA-matched or mismatched unrelated donors | Standard myeloablative<br>Escalated dose busulfan<br>Non-myeloablative<br>Reduced toxicity |
| Pidala 2015 (14) | AML, MDS, CML, ALL, CLL, sAA, MM, and lymphoma | 49 (25–68) | 37/37 | Only 8/8 or more HLA-matched sibling or unrelated donors | Bu/pent, Flu/Mel, Flu/Mel |
| Sandmaier 2019 (15) | Advanced hematological malignancies. | 63 (58–68) | 90/77 | At least 9/10 HLA-matched unrelated donors | Fludarabine+TBI |
| Kornblit 2014 (16) | AML, ALL, MDS, CML, CLL, MM, and lymphoma | 61 (15–76) | 68/71 | HLA-matched or mismatched unrelated donors | Nonmyeloablative regimen (fludarabine and 2 Gy TBI) |

*SRL, sirolimus; ALL, acute lymphoblastic leukemia; AML, acute myeloid leukemia; CLL, chronic lymphocytic leukemia; CML, chronic myelogenous leukemia; CR, complete remission; MDS, myelodysplastic syndrome; SAA, severe aplastic anemia; MM, multiple myeloma; HLA, human leukocyte antigen; MUD, matched unrelated donor; URD, unrelated donor; TBI, total body irradiation; CY, cyclophosphamide; RIC, reduced-intensity conditioning; Bu, busulfan; ATG, anti-thymocyte globulin; Flu, fludarabine; Mel, melphalan; NMA, non-myeloablative; HCT, allogeneic hematopoietic cell transplantation.*

**TABLE 2** | Characteristics of the included RCTs, comparing the SRL-based and non–SRL-based groups.

| First author and year | SRL usage and dosage | Grouping scheme | SRL administration time | Follow-up time (months) | SRL-based benefit outcomes ($p < 0.05$) |
|---|---|---|---|---|---|
| Armand 2016 (10) | 12 mg orally on day -3, then 4 mg daily to 360 days, with 5~12 ng/ml | TAC+MTX *vs.* TAC+MTX+SRL | -3 days~+360 days | 22 (NA) | II–IV aGVHD, yes; III–IV aGVHD, no; cGVHD, no; relapse, no; TMA, no; PFS, no; OS, no |
| Pulsipher 2014 (11) | 4 mg/m$^2$ on day 0, maintaining for 6 months, with 3~12 ng/ml level, followed by a 1-month taper | TAC+MTX *vs.* TAC+MTX+SRL | 0 days~+180 days | 26 (23~38) | II–IV aGVHD, yes; III–IV aGVHD, no; cGVHD, no; relapse, no; TMA, no; VOD, no; OS, no; NRM, no |
| Cutler 2014 (12) | Started on day -3 with 12 mg, followed by a daily dose of 4 mg, maintaining a 3~12-ng/ml level | TAC+MTX *vs.* TAC+SRL | -3 days~+100 days | 24 (NA) | II–IV aGVHD, no; III–IV aGVHD, yes; cGVHD, no; relapse, no; TMA, no; VOD, no; OS, no; NRM, no |
| Khimani 2017 (13) | 9 mg oral loading dose on day -1, kept at 5–14 ng/ml concentration, and continued for at least 1 year | TAC+MTX *vs.* TAC+SRL | -1 day~+365 days | 23.7(11.1-73.1) | II–IV aGVHD, yes; III–IV aGVHD, no; cGVHD, no; relapse, no; VOD, no; OS, yes; NRM, no |
| Pidala 2015 (14) | Started on day -1 with 9 mg, maintaining 5~14 ng/ml level, continued for at least 1 year | TAC+MTX *vs.* TAC+SRL | -1 day~+365 days | 41(27~60) | II–IV aGVHD, yes; cGVHD, yes; relapse, yes; TMA, no; VOD, no; OS, no; NRM, no. |
| Sandmaier 2019 (15) | Started on day -3 at 2 mg/day, maintaining 3~12 ng/ml to day 150, and tapered off by day 180 | CsA+MMF *vs.* CsA+MMF+SRL | -3 days~+180 days | 48 (31–60) | II–IV aGVHD, yes; III–IV aGVHD, yes; cGVHD, no; relapse, no; OS, yes; PFS, no; NRM, yes |
| Kornblit 2014 (16) | Started on day -3 at 2 mg, maintaining 3–12 ng/ml. Stopped on day 80 without a taper | TAC+MMF *vs.* TAC+MMF+SRL | -3 days~+80 days | 59 (6–101) | II–IV aGVHD, yes; III–IV aGVHD, no; cGVHD, no; relapse, no; EFS, no; OS, no; PFS, no |

*TAC, tacrolimus; MTX, methotrexate; CSA, cyclosporine; MMF, mycophenolate mofetil; aGVHD, acute graft-versus-host disease; OS, overall survival; PFS, progression-free survival; NRM, non-relapse mortality; TMA, thrombotic microangiopathy; VOD, veno-occlusive disease.*

## Study Outcome Analysis

### Primary Outcomes: GVHD, Including aGVHD and cGVHD

All seven studies reported the incidence of Grade II–IV aGVHD. Interstudy heterogeneity was observed to be significant, and the random-effect model was used ($I^2$ = 76%, $p < 0.0001$). By Stata analysis, Begg's test showed that $p = 0.548 > 0.5$, which suggests that there is no publication bias. Based on the results of modeling, SRL-based regimens significantly decreased the incidence of Grade II–IV aGVHD (RR, 0.75; 95% CI, 0.68–0.82; **Figure 3**). Interestingly, six studies reported the incidence of Grade III–IV aGVHD and the results did not support that addition of SRL can also reduce Grade III–IV aGVHD (RR, 0.78; 95% CI, 0.59–1.03, $p = 0.08$; **Figure 4**).

Additionally, SRL-based prophylaxis also cannot reduce the incidence of cGVHD. All seven studies reported that the incidence of cGVHD was not impacted by SRL-based prophylaxis regimens. There was no statistical difference in cGVHD prevention between SRL-based and non-SRL groups (RR, 1.01; 95% CI, 0.91-1.12, *P*=0.89; **Figure 5**).

### Secondary Outcomes: TMA, VOD, and OS

Regarding TMA, five studies included in this meta-analysis analyzed the risk of developing TMA. Pooled analysis suggested that all the SRL-based regimens led to an increased TMA incidence (RR, 2.69; 95% CI, 1.85–3.92, $p < 0.00001$; **Figure 6**). Regarding VOD risk, four studies mentioned that SRL-based prophylaxis increased the incidence of VOD, and only one reported that there was no VOD on either arm. Pooled analysis also hinted that SRL-based regimens increase VOD risk (RR, 3.00; 95% CI, 1.96–4.57, $p < 0.00001$; **Figure 7**). It is hypothesized that rapamycin can cause endothelial cell damage through macrophage activation (17) and calcium overload (18).

Our analysis includes seven RCTs to analyze OS. The pooled meta-analysis showed that there are no differences in OS (RR, 1.00; 95% CI, 0.92–1.09, $p = 0.98$; **Figure 8**). Moreover, SRL-based interventions had no statistical effect on PFS, relapse, NRM, bacterial and fungal infection, and CMV reactivation (**Supplementary File 1**).

## Publication Bias Assessment and Sensitivity Analysis

Stata 15.0 software was used to test the publication bias. The results showed that there was no significant publication bias ($p > 0.05$). The heterogeneity of two indexes (II–IV aGVHD and bacterial infection) displayed that the $I^2$ value was greater than 50%. We used sensitivity analysis with Stata software to determine the stability of the results. The sensitivity analysis showed that the research results were stable and reliable (**Supplementary File 2**).

# DISCUSSION

Effective prophylaxis of GVHD is the key to successful allo-HSCT. Sirolimus, in combination with a calcineurin inhibitor or post-transplantation cyclophosphamide, is a common regimen for GVHD prophylaxis. This meta-analysis specifically focuses on sirolimus-based GVHD prophylaxis, but there are indeed many other prophylaxis regimens, each with their own advantages and disadvantages depending on the transplant setting and GVHD risk factors.

In this study, we systematically evaluated the effect of SRL on GVHD as a prophylactic drug and included seven RCTs. Statistical results show that SRL prophylaxis regimens can significantly reduce the incidence of Grade II–IV aGVHD. There was no significant difference between the SRL group and the non-SRL group in reducing the incidence of III–IV aGVHD and cGVHD, which indicated that the sirolimus-containing

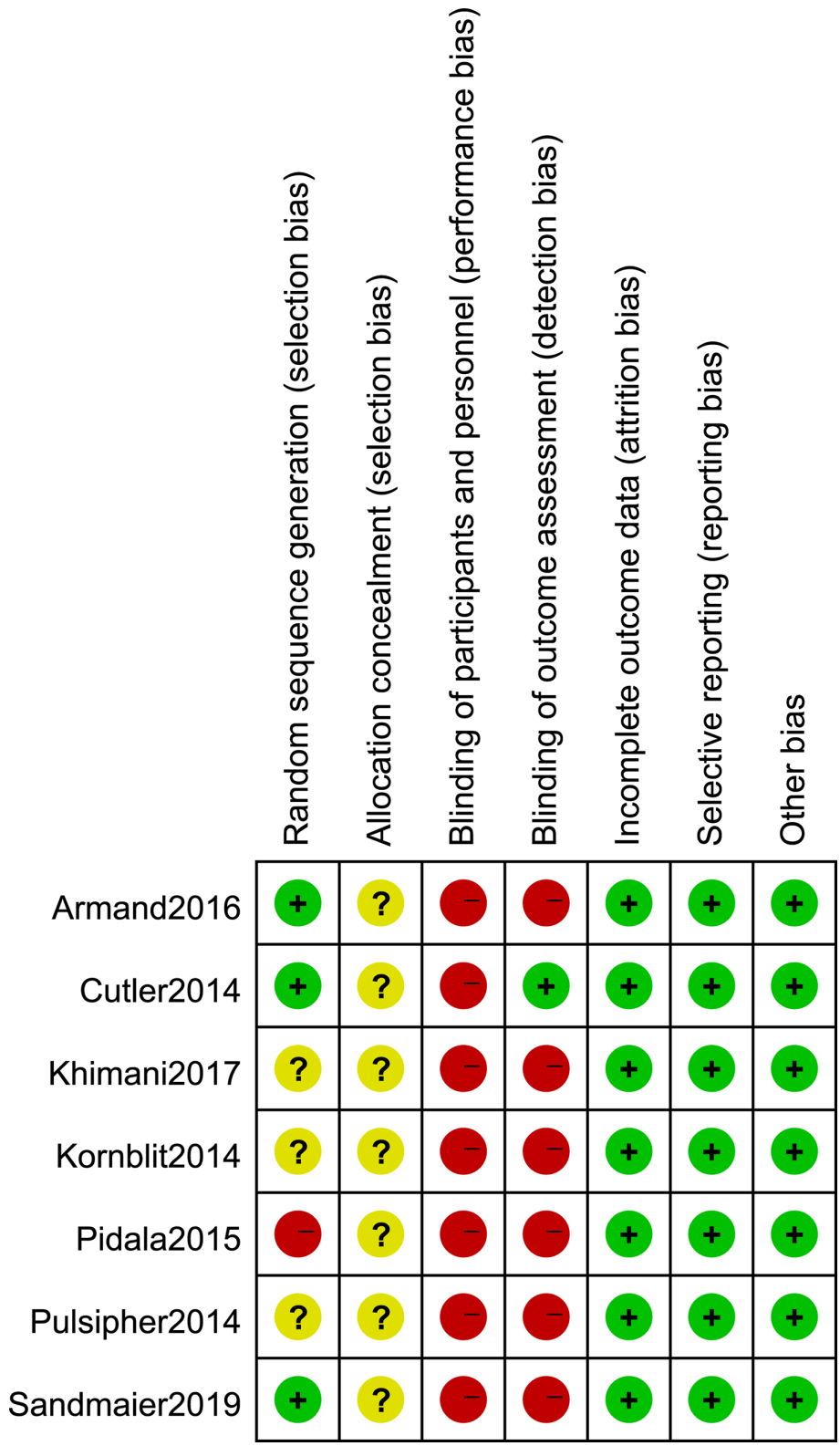


**FIGURE 2** | Risk of bias of included randomized controlled trials.

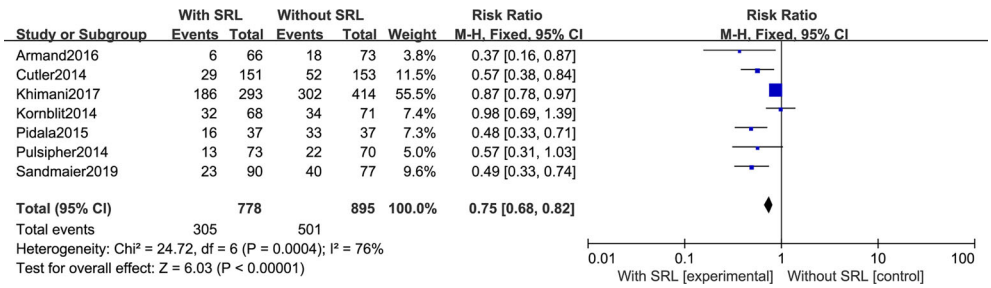


**FIGURE 3** | The effect of addition of SRL to prophylaxis on Grade II to IV aGVHD.

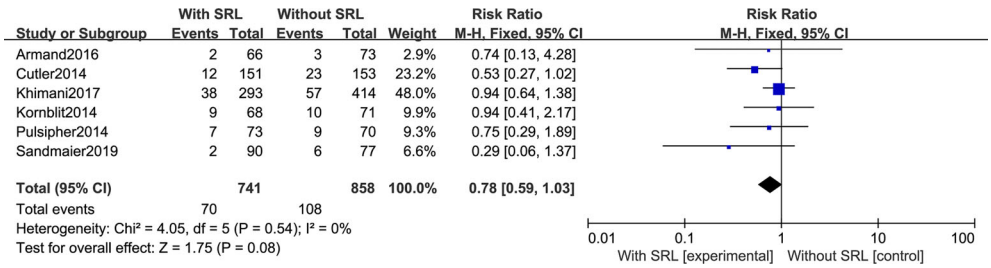


**FIGURE 4** | The effect of addition of SRL to prophylaxis on Grade III to IV aGVHD.

regimen may not prevent all forms of GVHD. This suggests that additional steps may be necessary to prevent cGVHD in the clinic in patients treated with SRL-based regimens.

Meta-analysis showed that the prophylactic regimen containing SRL could reduce acute GVHD but had no effect on OS and PFS. It is known that factors affecting OS and PFS in patients with HSCT are complex, and SRL prophylaxis is not the only factor. Khimani et al. (13) divided the patients into four subgroups according to the hematopoietic cell transplantation–comorbidity index (HCT-CI: creatinine, ejection fraction, FEV1, aspartate aminotransferase, ALT, and bilirubin) (19). Patients with HCT-CI ≥ 4 had significantly worse OS with MTX/TAC than the SRL/TAC group. Thus, it is possible that SRL may improve outcomes in high-risk populations. In addition, SRL combined with post-transplant cyclophosphamide can also provide better survival outcomes in patients after allo-HSCT (20–23). Additional RCTs are required to carefully assess the role of SRL in transplant patient outcomes.

TMA and VOD are both thrombotic diseases that commonly develop post-transplant, and, at present, the pathogenesis of these diseases is unknown. It has been reported that the occurrence of TMA and VOD is related to different regimens, aGVHD, bacterial or fungal infection, HLA mismatch, and combination of drugs (tacrolimus and sirolimus), which caused endothelial injury, thrombosis, and microcirculatory fibrin deposition. Meta-analysis showed that the SRL-based prophylaxes increased the risk of TMA and VOD, suggesting that administration of SRL should be stopped in time when a

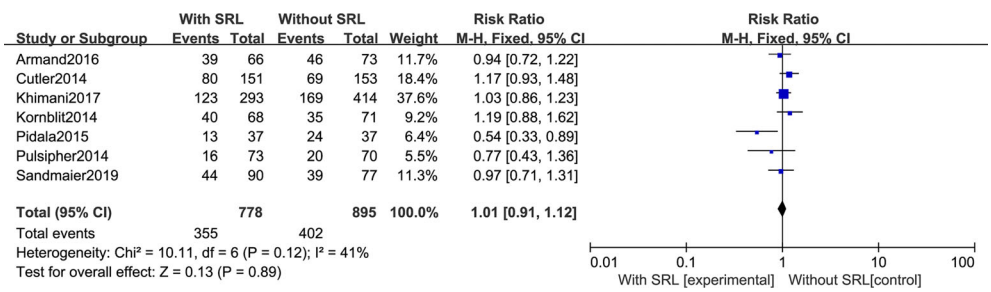


**FIGURE 5** | The effect of addition of SRL to prophylaxis on chronic GVHD.

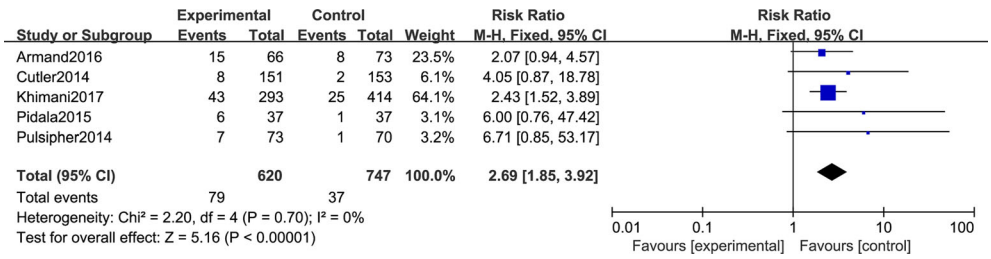


**FIGURE 6** | The effect of SRL-based and non-SRL-based prophylaxis on TMA.

toxic reaction arises caused by thrombogenesis. However, it should be noted that the occurrence of TMA is not necessarily caused by SRL. Pidala et al. (14) reported that the occurrence of TMA in their study was related to use of tacrolimus, which indicates that TMA may also be a result of the combined effect of SRL and TAC. SRL-induced TMA may be attributable to enhanced platelet activation and aggregation, leading to endothelial damage. Another theory involves the pharmacokinetic interaction between sirolimus and calcineurin inhibitors, which may potentially lead to increased serum and kidney levels of these agents (24). TMA is a multifactorial complication, which may be caused by pathogenic microorganism infection (CMV, BK virus, etc.), calcineurin inhibitor and mTOR inhibitor, GVHD, cytokines (IL-6, INF-a, etc), and neutrophil extracellular traps (NET). TMA might primarily be an effect of high-dose Bu treatment, especially in combination with tacrolimus-based GVHD prophylaxis (25).

The addition of SRL on the basis of the prevention of the two drugs may aggravate the immunosuppression and increase the chance of infection in the later stage. However, there were contrary opinions that sirolimus-based GVHD prophylaxis significantly reduced CMV reactivation (26). Additionally, SRL also exerts anti-EB viral (27) and antifungal (28) actions. Our meta-analysis showed that the SRL-containing regimen neither increased nor decreased bacterial, fungal, and CMV infection. Therefore, more RCTs are needed to confirm this conclusion.

In the seven articles, almost all recipients received identical transplants, including HLA-matched sibling or unrelated donors, with no more than a single allele disparity. Only one paper mentioned mismatched unrelated donor (MMUD); in this report, in the SRL/TAC group, 15% of the patients received MMUD, and in the TAC/MTX group, 22% patients received MMUD (13). Although donor source mismatch unrelated and matched sibling have no difference in OS rate according to the

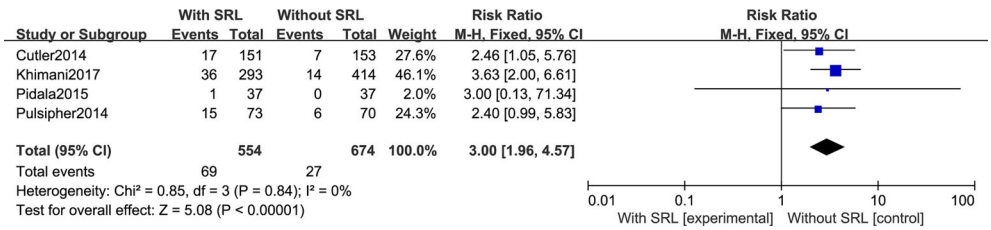


**FIGURE 7** | Impact of SRL-based prophylaxis *versus* non-SRL-based prophylaxis on VOD.

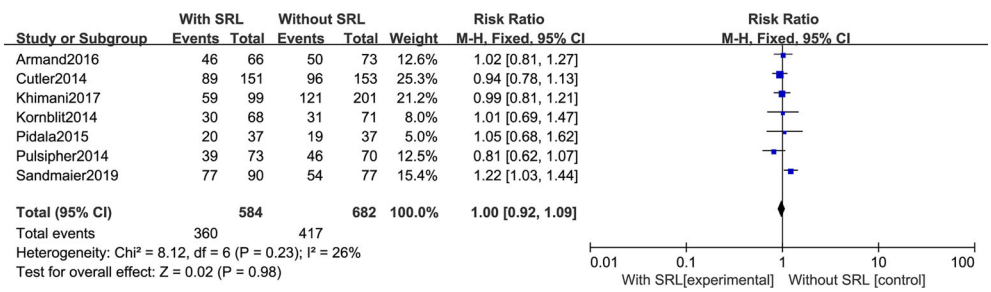


**FIGURE 8** | Impact of SRL-based prophylaxis *versus* non-SRL-based prophylaxis on OS.

GVHD prophylaxis group, it is worth noting that SRL/TAC has been associated with improved OS among patients at high risk for GVHD based on subgroup analysis (13). There are many factors affecting the clinical outcomes of allo-HSCT, including disease status, conditioning regimen, and GVHD prophylaxis. Whether SRL-based prophylaxis is suitable for haploid transplantation requires additional clinical studies.

Due to different classifications of HSCT, such as HLA-matched or mismatched, sibling, or unrelated donors, the prophylaxis schemes of GVHD are different. To minimize heterogeneity, we strictly chose seven papers for this meta-analysis; from the results, addition of sirolimus could be an effective and safe prophylaxis option for GVHD, although the association of SRL with increased thrombotic complications must be carefully monitored and effectively managed. While SRL has some advantages, it is not a first choice for GVHD prophylaxis; however, subgroup analysis may identify additional advantages in high-risk (≥HCT-CI) groups. More adequately powered RCTs are required to better understand the impact of SRL-based GVHD prophylactic regimens.

## DATA AVAILABILITY STATEMENT

The raw data supporting the conclusions of this article will be made available by the authors, without undue reservation.

## AUTHOR CONTRIBUTIONS

YF wrote the original draft and revised the manuscript. XC and YF completed the literature search, data extraction, data analysis, and chart making. KC, HS, LW, TC, HY, SY, and XZ edited this review. XC, XZ, and YF funded the work. All authors contributed to the article and approved the submitted version.

## FUNDING

This work was supported by Chongqing Science and Technology Commission joint project (2021MSXM299) and the Natural Science Foundation of Chongqing (cstc2019jcyj-msxmX0273, cstc2020jcyj-msxmX1086 and cstc2020jcyj-msxmX0448), Science and Technology Innovation Capacity Promotion Project of Army Medical University (2019XLC3014), Special Projects in the Frontier of Military Medicine Natural Science of Xinqiao Hospital (2018 YQYLY002), and National Key Research Program (2017YFA0105502).

## SUPPLEMENTARY MATERIAL

The Supplementary Material for this article can be found online at: https://www.frontiersin.org/articles/10.3389/fonc.2021.683263/full#supplementary-material

## REFERENCES

1. Fuchs EJ, Huang XJ, Miller JS. HLA-Haploidentical Stem Cell Transplantation for Hematologic Malignancies. *Biol Blood Marrow Transplant* (2010) 16:S57–63. doi: 10.1016/j.bbmt.2009.10.032
2. Xu T, Sun D, Chen Y, Ouyang L. Targeting Mtor for Fighting Diseases: A Revisited Review of mTOR Inhibitors. *Eur J Med Chem* (2020) 199:112391. doi: 10.1016/j.ejmech.2020.112391
3. Feng YM, Xiao YS, Yan HJ, Wang P, Zhu W, Cassady K, et al. Sirolimus as Rescue Therapy for Refractory/Relapsed Immune Thrombocytopenia: Results of a Single-Center, Prospective, Single-Arm Study. *Front Med* (2020) 7:110. doi: 10.3389/fmed.2020.00110
4. Feng Y, Chen X, Cassady K, Zou Z, Yang S, Wang Z, et al. The Role of Mtor Inhibitors in Hematologic Disease: From Bench to Bedside. *Front Oncol* (2021) 10:611690. doi: 10.3389/fonc.2020.611690
5. Johnston L, Florek M, Armstrong R, McCune JS, Arai S, Brown J, et al. Sirolimus and Mycophenolate Mofetil as GVHD Prophylaxis in Myeloablative, Matched-Related Donor Hematopoietic Cell Transplantation. *Bone Marrow Transplant* (2012) 47:581–8. doi: 10.1038/bmt.2011.104
6. Furlong T, Kiem HP, Appelbaum FR, Carpenter PA, Deeg HJ, Doney K, et al. Sirolimus in Combination With Cyclosporine or Tacrolimus Plus Methotrexate for Prevention of Graft-*Versus*-Host Disease Following Hematopoietic Cell Transplantation From Unrelated Donors. *Biol Blood Marrow Transplant* (2008) 14:531–7. doi: 10.1016/j.bbmt.2008.02.009
7. Cutler C, Henry NL, Magee C, Li S, Kim HT, Alyea E, et al. Sirolimus and Thrombotic Microangiopathy After Allogeneic Hematopoietic Stem Cell Transplantation. *Biol Blood Marrow Transplant* (2005) 11:551–7. doi: 10.1016/j.bbmt.2005.04.007
8. Labrador J, Lopez-Corral L, Lopez-Godino O, Vazquez L, Cabrero-Calvo M, Perez-Lopez R, et al. Risk Factors for Thrombotic Microangiopathy in Allogeneic Hematopoietic Stem Cell Recipients Receiving GVHD Prophylaxis With Tacrolimus Plus MTX or Sirolimus. *Bone Marrow Transplant* (2014) 49:684–90. doi: 10.1038/bmt.2014.17
9. Higgins JP, Thompson SG. Quantifying Heterogeneity in a Meta-Analysis. *Stat Med* (2002) 21:1539–58. doi: 10.1002/sim.1186
10. Armand P, Kim HT, Sainvil MM, Lange PB, Giardino AA, Bachanova V, et al. The Addition of Sirolimus to the Graft-*Versus*-Host Disease Prophylaxis Regimen in Reduced Intensity Allogeneic Stem Cell Transplantation for Lymphoma: A Multicentre Randomized Trial. *Br J Haematol* (2016) 173:96–104. doi: 10.1111/bjh.13931
11. Pulsipher MA, Langholz B, Wall DA, Schultz KR, Bunin N, Carroll WL, et al. The Addition of Sirolimus to Tacrolimus/Methotrexate GVHD Prophylaxis in Children With ALL: A Phase 3 Children's Oncology Group/Pediatric Blood and Marrow Transplant Consortium Trial. *Blood* (2014) 123:2017–25. doi: 10.1182/blood-2013-10-534297
12. Cutler C, Logan B, Nakamura R, Johnston L, Choi S, Porter D, et al. Tacrolimus/Sirolimus *vs* Tacrolimus/Methotrexate as GVHD Prophylaxis After Matched, Related Donor Allogeneic HCT. *Blood* (2014) 124:1372–7. doi: 10.1182/blood-2014-04-567164
13. Khimani F, Kim J, Chen L, Dean E, Rizk V, Betts B, et al. Predictors of Overall Survival Among Patients Treated With Sirolimus/Tacrolimus vs Methotrexate/Tacrolimus for GvHD Prevention. *Bone Marrow Transplant* (2017) 52:1003–9. doi: 10.1038/bmt.2017.63
14. Pidala J, Kim J, Alsina M, Ayala E, Betts BC, Fernandez HF, et al. Prolonged Sirolimus Administration After Allogeneic Hematopoietic Cell Transplantation Is Associated With Decreased Risk for Moderate-Severe Chronic Graft-*Versus*-Host Disease. *Haematologica* (2015) 100:970–7. doi: 10.3324/haematol.2015.123588
15. Sandmaier BM, Kornblit B, Storer BE, Olesen G, Maris MB, Langston AA, et al. Addition of Sirolimus to Standard Cyclosporine Plus Mycophenolate Mofetil-Based Graft-*Versus*-Host Disease Prophylaxis for Patients After Unrelated Non-Myeloablative Haemopoietic Stem Cell Transplantation: A Multicentre, Randomised, Phase 3 Trial. *Lancet Haematol* (2019) 6:e409–18. doi: 10.1016/S2352-3026(19)30088-2
16. Kornblit B, Maloney DG, Storer BE, Maris MB, Vindelov L, Hari P, et al. A Randomized Phase II Trial of Tacrolimus, Mycophenolate Mofetil and Sirolimus After Non-Myeloablative Unrelated Donor Transplantation. *Haematologica* (2014) 99:1624–31. doi: 10.3324/haematol.2014.108340
17. Park SJ, Kang SJ, Virmani R, Nakano M, Ueda Y. In-Stent Neoatherosclerosis: A Final Common Pathway of Late Stent Failure. *J Am Coll Cardiol* (2012) 59:2051–7. doi: 10.1016/j.jacc.2011.10.909

18. Long C, Cook LG, Hamilton SL, Wu GY, Mitchell BM. FK506 Binding Protein 12/12.6 Depletion Increases Endothelial Nitric Oxide Synthase Threonine 495 Phosphorylation and Blood Pressure. *Hypertension* (2007) 49:569–76. doi: 10.1161/01.HYP.0000257914.80918.72
19. Sorror ML, Maris MB, Storb R, Baron F, Sandmaier BM, Maloney DG, et al. Hematopoietic Cell Transplantation (HCT)-Specific Comorbidity Index: A New Tool for Risk Assessment Before Allogeneic HCT. *Blood* (2005) 106:2912–9. doi: 10.1182/blood-2005-05-2004
20. Montoro J, Roldan E, Pinana JL, Barba P, Chorao P, Quintero A, et al. *Ex Vivo* T-Cell Depletion vs Post-Transplant Cyclophosphamide, Sirolimus, and Mycophenolate Mofetil as Graft-vs-Host Disease Prophylaxis for Allogeneic Hematopoietic Stem Cell Transplantation. *Eur J Haematol* (2021) 106:114–25. doi: 10.1111/ejh.13529
21. Jaiswal SR, Chatterjee S, Mukherjee S, Ray K, Chakrabarti S. Pre-Transplant Sirolimus Might Improve the Outcome of Haploidentical Peripheral Blood Stem Cell Transplantation With Post-Transplant Cyclophosphamide for Patients With Severe Aplastic Anemia. *Bone Marrow Transplant* (2015) 50:873–5. doi: 10.1038/bmt.2015.50
22. Jaiswal SR, Bhakuni P, Zaman S, Bansal S, Bharadwaj P, Bhargava S, et al. T Cell Costimulation Blockade Promotes Transplantation Tolerance in Combination With Sirolimus and Post-Transplantation Cyclophosphamide for Haploidentical Transplantation in Children With Severe Aplastic Anemia. *Transpl Immunol* (2017) 43-44:54–9. doi: 10.1016/j.trim.2017.07.004
23. Jaiswal SR, Bhakuni P, Aiyer HM, Soni M, Bansal S, Chakrabarti S. CTLA4Ig in an Extended Schedule Along With Sirolimus Improves Outcome With a Distinct Pattern of Immune Reconstitution Following Post-Transplantation Cyclophosphamide-Based Haploidentical Transplantation for Hemoglobinopathies. *Biol Blood Marrow Transplant* (2020) 26:1469–76. doi: 10.1016/j.bbmt.2020.05.005
24. Shayani S, Palmer J, Stiller T, Liu X, Thomas SH, Khuu T, et al. Thrombotic Microangiopathy Associated With Sirolimus Level After Allogeneic Hematopoietic Cell Transplantation With Tacrolimus/Sirolimus-Based Graft-*Versus*-Host Disease Prophylaxis. *Biol Blood Marrow Transplant* (2013) 19:298–304. doi: 10.1016/j.bbmt.2012.10.006
25. Hassan Z, Hellstrom-Lindberg E, Alsadi S, Edgren M, Hagglund H, Hassan M. The Effect of Modulation of Glutathione Cellular Content on Busulphan-Induced Cytotoxicity on Hematopoietic Cells *In Vitro* and *In Vivo*. *Bone Marrow Transplant* (2002) 30:141–7. doi: 10.1038/sj.bmt.1703615
26. Marty FM, Bryar J, Browne SK, Schwarzberg T, Ho VT, Bassett IV, et al. Sirolimus-Based Graft-*Versus*-Host Disease Prophylaxis Protects Against Cytomegalovirus Reactivation After Allogeneic Hematopoietic Stem Cell Transplantation: A Cohort Analysis. *Blood* (2007) 110:490–500. doi: 10.1182/blood-2007-01-069294
27. Krams SM, Martinez OM. Epstein-Barr Virus, Rapamycin, and Host Immune Responses. *Curr Opin Organ Transplant* (2008) 13:563–8. doi: 10.1097/MOT.0b013e3283186ba9
28. Vezina C, Kudelski A, Sehgal SN. Rapamycin (AY-22,989), a New Antifungal Antibiotic. I. Taxonomy of the Producing Streptomycete and Isolation of the Active Principle. *J Antibiot (Tokyo)* (1975) 28:721–6. doi: 10.7164/antibiotics.28.721

**Conflict of Interest:** The authors declare that the research was conducted in the absence of any commercial or financial relationships that could be construed as a potential conflict of interest.

**Publisher's Note:** All claims expressed in this article are solely those of the authors and do not necessarily represent those of their affiliated organizations, or those of the publisher, the editors and the reviewers. Any product that may be evaluated in this article, or claim that may be made by its manufacturer, is not guaranteed or endorsed by the publisher.

frontiers in Oncology

ORIGINAL RESEARCH
published: 10 September 2021
doi: 10.3389/fonc.2021.731478

# Treosulfan-Based Conditioning Regimen Prior to Allogeneic Stem Cell Transplantation: Long-Term Results From a Phase 2 Clinical Trial

*Lorenzo Lazzari[1], Annalisa Ruggeri[1], Maria Teresa Lupo Stanghellini[1], Sara Mastaglio[1], Carlo Messina[1], Fabio Giglio[1], Alessandro Lorusso[2], Tommaso Perini[1], Simona Piemontese[1], Magda Marcatti[1], Francesca Lorentino[1,3], Elisabetta Xue[1], Daniela Clerici[1], Consuelo Corti[1], Massimo Bernardi[1], Andrea Assanelli[1], Raffaella Greco[1]*, Fabio Ciceri[1,4]* and Jacopo Peccatori[1]*

[1] Haematology and Bone Marrow Transplant Unit, IRCCS San Raffaele Scientific Institute, Milan, Italy, [2] Department of Hematology, Oncology and Tumor Immunology Charité-Universitätsmedizin Berlin, Berlin, Germany, [3] PhD Program in Public Health, Department of Medicine and Surgery, University of Milano Bicocca, Milan, Italy, [4] Università Vita-Salute San Raffaele, Milan, Italy

OPEN ACCESS

**Edited by:**
Monica Thakar,
Fred Hutchinson Cancer Research Center, United States

**Reviewed by:**
Eneida Nemecek,
Oregon Health & Science University, United States
Filippo Milano,
Fred Hutchinson Cancer Research Center, United States

***Correspondence:**
Raffaella Greco
greco.raffaella@hsr.it
Fabio Ciceri
ciceri.fabio@hsr.it

**Specialty section:**
This article was submitted to Hematologic Malignancies, a section of the journal Frontiers in Oncology

**Received:** 27 June 2021
**Accepted:** 23 August 2021
**Published:** 10 September 2021

**Citation:**
Lazzari L, Ruggeri A, Lupo Stanghellini MT, Mastaglio S, Messina C, Giglio F, Lorusso A, Perini T, Piemontese S, Marcatti M, Lorentino F, Xue E, Clerici D, Corti C, Bernardi M, Assanelli A, Greco R, Ciceri F and Peccatori J (2021) Treosulfan-Based Conditioning Regimen Prior to Allogeneic Stem Cell Transplantation: Long-Term Results From a Phase 2 Clinical Trial. Front. Oncol. 11:731478. doi: 10.3389/fonc.2021.731478

**Introduction:** Reducing toxicities while preserving efficacy in allogeneic stem cell transplant (allo-HCT) remains a particularly challenging problem. Different strategies to enhance the antitumor activity without increasing early and late adverse toxicities of the conditioning regimens have been investigated.

**Methods:** The aim of "AlloTreo" prospective phase 2 clinical trial was to evaluate the efficacy and safety of a conditioning regimen based on Treosulfan (42 g/m$^2$) and fludarabine (https://clinicaltrials.gov/ct2/show/NCT00598624). We enrolled 108 patients with hematological diseases who received a first allo-HCT between June 2005 and January 2011, inside the frame of this trial at our center. Median age at allo-HCT was 49 (21–69) years. Disease Risk Index was low in 14 (13%) patients, intermediate in 73 (67.7%), high in 17 (15.7%), and very high in 4 (3.7%). Donors were human leukocyte antigen (HLA)-matched related in 50 cases, 10/10-matched unrelated in 36, and 9/10-mismatched unrelated in 22. Graft-*versus*-host disease (GvHD) prophylaxis consisted of cyclosporine-A and methotrexate. Anti-T-lymphocyte globulin (ATLG) was administered in patients receiving unrelated allo-HCT. Stem cell source was mainly peripheral blood stem cells (95%).

**Results:** Conditioning regimen was well tolerated. Full donor chimerism was documented for most patients (88%) at day +30. At 12 years, overall survival (OS) was 41.7% (32.2%–50.9%), progression-free survival (PFS) was 31.7% (23%–40.7%), GvHD-free/relapse-free survival was 20.9% (13.7%–29.1%), cumulative incidence (CI) of relapse was 44.5% (34.9%–53.6%), and transplant-related mortality (TRM) was 22.5% (15.1%–30.9%). CI of acute GvHD grades II–IV was 27.8% (19.7%–36.5%) at 100 days; 12-year CI of chronic GvHD was 40.7% (31.3%–49.9%). Relevant long-term adverse effects were 10 secondary malignancy, 3 fatal cardiovascular events, and 1 late-onset transplant-associated thrombotic microangiopathy. Ten successful pregnancies were reported

after allo-HCT. In multivariate analysis, older age (≥60 years) at transplant [hazard ratio (HR), 2.157; p = 0.004] and a high/very high disease risk index (HR, 1.913; p = 0.026) were significantly associated with a lower OS.

**Conclusions:** Overall, our data confirmed the myeloablative potential and safe toxicity profile of full dose Treo (42 g/m$^2$) especially for the younger population.

**Keywords: Treosulfan, ATLG, allogeneic transplant, reduced toxicity, conditioning regimen**

## INTRODUCTION

Allogeneic hematopoietic stem cell transplantation (allo-HCT) is an increasingly offered treatment option for the management of hematological malignancies (1). Transplant-related mortality (TRM) has fallen in the past 40 years; however, the major causes of treatment failure remain disease relapse and treatment toxicities (2). The use of reduced intensity conditioning regimens (RICs) coupled with expansion of alternative donor stem cell sources has dramatically increased the number of patients who can benefit from allo-HCT. The introduction into clinical practice of less toxic chemotherapeutic agents, new antimicrobials, and more effective graft-*versus*-host disease (GvHD) treatments has significantly reduced TRM over the last decades (3). In this context, optimization of both patient selection and conditioning regimen is critical to improve outcomes.

The conditioning regimen given prior to allo-HCT has the aim of suppressing host immunity, allowing donor cell engraftment, and ablating the underlying malignancy. Bacigalupo et al. (4) have classified the intensity of conditioning regimens into myeloablative (MAC), RIC, and non-myeloablative based on the expected duration and reversibility of cytopenias. Even if more effective against disease relapse, MAC regimens also enhance toxicities, further limiting the overall outcome of allo-HCT. Reduced-toxicity conditioning (RTC) regimens, based on the use of fludarabine and an alkylating agent, have been designed to allow a safer administration of dose-intensive myeloablative therapy (5, 6). This area of investigation will likely continue to be of interest in terms of optimizing transplant results.

Treosulfan (Treo), a water-soluble bifunctional alkylating drug, demonstrated an advantageous toxicity profile over standard conditioning regimens in preliminary experiences (7, 8). It has been increasingly applied to pediatric and adult patients with hematological malignancies, showing low risk of organ toxicity and treatment-related mortality combined with effective immunosuppressive and cytotoxic properties (9–14). In a recent multicenter randomized phase 3 trial, Treo demonstrated non-inferiority over busulfan (Bu) when used in combination with fludarabine in patients with advanced age or comorbidities, suggesting a potential to become a standard preparative regimen in this population (15).

The aim of the "AlloTreo" study—a prospective, multicenter, non-randomized, open-label, phase 2 clinical trial—was to evaluate the efficacy and safety of Treo in combination with fludarabine as a preparative regimen for allo-HCT. Herein, we report the long-term outcomes for this study population.

## MATERIALS AND METHODS

This is a long-term, single-center, retrospective analysis of prospectively collected data from the clinical phase 2 multicentric trial "AlloTreo." Primary endpoint of this trial was neutrophil engraftment and the incidence of CTC-AE grade 3 and 4 adverse events. Secondary endpoints were the evaluation of overall survival (OS), progression-free survival (PFS), TRM, cumulative incidence (CI) of relapse/progression, CI of acute GvHD (aGvHD) and chronic GvHD (cGvHD), bone marrow donor chimerism at +28 and +100, and the incidence of Epstein–Barr virus (EBV) reactivations. The study protocol was approved by the institutional review board of San Raffaele Scientific Institute and complied with our country-specific regulatory requirements. The study was conducted in accordance with the Declaration of Helsinki and good clinical practice guidelines. Written informed consent was provided by all patients. Inclusion and exclusion criteria of the trial are provided in **Table S1**.

We included in this long-term analysis those patients who received an allo-HCT at our center from a matched-related or unrelated donor using peripheral blood stem cell (PBSC) or bone marrow (BM) as a source. Overall, we included in this study 108 patients with hematological diseases—99 enrolled in the "AlloTreo" study and 9 inside a pilot project performed before starting with the trial—who received a first allo-HCT at San Raffaele Scientific Institute in Milan between June 2005 and January 2011. The last follow-up was January 1, 2021.

The RTC regimen consisted of Treo 14 g/m$^2$ daily for 3 days (from day −6 to −4) and fludarabine 30 mg/m$^2$ for 5 days (from day −6 to −2) (**Figure S1**). GvHD prophylaxis consisted of cyclosporine-A (CSA) from day −1 and methotrexate 15 mg/m$^2$ on day +1, with consecutive doses of 10 mg/m$^2$ given on days +3 and +6. Anti T-lymphocyte globulin (ATLG, Neovii) was given as part of the conditioning regimen (10 mg/kg from day −4 to −2) to patients receiving grafts from an unrelated donor. A single dose of Rituximab 500 mg was added in these cases considering the high risk of posttransplant lymphoproliferative disorders related to the *in vivo* T-cell depletion. Supportive care and antimicrobial prophylaxis followed institutional guidelines.

### Study Definitions

Complete remission was defined in case of absence of disease activity by BM evaluation or imaging, according to the underlying disease. All patients not falling within this definition were categorized as having active disease. Additionally, patients were

stratified by status at the time of transplantation according to the disease risk index (DRI) defined by Armand et al. (16). Comorbidities at time of transplantation were evaluated according to the hematopoietic cell transplantation-specific comorbidity index (HCT-CI) (17). Human leukocyte antigen (HLA) compatibility among donor–recipient pairs was assessed by 10 loci molecular typing (HLA-A, HLA-B, HLA-C, HLA-DRB1, and HLA-DQB1) at the allelic level.

Neutrophil engraftment was defined as the first of 3 consecutive days with neutrophil counts $\geq 0.5 \times 10^9$/L after transplantation, and platelet engraftment was defined as platelet counts $\geq 20 \times 10^9$/L in the absence of growth factors or transfusions during the preceding 7 days. Disease follow-up during posttransplant period consisted of BM evaluations carried out monthly for the first 3 months and then two times a year for the first 5 years. Donor-recipient chimerism was assessed on unfractionated BM aspirate samples with a commercial assay based on short-tandem repeats analysis (AmpFISTR Profiler Plus PCR Kit; Applied Biosystem, Carlsbad, CA). Patients were considered fully chimeric if their unfractionated BM samples were ≥95% donor.

Clinical diagnosis and grading of aGvHD were made according the Glucksberg criteria (18), while cGvHD diagnosis and grading were based on the National Institutes of Health consensus criteria (19). GvHD was treated per institutional protocols considering the European Society for Blood and Marrow Transplantation recommendations. Tapering of GvHD prophylaxis occurred as per protocol, in the absence of GvHD signs, starting from day +90 after allo-HCT, and definitively withdrawn at day +180. Cytomegalovirus (CMV) and EBV were monitored at least weekly until day +100 in peripheral blood plasma samples.

## Statistical Analysis

Primary endpoint of our retrospective analysis was OS. Secondary endpoints were PFS, TRM, incidence of neutrophils and platelets engraftment, CI of relapse/progression (RI), and CI of acute and chronic GvHD. OS was defined as the time from transplant to death from all causes. PFS was defined as the time to death or relapse/progression, whichever came first. TRM was defined as death without evidence of relapse. Competing risks were as follows: death without engraftment for engraftment, death without relapse for RI, relapse for TRM, and death without GvHD for aGvHD and cGvHD.

Main clinical characteristics were studied for associations with outcomes by univariate analysis using the log-rank test for PFS, OS, and GvHD-free/relapse-free survival (GRFS), while Grey's test was employed for CI of aGvHD, cGvHD, RI, and TRM. A 95% confidence interval (95% CI) was considered. A p-value lower than 0.05 was interpreted as significant.

Multivariate analysis was performed using the Cox proportional-hazard model. All factors known to influence outcome and factors associated with a univariate analysis $p < 0.10$ were first included in the model. Subsequently, a stepwise backward procedure was used with a cutoff significance level of 0.10 for deleting factors from the model. The type I error rate was fixed at 0.05 for determination of factors associated with time to event.

Analyses were performed using SPSS version 25.0 (IBM Corporation, Armonk, NY) and R statistical software version 4.0.4 (R Development Core Team, Vienna, Austria).

# RESULTS

Patients' and transplant characteristics are provided in **Table 1**. Acute myeloid leukemia (AML) was the most common disease with 36 cases (33.3%), followed by non-Hodgkin's lymphoma (NHL; n = 21, 19.5%) and myelodysplastic syndrome (MDS; n = 15, 13.9%). Donor types were as follows: matched related donor (MRD) in 50 cases, 10/10-matched unrelated donor (MUD) in 36, and 9/10-mismatched unrelated donor (MMUD) in 22 patients. The source of stem cells mainly consisted in unmanipulated PBSC (95%); only five patients underwent a BM allo-HCT. Almost half of the patients (45%) were transplanted in complete remission: 37 in first complete remission (CR1) and 12 in second or subsequent complete remission (CR ≥ 2). Disease status at the time of allo-HCT for the remaining 55 patients was partial remission (PR) in 18 (16.7%) cases and active/advanced disease (AD) in 37 (34.3%), 19 (17.6%) of which, mainly suffering from myelodysplastic syndrome or primary myelofibrosis, received an upfront allo-HCT. DRI was low/intermediate in 87 (80.6%) patients and high/very high in 21 (19.4%). Median HCT-CI was 1 (range, 0–7): 0–1 in 57 (52.8%) patients, 2–3 in 35 (32.4%), and ≥4 in 16 (14.8%) cases. Median follow-up was 148 (range, 58–189) months.

## OS, PSF, and GRFS

At 12 years, OS was 41.7% (95% CI, 32.2%–50.9%), PFS was 31.7% (95% CI, 23%–40.7%), and GRFS was 20.9% (95% CI, 13.7%–29.1%) (**Figure 1**).

Results of the univariate analysis are reported in **Table 2**. In multivariate analysis, risk factors for a lower OS were age ≥60 years and having a high/very high DRI. Transplantation using a MUD and a high/very high DRI were independently associated with lower PFS (**Table 3**).

## Toxicity, Viral Infections, and Fertility

Conditioning regimen was well tolerated: non-hematological adverse events mainly consisted of low grade (CTC-AE grades 1 and 2) gastrointestinal mucositis and skin rash. Two patients died due to infectious complications before neutrophil engraftment. No other CTC-AE grade 3 or 4 conditioning-related adverse events occurred. Hepatic sinusoidal obstruction syndrome (SOS) cases were not documented.

CMV reactivations occurred in 63 (58.3%) patients. Five cases developed a CMV disease and were treated according to institutional guidelines. EBV reactivation occurred in three (2.8%) patients, prompting the need for Rituximab treatment in two of them according to institutional guidelines. No cases of post-transplant lymphoproliferative disease were documented.

Ten (22%) of our 45 long-term survivors were diagnosed with a second cancer during follow-up. Median time from allo-HCT

**TABLE 1** | Patients' and transplant characteristics.

| | | TOTAL (*N*=108) |
|---|---|---|
| **Patient age years, median (range)** | | 49 (21-69) |
| **Patient sex, male (%)** | | 76 (70) |
| **HCT-CI, median (range)** | | 1 (0-7) |
| **Diagnosis, *n* (%)** | AML | 36 (33.3) |
| | ALL | 11 (10.2) |
| | MPAL | 1 (0.9) |
| | MDS | 15 (13.9) |
| | CML | 1 (0.9) |
| | MPD | 7 (6.5) |
| | MDS/MPN | 2 (1.9) |
| | MM | 5 (4.6) |
| | HL | 4 (3.7) |
| | NHL | 21 (19.4) |
| | CLL | 4 (3.7) |
| | Other | 1 (0.9) |
| **Disease status at transplant, *n* (%)** | CR1 | 40 (37) |
| | CR≥2 | 13 (12) |
| | PR | 18 (16.7) |
| | Relapse/PD | 18 (16.7) |
| | Upfront | 19 (17.6) |
| **DRI, *n* (%)** | Low | 14 (13) |
| | Intermediate | 73 (67.6) |
| | High | 17 (15.7) |
| | Very high | 4 (3.7) |
| **Type of donor, *n* (%)** | MRD | 50 (46.3) |
| | MUD | 36 (33.3) |
| | MMUD | 22 (20.4) |
| **ATLG, *n* (%)** | | 58 (53.7) |
| **Stem cell source, *n* (%)** | PBSC | 103 (95.4) |
| | BM | |
| **PBSC graft content, median (range)** | CD45+ cells x$10^8$/Kg | 8.7 (1.3-25.5) |
| | CD34+ cells x$10^6$/Kg | 7.0 (2.6-17.8) |
| | CD3+ cells x$10^8$/Kg | 3.0 (0.6-9.9) |
| **BM graft content, median (range)** | CD45+ cells x$10^8$/Kg | 3.1 (2.6-8.5) |
| | CD34+ cells x$10^6$/Kg | 4.0 (2.4-7.0) |
| | CD3+ cells x$10^6$/Kg | 0.8 (0.3-12.2) |
| **H/D CMV status, *n* (%)** | pos/pos | 62 (57.5) |
| | pos/neg | 31 (28.7) |
| | neg/pos | 6 (5.5) |
| | neg/neg | 9 (8.3) |

*HCT-CI, Hematopoietic cell transplantation-comorbidity index; AML, acute myeloid leukemia; ALL, acute lymphoblastic leukemia; MPAL, mixed phenotype acute leukemia; MDS, myelodysplastic syndromes; CML, chronic myeloid leukemia; MPN, myeloproliferative neoplasm; MDS/MPN, myelodysplastic-myeloproliferative neoplasms; MM, multiple myeloma; HL, Hodgkin lymphoma; NHL, non-Hodgkin lymphoma; CLL, chronic lymphocytic leukemia; CR1, first complete remission; CR2, second complete remission; PR, partial remission; PD, progressive disease; DRI, Disease Risk Index; MRD, matched related donor; MUD, matched unrelated donor; MMUD, mismatched unrelated donor; ATLG, anti T-lymphocyte globulin; PBSC, peripheral blood stem cells; BM, bone marrow; H/D, host/donor; CMV, cytomegalovirus.*

to diagnosis of the secondary solid tumor was 7.9 (1.3–11) years. Second cancer types were as follows: three non-melanoma skin cancer (one basal and two squamous cell carcinomas), one renal neoplasia, one metastatic colon cancer, four pulmonary neoplasms, and one gastric tumor. Four of these patients were previously diagnosed with cGvHD and received an immunosuppressive treatment before the development of the second malignancy. Three of these patients died due to cancer-related complications. Two women were diagnosed with a human papillomavirus-related cervical intraepithelial neoplasia after allo-HCT. No secondary hematological malignancies were observed during the follow-up.

Other toxicities diagnosed during long-term follow-up in long-term survivors were hypothyroidism (five cases), acute myocardial infarction (two cases), ischemic stroke (two cases), heart failure associated with chronic atrial fibrillation (one case), cutaneous herpes zoster (five cases), postherpetic neuralgia (two cases), secondary hemosiderosis treated with deferasirox or phlebotomy (six cases), and avascular necrosis of the femoral head (four cases).

At last follow-up, 10 successful pregnancies were reported after allo-HCT by 6 patients (5 men and 1 woman). Median age at transplant of this group was 31 (range, 25–41) years. The pregnancies resulted in successful deliveries of 10 live-born singletons (3 boys and 7 girls). Pregnancy outcome was uncomplicated in all cases, and there was no delivery-related complication in the mothers. Seven pregnancies were achieved with spontaneous conception, while two men reported use of

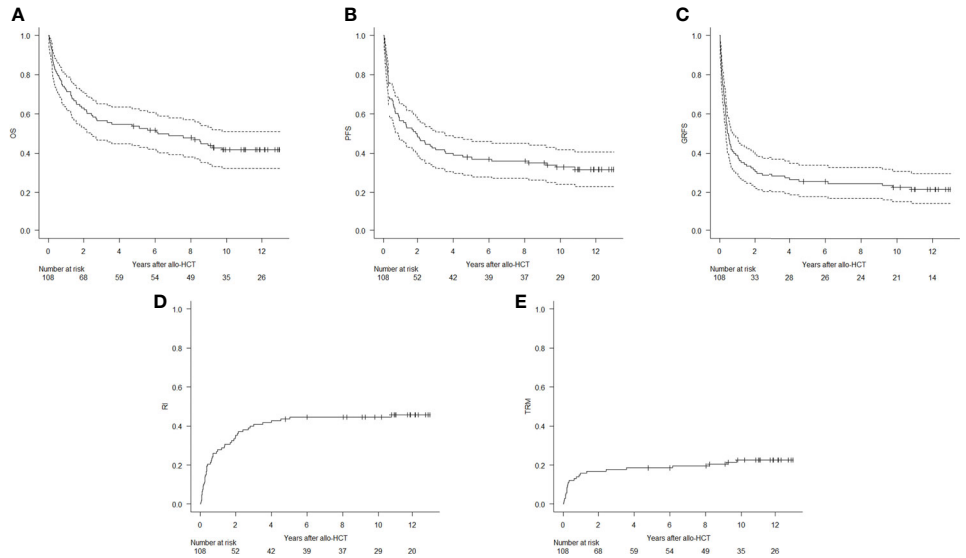


**FIGURE 1** | Kaplan–Meier estimates of overall survival (OS, **A**), progression-free survival (PFS, **B**), and graft-*versus*-host-free/relapse-free survival (GRFS, **C**), and cumulative incidence of relapse/progression (RI, **D**) and transplant-related mortality (TRM, **E**).

cryopreserved sperm (one case unknown). The only woman that successfully carried a pregnancy to term was transplanted from her HLA-identical sister at the age of 28 for an intermediate risk AML in CR1. During the posttransplant period, she was diagnosed with moderate cGvHD at day +192 managed with topical therapy and immunosuppression adjustments; CSA was definitively suspended after 9 months from diagnosis. Pregnancy was reported after 7 years from the date of allo-HCT. No sign of disease recurrence or GvHD flare-up was documented at last follow-up.

## Engraftment and GvHD

The CI of engraftment was 96% at day +28 for neutrophils and 95% at day +100 for platelets. Median time to neutrophil and platelet engraftment was 16 (range, 11–39) days and 14 (range, 8–47) days, respectively. No primary or secondary graft failure was observed. Day +28 chimerism was evaluable in 101 patients, 95 of which displayed a ≥95% donor chimerism. Three more patients converted to full donor chimerism at the evaluation of day +100.

**TABLE 2** | Univariate analysis for significant transplant outcomes at 12 years.

| Variables | Median (95% CI) | | | | |
|---|---|---|---|---|---|
| | OS | PFS | GRFS | TRM | RI |
| **Recipient age** | | | | | |
| **<60 years** | 50.1% (38.7–60.5) | 39.3% (28.7–49.8) | 24.6% (15.8–34.4) | 16.2% (9.2–25.1) | 44.4% (33.3–54.9) |
| **≥60 years** | 16.5% (5.3–33) | 6.7% (0.6–23.7) | 6.9% (0.7–24.3) | 41.6% (22.1–60) | 51.1% (27.3–70.7) |
| | ***p = 0.001*** | ***p = 0.019*** | *p = 0.199* | ***p = 0.004*** | *p = 0.916* |
| **DRI** | | | | | |
| **Low/intermediate** | 46.1% (35.2–56.4) | 38.7% (28.4–48.8) | 25.1% (16.5–24.6) | 22.1% (14–31.5) | 39.1% (28.8–49.3) |
| **High/very high** | 23.8% (8.7–43.1) | 4.8% (0.3–19.7) | 4.8% (0.3–19.7) | 23.8% (8.2–43.9) | 71.4% (44–87.1) |
| | ***p = 0.015*** | ***p < 0.001*** | ***p = 0.008*** | *p = 0.986* | ***p = 0.002*** |
| **Donor type** | | | | | |
| **MRD** | 48.5% (33.8–61.8) | 43.1% (28.9–56.4) | 21.7% (11.5–33.9) | 14.8% (6.4–26.6) | 42% (28.1–55.3) |
| **MUD** | 32.7% (18.2–48.2) | 11.9% (3.6–25.7) | 12.2% (3.7–26) | 30.8% (16.4–46.3) | 57.1% (37.9–72.4) |
| **MMUD** | 40.9% (20.9–60.1) | 36.4% (17.4–55.7) | 31.8% (14.2–51.1) | 27.3% (10.7–47) | 36.4% (16.8–56.3) |
| | *p = 0.161* | ***p = 0.016*** | *p = 0.331* | *p = 0.097* | *p = 0.373* |
| **ATLG** | | | | | |
| **Yes** | 35.8% (23.7–48) | 21.8% (12.2–33.3) | 21.7% (11.5–33.9) | 29.4% (18.2–41.5) | 48.6% (35–61) |
| **No** | 48.5% (33.8–61.8) | 43.1% (28.9–56.4) | 20.3% (11–31.5) | 14.8% (6.4–26.6) | 42% (28.1–55.3) |
| | *p = 0.073* | ***p = 0.02*** | *p = 0.537* | ***p = 0.031*** | *p = 0.731* |

*Outcomes were not statistically different if patients were grouped according to HCT-CI score, host/donor CMV mismatch, or stem cell source (not shown).*
*CI, confidence interval; OS, overall survival; PFS, progression-free survival; GRFS, graft-versus-host-free/relapse-free survival; TRM, transplant-related mortality; RI, relapse incidence; DRI, disease risk index; MRD, matched related donor; MUD, matched unrelated donor; MMUD, 9/10-mismatched unrelated donor; ATLG, anti T-lymphocyte globulin.*
*Bold values were statistically significant.*

**TABLE 3** | Multivariate analysis for main outcomes.

| | HR | 95%CI per HR | | p-value |
|---|---|---|---|---|
| | | Lower | Upper | |
| ***OS*** | | | | |
| **Age ≥60 *vs*. <60** | **2.157** | **1.286** | **3.616** | **0.004** |
| **HCT-CI ≥3 *vs*. <3** | 1.233 | 0.733 | 2.076 | 0.430 |
| **DRI H/VH *vs*. L/I** | **1.913** | **1.081** | **3.386** | **0.026** |
| **MMUD *vs*. MRD** | 1.253 | 0.636 | 2.470 | 0.515 |
| **MUD *vs*. MRD** | 1.543 | 0.875 | 2.722 | 0.134 |
| **ATLG *vs*. no ATLG** | 1.205 | 0.606 | 2.395 | 0.594 |
| ***PFS*** | | | | |
| **Age ≥60 *vs*. <60** | 1.588 | 0.972 | 2.596 | 0.065 |
| **HCT-CI ≥3 *vs*. <3** | 1.242 | 0.764 | 2.019 | 0.383 |
| **DRI H/VH *vs*. L/I** | **2.304** | **1.351** | **3.930** | **0.002** |
| **MMUD *vs*. MRD** | 1.335 | 0.704 | 2.530 | 0.376 |
| **MUD *vs*. MRD** | **1.880** | **1.117** | **3.167** | **0.018** |
| **ATLG *vs*. no ATLG** | 1.281 | 0.671 | 2.447 | 0.453 |
| ***TRM*** | | | | |
| **Age ≥60 *vs*. <60** | **3.072** | **1.381** | **6.831** | **0.006** |
| **HCT-CI ≥3 *vs*. <3** | 1.449 | 0.647 | 3.245 | 0.367 |
| **DRI H/VH *vs*. L/I** | 1.209 | 0.445 | 3.285 | 0.709 |
| **MMUD *vs*. MRD** | 1.398 | 0.528 | 3.700 | 0.500 |
| **MUD *vs*. MRD** | 1.734 | 0.585 | 5.142 | 0.321 |
| **ATLG *vs*. no ATLG** | 2.230 | 0.922 | 5.394 | 0.075 |
| ***RI*** | | | | |
| **Age ≥60 *vs*. <60** | 1.115 | 0.586 | 2.122 | 0.741 |
| **HCT-CI ≥3 *vs*. <3** | 1.072 | 0.581 | 1.979 | 0.824 |
| **DRI H/VH *vs*. L/I** | **3.086** | **1.664** | **5.724** | **<0.001** |
| **MMUD *vs*. MRD** | 1.061 | 0.466 | 2.415 | 0.889 |
| **MUD *vs*. MRD** | 1.607 | 0.865 | 2.984 | 0.133 |
| **ATLG *vs*. no ATLG** | 1.029 | 0.446 | 2.378 | 0.946 |

*CI, confidence interval; HR, hazard ratio; OS, overall survival; PFS, progression-free survival; TRM, transplant-related mortality; RI, relapse incidence; HCT-CI, hematopoietic cell transplantation-specific comorbidity index; DRI, disease risk index; H, high; VH, very high; L, low; I, intermediate; MMUD, 9/10-mismatched unrelated donor; MUD, 10/10-matched unrelated donor; ATLG, anti T-lymphocyte globulin.*

*Bold values were statistically significant.*

The 100-day CI of aGvHD grade II–IV and grade III–IV was 27.8% (95% CI, 19.7%–36.5%) and 14.8% (95% CI, 8.9%–22.2%), respectively (**Figure 2**). Median time to development of aGvHD was 68 days. Skin was the most frequent organ affected by aGvHD: 30 cases displayed an isolated cutaneous form, while other 16 cases developed a skin involvement in association with a visceral one (6 with lower gastrointestinal and 10 with liver disease). Acute GvHD with isolated visceral organ involvement was diagnosed in 10 cases (2 lower gastrointestinal and 8 liver disease). In univariate analysis, the administration of ATLG did not show a significant difference in the CI of aGvHD grade II–IV [32.8% (95% CI, 21%–45%) for the ATLG group *versus* 22% (95% CI, 11.7%–34.4%); p = 0.432] and grade III–IV [15.5% (95% CI, 7.6%–26%) for the ATLG group *versus* 14% (95% CI, 6.1%–25.1%); p = 0.61] (**Figure 3**). Similarly, disease status at transplant and donor type had no impact for these two outcomes.

At 6 years, the CI of cGvHD and moderate-to-severe cGvHD was 40.7% (95% CI, 31.3%–49.9%) and 21.3% (95% CI, 14.1%–29.5%), respectively (**Figure 2**). Median time to cGvHD occurrence was 267 days. In univariate analysis, ATLG administration was associated with a significant reduction in the 6-year CI of moderate-to-severe cGvHD [13.8% (95% CI, 6.4%–24.1%) for the ATLG group *versus* 30% (95% CI, 17.9%–43.1%); p = 0.0475], while there was no difference in the CI of cGvHD all grades [34.5% (95% CI, 22.4%–46.9%) for the ATLG group *versus* 48% (95% CI, 33.4%–61.2%); p = 0.178] (**Figure 3**). Median length of CSA administration was 220 (range, 25–1,966) days. Overall, 25 (15 MRD, 6 MUD, and 4 MMUD) patients developed a moderate-to-severe cGvHD requiring a prolonged systemic immunosuppressive therapy. Organ involvements of patients diagnosed with cGvHD are displayed in **Figure 4** and **Figure S2**. At the time of last follow-up, 41 of 47 patients were alive and off their assigned immunosuppression.

## Relapse and TRM

RI was 44.5% (95% CI, 34.9%–53.6%) at 12 years (**Figure 1**). Median time for relapse occurrence was 8 (range, 0.4–131.5) months. Overall, forty-nine (45%) patients died from disease relapse/progression. There was no difference in the 12-year RI between the four more frequent disease types in our cohort [44% (95% CI, 27.6%–60%) for AML, 36.4% (95% CI, 10%–64.2%) for acute lymphoblastic leukemia, 35% (95% CI, 11.1%–60.6%) for MDS, and 42.9% (95% CI, 21.1%–63.1%) for NHL; p = 0.865].

Twenty patients received a second allo-HCT for disease relapse after a median of 256 (range, 28–1,870) days from the first allo-HCT. In 11 cases a different donor was chosen: 10 patients underwent a haploidentical family donor allo-HCT and

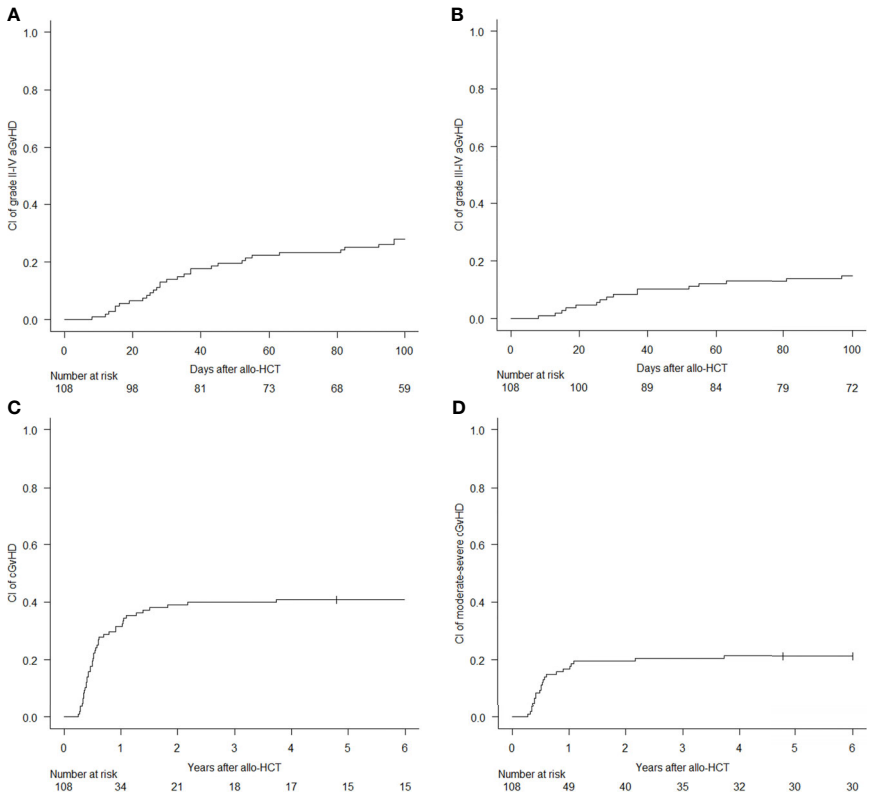


**FIGURE 2** | Cumulative incidence (CI) of acute graft-*versus*-host disease (GvHD) grade II–IV **(A)** and III-IV **(B)**, and CI of chronic GvHD all grades **(C)** and moderate-to-severe **(D)**.

1 patient a cord blood transplant. As for the other nine patients, we made use of the cryopreserved PBSC from the first donor. Treo in association with a purine nucleoside analog (fludarabine or clofarabine) was the most frequent conditioning regimen used (10 cases), while an intensification with 4 Gy of total-body irradiation was used in 4 cases. At last follow-up, 3 out of these 20 patients are alive and in complete remission; 11 died from disease progression and 6 for causes related to the second allogeneic procedure. One patient underwent a third allo-HCT using a haploidentical family donor and a MAC regimen to treat a further disease relapse diagnosed 2 years after the second transplant: she is alive and in complete remission 6 years after the third allo-HCT.

CI of TRM was 10.2% at 100 days (95% CI, 5.4%–16.8%) and 22.5% (95% CI, 15.1%–30.9%) at 12 years (**Figure 1**). Twenty-five patients died from transplant-related causes: six from infections (three sepsis and three pneumonias), three from GvHD, three from multiorgan failure, one from arrhythmia, one from stroke, one from acute myocardial infarction, one from late-onset transplant-associated thrombotic microangiopathy, three from secondary malignancies, and six for unknown causes.

Results of the univariate analysis are reported in **Table 2**. In multivariate analysis, age ≥60 years was independently associated with a higher risk of TRM. High/very high DRI was a risk factor for higher RI (**Table 3**).

## DISCUSSION

Allo-HCT conditioning regimen has rapidly changed from a one regimen that fits all to multiple potential regimens tailored on disease characteristics and patient comorbidities. In this setting, even in advanced disease stages, Treo has increasingly been employed owing to its low risk of organ toxicity and TRM (7, 15, 20–24).

At the time of this phase 2 clinical trial accrual, Treo was approved only for the treatment of advanced ovarian carcinoma. Treo exhibited low inter- and intrapatient variability in pharmacokinetic studies; gastrointestinal mucositis, skin toxicity, and metabolic acidosis were reported as dose-limiting adverse effects (25, 26). Preliminary clinical trials in the allo-HCT setting demonstrated an advantageous toxicity profile of Treo up to a dose of 42 g/m$^2$ when compared with other standard conditioning regimens (7, 8). Thereafter, Treo was approved by the European Medicines Agency (EMA) at a total dose of 30 g/m$^2$ according to the results of a multicenter randomized phase 3 trial in older and comorbid patients.[15]

Although potentially limited by the presence of single-center data, our long-term analysis confirms that a full-dose Treo-based conditioning regimen displays a strong myeloablative and immunosuppressive potential coupled with a good safety profile, in line with other recent studies (9, 15, 20–23, 27–29).

A fast and stable full donor engraftment was achieved by most of our patients, toxicities were limited, and no case of SOS was reported. Importantly, in our series, 20 patients were able to proceed to a second allo-HCT for the treatment of disease relapse, a further proof of the low cumulative toxicity of this conditioning combination. We were able to report detailed long-term adverse events in our population: 10 patients were diagnosed with a secondary malignancy, 3 patients died from

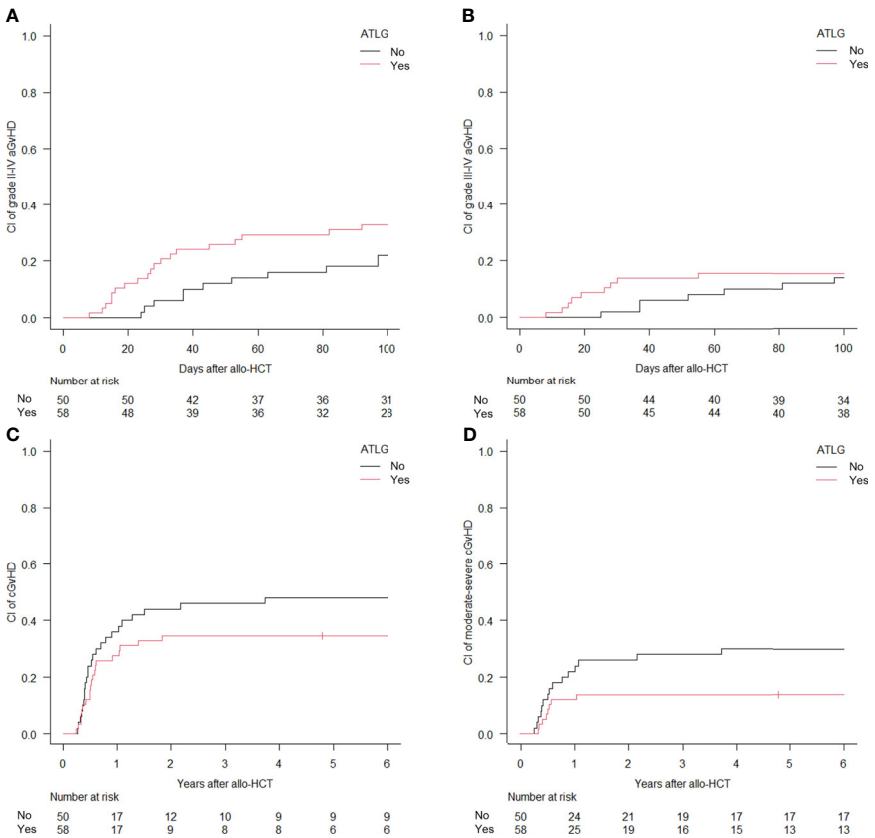


**FIGURE 3** | Cumulative incidence (CI) of acute graft-*versus*-host disease (GvHD) grade II–IV **(A)** and III–IV **(B)** and CI of chronic GvHD all grades **(C)** and moderate-to-severe **(D)** according to anti T-lymphocyte globulin administration.

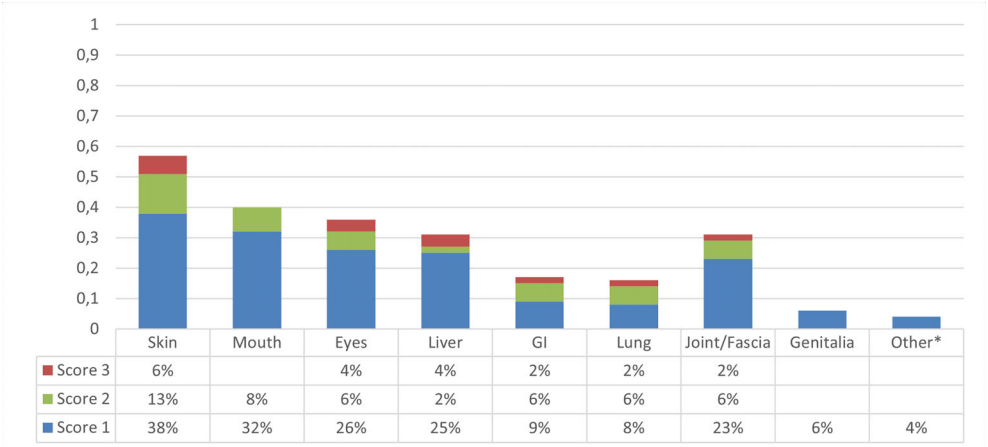


**FIGURE 4** | Graphic representation of the distribution of organs involved by chronic graft-*versus*-host disease (cGvHD) in the overall population. *Renal cGvHD.

cardiovascular diseases, 1 patient died from a late-onset transplant-associated thrombotic microangiopathy. Six long-term survivors from our study were able to achieve a successful pregnancy or fatherhood after allo-HCT, underlining the lower gonadal toxicity of Treo as compared with other alkylating agents such as Bu (30, 31).

The results of our study are in line with those regarding Bu-based conditioning regimens (15, 20, 21, 23, 32, 33). The immunosuppressive activity of Treo facilitates stem cell engraftment, making it an attractive candidate for this clinical context (21, 27, 34).

In our study, older age at transplant was associated with a lower OS and an increased TRM. Age is a known factor associated with TRM due to the burden of comorbidities and frailty. Indeed, in our series, the use of Treo at a daily dose of 14 g/m$^2$ may in part explain this finding. Considering that RI was similar between the two age groups, reducing the Treo dose could possibly improve allo-HCT outcomes in the older population, as also confirmed in other trials (5, 15, 23).

Disease recurrence was a major issue in our study, especially for patients with a high/very high DRI. Intensification of the conditioning regimen with the addition of a second alkylating agent or total body irradiation based on the underlying disease type could be implemented in this group of patients to counteract posttransplant disease relapse. Furthermore, owing to the fast and stable recovery provided with this conditioning protocol, the use of preemptive maintenance therapies in the early posttransplant period may be explored in these high-risk patients (35). Moreover, an additional limitation to our study, mainly related to its long-standing enrollment phase, is the absence of detailed data on measurable residual disease, a rich field of research where many advances have been made in recent years (36).

The use of *in vivo* T-cell depletion with ATLG for patients undergoing unrelated donor allo-HCT was able to significantly reduce the incidence of moderate-to-severe cGvHD at the expense of a higher risk of TRM and worse PFS, with a trend towards a lower OS in univariate analysis. At the time of this trial, T-cell depletion with ATLG was not considered a standard practice in matched-related transplants but rather widely recommended. Switching to a different T-cell depletion approach in this setting, mainly using posttransplant cyclophosphamide (PTCy), could possibly improve both GvHD incidence and transplant outcomes, as also suggested by recent experiences (13, 37, 38).

Overall, our data confirmed that full-dose Treo (42 g/m$^2$) displays a myeloablative potential associated with a prompt achievement of full donor chimerism and a safe toxicity profile, mostly in the younger population. A lower Treo dose should be adopted for older patients, according to the EMA schedule (30 g/m$^2$). This conditioning regimen can be safely adopted as a backbone for newly transplant strategies implementing different GvHD prophylaxis or posttransplant maintenance therapies.

## DATA AVAILABILITY STATEMENT

The raw data supporting the conclusions of this article will be made available by the authors, without undue reservation.

## ETHICS STATEMENT

The studies involving human participants were reviewed and approved by San Raffaele's Hospital Ethics Committee. The patients/participants provided their written informed consent to participate in this study.

## AUTHOR CONTRIBUTIONS

All authors contributed to patient clinical care and data collection. LL, ML, SM, RG, FC, and JP updated and interpreted the long-term follow-up data. LL and AR performed statistical analysis and prepared the figures and tables. FC and JP designed the study. LL, AR, ML, RG, FC, and JP wrote the manuscript. All authors contributed to the article and approved the submitted version.

## ACKNOWLEDGMENTS

This study was supported in part by Fresenius and Medac for data management. The authors would also like to thank the San Raffaele URC (clinical trial office), the participating patients and their families, all nurses, and data managers who contributed to this study.

## SUPPLEMENTARY MATERIAL

The Supplementary Material for this article can be found online at: https://www.frontiersin.org/articles/10.3389/fonc.2021.731478/full#supplementary-material

## REFERENCES

1. Passweg JR, Baldomero H, Chabannon C, Basak GW, de la Cámara R, Corbacioglu S, et al. Hematopoietic Cell Transplantation and Cellular Therapy Survey of the EBMT: Monitoring of Activities and Trends Over 30 Years. *Bone Marrow Transplant* (2021) 56(7):1651–64. doi: 10.1038/s41409-021-01227-8
2. Penack O, Peczynski C, Mohty M, Yakoub-Agha I, Styczynski J, Montoto S, et al. How Much has Allogeneic Stem Cell Transplant-Related Mortality Improved Since the 1980s? A Retrospective Analysis From the EBMT. *Blood Adv* (2020) 4(24):6283–90. doi: 10.1182/bloodadvances.2020003418
3. Gooley TA, Chien JW, Pergam SA, Hingorani S, Sorror ML, Boeckh M, et al. Reduced Mortality After Allogeneic Hematopoietic-Cell Transplantation. *N Engl J Med* (2010) 363(22):2091–101. doi: 10.1056/nejmoa1004383

4. Bacigalupo A, Ballen K, Rizzo D, Giralt S, Lazarus H, Ho V, et al. Defining the Intensity of Conditioning Regimens: Working Definitions. *Biol Blood Marrow Transplant* (2009) 15(12):1628–33. doi: 10.1016/j.bbmt.2009.07.004
5. Gagelmann N, Kröger N. Dose Intensity for Conditioning in Allogeneic Hematopoietic Cell Transplantation: Can We Recommend "When and for Whom" in 2021? *Haematologica* (2021) 106(7):1794–804. doi: 10.3324/haematol.2020.268839
6. Champlin R, Khouri I, Shimoni A, Gajewski J, Kornblau S, Molldrem J, et al. Harnessing Graft-*Versus*-Malignancy: non-Myeloablative Preparative Regimens for Allogeneic Haematopoietic Transplantation, an Evolving Strategy for Adoptive Immunotherapy. *Br J Haematol* (2000) 111(1):18–29. doi: 10.1111/j.1365-2141.2000.02196.x
7. Casper J, Knauf W, Kiefer T, Wolff D, Steiner B, Hammer U, et al. Treosulfan and Fludarabine: A New Toxicity-Reduced Conditioning Regimen for Allogeneic Hematopoietic Stem Cell Transplantation. *Blood* (2004) 103 (2):725–31. doi: 10.1182/blood-2002-11-3615
8. Beelen DW, Trenschel R, Casper J, Freud M, Basara N, Fauser A. Evaluation of Safety, Efficacy and Pharmacokinetics of Dose-Escalated Treosulfan (TREO)/cyclophosphamide (CY) Conditioning Prior to Allogeneic Transplantation of High-Risk Leukemia Patients. *Blood* (2002) 100):415a.
9. Casper J, Wolff D, Knauf W, Blau IW, Ruutu T, Volin L, et al. Allogeneic Hematopoietic Stem-Cell Transplantation in Patients With Hematologic Malignancies After Dose-Escalated Treosulfan/Fludarabine Conditioning. *J Clin Oncol* (2010) 28(20):3344–51. doi: 10.1200/JCO.2009.23.3429
10. Boztug H, Sykora KW, Slatter M, Zecca M, Veys P, Lankester A, et al. European Society for Blood and Marrow Transplantation Analysis of Treosulfan Conditioning Before Hematopoietic Stem Cell Transplantation in Children and Adolescents With Hematological Malignancies. *Pediatr Blood Cancer* (2016) 63(1):139–48. doi: 10.1002/pbc.25764
11. Peccatori J, Forcina A, Clerici D, Crocchiolo R, Vago L, Stanghellini MT, et al. Sirolimus-Based Graft-*Versus*-Host Disease Prophylaxis Promotes the In Vivo Expansion of Regulatory T Cells and Permits Peripheral Blood Stem Cell Transplantation From Haploidentical Donors. *Leukemia* (2015) 29(2):396–405. doi: 10.1038/leu.2014.180
12. Cieri N, Greco R, Crucitti L, Morelli M, Giglio F, Levati G, et al. Post-Transplantation Cyclophosphamide and Sirolimus After Haploidentical Hematopoietic Stem Cell Transplantation Using a Treosulfan-Based Myeloablative Conditioning and Peripheral Blood Stem Cells. *Biol Blood Marrow Transplant* (2015) 21(8):1506–14. doi: 10.1016/j.bbmt.2015.04.025
13. Greco R, Lorentino F, Morelli M, Giglio F, Mannina D, Assanelli A, et al. Posttransplantation Cyclophosphamide and Sirolimus for Prevention of GVHD After HLA-Matched PBSC Transplantation. *Blood* (2016) 128 (11):1528–31. doi: 10.1182/blood-2016-06-723205
14. Kröger N, Bornhäuser M, Stelljes M, Pichlmeier U, Trenschel R, Schmid C, et al. Allogeneic Stem Cell Transplantation After Conditioning With Treosulfan, Etoposide and Cyclophosphamide for Patients With ALL: A Phase II-Study on Behalf of the German Cooperative Transplant Study Group and ALL Study Group (GMALL). *Bone Marrow Transplant* (2015) 50(12):1503–7. doi: 10.1038/bmt.2015.202
15. Beelen DW, Trenschel R, Stelljes M, Groth C, Masszi T, Reményi P, et al. Treosulfan or Busulfan Plus Fludarabine as Conditioning Treatment Before Allogeneic Haemopoietic Stem Cell Transplantation for Older Patients With Acute Myeloid Leukaemia or Myelodysplastic Syndrome (MC-FludT.14/L): A Randomised, non-Inferiority, Phase 3 Trial. *Lancet Haematol* (2020) 7(1): e28–39. doi: 10.1016/S2352-3026(19)30157-7
16. Armand P, Gibson CJ, Cutler C, Ho VT, Koreth J, Alyea EP, et al. A Disease Risk Index for Patients Undergoing Allogeneic Stem Cell Transplantation. *Blood* (2012) 120(4):905–13. doi: 10.1182/blood-2012-03-418202
17. Sorror ML, Maris MB, Storb R, Baron F, Sandmaier BM, Maloney DG, et al. Hematopoietic Cell Transplantation (HCT)-Specific Comorbidity Index: A New Tool for Risk Assessment Before Allogeneic HCT. *Blood* (2005) 106 (8):2912–9. doi: 10.1182/blood-2005-05-2004
18. Glucksberg H, Storb R, Fefer A, Buckner CD, Neiman PE, Clift RA, et al. Clinical Manifestations of Graft-*Versus*-Host Disease in Human Recipients of Marrow From HL-A-Matched Sibling Donors1. *Transplantation* (1974) 18 (4):295–304. doi: 10.1097/00007890-197410000-00001
19. Filipovich AH, Weisdorf D, Pavletic S, Socie G, Wingard JR, Lee SJ, et al. National Institutes of Health Consensus Development Project on Criteria for Clinical Trials in Chronic Graft-*Versus*-Host Disease: I. Diagnosis and Staging Working Group Report. *Biol Blood Marrow Transplant* (2005) 11(12):945–56. doi: 10.1016/j.bbmt.2005.09.004
20. Sakellari I, Mallouri D, Gavriilaki E, Batsis I, Kaliou M, Constantinou V, et al. Survival Advantage and Comparable Toxicity in Reduced-Toxicity Treosulfan-Based *Versus* Reduced-Intensity Busulfan-Based Conditioning Regimen in Myelodysplastic Syndrome and Acute Myeloid Leukemia Patients After Allogeneic Hematopoietic Cell Transplantation. *Biol Blood Marrow Transplant* (2017) 23(3):445–51. doi: 10.1016/j.bbmt.2016.11.023
21. Danylesko I, Shimoni A, Nagler A. Treosulfan-Based Conditioning Before Hematopoietic SCT: More Than a BU Look-Alike. *Bone Marrow Transplant* (2012) 47(1):5–14. doi: 10.1038/bmt.2011.88
22. Michallet M, Sobh M, Milpied N, Bay JO, Fürst S, Harousseau JL, et al. Phase II Prospective Study of Treosulfan-Based Reduced-Intensity Conditioning in Allogeneic HSCT for Hematological Malignancies From 10/10 HLA-Identical Unrelated Donor. *Ann Hematol* (2012) 91(8):1289–97. doi: 10.1007/s00277-012-1429-y
23. Shimoni A, Labopin M, Savani B, Hamladji RM, Beelen D, Mufti G, et al. Intravenous Busulfan Compared With Treosulfan-Based Conditioning for Allogeneic Stem Cell Transplantation in Acute Myeloid Leukemia: A Study on Behalf of the Acute Leukemia Working Party of European Society for Blood and Marrow Transplantation. *Biol Blood Marrow Transplant* (2018) 24 (4):751–7. doi: 10.1016/j.bbmt.2017.12.776
24. Remberger M, Törlen J, Serafi I, Garming-Legert K, Björklund A, Ljungman P, et al. Toxicological Effects of Fludarabine and Treosulfan Conditioning Before Allogeneic Stem-Cell Transplantation. *Int J Hematol* (2017) 106(4):471–5. doi: 10.1007/s12185-017-2320-3
25. Ten Brink MH, Zwaveling J, Swen JJ, Bredius RGM, Lankester AC, Guchelaar HJ. Personalized Busulfan and Treosulfan Conditioning for Pediatric Stem Cell Transplantation: The Role of Pharmacogenetics and Pharmacokinetics. *Drug Discov Today* (2014) 19(10):1572–86. doi: 10.1016/j.drudis.2014.04.005
26. Galaup A, Paci A. Pharmacology of Dimethanesulfonate Alkylating Agents: Busulfan and Treosulfan. *Expert Opin Drug Metab Toxicol* (2013) 9(3):333–47. doi: 10.1517/17425255.2013.737319
27. Nagler A, Labopin M, Beelen D, Ciceri F, Volin L, Shimoni A, et al. Long-Term Outcome After a Treosulfan-Based Conditioning Regimen for Patients With Acute Myeloid Leukemia: A Report From the Acute Leukemia Working Party of the European Society for Blood and Marrow Transplantation. *Cancer* (2017). doi: 10.1002/cncr.30646
28. Shimoni A, Vago L, Bernardi M, Yerushalmi R, Peccatori J, Greco R, et al. Missing HLA C Group 1 Ligand in Patients With AML and MDS Is Associated With Reduced Risk of Relapse and Better Survival After Allogeneic Stem Cell Transplantation With Fludarabine and Treosulfan Reduced Toxicity Conditioning. *Am J Hematol* (2017) 92(10):1011–9. doi: 10.1002/ajh.24827
29. Yerushalmi R, Shem-Tov N, Danylesko I, Avigdor A, Nagler A, Shimoni A. Fludarabine and Treosulfan Compared With Other Reduced-Intensity Conditioning Regimens for Allogeneic Stem Cell Transplantation in Patients With Lymphoid Malignancies. *Bone Marrow Transplant* (2015) 50 (12):1526–35. doi: 10.1038/bmt.2015.174
30. Faraci M, Diesch T, Labopin M, Dalissier A, Lankester A, Gennery A, et al. Gonadal Function After Busulfan Compared With Treosulfan in Children and Adolescents Undergoing Allogeneic Hematopoietic Stem Cell Transplant. *Biol Blood Marrow Transplant* (2019) 25(9):1786–91. doi: 10.1016/j.bbmt.2019.05.005
31. Levi M, Stemmer SM, Stein J, Shalgi R, Ben-Aharon I. Treosulfan Induces Distinctive Gonadal Toxicity Compared With Busulfan. *Oncotarget* (2018) 9 (27):19317–27. doi: 10.18632/oncotarget.25029
32. Rambaldi A, Grassi A, Masciulli A, Boschini C, Micò MC, Busca A, et al. Busulfan Plus Cyclophosphamide *Versus* Busulfan Plus Fludarabine as a Preparative Regimen for Allogeneic Haemopoietic Stem-Cell Transplantation in Patients With Acute Myeloid Leukaemia: An Open-Label, Multicentre, Randomised, Phase 3 Trial. *Lancet Oncol* (2015) 16 (15):1525–36. doi: 10.1016/S1470-2045(15)00200-4
33. Shimoni A, Shem-Tov N, Volchek Y, Danylesko I, Yerushalmi R, Nagler A. Allo-SCT for AML and MDS With Treosulfan Compared With BU-Based Regimens: Reduced Toxicity *vs* Reduced Intensity. *Bone Marrow Transplant* (2012) 47(10):1274–82. doi: 10.1038/bmt.2012.4
34. Casper J, Holowiecki J, Trenschel R, Wandt H, Schaefer-Eckart K, Ruutu T, et al. Allogeneic Hematopoietic SCT in Patients With AML Following

Treosulfan/Fludarabine Conditioning. *Bone Marrow Transplant* (2012) 47 (9):1171–7. doi: 10.1038/bmt.2011.242

35. DeFilipp Z, Chen YB. Strategies and Challenges for Pharmacological Maintenance Therapies After Allogeneic Hematopoietic Cell Transplantation. *Biol Blood Marrow Transplant* (2016) 22(12):2134–40. doi: 10.1016/j.bbmt.2016.08.021
36. Schuurhuis GJ, Heuser M, Freeman S, Béné MC, Buccisano F, Cloos J, et al. Minimal/measurable Residual Disease in AML: A Consensus Document From the European LeukemiaNet MRD Working Party. *Blood* (2018) 131(12):1275–91. doi: 10.1182/blood-2017-09-801498
37. Sanz J, Galimard JE, Labopin M, Afanasyev B, Angelucci E, Ciceri F, et al. Post-Transplant Cyclophosphamide After Matched Sibling, Unrelated and Haploidentical Donor Transplants in Patients With Acute Myeloid Leukemia: A Comparative Study of the ALWP EBMT. *J Hematol Oncol* (2020) 13(1):46. doi: 10.1186/s13045-020-00882-6
38. Greco R, Lorentino F, Albanese S, Lupo Stanghellini MT, Giglio F, Piemontese S, et al. Post-Transplant Cyclophosphamide and Sirolimus Based Graft-*Versus*-Host-Disease Prophylaxis in Allogeneic Stem Cell Transplant. *Transplant Cell Ther* (2021) 27(9):776.e1–13. doi: 10.1016/j.jtct.2021.05.023

**Conflict of Interest:** The authors declare that the research was conducted in the absence of any commercial or financial relationships that could be construed as a potential conflict of interest.

**Publisher's Note:** All claims expressed in this article are solely those of the authors and do not necessarily represent those of their affiliated organizations, or those of the publisher, the editors and the reviewers. Any product that may be evaluated in this article, or claim that may be made by its manufacturer, is not guaranteed or endorsed by the publisher.

frontiers in Oncology

ORIGINAL RESEARCH
published: 13 September 2021
doi: 10.3389/fonc.2021.712747

# High *EVI1* Expression Predicts Adverse Outcomes in Children With *De Novo* Acute Myeloid Leukemia

*Yongzhi Zheng[1†], Yan Huang[1†], Shaohua Le[1], Hao Zheng[1], Xueling Hua[1], Zaisheng Chen[1], Xiaoqin Feng[2], Chunfu Li[3], Mincui Zheng[4], Honggui Xu[5], Yingyi He[6], Xiangling He[7], Jian Li[1*] and Jianda Hu[1*]*

*[1] Department of Hematology, Fujian Institute of Hematology, Fujian Provincial Key Laboratory on Hematology, Fujian Medical University Union Hospital, Fuzhou, China, [2] Department of Pediatrics, Southern Medical University/Nanfang Hospital, Guangzhou, China, [3] Nanfang-Chunfu Children's Institute of Hematology & Oncology, TaiXin Hospital, Dongguan, China, [4] Hematology and Oncology, Hunan Children's Hospital, Changsha, China, [5] Department of Pediatric Hematology & Oncology, Sun Yat-sen Memorial Hospital, Guangzhou, China, [6] Department of Pediatric Hematology/Oncology, Guangzhou Women and Children's Medical Center, Guangzhou, China, [7] Pediatrics, People's Hospital of Hunan Province, Changsha, China*

OPEN ACCESS

**Edited by:**
*Gurvinder Kaur, All India Institute of Medical Sciences, India*

**Reviewed by:**
*Michael Diamantidis, University Hospital of Larissa, Greece*
*Branko Cuglievan, University of Texas MD Anderson Cancer Center, United States*
*Barbara McClure, South Australian Health and Medical Research Institute (SAHMRI), Australia*

***Correspondence:**
*Jianda Hu*
*drjiandahu@163.com*
*Jian Li*
*1354113723@qq.com*

*[†]These authors have contributed equally to this work*

**Specialty section:**
*This article was submitted to Hematologic Malignancies, a section of the journal Frontiers in Oncology*

**Received:** *21 May 2021*
**Accepted:** *09 August 2021*
**Published:** *13 September 2021*

**Citation:**
*Zheng Y, Huang Y, Le S, Zheng H, Hua X, Chen Z, Feng X, Li C, Zheng M, Xu H, He Y, He X, Li J and Hu J (2021) High EVI1 Expression Predicts Adverse Outcomes in Children With De Novo Acute Myeloid Leukemia. Front. Oncol. 11:712747. doi: 10.3389/fonc.2021.712747*

**Background:** A high ecotropic viral integration site 1 (*EVI1*) expression (*EVI1*$^{high}$) is an independent prognostic factor in adult acute myeloid leukemia (AML). However, little is known of the prognostic value of *EVI1*$^{high}$ in pediatric AML. This study aimed to examine the biological and prognostic significance of *EVI1*$^{high}$ in uniformly treated pediatric patients with AML from a large cohort of seven centers in China.

**Methods:** A diagnostic assay was developed to determine the relative *EVI1* expression using a single real-time quantitative polymerase chain reaction in 421 newly diagnosed pediatric AML patients younger than 14 years from seven centers in southern China. All patients were treated with a uniform protocol, but only 383 patients were evaluated for their treatment response. The survival data were included in the subsequent analysis (n = 35 for *EVI1*$^{high}$, n = 348 for *EVI1*$^{low}$).

**Results:** *EVI1*$^{high}$ was found in 9.0% of all 421 pediatric patients with *de novo* AML. *EVI1*$^{high}$ was predominantly found in acute megakaryoblastic leukemia (FAB M7), *MLL* rearrangements, and unfavorable cytogenetic aberrance, whereas it was mutually exclusive with t (8; 21), inv (16)/t (16; 16), *CEBPA*, *NPM1*, or *C-KIT* mutations. In the univariate Cox regression analysis, *EVI1*$^{high}$ had a significantly adverse 5-year event-free survival (EFS) and overall survival (OS) [hazard ratio (HR) = 1.821 and 2.401, $p = 0.036$ and 0.005, respectively]. In the multivariate Cox regression analysis, *EVI1*$^{high}$ was an independent prognostic factor for the OS (HR = 2.447, $p = 0.015$) but not EFS (HR = 1.556, p = 0.174). Furthermore, *EVI1*$^{high}$ was an independent adverse predictor of the OS and EFS of patients with *MLL* rearrangements (univariate analysis: HR = 9.921 and 7.253, both $p < 0.001$; multivariate analysis: HR = 7.186 and 7.315, $p = 0.005$ and 0.001, respectively). Hematopoietic stem cell transplantation (HSCT) in first complete remission (CR1) provided *EVI1*$^{high}$ patients with a tendential survival benefit when compared with chemotherapy as a consolidation (5-year EFS: 68.4% *vs.* 50.8%, $p = 0.26$; 5-year OS: 65.9% *vs.* 54.8%, $p = 0.45$).

**Conclusion:** It could be concluded that *EVI1*$^{high}$ can be detected in approximately 10% of pediatric AML cases. It is predominantly present in unfavorable cytogenetic subtypes and predicts adverse outcomes. Whether pediatric patients with *EVI1*$^{high}$ AML can benefit from HSCT in CR1 needs to be researched further.

**Keywords: *EVI1*, prognostic factor, acute myeloid leukemia, pediatric, adverse outcome, transplantation**

# 1 INTRODUCTION

Acute myeloid leukemia (AML) accounts for approximately 20% of pediatric leukemia diagnoses, and its long-term survival rate has dramatically increased from less than 20% to approximately 70% in the past 50 years (1). One of the most important reasons for these dramatic improvements is the accurate prediction of the prognosis to initiate the appropriate therapy regimens. Cytogenetic abnormalities and gene mutations are the classical and most important framework for risk stratification (2, 3). In addition to genetic alterations, aberrant overexpression of specific genes may also serve as biomarkers to evaluate the risk of treatment failure or relapse; ecotropic viral integration site 1 (*EVI1*) is a representative of this group (4, 5).

The *EVI1* gene encodes a zinc-finger protein that functions as a transcription factor essential for hematopoietic stem cell (HSC) proliferation and differentiation, and is located on chromosome 3q26 (6). Aberrantly high *EVI1* expression (*EVI1*$^{high}$) plays an important role in the pathogenesis of hematological malignancies, including AML, chronic myeloid leukemia, and myelodysplastic syndrome (MDS) (7). In adult AML, *EVI1*$^{high}$ is frequently associated with cytogenetic abnormalities of 3q, especially 3q26, whereas in pediatric AML, it is rarely correlated with the cytogenetic rearrangements of this locus (8). In pediatric AML, *EVI1*$^{high}$ is commonly found together with mixed lineage leukemia (*MLL*) rearrangements, which indicates that the pathogenetic and prognostic significance of *EVI1*$^{high}$ may be different between adult and pediatric patients with AML (9, 10).

In the past decade, several studies have shown that *EVI1*$^{high}$ is a poor independent prognostic predictor for the complete remission (CR), overall survival (OS), relapse-free (RFS), and event-free survival (EFS) in adult AML, irrespective of the cytogenetic abnormalities of 3q (8). However, few studies have examined how *EVI1*$^{high}$ affects the prognosis in pediatric AML, and some of its effects are contradictory to those of adult AML. Using multivariate analysis, Balgobind et al. (10) and Ho et al. (9) reported that *EVI1*$^{high}$ had a significantly lower EFS but was not independently associated with an inferior OS and EFS in pediatric AML. In consideration of the inconsistent conclusions, the aim of our study was to examine the biological and prognostic significance of *EVI1*$^{high}$ in uniformly treated pediatric AML patients from a large cohort of seven centers in China.

# 2 MATERIAL AND METHODS

## 2.1 Patients and Treatment

A total of 421 newly diagnosed pediatric patients with AML (≤14 years) were enrolled in this retrospective study. Patients with acute promyelocytic leukemia, secondary AML, constitutional trisomy 21, or antecedent MDS were excluded. These patients were consecutively diagnosed at seven centers in southern China between January 2015 and December 2020. Morphological, flow cytometric, cytogenetic, and molecular analyses were performed on all patients at diagnosis, and the results were available for all patients included in this study. AML was diagnosed and classified according to the World Health Organization (2016) classification (11).

All patients were treated using the C-HUANAN-AML15 protocol. In the C-HUANAN-AML15 protocol, two tandem courses of the FLAG-IDA or DAE regimen were applied as induction chemotherapy. One course of homoharringtonine cytarabine/etoposide and one course of mitoxantrone/cytarabine in consolidation chemotherapy were uniformly administered to both groups. Intermediate-risk patients who had human leukocyte antigen (HLA) matched donors and high-risk patients were advised to undergo HSC transplantation (HSCT) in CR1. Details of the treatment protocols are provided in the **Supplementary Data** section. This study was approved by the ethics committee of all seven centers. All patients and volunteers provided a written informed consent, in accordance with the Declaration of Helsinki, to participate in the present study.

## 2.2 Quantitative Real-Time Polymerase Chain Reaction (qRT-PCR)

Total RNA was isolated from nucleated cells of the bone marrow using the Trizol Reagent (Invitrogen, Carlsbad, CA, USA), and subsequent reverse transcription was performed on 1 μg of the total diagnostic RNA using the standard protocol (Invitrogen, Carlsbad, CA, USA). *EVI1* expression was measured by qRT-PCR using the TaqMan Universal PCR Master Mix and TaqMan *EVI1* Gene Expression Assay (Applied Biosystems, Foster City, CA) with a primer/probe set designed to hybridize within a region spanning exons 2 and 3, as follows:

Forward primer: 5'-GTACTTGAGCCAGCTTCCAACA-3' (in exon 3)

Reverse primer: 5'-CTTCTTGACTAAAGCCCTTGGA-3' (in exon 2)

Probe: 5'-FAM-TCTTAGACGAATTTTACAATGTGAAGTT CTGCATAGATG-TAMRA-3' (in exon 3).

Abelson murine leukemia viral oncogene homolog *(ABL)* was used as a control gene, and the corresponding primers and probes were based on a report from the Europe Against Cancer Program (12). The primer of *EVI1* can detect the expression of the total *EVI1* (including *EVI1-1A*, *1B*, *1C*, and

*1D*), and the *MDS1* and *EVI1* complex fusion transcript. A total of 15 bone marrow samples from healthy donors were processed as calibrators for quantification. *EVI1* transcript levels were calculated as the percentage of the target transcript copies/*ABL* copies. The mean value of *EVI1* in the 15 normal controls was considered as the baseline. Relative quantification was performed using the $2^{-\triangle\triangle Ct}$ method (13). The relative expression level of *EVI1* is expressed as a percentage. The percentile of the expression level in all *EVI1* test results in the present study was used as a percentage. *EVI1* expression levels were dichotomized based on a cutoff value of 75% (approximately 10 times the baseline), according to Santamaría et al. (14). A total of 38 patients were defined as having $EVI1^{high}$ and the remainder as $EVI1^{low}$.

## 2.3 Statistical Analysis

Continuous variables of patient characteristics were compared using the Wilcoxon rank-sum test (abnormal distribution) or Mann–Whitney U test (normal distribution), while categorical variables were compared using Pearson's $\chi^2$ test or Fisher's exact test when data were sparse. A total of 38 children (3 children with $EVI1^{high}$ and 35 children with $EVI1^{low}$), including those that were lost during the follow-up (n = 21), discontinued the treatment (n = 12), or were transferred (n = 5) before completing two courses of chemotherapy or were excluded from the survival analysis. The cutoff date for follow-up was February 28, 2021. OS endpoints were death (failure) and being alive at the last follow-up (censored), measured from the onset to the start of chemotherapy. EFS endpoints were disease relapse or death from any cause, measured from the onset to the start of chemotherapy. Distribution estimations and survival distributions of the OS and EFS were calculated using the Kaplan-Meier method and log-rank test, respectively. Univariate analyses were performed using the unadjusted Cox proportional hazards model to calculate the hazard ratios (HRs). Variables that were significant in the univariate analyses were included in the multivariate analyses. Multivariate analyses were performed using the Cox proportional hazards model to identify the independent prognostic factors. All tests were two-sided, and a *p*-value of less than 0.05 was considered statistically significant. All statistical analyses were performed using the Statistical Software Environment R, version 4.0.4.

# 3 RESULTS

## 3.1 Clinical Characteristics of Pediatric Patients With Acute Myeloid Leukemia (AML) and a High Ecotropic Viral Integration Site 1 Expression ($EVI1^{high}$)

The clinical features of all 421 patients are summarized in **Table 1**. The median age was 74 months (range, 7–176 months), and 12 patients had infant AML. The most common cytogenetic changes included t (8; 21) and 11q23 chromosome abnormality. In 47/421 (11.2%) patients, FLT3-ITD mutations were detected, while ASXL1 mutations occurred in 11.6%. $EVI1^{high}$, which was found in 9.0% (38/421) of all the patients, was not detected in infant patients. $EVI1^{high}$ was not correlated with age, sex, or white blood cells (WBC), whereas patients with $EVI1^{high}$ had a significantly higher frequency of (1) acute megakaryoblastic leukemia (FAB-M7) (23.7% *vs.* 6.0%, $p$ = 0.001) (2), *MLL* rearrangements (39.5% *vs.* 14.4%, $p < 0.0001$), especially *MLL-AF9* (15.8% *vs.* 6.8%, $p = 0.046$) (3); unfavorable cytogenetic aberrance (55.3% *vs.* 24.8%, $p < 0.0001$), but only one

**TABLE 1** | Clinical and genetic characteristics according to the *EVI1* status.

| Characteristic | All patients (n = 421) | $EVI1^{high}$ group (n = 38) | $EVI1^{low}$ group (n = 383) | *P-value* |
|---|---|---|---|---|
| **Age, months** | | | | **0.964** |
| **Median (range)** | 74 (7–176) | 44 (12–163) | 75 (7–176) | |
| **Sex, n%** | | | | **0.487** |
| **Male** | 264 (62.7) | 26 (68.4) | 238 (62.1) | |
| **Female** | 157 (37.3) | 12 (31.6) | 145 (37.9) | |
| **WBC, ×10⁹/L** | | | | **0.137** |
| **<50** | 294 (69.8) | 31 (81.6) | 263 (68.7) | |
| **≥50** | 127 (30.2) | 7 (18.4) | 120 (31.3) | |
| **FAB subtype, n%** | | | | **0.001** |
| **M7** | 32 (7.6) | 9 (23.7) | 23 (6.0) | |
| **Other types** | 389 (92.4) | 29 (76.3) | 360 (94.0) | |
| ***Cytogenetic characteristics, n (%)** | | | | |
| **t (8;21)** | 106 (25.2) | 0 (0) | 106 (27.7) | **<0.001** |
| **inv (16)/t (16;16)** | 28 (6.7) | 0 (0) | 28 (7.3) | **0.072** |
| **t (v;11q23)** | 70 (16.6) | 15 (39.5) | 55 (14.4) | **<0.001** |
| **t (9;11)** | 32 (7.6) | 6 (15.8) | 26 (6.8) | **0.046** |
| **-7 or del (7q)** | 17 (4.0) | 3 (7.9) | 14 (3.7) | **0.385** |
| **Complex karyotype** | 13 (3.1) | 3 (7.9) | 10 (2.6) | **0.390** |
| **†Cytogenetic risk** | | | | **<0.001** |
| **Favorable** | 128 (30.4) | 0 (0) | 128 (33.4) | |
| **Intermediate** | 177 (42.0) | 17 (44.7) | 160 (41.8) | |
| **Unfavorable** | 116 (27.6) | 21 (55.3) | 95 (24.8) | |
| **Molecular abnormalities** | | | | |
| **FLT3-ITD** | 47 (11.2) | 3 (7.9) | 44 (11.5) | **0.602** |
| **ASXL1** | 49 (11.6) | 3 (7.9) | 46 (12.0) | **0.600** |
| **CEBPA-mutation** | 13 (3.1) | 0 (0) | 13 (3.4) | **0.309** |
| **NPM1- mutation** | 9 (2.1) | 0 (0) | 9 (2.3) | **0.462** |
| **C-KIT-mutation** | 40 (9.5) | 0 (0) | 40 (10.4) | **0.020** |
| **#CR after induction 2nd** | | | | **0.364** |
| **Yes** | 342 (81.4) | 29 (76.3) | 313 (81.9) | |
| **No** | 31 (7.4) | 2 (5.3) | 29 (7.6) | |
| **Missing** | 47 (11.2) | 7 (18.4) | 40 (10.5) | |
| **#Blast>15% in BM after induction 1st** | | | | **1.000** |
| **Yes** | 20 (4.8) | 2 (5.3) | 18 (4.7) | |
| **No** | 390 (92.6) | 35 (92.1) | 355 (92.7) | |
| **Missing** | 11 (2.6) | 1 (2.6) | 10 (2.6) | |

**Patients may be counted more than once owing to the coexistence of more than one cytogenetic abnormality in the leukemic clone.*

*†Favorable risk: t (15;17), t (8;21), inv (16)/t (16;16); unfavorable risk: inv (3) or t (3;3),t (6;9), t (v;11q23) other than t (9;11), -5 or del (5q), -7 or del (7q), abn (17p), complex karyotype (three or more abnormalities in the absence of a WHO designated recurring chromosome abnormality); intermediate risk: all chromosome abnormalities not classified as favorable or unfavorable. #Only 383 patients were included in this part, for 38 cases giving up treatment or loss to follow-up.*

*Bold values indicated statistically significant differences.*

patient harbored a 3q26 rearrangement. *EVI1*$^{high}$ was not found in the favorable subtypes, including t (8;21) and inv (16). We also studied *EVI1*$^{high}$ in relation to five common single-gene mutations. Three patients with *EVI1*$^{high}$ had an internal tandem duplication of FMS-like tyrosine kinase 3 (*FLT3-ITD)*, and three patients with *EVI1*$^{high}$ had an *ASXL1* mutation; this association was not statistically significant compared to patients with *EVI1*$^{low}$. *EVI1*$^{high}$ was not found in patients with *NPM1*, *C-KIT*, or *CEBPA*-biallelic mutations.

## 3.2 Survival Analysis of Whole Pediatric Acute Myeloid Leukemia (AML)

An evaluation of the treatment response and the survival data were only available for 383 patients, including 35 patients with *EVI1*$^{high}$, because some of them discontinued treatment or were lost to follow-up. The median follow-up time for survival was 32.5 (range, 2.6–134.1) months. Of the 383 cases, the CR rate was 85.6% (328/383) and 91.7% (342/373) after the first and second courses of induction, respectively; the relapse rate was 19.5% (64/328) and the chemotherapy-related mortality was 4.7% (18/383). The 5-year EFS and OS were 66.7% and 75.2%, respectively.

## 3.3 Survival Analysis of Pediatric Acute Myeloid Leukemia (AML) With a High Ecotropic Viral Integration Site 1 Expression (*EVI1*$^{high}$)

For the 35 patients with *EVI1*$^{high}$, 32 patients (91.4%) achieved CR and 26 (74.3%) patients achieved MRD negative after the first course of induction, whereas 27 patients (93.1%) achieved CR and 25 (86.2%) patients achieved MRD negative after the second course of induction, respectively; the relapse rate was 20% (7/35) and the chemotherapy-related mortality was 2.9% (1/35).

The proportion of patients with bone marrow blasts >15% after the first course of induction, and CR rate after the second course of induction was not statistically different between the *EVI1*$^{high}$ and *EVI1*$^{low}$ subgroups. Patients with *EVI1*$^{high}$ had a significantly worse 5-year EFS and OS than those with *EVI1*$^{low}$ (EFS: 51.7% *vs.* 68.1%, $p = 0.041$; OS: 53.1% *vs.* 77.0%, $p = 0.041$) (**Figure 1**).

Risk factors, including age, sex, WBC, FAB type, risk category, and genetic abnormalities, were evaluated using a univariate Cox analysis (**Figure 2**). *EVI1*$^{high}$ was a significant factor for the decreased EFS and OS (HR = 1.821 and 2.401, $p = 0.036$ and 0.005, respectively). In addition, poor prognostic predictors also included WBC $\geq 50 \times 10^9$/L, risk category, *FLT3-ITD* mutation, failure to achieve CR after the second course of induction, and the proportion of bone marrow blasts higher than 15% after the first course of induction (all HR > 1 and $p < 0.05$). In contrast, an *AML1-ETO* as a favorable predictor of improved the EFS and OS (HR = 0.442 and 0.465, $p = 0.002$ and 0.015, respectively).

A multivariate Cox analysis was then performed to evaluate the independent prognostic factors (**Figure 3**). The results showed that *EVI1*$^{high}$ significantly affected the OS (HR = 2.447, $p = 0.015$) but not EFS (HR = 1.556, $p = 0.174$). Similarly, the risk category based on the treatment program was a poor independent prognostic predictor for the OS (HR = 1.759, $p = 0.033$) and tendentially predicted a worse EFS (HR = 1.569, $p = 0.058$). A WBC count $\geq 50 \times 10^9$/L and a proportion of bone marrow blasts greater than 15% after the first course were independent risk predictors for the OS and EFS (all HR > 1 and $p < 0.05$). However, failure to achieve CR after two courses of induction treatment was an independent prognostic factor for an inferior EFS (HR = 1.915, $p = 0.047$), excluding the OS (HR = 1.591, $p = 0.25$).

## 3.4 Characteristics and Prognostic Value of High Ecotropic Viral Integration Site 1 Expression (*EVI1*$^{high}$) in Patients With *MLL* Rearrangements

As noted above, *EVI1*$^{high}$ was associated with *MLL* rearrangement. *EVI1*$^{high}$ was detected in 21.4% (15/70) of all patients with *MLL* rearrangements and 18.8% (6/32) of patients with *MLL-AF9*. The characteristics of patients with *MLL* rearrangements categorized according to the *EVI1* status are shown in **Supplementary Table S2**. *EVI1*$^{high}$ was significantly correlated to an unfavorable cytogenetic aberrance (73.3% *vs.* 38.2%, both $p < 0.02$). *EVI1*$^{high}$ had a significantly adverse 5-year EFS and OS in all patients with *MLL* rearrangements (EFS: 34.5% *vs.* 84.5%, OS: 34.8% *vs.* 89.7%, both $p < 0.0001$) (**Figure 4**). The same conclusion was found in patients with *MLL-AF9* (EFS: 50.0% *vs.* 87.7%, $p = 0.013$; OS: 50.0% *vs.* 93.7%, $p = 0.0035$) (**Figure 4**).

A Cox regression analysis was performed. Only 65 patients with *MLL* rearrangements were included. The results revealed that *EVI1*$^{high}$ was an independent adverse predictor of the OS and EFS in patients with *MLL* rearrangements (univariate analysis: HR = 9.921 and 7.253, both $p < 0.001$; multivariate analysis: HR = 7.186 and 7.315, $p = 0.005$ and 0.001, respectively) (**Table 2**). Among the AML patients with *MLL-AF9*, significant differences in the OS and EFS were observed in the univariate analysis (HR = 13.349 and 7.112, $p = 0.025$ and 0.032, respectively); however, multivariate analysis did not identify *EVI1*$^{high}$ as an independent prognostic factor for the OS and EFS (HR = 13.056 and 10.091, $p = 0.060$ and 0.066, respectively; **Table S2**).

## 3.5 The Impact of a Different Induction Regimen and Effect of Hematopoietic Stem Cell Transplantation (HSCT) after First Complete Remission (CR1) in Patients With a High Ecotropic Viral Integration Site 1 Expression (*EVI1*$^{high}$)

Of the 35 patients with *EVI1*$^{high}$ who underwent an evaluation of the treatment response and survival data, the CR rate after the first course of chemotherapy of the 26 patients who received FLAG-IDA induction was significantly higher than that of the remaining 9 patients who received DAE induction (100% *vs.* 66%, $p = 0.013$). The Kaplan-Meier analysis showed that the FLAG-IDA group had a trend for a better 5-year EFS and OS, without a significant statistical difference (EFS: 62.7% *vs.* 41.7%, $p = 0.37$; OS: 65.7% *vs.* 38.9%, $p = 0.19$). A total of 14 patients with *EVI1*$^{high}$ who underwent HSCT after CR1 had a better

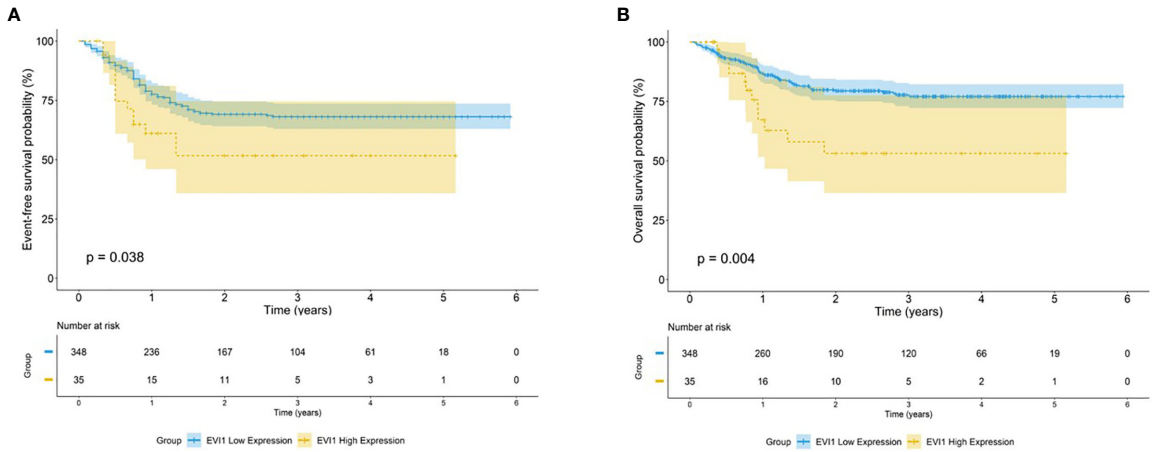


**FIGURE 1** | Survival outcome for high EVI1 expression in pediatric AML. Kaplan–Meier curve estimates for the **(A)** EFS and **(B)** OS in the total cohort between *EVI1*$^{high}$ and *EVI1*$^{low}$ patients.

5-year EFS and OS, but this difference was not statistically different (EFS: 68.4% *vs.* 50.8%, $p = 0.26$; OS: 65.9% *vs.* 54.8%, $p = 0.45$) (**Figure 5**).

## 4 DISCUSSION

In the present study, we retrospectively analyzed the characteristics and prognostic value of *EVI1*$^{high}$ in pediatric patients with AML. Our study enrolled pediatric patients aged 7–176 months in a large cohort of 421 pediatric patients with AML who received uniform treatments from multiple centers, with the inclusion of the respective FAB subtypes, cytogenetic characteristics, and molecular genetic characteristics, which are broadly representative. This study showed that *EVI1*$^{high}$ significantly correlated with unfavorable types, including MLL rearrangements, FAB-M7, and a complex karyotype, but was mutually exclusive for favorable types, including t (8;21), inv (16), an *NPM1*-mutation, and *CEBPA*-biallelic mutations. Furthermore, our results demonstrate that *EVI1*$^{high}$ is a poor independent prognostic factor for the survival in pediatric AML, especially in patients with *MLL* rearrangements. In view of its significant correlation with the survival, *EVI1*$^{high}$ is expected to be an excellent prognostic marker.

In this cohort, *EVI1*$^{high}$ was detected in 9.0% of cases, which was consistent with a previous pediatric study by Balgobind et al. (10), and several adult studies that indicated a percentage of 6%–11% (15, 16). However, the prevalence of *EVI1*$^{high}$ in our study was lower than the 28% reported by Ho et al. (9) (58/206) and 16% reported by Jo et al. (17) (21/130). This difference may reflect the distinct definitions in the studies, including the detection method, the cutoff value selection method, and the control gene used for normalization. In the study of Balgobind et al. (10), the cumulative relative expression of *EVI1-1A*, *-1B*, *and -3L* to a GAPDH above 1.5% is consistent with our definition of *EVI1*$^{high}$, showing the highest correlation with *EVI1*$^{high}$ cases based on the gene expression profiling; all normal bone marrow samples were below this threshold. In the study of Ho et al. (9), beta glucuronidase was quantified as an internal control, and *EVI1*$^{high}$ was defined as the cumulative relative expression of the total *EVI1 (*including *EVI1-1A*, *1B*, *1C*, *and 1D*), and the *MDS1* and *EVI1* complex fusion transcript, which was >1.0-fold increase compared to the normal peripheral blood controls. In the study of Jo et al. (17), patients with an *EVI1/ABL1* ratio higher than 0.1 were defined as *EVI1*$^{high}$. In our study, to avoid the inclusion of false-positive cases, patients were defined as *EVI1*$^{high}$ with an expression level of 10 or higher compared to a pool of 15 healthy bone marrow controls. The definition of *EVI1*$^{high}$ is still debatable, as the AML patient groups selected by the different definitions vary in size and may have an inferior prognosis. Thus, the studies may not be directly comparable, and standardization of *EVI1* transcript testing and reporting is required.

Previous studies have indicated that *EVI1*$^{high}$ is strongly associated with specific genetic and morphological subtypes in both pediatric and adult AML (9, 10, 15, 17), and the similarities and differences regarding *EVI1*$^{high}$ in pediatric vs. adult AML are shown in **Supplementary Table S4**. *EVI1*$^{high}$ in adult AML is frequently associated with and presumed to directly result from alterations in 3q26. In contrast, we detected only one patient with chromosomal rearrangements of 3q26 in our study. In pediatric AML, 3q26 abnormalities are rare. In the study of Balgobind et al., no 3q26 abnormalities were identified in pediatric AML patients with *EVI1* overexpression (10). A similar result was shown by the research of Jo et al., and the 3q26 abnormality was not detected either at the level of conventional cytogenetics or cryptically in the whole genome and transcriptome sequencing data (17). The mechanisms of *EVI1* overexpression in pediatric AML appear to be different from that of adult patients. We speculate that *EVI1* overexpression may not be the driving factor in pediatric AML, but a secondary event after leukemogenesis.

All patients with *EVI1*$^{high}$ in this study belonged to the intermediate- or high-risk cytogenetic/molecular aberrance group based on the current risk stratification (3, 18), as they showed *MLL*

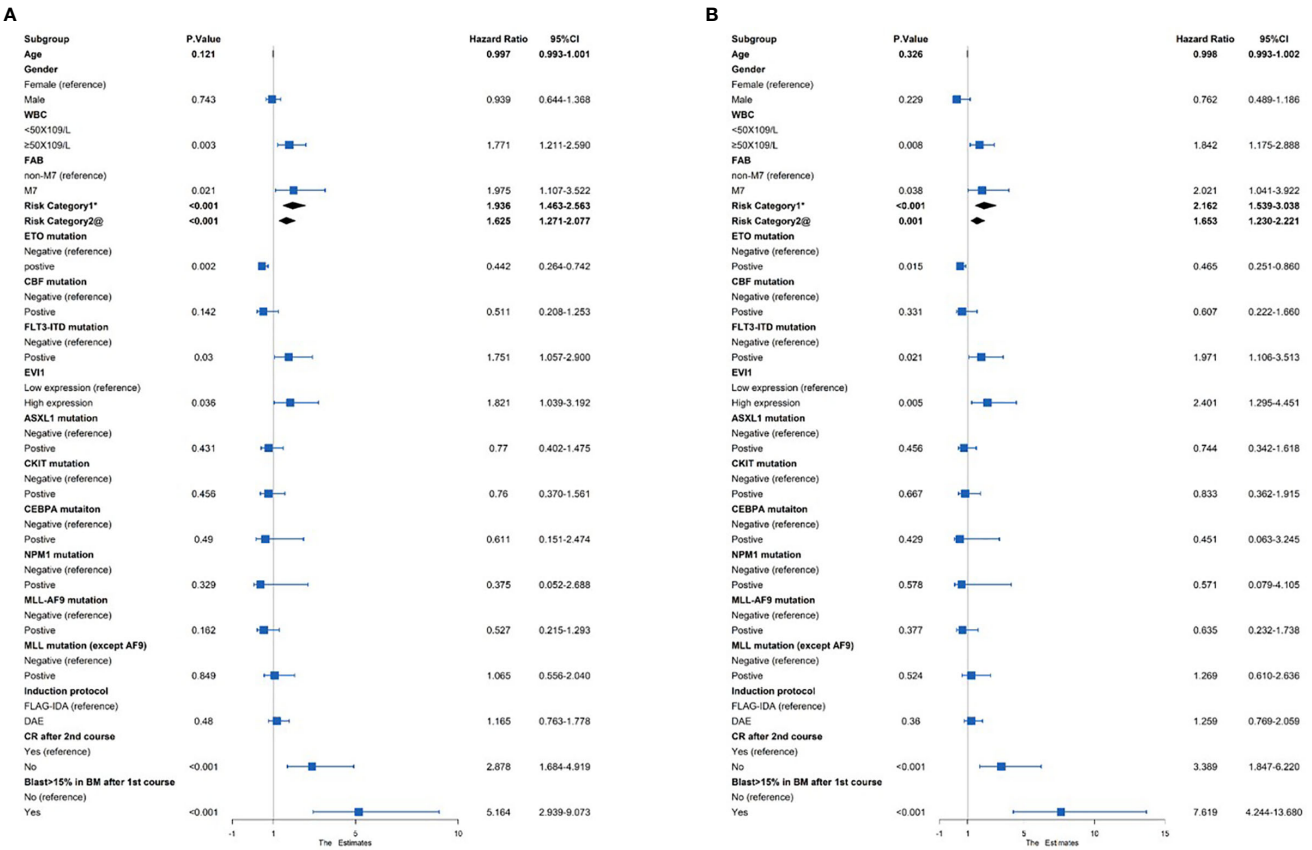


**FIGURE 2** | Univariate Cox regression analysis of the **(A)** EFS and **(B)** OS among 383 pediatric AML patients. *Risk category based on treatment regimens. Refer to **Supplementary Table S1**. @Risk category based on cytogenetic stratification of ELN 2017.

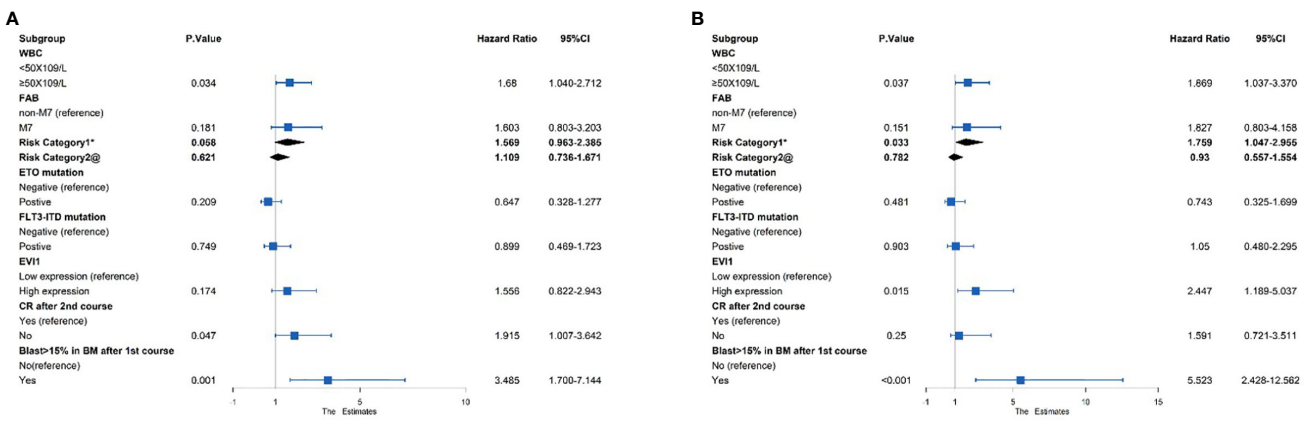


**FIGURE 3** | Multivariate Cox regression analysis of the **(A)** EFS and **(B)** OS among 383 pediatric AML patients. *Risk category based on treatment regimens. Refer to **Supplementary Table S1**. @Risk category based on cytogenetic stratification of ELN 2017.

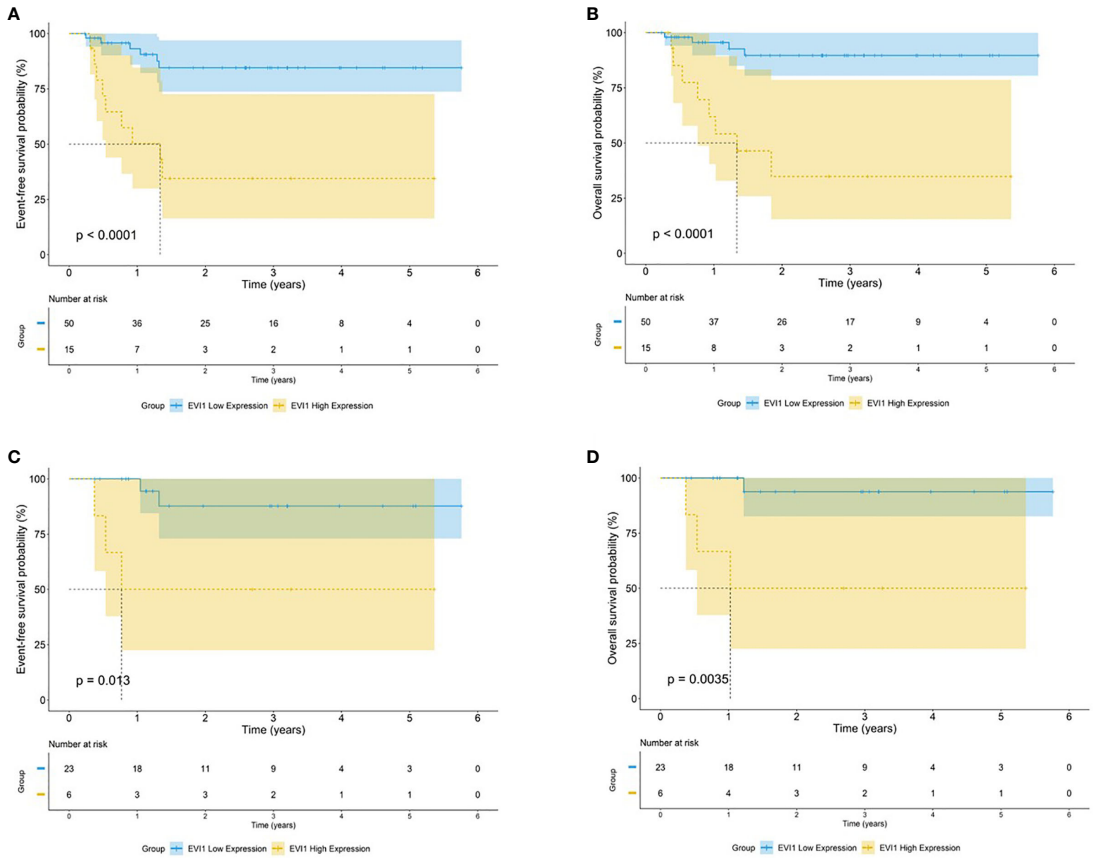


**FIGURE 4** | Survival outcomes by *EVI1* expression among patients carrying t(v;11). Kaplan–Meier curve estimates for the **(A)** EFS and **(B)** OS in the cohort of MLL rearranged AML between *EVI1*$^{high}$ and *EVI1*$^{low}$ patients. Kaplan–Meier curve estimates for the **(C)** EFS and **(D)** OS in the cohort of *MLL-AF9* rearranged AML between *EVI1*$^{high}$ and *EVI1*$^{low}$ patients.

rearrangements and complex karyotypes. Furthermore, consistent with previous pediatric studies (9, 10, 17), *EVI1*$^{high}$ was also significantly associated with a FAB class M7 unrelated to trisomy 21, which has been reported to confer a poor prognosis in pediatric AML (19, 20), while *EVI1*$^{high}$ had a higher incidence of FAB-M5 in adult AML (21). Moreover, *EVI1*$^{high}$ was mutually exclusive with t (8;21), inv (16), *NPM1*-mutations, and *CEBPA*-biallelic mutations, representing favorable types of pediatric AML.

Although almost all relevant studies have shown an adverse impact of *EVI1*$^{high}$ on the therapeutic response and prognosis in adult AML (8, 15, 16), this was not completely consistent in pediatric AML. The reasons for these differences may lie with the therapy and prognosis between adults and children, but also in the different definitions of *EVI1*$^{high}$ and smaller sample sizes. In previous pediatric studies (9, 10, 17), *EVI1*$^{high}$ had significantly lower rates of EFS and OS but had no independent prognostic value for pediatric AML. In the present study, 421 pediatric patients with *de novo* AML were included, and patients with *EVI1*$^{high}$ had a significantly lower 5-year OS and EFS rates. Furthermore, *EVI1*$^{high}$ was also a significant predictor of a decreased OS and EFS in a separate univariate model and an independent prognostic factor for the OS but not EFS in a multivariate model including *EVI1*$^{high}$ and the aforementioned risk groups. To our knowledge, this study is the first to indicate that *EVI1*$^{high}$ has an independent prognostic value for pediatric AML.

*MLL* rearrangements are present in 15%–20% of pediatric patients with *de novo* AML and are associated with a poor prognosis (22). However, *MLL* rearrangements comprise a biologically and clinically heterogeneous group (23). A large international study of pediatric AML with *MLL* rearrangements identified specific translocations with prognostic associations (24). Previous studies have indicated that *EVI1* is a transcriptional target of *MLL* oncoproteins in hematopoietic stem cells and plays a critical role in tumor growth in a subset of *MLL*-r AML (25, 26). In a report of adult AML, *EVI1*$^{high}$ was the sole prognostic factor for the inferior OS, RFS, and EFS in both patients with *MLL*-r AML and patients with *MLL-AF9* (27). However, there have been inconsistent conclusions in the pediatric studies. Ho et al. (9) showed that *EVI1*$^{high}$ could not determine its prognostic value in pediatric AML with *MLL* rearrangements. Jo et al. (17) revealed that *EVI1*$^{high}$ was mainly detected and had a prognostic significance in myelomonocytic-lineage leukemia with *MLL* rearrangements.

**TABLE 2** | Univariate and multivariate analysis of patients with *MLL* rearrangement.

| Cases (n = 65) | EFS | | | OS | | |
|---|---|---|---|---|---|---|
| **Univariate Analysis** | ***HR*** | **95% CI** | ***P*-value** | ***HR*** | **95% CI** | ***P*-value** |
| Age (+1 year) | 0.993 | 0.981–1.006 | 0.292 | 0.997 | 0.984–1.009 | 0.602 |
| Gender (Male) | 0.824 | 0.299–2.274 | 0.709 | 0.706 | 0.227–2.191 | 0.547 |
| WBC (≥50X109/L) | 2.600 | 0.943–7.173 | 0.065 | 3.115 | 0.988–9.816 | 0.052 |
| FAB (M7) | 2.333 | 0.522–10.418 | 0.267 | 1.203 | 0.155–9.348 | 0.860 |
| Risk Category1* | *2.259* | 0.771–6.616 | 0.137 | 3.287 | 1.041–10.381 | **0.043** |
| Risk Category2@ | 2.599 | 0.888–7.606 | 0.081 | 3.924 | 1.062–14.504 | **0.040** |
| FLT3-ITD mutation | 1.078 | 0.142–8.210 | 0.942 | 1.443 | 0.186–11.192 | 0.726 |
| *EVI1*$^{high}$ | 7.253 | 2.559–20.561 | **<0.001** | 9.921 | 2.954–33.319 | **<0.001** |
| ASXL1 mutation | 0.041 | 0.000–39.818 | 0.363 | 0.041 | 0.000–97.422 | 0.421 |
| Induction protocol (DAE) | 3.390 | 1.226–9.371 | **0.019** | 2.704 | 0.857–8.528 | 0.090 |
| No CR after 2nd course | 8.280 | 2.252–30.448 | **0.001** | 6.891 | 1.438–33.021 | **0.016** |
| Blast>15% in BM after 1st course | 1.962 | 0.442–8.705 | 0.376 | 2.760 | 0.604–12.618 | 0.190 |
| **Multivariate Analysis** | **HR** | **95% CI** | ***P*-value** | **HR** | **95% CI** | ***P*-value** |
| Risk Category1* | / | / | / | 0.985 | 0.206–4.715 | 0.985 |
| Risk Category2@ | / | / | / | 1.593 | 0.331–7.667 | 0.561 |
| Induction protocol (DAE) | 3.284 | 0.849–12.707 | 0.085 | / | / | / |
| *EVI1*$^{high}$ | 7.315 | 2.208–24.229 | **0.001** | 7.186 | 1.843–28.019 | **0.005** |
| **No CR after 2nd course** | 3.046 | 0.625–14.835 | 0.168 | 4.840 | 0.836–28.032 | 0.078 |

**Risk category based on treatment regimens. Refer to* ***Supplementary Table S1****.*
*@Risk category based on cytogenetic stratification of ELN 2017.*
*Bold values indicated statistically significant differences.*

Matsuo et al. (28) also showed that *EVI1*$^{high}$ was an independent poor prognostic factor for the EFS but not OS in children with *MLL*-r AML. In the present study, *EVI1*$^{high}$ was associated with adverse EFS and OS in both the *MLL*-r and *MLL-AF9* subgroups. A multivariate analysis identified *EVI1*$^{high}$ as an independent prognostic factor predicting a poor EFS and OS in the total cohort of *MLL*-r AML, but not in the *MLL-AF9* subgroup, which may be caused by the smaller sample size.

At present, chemotherapy remains the front-line treatment for newly diagnosed pediatric AML, but the regimen for patients with *EVI1*$^{high}$ is not unified. Based on the medical research council AML15 trial (29), we have considered the FLAG-IDA or DAE regimen as induction chemotherapy. In the present study, the excellent CR rate of the FLAG-IDA regimen was significantly higher than that of the DAE regimen, which may indicate that the FLAG-IDA regimen is more suitable for induction in children with *EVI1*$^{high}$. Studies on whether pediatric AML patients with *EVI1*$^{high}$ need to undergo HSCT in CR1 are few. However, *EVI1*$^{high}$ is predominantly present in unfavorable cytogenetic subtypes (high or intermediate risk) and predicts adverse outcomes for all AML patients (also for the *MLL-r* subtype). Furthermore, previous research has shown that HSCT significantly improved the prognosis of adult AML patients with *EVI1*$^{high}$ and those with the *MLL*-r subtype as well (15, 27). Moreover, patients with *EVI1*$^{high}$ who underwent HSCT after CR1 had a higher OS and EFS than those who only received chemotherapy. Therefore, we suggest that pediatric AML patients (also in *MLL*-r subtype) with *EVI1*$^{high}$ should undergo HSCT in the first CR. However, it is still essential to conduct prospective multicenter clinical studies including more patients to confirm whether HSCT could improve the long-term survival of pediatric patients with AML and *EVI1*$^{high}$.

Moreover, novel therapeutic strategies effective for pediatric patients with *EVI1*$^{high}$ are also constantly being explored. Saito et al. (30) found that CD52 was highly expressed in most *EVI1*$^{high}$ leukemia cells, and humanized anti-CD52 monoclonal antibody CAMPATH-1H could inhibit cell growth and induce the apoptosis of *EVI1*$^{high}$ leukemia cells. These suggest that CAMPATH-1H may be effective in treating myeloid leukemia with *EVI1*$^{high}$. However, the correlation between CD52 and *EVI1*$^{high}$ in AML patients still needs to be verified because CD52 is not tested routinely during flow cytometry for establishing a diagnosis. Furthermore, whether CAMPATH-1H is effective in treating myeloid leukemia with *EVI1*$^{high}$ also needs to be clarified in clinical studies. Mittal et al. (31) reported that *EVI1*-induced hypermethylation and downregulation of miR-9 play an important role in leukemogenesis in pediatric patients with AML and *EVI1*$^{high}$, indicating that hypomethylating agents may be a potential therapeutic strategy for these patients. Nguyen et al. (32) showed that *EVI1* plays an important role in the key properties of AML leukemic stem cells, and all-trans retinoic acid (ATRA) enhances the effects of *EVI1* on AML stemness, thus, raising the possibility of using RAR antagonists in the therapy of *EVI1*$^{high}$ AML. However, Steinmetz et al. (33) and Verhagen et al. (34) demonstrated that primary AML cells with *EVI1*$^{high}$ were sensitive to ATRA, indicating that ATRA may be a candidate for patients with AML and *EVI1*$^{high}$. As noted above, *EVI1*$^{high}$ was associated with *MLL* rearrangement. As a highly effective inhibitor targeting MLL, Menin reduced leukemia burden significantly and prolonged survival in *in vivo* experiments, which indicated that Menin may be effective in treating myeloid leukemia with *EVI1*$^{high}$ (35, 36).

The limitation of this study is that it was a retrospective study and only 35 patients expressed *EVI1*$^{high}$, and it will be necessary to explore more effective treatments through prospective

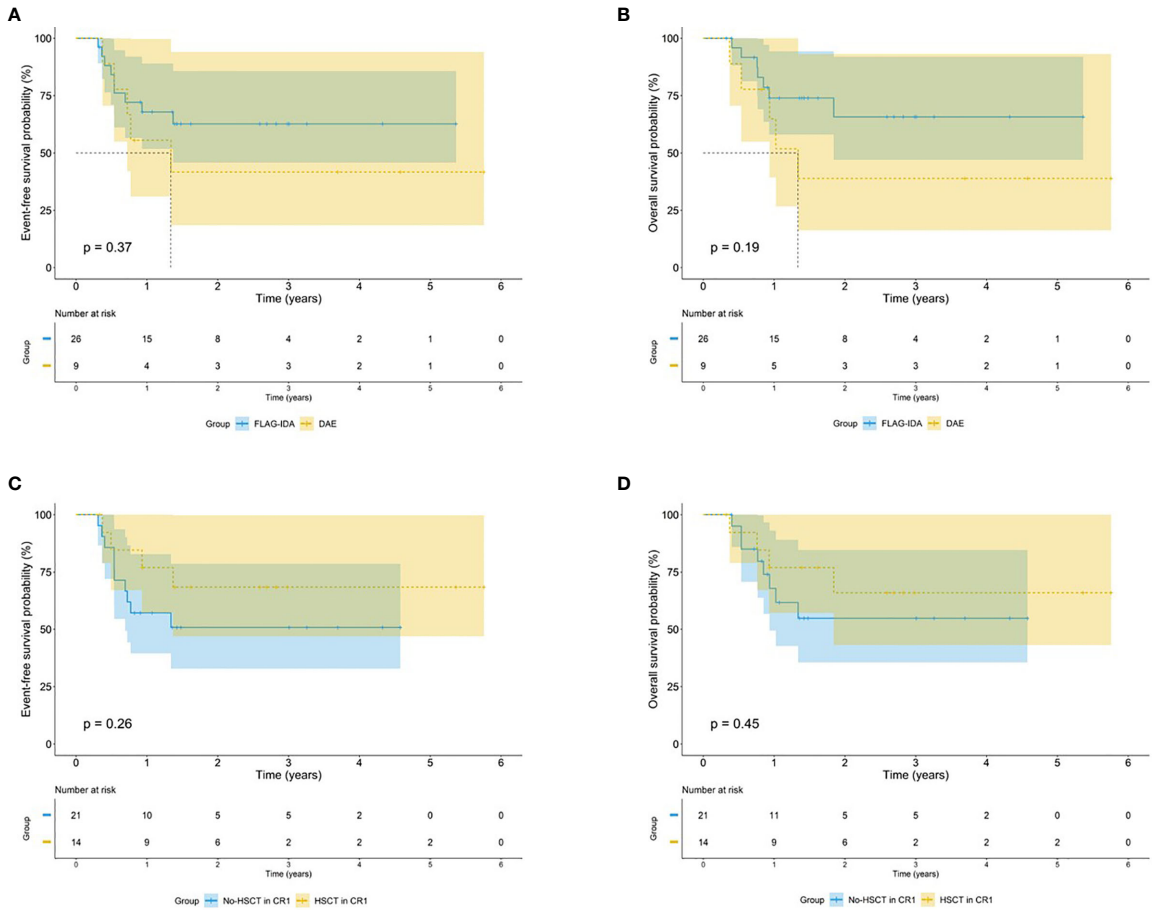


**FIGURE 5** | Survival outcomes by treatment regimens among *EVI1*$^{high}$ patients. Kaplan–Meier curve estimates the impact of different induction regimens on the **(A)** EFS and **(B)** OS in the cohort of *EVI1*$^{high}$ patients. Kaplan–Meier curve estimates the impact of HSCT after CR1 on the **(C)** EFS and **(D)** OS in the cohort of *EVI1*$^{high}$ patients.

multicenter studies to improve long-term outcomes of pediatric patients with AML and *EVI1*$^{high}$.

In conclusion, *EVI1*$^{high}$ is significantly associated with specific unfavorable cytogenetic (*MLL* rearrangements and complex karyotypes) and morphologic (FAB-M7) subtypes in pediatric AML. Furthermore, this study is the first to indicate that *EVI1*$^{high}$ is an independent adverse prognosis predictor for survival, especially in *MLL*-r AML. These results may be conducive to risk stratification and therapy decisions in pediatric patients with AML, and *EVI1* transcript levels should be routinely assessed at diagnosis for risk stratification once a standard laboratory protocol is established and the cutoff value is determined.

## DATA AVAILABILITY STATEMENT

The original contributions presented in the study are included in the article/**Supplementary Material**. Further inquiries can be directed to the corresponding authors.

## ETHICS STATEMENT

The studies involving human participants were reviewed and approved by the ethics committees from Fujian Medical University Union Hospital, Nanfang Hospital, TaiXin Hospital, Hunan Children's Hospital, Sun Yat-sen Memorial Hospital, Guangzhou Women and Children's Medical Center, and People's Hospital of Hunan Province. Written informed consent to participate in this study was provided by the participants' legal guardian/next of kin.

## AUTHOR CONTRIBUTIONS

YZ, JL, and JH conceived and designed the experiments. YZ performed the experiments. YZ, SL, HZ, XHu, ZC, XF, CL, MZ, HX, YHe, and XHe collected the clinical data. YZ and YHu analyzed and interpreted the data. YZ and YHu wrote the manuscript. JH critically revised the manuscript. All authors contributed to the article and approved the submitted version.

## FUNDING

This work was supported by the Construction Project of the Fujian Medical Center of Hematology (Min201704), Startup fund of scientific research, Fujian medical university (2019QH1022, 2019QH1032).

## ACKNOWLEDGMENTS

We would like to express our deepest gratitude to patients who donated samples for research purpose. We would like to express our sincere thanks to the doctors of the cooperative units for providing the clinical data.

## SUPPLEMENTARY MATERIAL

The Supplementary Material for this article can be found online at: https://www.frontiersin.org/articles/10.3389/fonc.2021.712747/full#supplementary-material

**Supplementary Figure 1 |** C-HUANAN-AML15 protocol workflow. FLAG-IDA: Fludarabine 30 mg/m2/d d2-6, cytarabine 2g/m2/d d2-6, Idarubicin 8 mg/m2/d d4-6, Granulocyte Colony Stimulating Factor (G-CSF) 5μg/kg/d d1-7. DAE (3 + 10 +5): Daunorubicin 50 mg/m2/d d1,3,5; Cytarabine 100mg/m2 q12h d1-10, Etoposide 100mg/m2/d d1-5. DAE (3 + 8+5): Daunorubicin 50 mg/m2/d d1,3,5; Cytarabine 100mg/m2 q12h d1-8, Etoposide 100mg/m2/d d1-5. HAE: Homoharringtonine 3mg/m2/d d1-5, Cytarabine 100mg/m2 q12h d1-7, Etoposide 100mg/m2/d d1-5. HHA: Homoharringtonine 3mg/m2/d d1-7, Cytarabine 2g/m2 q12h d1-3. MidAc: Mitoxantrone 10mg/m2/d d1-5, Cytarabine 1g/m2 q12h d1-3.

## REFERENCES

1. Kolb EA, Meshinchi S. Acute Myeloid Leukemia in Children and Adolescents: Identification of New Molecular Targets Brings Promise of New Therapies. *Hematol Am Soc Hematol Educ Program* (2015) 2015(1):507–13. doi: 10.1182/asheducation-2015.1.507
2. Taga T, Tomizawa D, Takahashi H, Adachi S. Acute Myeloid Leukemia in Children: Current Status and Future Directions. *Pediatr Int* (2016) 2:71–80. doi: 10.1111/ped.12865
3. Döhner H, Estey E, Grimwade D, Amadori S, Appelbaum FR, Büchner T, et al. Diagnosis and Management of AML in Adults: 2017 ELN Recommendations From an International Expert Panel. *Blood* (2017) 4:424–47. doi: 10.1182/blood-2016-08-733196
4. Mawad R, Estey EH. Acute Myeloid Leukemia With Normal Cytogenetics. *Curr Oncol Rep* (2012) 5:359–68. doi: 10.1007/s11912-012-0252-x
5. Qin YZ, Zhao T, Zhu HH, Wang J, Jia JS, Lai YY, et al. High EVI1 Expression Predicts Poor Outcomes in Adult Acute Myeloid Leukemia Patients With Intermediate Cytogenetic Risk Receiving Chemotherapy. *Med Sci Monit* (2018) 24:758–67. doi: 10.12659/msm.905903
6. Kataoka K, Kurokawa M. Ecotropic Viral Integration Site 1, Stem Cell Self-Renewal and Leukemogenesis. *Cancer Sci* (2012) 8:1371–7. doi: 10.1111/j.1349-7006.2012.02303.x
7. Goyama S, Kurokawa M. Pathogenetic Significance of Ecotropic Viral Integration Site-1 in Hematological Malignancies. *Cancer Sci* (2009) 6:990–5. doi: 10.1111/j.1349-7006.2009.01152.x
8. Hinai AA, Valk PJ. Review: Aberrant EVI1 Expression in Acute Myeloid Leukaemia. *Br J Haematol* (2016) 6:870–8. doi: 10.1111/bjh.13898
9. Ho PA, Alonzo TA, Gerbing RB, Pollard JA, Hirsch B, Raimondi SC, et al. High EVI1 Expression is Associated With MLL Rearrangements and Predicts Decreased Survival in Paediatric Acute Myeloid Leukaemia: A Report From the Children's Oncology Group. *Br J Haematol* (2013) 5:670–7. doi: 10.1111/bjh.12444
10. Balgobind BV, Lugthart S, Hollink IH, Arentsen-Peters ST, van Wering ER, de Graaf SS, et al. EVI1 Overexpression in Distinct Subtypes of Pediatric Acute Myeloid Leukemia. *Leukemia* (2010) 5:942–9. doi: 10.1038/leu.2010.47
11. Arber DA, Orazi A, Hasserjian R, Thiele J, Borowitz MJ, Le Beau MM, et al. The 2016 Revision to the World Health Organization Classification of Myeloid Neoplasms and Acute Leukemia. *Blood* (2016) 20:2391–405. doi: 10.1182/blood-2016-03-643544
12. Beillard E, Pallisgaard N, van der Velden VH, Bi W, Dee R, van der Schoot E, et al. Evaluation of Candidate Control Genes for Diagnosis and Residual Disease Detection in Leukemic Patients Using 'Real-Time' Quantitative Reverse-Transcriptase Polymerase Chain Reaction (RQ-PCR) - a Europe Against Cancer Program. *Leukemia* (2003) 12:2474–86. doi: 10.1038/sj.leu.2403136
13. Schmittgen TD, Livak KJ. Analyzing Real-Time PCR Data by the Comparative C(T) Method. *Nat Protoc* (2008) 6:1101–8. doi: 10.1038/nprot.2008.73
14. Santamaría CM, Chillón MC, García-Sanz R, Pérez C, Caballero MD, Ramos F, et al. Molecular Stratification Model for Prognosis in Cytogenetically Normal Acute Myeloid Leukemia. *Blood* (2009) 1:148–52. doi: 10.1182/blood-2008-11-187724
15. Gröschel S, Lugthart S, Schlenk RF, Valk PJ, Eiwen K, Goudswaard C, et al. High EVI1 Expression Predicts Outcome in Younger Adult Patients With Acute Myeloid Leukemia and is Associated With Distinct Cytogenetic Abnormalities. *J Clin Oncol* (2010) 12:2101–7. doi: 10.1200/jco.2009.26.0646
16. Lugthart S, van Drunen E, van Norden Y, van Hoven A, Erpelinck CA, Valk PJ, et al. High EVI1 Levels Predict Adverse Outcome in Acute Myeloid Leukemia: Prevalence of EVI1 Overexpression and Chromosome 3q26 Abnormalities Underestimated. *Blood* (2008) 8:4329–37. doi: 10.1182/blood-2007-10-119230
17. Jo A, Mitani S, Shiba N, Hayashi Y, Hara Y, Takahashi H, et al. High Expression of EVI1 and MEL1 is a Compelling Poor Prognostic Marker of Pediatric AML. *Leukemia* (2015) 5:1076–83. doi: 10.1038/leu.2015.5
18. Rau RE, Loh ML. Using Genomics to Define Pediatric Blood Cancers and Inform Practice. *Hematol Am Soc Hematol Educ Program* (2018) 1:286–300. doi: 10.1182/asheducation-2018.1.286
19. Teyssier AC, Lapillonne H, Pasquet M, Ballerini P, Baruchel A, Ducassou S, et al. Acute Megakaryoblastic Leukemia (Excluding Down Syndrome) Remains an Acute Myeloid Subgroup With Inferior Outcome in the French ELAM02 Trial. *Pediatr Hematol Oncol* (2017) 8:425–7. doi: 10.1080/08880018.2017.1414905
20. Schweitzer J, Zimmermann M, Rasche M, von Neuhoff C, Creutzig U, Dworzak M, et al. Improved Outcome of Pediatric Patients With Acute Megakaryoblastic Leukemia in the AML-BFM 04 Trial. *Ann Hematol* (2015) 8:1327–36. doi: 10.1007/s00277-015-2383-2
21. He X, Wang Q, Cen J, Qiu H, Sun A, Chen S, et al. Predictive Value of High EVI1 Expression in AML Patients Undergoing Myeloablative Allogeneic Hematopoietic Stem Cell Transplantation in First CR. *Bone Marrow Transplant* (2016) 7:921–7. doi: 10.1038/bmt.2016.71
22. Conneely S, Rau R. The Genomics of Acute Myeloid Leukemia in Children. *Cancer Metastasis Rev* (2020) 1:189–209. doi: 10.1007/s10555-020-09846-1
23. Winters A, Bernt K. MLL-Rearranged Leukemias-An Update on Science and Clinical Approaches. *Front Pediatr* (2017) 4:4. doi: 10.3389/fped.2017.00004
24. Balgobind BV, Raimondi SC, Harbott J, Zimmermann M, Alonzo TA, Auvrignon A, et al. Novel Prognostic Subgroups in Childhood 11q23/MLL-Rearranged Acute Myeloid Leukemia: Results of an International Retrospective Study. *Blood* (2009) 12:2489–96. doi: 10.1182/blood-2009-04-215152
25. Arai S, Yoshimi A, Shimabe M, Ichikawa M, Nakagawa M, Imai Y, et al. Evi-1 Is a Transcriptional Target of Mixed-Lineage Leukemia Oncoproteins in Hematopoietic Stem Cells. *Blood* (2011) 23:6304–14. doi: 10.1182/blood-2009-07-234310
26. Bindels EM, Havermans M, Lugthart S, Erpelinck C, Wocjtowicz E, Krivtsov AV, et al. EVI1 is Critical for the Pathogenesis of a Subset of MLL-AF9-Rearranged AMLs. *Blood* (2012) 24:5838–49. doi: 10.1182/blood-2011-11-393827

27. Gröschel S, Schlenk RF, Engelmann J, Rockova V, Teleanu V, Kühn MW, et al. Deregulated Expression of EVI1 Defines a Poor Prognostic Subset of MLL-Rearranged Acute Myeloid Leukemias: A Study of the German-Austrian Acute Myeloid Leukemia Study Group and the Dutch-Belgian-Swiss HOVON/SAKK Cooperative Group. *J Clin Oncol* (2013) 1:95–103. doi: 10.1200/jco.2011.41.5505
28. Matsuo H, Kajihara M, Tomizawa D, Watanabe T, Saito AM, Fujimoto J, et al. EVI1 Overexpression is a Poor Prognostic Factor in Pediatric Patients With Mixed Lineage Leukemia-AF9 Rearranged Acute Myeloid Leukemia. *Haematologica* (2014) 11:e225–7. doi: 10.3324/haematol.2014.107128
29. Burnett AK, Russell NH, Hills RK, Hunter AE, Kjeldsen L, Yin J, et al. Optimization of Chemotherapy for Younger Patients With Acute Myeloid Leukemia: Results of the Medical Research Council AML15 Trial. *J Clin Oncol* (2013) 27:3360–8. doi: 10.1200/jco.2012.47.4874
30. Saito Y, Nakahata S, Yamakawa N, Kaneda K, Ichihara E, Suekane A, et al. CD52 as a Molecular Target for Immunotherapy to Treat Acute Myeloid Leukemia With High EVI1 Expression. *Leukemia* (2011) 6:921–31. doi: 10.1038/leu.2011.36
31. Mittal N, Li L, Sheng Y, Hu C, Li F, Zhu T, et al. A Critical Role of Epigenetic Inactivation of miR-9 in EVI1(high) Pediatric AML. *Mol Cancer* (2019) 1:30. doi: 10.1186/s12943-019-0952-z
32. Nguyen CH, Bauer K, Hackl H, Schlerka A, Koller E, Hladik A, et al. All-Trans Retinoic Acid Enhances, and a Pan-RAR Antagonist Counteracts, the Stem Cell Promoting Activity of EVI1 in Acute Myeloid Leukemia. *Cell Death Dis* (2019) 12:944. doi: 10.1038/s41419-019-2172-2
33. Steinmetz B, Hackl H, Slabáková E, Schwarzinger I, Smějová M, Spittler A, et al. The Oncogene EVI1 Enhances Transcriptional and Biological Responses of Human Myeloid Cells to All-Trans Retinoic Acid. *Cell Cycle* (2014) 18:2931–43. doi: 10.4161/15384101.2014.946869
34. Verhagen HJ, Smit MA, Rutten A, Denkers F, Poddighe PJ, Merle PA, et al. Primary Acute Myeloid Leukemia Cells With Overexpression of EVI-1 are Sensitive to All-Trans Retinoic Acid. *Blood* (2016) 4:458–63. doi: 10.1182/blood-2015-07-653840
35. Dzama MM, Steiner M, Rausch J, Sasca D, Schönfeld J, Kunz K, et al. Synergistic Targeting of FLT3 Mutations in AML via Combined Menin-MLL and FLT3 Inhibition. *Blood* (2020) 21:2442–56. doi: 10.1182/blood.2020005037
36. Krivtsov AV, Evans K, Gadrey JY, Eschle BK, Hatton C, Uckelmann HJ, et al. A Menin-MLL Inhibitor Induces Specific Chromatin Changes and Eradicates Disease in Models of MLL-Rearranged Leukemia. *Cancer Cell* (2019) 6:660–73.e11. doi: 10.1016/j.ccell.2019.11.001

**Conflict of Interest:** The authors declare that the research was conducted in the absence of any commercial or financial relationships that could be construed as a potential conflict of interest.

frontiers in Oncology

MINI REVIEW
published: 24 September 2021
doi: 10.3389/fonc.2021.731323

# Steering Mast Cells or Their Mediators as a Prospective Novel Therapeutic Approach for the Treatment of Hematological Malignancies

*Deeksha Mehtani and Niti Puri* *

*Cellular and Molecular Immunology Lab, School of Life Sciences, Jawaharlal Nehru University, New Delhi, India*

Tumor cells require signaling and close interaction with their microenvironment for their survival and proliferation. In the recent years, Mast cells have earned a greater importance for their presence and role in cancers. It is known that mast cells are attracted towards tumor microenvironment by secreted soluble chemotactic factors. Mast cells seem to exert a pro-tumorigenic role in hematological malignancies with a few exceptions where they showed anti-cancerous role. This dual role of mast cells in tumor growth and survival may be dependent on the intrinsic characteristics of the particular tumor, differences in tumor microenvironment according to tumor type, and the interactions and heterogeneity of mediators released by mast cells in the tumor microenvironment. In many studies, Mast cells and their mediators have been shown to affect tumor survival and growth, prognosis, inflammation, tumor vascularization and angiogenesis. Modulating mast cell accumulation, viability, activity and mediator release patterns may thus be important in controlling these malignancies. In this review, we emphasize on the role of mast cells in lymphoid malignancies and discuss strategies for targeting and steering mast cells or their mediators as a potential therapeutic approach for the treatment of these malignancies.

**Keywords: hematological malignancy, mast cells, lymphoid neoplasms, lymphoma, leukemia, blood cancer, cancer therapeutics, myeloma**

OPEN ACCESS

***Edited by:***
*Gurvinder Kaur,*
*All India Institute of Medical Sciences, India*

***Reviewed by:***
*Jean Sylvia Marshall,*
*Dalhousie University, Canada*
*Tijana Martinov,*
*Fred Hutchinson Cancer Research Center, United States*

***Correspondence:**
*Niti Puri*
*purin@mail.jnu.ac.in*

***Specialty section:***
*This article was submitted to Hematologic Malignancies, a section of the journal Frontiers in Oncology*

***Received:*** *26 June 2021*
***Accepted:*** *09 September 2021*
***Published:*** *24 September 2021*

***Citation:***
*Mehtani D and Puri N (2021) Steering Mast Cells or Their Mediators as a Prospective Novel Therapeutic Approach for the Treatment of Hematological Malignancies. Front. Oncol. 11:731323. doi: 10.3389/fonc.2021.731323*

## 1. INTRODUCTION

Cancer is a complicated disease and a leading cause of mortalities, the world over. Hematological malignancies are the most common and frequently occurring cancers in children and the elderly (1, 2). Development of these malignancies is characterized by a crucial transition of hematopoietic cells of a particular lineage to cancerous cells with altered and abnormal cellular proliferation. One such condition that is most commonly seen in elderly people is clonal hematopoiesis, a premalignant disorder characterized by aberrant proliferation of clonally-derived hematopoietic stem cells carrying somatic mutations in leukemia-related genes. Aside from age advancement, this phenomenon is more common in solid or lymphoid tumors and is linked to genotoxic stress (3). Leukemia refers to the clonal expansion of abnormal leukocyte cells in the bone marrow (BM),

which leads to the elevated levels of affected cells in the blood circulation. While lymphoma or lymphoid malignancies show elevated numbers of B or T lymphocytes which are present as tumor in the lymphatic tissue (1). Due to their complexity, the hematologic malignancies become challenging to manage.

Cancer pathogenesis involves multiple interactions between neoplastic cells and their microenvironment resulting in maintenance and progression or rejection of growing tumor. For hematological malignancies, BM or secondary lymphoid organs form the cancer microenvironment which is composed of stromal cells, fibroblasts, immune cells and vascular endothelial cells (4). Dynamic signaling by soluble mediators or cell-cell interactions between leukemia or lymphoma cells and immune cells in the tumor or surrounding microenvironment strongly determines the malignant progression or eradication of tumor. Presence of immune cells also plays a greater role in tumor development or elimination. $CD8^+$ T cells and NK cells eradicate immunogenic cancer cells which leave the variants of cells that are non-immunogenic, making it difficult for the immune system to recognize them (5). Many studies have associated the presence of Mast cells (MCs) and release of various mediators with the remodeling of tumor microenvironment.

MCs are innate immune granulocytes, derived from bone marrow, that migrate to peripheral tissues to mature and reside in mucosal layers and near blood vessels remaining close to the external environment so as to respond quickly to an invasion by a pathogen or allergen (6). Years ago, Paul Ehrlich discovered MCs and found them to be present in close proximity to a tumor (7). MCs have a wide range of surface receptors like FcεRI, histamine receptors, c-KIT receptor, Pattern recognition receptors (PRRs) which on activation make them capable of releasing diverse set of mediators in response to various stimuli (8). In tumor microenvironment, MCs release molecules like Vascular endothelial growth factor (VEGF), heparin, tryptase, Fibroblast growth factor (FGF-2) which can initiate tumor angiogenesis and molecules like Matrix metalloproteinases (MMP-9 and MMP-2) which can enable tumor niche remodeling, migration and invasiveness collectively leading to cancer progression (9). Whereas secreted molecules like histamine, IL-4, IL-8, Tumor necrosis factor (TNF-α) contribute in inhibiting tumor cell survival or growth and inducing apoptosis (9). MC functions are extremely context-dependent and cross-talk between tumor cells-MCs and other tumor-associated immune cells are likely to play a role in determining whether a tumor will be eliminated or progressed.

The existing anti-cancerous treatments focus on targeting the mechanisms behind the abnormally proliferating cells. Therefore, an unmet need in cancer research is to understand the cancer microenvironment and the interplay between tumor cells and the immune cells like MCs which on activation release a diverse variety of mediators having capacity to modulate the tumor microenvironment in favor of or for rejection of cancer. In this review, we emphasize on the role of MCs in hematological malignancies and discuss the strategies to target and steer MCs or their mediators as a potential therapeutic approach for these malignancies.

## 1.1 Dual Role of MCs in Hematological Malignancies

The contribution of immune and inflammatory cells, such as MCs, is well known in the control, progression and invasion of malignant cells. Here we discuss the studies highlighting the correlation between the amount of tumor-infiltrating MCs and the extent of tumor aggressiveness and propagation, implying a significant role of MCs in various hematological malignancies. The characteristics of the studies reviewed have been compiled in **Tables 1** and **2**.

### 1.1.1 The Role of Mast Cells in Lymphomas

MCs have been documented to be involved in shaping the microenvironment in lymphomas, mostly by increasing the microvessel density, increasing angiogenesis and fibrosis thus leading to rogue advancement of lymphomas. Hodgkin's lymphoma (HL), derived from mature B cells, is characterized by tumor cells, Hodgkin's and Reed-Sternberg (HRS) cells in a smoldering inflammatory microenvironment (33). Abundance in tryptase positive MCs has been predominantly associated with inflammation and poor prognosis in patients with HL. Infiltration of TGF-β producing MCs in HL's subtype-nodular sclerosis has been associated with the invasion of neoplastic cells, the development of fibrosis and progression of HL by the promotion of angiogenesis (10, 25). MCs were shown to promote HL cell growth in SCID mice *in vivo* (25). In HL, MCs have also been reported to interact directly with tumor cells *via* CD30-CD30L, causing HRS cells to become activated and proliferate could be important for HL pathogenesis (10–12). Indirect interactions between tumor cells and MCs caused by soluble factors produced by HRS cells, such as IL-9, IL-13, CCL5/RANTES are important for MC infiltration and proliferation (10, 11, 13, 26). MCs are, therefore, involved in shaping the HL microenvironment in terms of angiogenesis and fibrosis leading to advancement of tumor cells towards invasion and nodular progression.

Splenic marginal zone lymphoma (SMZL), is characterized by indolent neoplastic B cells that infiltrate the spleen and sometimes the BM (34). MCs are directly recruited by neoplasm cells in the tumor microenvironment and support the stromal cell proliferation, angiogenesis, extracellular matrix (ECM) remodeling in this B cell malignancy. Also, stromal cells highly express CD40 which recruits MCs expressing CD40 ligand, lead to the release of IL-6 with other pro-inflammatory cytokines, thereby activating B cells, increasing the survival and proliferation of neoplastic cells and contributing to pathobiology of SMZL progression (14).

B cell lymphoma (BCL) accounts for 90% of lymphoid neoplasms worldwide. The most common and aggressive form of non-Hodgkin lymphoma that occurs within the lymph nodes, but can be present anywhere in the body outside the lymphoid system, is diffuse large B cell lymphoma (DLBCL). Marinaccio et al. speculated that a decrease in MC density would result in reduced inflammatory signals and increased pro-angiogenic signals by regulatory T cells ($T_{regs}$) (17). Whereas, an increase in MC density can enhance inflammation and suppress the functions of $T_{regs}$ thereby allowing the differentiation and expansion of $T_h17$ lymphocytes leading to angiogenesis (17).

**TABLE 1** | Characteristics of clinical studies included in this review mentioning the stage of hematological malignancies and number of mast cells.

| Type of hematological malignancy | Stage of hematological malignancy | Mast cell number | Role played by MCs | Year of publication | Reference |
|---|---|---|---|---|---|
| Hodgkin's Lymphoma | subtypes of CHL (NSCHL and non-NSCHL) | Higher number of MCs in IL-13 positive HRS cell group | Pro-tumorigenic | 2016 | (10) |
| | Stage I-IIA<br>Stage IIB-IV | The disease-free survival rate and overall survival rate were both lower in patients with a higher MC count | | 2002 | (11) |
| | NS subtype, non NS subtype,<br>MxC subtype | CD30L is expressed by MCs, and there is no difference in MCs numbers between groups. | | 2001 | (12) |
| | Stage I-II<br>Stage III-IV, Histological type-NS subtype<br>MxC subtype | MCs were more in nodular sclerosis (NS) than mixed cellularity (MxC) subtype | | 2015 | (13) |
| Splenic Marginal Zone Lymphoma | Grouped according to IIL score (Low risk, intermediate risk, high risk) | MCs express CD40L | Pro-tumorigenic | 2014 | (14) |
| Primary Cutaneous Lymphoma (PCL) | Mycosis fungoides (MF)<br>Stage IA-IB<br>Stage IIA-IIB | MC number and density higher in early stages of MF IA and IB | Pro-tumorigenic | 2016 | (15) |
| | For MF, FMF, SS<br>Stage IA-IB<br>Stage IIA-IIB<br>Stage IIIB<br>Stage IVA | MC number and degranulation increase in CTCL and CBCL | | 2012 | (16) |
| B cell Lymphoma (BCL) | DLBCL (Diffuse large B cell lymphoma)<br>Stage III-IV | Not mentioned | Pro-tumorigenic | 2016 | (17) |
| | Stages Not mentioned<br>Samples from DLBCL, FL, Mantle cell lymphoma, marginal zone B cell lymphoma | | | 2011 | (18) |
| T cell Lymphoma (TCL) | Stages not mentioned, samples from BCL, TCL | MC numbers were higher in TCL than BCL | Pro-tumorigenic | 2001 | (19) |
| | Stage not mentioned.<br>Samples from AITL (Angioimmunoblastic T cell lymphoma), PCL | MC numbers were higher in AITL than PCL | | 2010 | (20) |
| Leukemia | CML Phases mentioned Chronic Phase, Accelerated Phase and Blast Phase (ALLT, AMLT) | MC numbers were highest in AMLT (Acute myeloid leukemia transformation stage) | Pro-tumorigenic | 2019 | (21) |
| Multiple Myeloma (MM) | Stage I, II, III | MC density was higher in advanced stages of MM | Pro-tumorigenic | 2013 | (22) |
| | Stage I, II, III | The diseased state had a higher MC density than the healthy control. | | 2015 | (23) |
| | Active MM (Stage I, II, III) | The diseased state had a higher MC density than the healthy control group, and it was even higher in advanced stages of MM. | | 2016 | (24) |

Feng et al. considered IL-9 to be a key driver of tumor growth by which $T_{regs}$ recruited and activated MCs to mediate immune suppression in the tumor region (18). The interplay of infiltrating $T_{regs}$ and MCs in the tumor microenvironment therefore promotes the formation of tumor vessels, maintains the growth and metastasis of tumor in BCL.

Primary cutaneous lymphoma (PCL) is a non-Hodgkin's lymphoma also known as lympho-proliferative neoplasm of clonal B cell or T cell lymphoma largely associated with the skin (35). Studies have shown that there is an increased number of MCs present in both the cutaneous B cell lymphoma (CBCL) and cutaneous T cell lymphoma (CTCL) in peripheral rims of skin (15). In CTCL presence of MCs is correlated with reduced survival and increased malignancy in patients with progressive disease or advanced disease stage in Folliculotropic mycosis fungoides and Se´zary syndrome compared to stable patients or early disease stage in Mycosis fungoides (MF) (16). MCs are not only present in advanced stages of CTCL and CBCL, but have also extensively degranulated, which is much more noticeable in progressive form of these neoplasms, whereas more non-degranulated form of MCs are present in MF (15). *In vitro* study has shown that the supernatant of MCs obtained by treatment with calcium ionophore can induce the production of cytokines such as IL-17, IL-6 from tumor cells and increase the proliferation of primary CTCL cells (16). For the first time, Rabenhorst et al. have used a connective tissue-MCs depleted mouse model to demonstrate the delay in development of PCL thus highlighting the crucial role of MCs in controlling the tumor progression (16). Rabenhorst et al. also demonstrated that adding MC supernatant increased the proliferation of Sezary and CTCL cell lines whereas MC supernatant had no effect on the proliferation of SeAx and Mac2B CTCL cell lines when MC degranulation was inhibited by cromolyn (16). Therefore MCs play a pro-tumorigenic role in PCL, which is critical in the advanced stages of the disease and can be linked to disease severity.

T cell lymphomas (TCLs) account for the rare group of non-Hodgkin's lymphoma group due to their low prevalence. Angioimmunoblastic TCL (AITL) is the uncommon aggressive subtype of the mature peripheral TCL that involves lymph node (36) and dysregulation of T cell immune response (37). The

**TABLE 2 |** Experimental setup of the studies included in this review.

| Type of hematological malignancy | Experimental setup | Demonstrated role played by mast cells | Year of publication | Reference |
|---|---|---|---|---|
| Hodgkin's Lymphoma | *In vitro* (human HL cell lines L428, HDLM2,KMH2; human leukemia cell line HL60; mouse BMMC, SPMCs | Pro-tumorigenic | 2012 | (25) |
| | *In vivo* (NOD/SCID mice) | | | |
| | Patient sample | | 2016 | (10) |
| | Patient sample | | 2002 | (11) |
| | Patient sample, *In vitro* (HMC-1, KU812) | | 2001 | (12) |
| | Patient Sample | | 2015 | (13) |
| | *In vitro* (HL cell lines CO, DEV, HDLM-2,KMH2,L540), umbilical cord derived CBMC | | 2003 | (26) |
| Splenic Marginal Zone Lymphoma | Patient Sample, *In vitro* | Pro-tumorigenic | 2014 | (14) |
| Primary Cutaneous Lymphoma (PCL) | Archival tissue samples of patients | Pro-tumorigenic | 2016 | (15) |
| | Patient samples | | 2012 | (16) |
| | *In vitro* (Mac2B, MyLa, SeAx, BJAB[30], Jurkat, HMC-1, EL4), *In vivo* (C57BL/6 *Kit*$^{W\text{-}sh/W\text{-}sh}$ mice and transgenic mast cell–deficient *Mcpt5-Cre*$^{+}$/*iDTR*$^{+}$ mice) | | | |
| B cell Lymphoma (BCL) | Patient samples | Pro-tumorigenic | 2016 | (17) |
| | Patient samples | | 2011 | (18) |
| | *In vitro* (mouse BCL cell line A20) | | | |
| | *In vivo* (BALB/c) | | | |
| T cell Lymphoma (TCL) | Patient samples | Pro-tumorigenic | 2001 | (19) |
| | Patient samples | | 2010 | (20) |
| | *In vitro* (BJAB, LAD2, ADMEC) | | | |
| | *In vitro* (murine TCL cell line EL4), RBL-2H3 mast cell line | | 2019 | (27) |
| | *In vitro* (murine TCL cell line YAC-1), RBL-2H3 mast cell line | Anti-cancerous | | |
| Leukemia | *In vitro* (murine leukemia cell line L1210), RBL-2H3 mast cell line | No effect | 2019 | (27) |
| | Patient sample | Pro-tumorigenic | 2019 | (21) |
| Multiple myeloma | Patient sample | Pro-tumorigenic | 2013 | (22) |
| | Patient sample | Not shown | 2020 | (28) |
| | Patient sample | Pro-tumorigenic | 2015 | (23) |
| | *In vivo* (syngeneic mouse MM model using IgA-producing plasmocytoma MOPC-315 cells, MOPC-104E and J588 plasmocytomas originating from Balb/c) | Not shown | 2015 | (29) |
| | Patient sample | Pro-tumorigenic | 2016 | (24) |
| Melanoma | *In vivo* (C57BL/6, B6.129S6-*Tnf*$^{tm1Gkl}$/J, B6.129S2-*Il6*$^{tm1Kopf}$/J, B6.129P2-*Ccl3*$^{tm1Unc}$/J, and B6.Cg-*Kit*$^{W\text{-}sh}$/HNihrJaeBsmJ (*Kit*$^{W\text{-}sh/W\text{-}sh}$) | Anti-cancerous | 2010 | (30) |
| | *In vitro* (B16.F10 cells, BMMC) | | | |
| Colon cancer | Patient sample | Anti-cancerous | 2016 | (31) |
| | *In vivo* (azoxymethane induced CAC model, *Cysltr1*$^{-/-}$C57BL/6) | | | |
| Colorectal cancer | Patient sample | Anti-cancerous | 2018 | (32) |

*BMMC, Bone marrow-derived mast cells; SPMC, Spleen-derived mast cells; CBMC, cord blood-derived mast cells; CAC, colitis-associated colorectal cancer.*

presence of micro-vessels with high endothelial venules is a prominent feature of AITL. There is strong correlation between MCs and number of blood vessels in TCL cases studied by Fukushima et al. Their study suggests that MCs are responsible for the angiogenesis and progression of AITL (19). Neoplastic follicular $T_h$ cells in AITL have been shown to produce CXCL-13, which is responsible for the accumulation of MCs strongly expressing IL-6 in AITL speculated to foster a pro-inflammatory microenvironment and deregulated angiogenesis (20). In addition to studies documenting the pro-tumorigenic role of MCs in TCL, YAC-1 T cell lymphoma cells in direct contact with MCs or tumor cell supernatant when added to MCs was shown to induce degranulation of MCs (27). Interestingly, after co-treatment with histamine receptor antagonists and MC mediators, it was discovered that histamine receptors H2 and H4 are involved in inhibition of YAC-1 cell growth whereas histamine receptors H1, H2 and H4 are involved in enhancement of EL4 T cell lymphoma cell growth and overall regulation of β catenin pathway (27). Furthermore, Rabenhorst et al. demonstrated that MCs are crucial for the progression of EL4 TCL tumors *in vivo* using an inducible mast cell deficiency mouse model *Mcpt5-Cre/iDTR* and *Kit* mutant mice. Increased proliferation of EL4 cells and release of pro-inflammatory cytokines on *in vitro* treatment with MC or BMMC supernatant was also observed (16). MCs exhibited a pro-tumorigenic role on the EL4 TCL cell line, but they exhibited an anti-cancerous role on the YAC-1 TCL cell line, implying that MCs may exist as picket cells in the lymphoma microenvironment and play a critical role in the suppression or advancement of tumorigenesis, depending on tumor characteristics and histamine receptor profile present on neoplastic cells (27).

### 1.1.2 The Role of Mast Cells in Leukemia

As discussed above there is a pro-inflammatory and pro-cancerous role of MCs in various lymphomas with an exception in a T cell lymphoma. It was also demonstrated that MCs showed no effect on the proliferation of L1210 cell line which is a murine lymphocytic leukemia cell line *in vitro* (27). Similar to lymphomas, tryptase positive MCs were found to be abundant in the BM of chronic myeloid leukemia (CML)

patients and increased MCs number in different stages of CML conformed to increased microvessel density and the advancement of CML to AML, which is the blast phase or the advanced stage (21). Interestingly, MCs count in acute lymphoblastic leukemia transformation (ALLT) stage was comparable to that of the healthy control group, implying that MCs control angiogenesis in the early stages of tumor development, whereas tumor cells drive growth and angiogenesis in later stages, and growth becomes MC-independent (21).

### 1.1.3 The Role of Mast Cells in Myeloma

Multiple myeloma (MM) is the malignancy of neoplastic plasma cells infiltrating the bone marrow. Similar to lymphomas and leukemias, patients with MM have an infiltration of tryptase positive MCs in their BM, associated with increased neovascularization and angiogenesis (22). Cytokines such as IL-6, VEGF, TNF-α, B cell activating factor, and receptor activator of NF-kB ligand are elevated in MM (28). IL-6 is required for the survival and proliferation of normal immature B cells in the BM, and it has been identified as the key growth and survival factor for myeloma cells (28). Raised IL-6 levels can be caused by both myeloma precursor cells and the presence of MCs (23, 29). Increased MC density has also been linked to increased angiogenesis factors found in BM of MM patients (24). Therefore, MC can either directly or indirectly contribute to the progression of MM.

## 1.2 Mast Cells and Conventional Cancer Therapy

Conventional cancer therapy involves chemotherapy and radiotherapy which are principally used to kill the rapidly dividing tumor cells. According to Soule et al, MCs are resistant to cytotoxicity after radiation, and radiation has no effect on Kit and FcεRI receptor expression. MCs degranulation is inhibited transiently and recovers within 24 hours after irradiation in human MCs, and MCs remain responsive to TLR-mediated signalling and produce cytokines (38). Westbury et al. observed a post-irradiation increase in the number of MCs (39). Radiation can also cause MC degranulation and the release of mediators like tryptase, as well as increase vascular permeability, which can lead to tissue injuries and fibrosis (40, 41). MCs may even be responsible for resistance to anti-PD1 therapy, which is linked to lower expression of HLA class1 in tumor cells, resulting in tumor escape from cytotoxic T cells (42). In prostate cancer, MCs can induce docetaxel resistance by phosphorylating p38 and radio-resistance by phosphorylating ATM, resulting in tumor cell survival and proliferation (43). Similarly, in inflammatory breast and pancreatic cancer, MCs have been implicated in tumor cell resistance to therapy and can also reduce the effect of anti-angiogenic therapy (44–46). As a result, MCs have emerged as important candidate cells in the tumor microenvironment to be targeted for therapies.

## 1.3 Various Strategies to Target Mast Cells as a Potential Therapeutic Approach

As discussed in section 1.1, accumulation of MCs and their precise role in almost all hematological malignancies were evidently correlated with detrimental effects, poor prognosis, angiogenesis, tumor aggressiveness and metastasis as summarized in **Figure 1**. Increase in number of MCs in early stages is correlated as an angiogenic switch which triggers the tumor towards the malignant advancement (21). Myeloid derived suppressor cells (MDSCs), Tregs, NK cells have been extensively studied for their tumor mediated immunosuppressive activity and ability to impair immunotherapy response (47). The interplay between MCs and MDSCs can be speculated as a builder for inflammatory tumor microenvironment as MCs secrete CCL2 which can recruit MDSCs and subsequent IL-17 secretion recruits Tregs producing IL-9 which is required for maintenance of MCs contributing to the immunosuppressive microenvironment (48, 49) making MCs as an important target for a responsive immunotherapy.

MCs are an excellent candidate for targeted immunotherapy in the microenvironment of hematological malignancies because of their increased number, selective release of variety of mediators upon activation, and interaction with other cells. In this section we will discuss various strategies that could potentially help target MCs in the hematological tumor microenvironment.

### 1.3.1 Strategies to Target Mast Cell Number

c-KIT receptor is critical for the survival and development of MCs as MC depletion is shown in mouse models with c-KIT mutation (50). The targeting of c-KIT receptor is therefore one such strategy that may help to reduce the number of MCs in the tumor microenvironment of hematological malignancies. c-KIT is a tyrosine kinase receptor and can be targeted by numerous tyrosine kinase inhibitors used as anti-cancer drugs such as imatinib, sunitinib, sofrafenib, which bind and inhibit Bcr-abl fusion protein tyrosine kinase and are currently being used in CML (51), gastro-intestinal cancers and in thymic carcinoma (52). Other United States Food and Drug Administration (FDA) approved anti-cancer drugs that are studied to target c-kit include Amuvatinib, which has been clinically tested for lymphoma and small cell lung carcinomas, Axitinib, was clinically tested for advanced renal cell carcinoma, Cabozantinib, for prostate cancers and Dasatinib, for Chronic myeloid leukemia (52). A biologic inhibitor of c-KIT, KT0158, which is a humanized monoclonal antibody, has been shown to decrease MC degranulation and reduce MC numbers in a preclinical study (53).

In addition to c-KIT inhibitors, interestingly Fluvastatin, a statin drug used in the treatment of hypercholesterolemia not only suppresses IgE signaling in MCs but also induces apoptosis by inhibiting stem cell factor (SCF) induced survival signals in primary and in c-KIT mutated MCs (54). Consequently, the strategy to target the number of MCs would serve as an anti-inflammatory approach with a potential to suppress neo-vascularization, leading to a considerable delay in the tumor growth prior to the initiation of angiogenic switch. This strategy could prove to be a rational and effective additional therapeutic strategy for lymphoid neoplasms negatively affected by MCs.

### 1.3.2 Mast Cell Stabilization

MCs release pre-formed mediators present within their granules and newly formed lipid mediators instantly upon activation and other newly synthesized mediators are released 3-12 hours later.

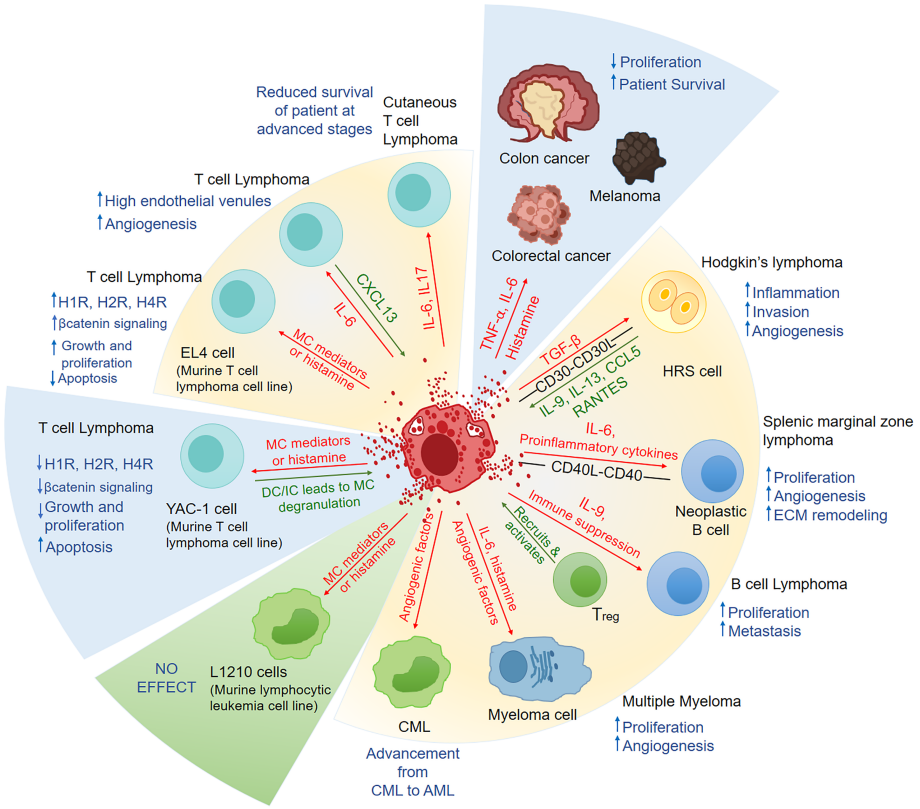


**FIGURE 1** | A summary of the factors released by mast cells and their physiological response in hematological malignancies and solid cancers. In Hodgkin's lymphoma, splenic marginal zone lymphoma, B cell lymphoma, CML, T cell lymphoma, and myeloma MCs have been shown to play pro-tumorigenic role. In an *in-vitro* study, MCs had an anti-tumorigenic effect in T cell lymphoma but had no effect in murine lymphocytic leukemia. In some solid cancers, like colon cancer, melanoma and colorectal cancers, MCs have been shown to play anti-cancerous role. The factors released by MCs are represented by red arrows in this figure, while the factors/chemokines released by leukemia/lymphoma cells are represented by green arrows. Blue upwards arrow represents the increase and blue downwards arrow represents the decrease, as a result of the effect of MC on the malignancy. In the pie representation, blue slice represents the anti-cancerous role, green slice represents No effect and yellow represents pro-tumorigenic role played by MCs. MC, Mast cell; HRS, Hodgkin's and Reed-Sternberg cells; ECM, extracellular matrix; Treg, Regulatory T cells; CML, Chronic myeloid leukemia; AML, acute myeloid leukemia; H1R:, H1 Histamine Receptor; H2R, H2 Histamine Receptor; H4R, H4 Histamine Receptor; DC, Direct contact; IC, Indirect contact means MCs treated with tumor cell supernatant only.

T cell lymphoma cells have been shown to activate MCs to a similar extent as an allergen and show similar release of pre-stored mediators (27). These mediators are further responsible for the inflammation and angiogenic progression in lymphoid neoplasms or the rejection of tumors as seen in some solid cancers like breast cancer. Therefore, if it is not possible to eliminate MCs, we can think about stabilization of MCs. MC Stabilization is a method of preventing the release of histamine and other mediators involved in rogue actions by impeding degranulation.

Bortezomib, an NF-Kβ inhibitor used to treat MM and other malignant hematological disorders, has been found to be minimally cytotoxic to MCs but can block MCs release, preventing fibrosis and vascularization in HL tumors *in vivo*. As a result, Bortezomib may be an interesting molecule to be used to kill malignant cells while simultaneously inactivating MCs in tumors, whereas Mizuno et al. claim that monotherapy may not work because the effect is transient (25).

Since histamine receptors are involved in responses to MC mediators, the use of MC antagonists may be helpful in reversing their response. Many MC stabilizers are now known to inhibit MC activation, such as H1 Histamine receptor antagonist Ketotifen, which is used to treat asthma and has been shown to suppress fibrosis (55). Azelastine, H1 receptor antagonist is a potent anti-inflammatory molecule that also inhibits release of histamine, tryptase and IL-6 from MCs (56). To inhibit histamine receptors in TCL cell lines, Pyrilamine as an antagonist for H1 Histamine receptor, Ranitidine as an antagonist for H2 histamine receptor, and JNJ7777120 as an antagonist for H4 receptor have been used (27). Some Tyrosine kinase inhibitors which are anti-cancerous agents such as Nilotinib, Sunitinib, Ibrutinib have been shown to have anti-histamine properties and can work as MC stabilizers (57–59). Not only chemical sources, but some natural sources of MC stabilizers such as flavonoids like luteolin, amentoflavone, bilobetin, quercetin (60, 61), phenols like curcumin (62) and alkaloids such as theanine present in green tea (63) have been shown to have antihistamine and MC stabilizing properties. It is therefore essential to identify and study how these stabilizers can be incorporated as add on therapeutic agents for the treatment of hematological malignancies.

### 1.3.3 MC Pre-Formed Mediators That Can Be Targeted or Incorporated in Cancer Therapies

As discussed in the section 1.1, MCs identified in haematological malignancies are tryptase-positive and are capable of causing neo-vascularization by secreting tryptase and chymase, which are potent angiogenic factors (64). Gabexate mesylate (GM), Nafamostat mesylate (NM) are tryptase inhibitors. NM is 100 times more potent than GM which is used in the treatment of acute pancreatitis and has been tested on several human cancer cell lines and Tranilast is used in the treatment of bronchial asthma and has a potential anti-tumor activity (65). Therefore, these molecules may be incorporated into treatments. As a result, targeting tryptase released by MC in the tumor microenvironment will serve as an anti-angiogenic strategy.

Although MCs have been shown to be involved in tumor progression, heparin, a MC mediator has been studied for its anti-cancerous role in many solid cancers (66). Heparin has been shown to attenuate metastasis in experimental cancer models possibly by inhibiting blood coagulation, inhibiting cancer cell–platelet and –endothelial interactions by selectin inhibition (67). It is therefore essential to study the role of heparin in hematological malignancies and thus strategies for including this molecule in cancer therapy.

Histamine is an important molecule that is pre-stored in MC granules and is the first molecule released when MCs are activated. Histamine has also been shown to be involved in cell proliferation, tumor development and embryonic development (68). The anti-cancerous properties of histamine in TCL have also been reported. Studies showed that histamine inhibits proliferation, decreases the survival and induces apoptosis in YAC-1 TCL cell line *in vitro* (27). Histamine dihydrochloride, a NOX2 inhibitor, targets MDSCs and improves immune-mediated clearance of neoplastic cells, thereby improving the immunotherapy efficacy of PD1 checkpoint blockade (69). Because of its receptor expression on immune cells as well as on tumor cells, histamine becomes an important molecule that can be strategically included in anti-cancer therapy and can have a detrimental effect on tumor depending on the construction of tumor microenvironment, cell types present and the histamine receptor expression profile.

### 1.3.4 Anti-Tumor Immune Responses of MCs

Apart from the pro-tumorogenic role, MCs have been shown to have an anti-tumor role in some solid cancers such as melanoma, colon cancer, and colorectal cancer where MC presence in tumor is associated with improved patient survival (30–32), and also in a haematological neoplasm *in vitro* (27).

The tumor microenvironment contains sufficient chemokines and alternate molecules that can activate MCs. Chemotherapy and radiotherapy, as well as injury, cause dead and dying cells to release molecules known as alarmins or Danger-associated molecular patterns (DAMPs), which can activate MCs *via* TLRs and other receptors (70, 71). In hematological malignancies, alarmins such as IL-33 and Hsp-70 are commonly released, and cytokines such as IL-1 have been found to activate MCs and cause the release of IL-6 and TNF-α, while chymase from MCs has been shown to degrade IL-33 and Hsp-70 due to their ability to cause inflammation (70, 72, 73). Depending on the activation molecule and receptor activated on MC, the anti-tumor mechanism involves recruiting immune effector cells such as NK cells and cytotoxic lymphocytes, which can eventually lead to tumor cell clearance or the development of anti-tumor immunity. Virus activated MCs have been shown to degranulate and produce type I and type III interferons, CXCL8, CXCR1, and TNF, which can recruit and activate IFN-γ producing NK cells and NKT cells, allowing them to carry out cytotoxic actions which eliminate transformed cells (74–76). Interferon-stimulated chemokines have been found in tumors (32), therefore interferon-induced MC activation and NK cells recruitment may play a role in anti-tumor immunity.

Histamine, an important mediator released by MCs, is involved in the conservation of cytotoxicity receptors (NKp46, NKG2D) on NK cells in AML that are likely to be inhibited by phagocytes, and histamine prevents this inhibition by targeting H2 receptors on phagocytes (77). Histamine was used as a protector for cytotoxic lymphocytes and NK cells from phagocytes in a clinical study on AML where IL-2 was to be given as immunotherapy, which delayed relapse in patients and significantly improved the therapy (78). When activated, MCs also produce lipid mediators such as prostaglandins, leukotrienes, which are also involved in the recruitment of cytotoxic lymphocytes. As demonstrated in colorectal cancers that Leukotriene B4 derived from MC is in charge of recruiting and homing CD8+ T cells to the tumor site in order to generate anti-tumor immunity (79). As a result, MCs contribute chemokines, granule-associated and *de novo* synthesized mediators in tumor microenvironment, which may be important for immune regulation and anti-tumor responses.

To improve the recruitment of effector cells by MCs, innate immune activators such as TLR targeting immune-therapeutic molecules could be used. TLR-2 activated MCs have been shown to recruit NK cells and T cells in a melanoma model (30), whereas TLR-3 receptor activation on MCs increases T cell recruitment and regulates its functions (80). Therefore, TLR agonists can be combined with molecules that inhibit the release of pro-tumorigenic factors by MCs (as discussed in previous section), resulting in an effective anti-tumor response.

## 2 CONCLUSION AND FUTURE PERSPECTIVES

The presence of MCs has been increasingly recognized in human cancers. Pathological studies of MCs in human tissues have revealed contradictory results, explaining both a positive and a negative correlation between the number of MCs and prognosis in various cancers. The role of MCs in hematological malignancies has been the focus of this mini review as the role of MCs in tumorigenesis is of increasing interest following the use of anti-tumor agents that affect tumor growth by inhibiting factors known to be crucial to MC function.

MCs are found to be beneficial for the tumor growth in hematological neoplasms, as discussed in this review, with the

exception of T cell lymphomas, where an *in vitro* study showed that MCs were detrimental to tumor cell growth. The role of MCs may be influenced by the stage of tumor development at which they infiltrate, their interaction with other cells, and the tumor microenvironment. MCs have been discussed to trigger the angiogenic switch in the tumors that helps to nourish the tumor and later on makes the tumor growth independent of MCs. MCs pro-tumorigenic effects are primarily mediated by angiogenic molecules secretion, tissue remodelling, tumor cell proliferation augmentation, and immunosuppression. Because MCs have the ability to influence cellular recruitment, proliferation, and functioning, they might be critical regulators of tumor microenvironment and, as a result tumor growth.

MCs can be activated by various molecules present in tumor microenvironment and are capable of secreting different mediators in response to different triggers. Sometimes they may only secrete cytokines without any release of pre-formed mediators. Also there is heterogeneity even in pre-stored mediators and their secretion is controlled by different secretion machinery (81). In such a scenario, it may be possible to specifically target and block secretion of pro-angiogenic factors and allow secretion of mediators which may have anti-tumor activities. Also it becomes important to understand the interactions of MCs with cancer stem cells or under hypoxic condition which is a hallmark of tumor microenvironment.

All of this tends to suggest that research into the role of MCs in hematological malignancies could have direct clinical implications in the use of targeted therapies, and that it should be investigated further using histopathological and appropriate multifaceted biological models. Some molecules or drugs that have been used for other purposes but can interfere with SCF-cKIT signaling could be repurposed, or some lysomotrophic drugs that cause granule permeabilization and eventually apoptosis of MCs could be geared at selectively limiting the number of MCs which may significantly reduce the inflammatory background that inevitably leads to aggravation and invasion of tumor cells. In addition, we discussed some therapeutic strategies which are available or can be considered to inhibit the viability, accumulation and interfere with activation of MCs and their mediator release to enhance the anti-tumor response. In the context of hematological malignancies, one potential therapeutic mechanism could be to activate MCs using TLR-activators after chemotherapy/radiotherapy to boost the innate immune response and effector cell recruitment. TLR-activators may be used in conjunction with histamine. Antihistamines or MC stabilizers could be used in cases where there is increase in pro-tumorigenic or angiogenic molecules, for example histamine regulates myeloma cell growth. Interplay between MCs and Tregs is responsible for angiogenesis in BCL, therefore could be inhibited by reducing the numbers of MCs and Tregs. Thus, a decision about how to incorporate MCs in immunotherapy can be made based on the malignancy's microenvironment, chemokines, alarmins released, and the extent and type of histamine receptors expressed.

## AUTHOR CONTRIBUTIONS

DM contributed to literature search, data curation and wrote the first draft of article. NP contributed to conception and design of the study, project administration and finalized the manuscript. All authors contributed to the article and approved the submitted version.

## FUNDING

This study was supported by research grants from Department of Science and Technology (DST) - Science & Engineering Board (SERB) Govt. of India (CRG/2019/003651) to NP. DM received senior research fellowship (2020-7400/SCR-BMS) from ICMR.

## REFERENCES

1. Bispo JAB, Pinheiro PS, Kobetz EK. Epidemiology and Etiology of Leukemia and Lymphoma. *Cold Spring Harbor Perspect Med* (2020) 10:a034819. doi: 10.1101/cshperspect.a034819
2. Satyanarayana L, Asthana S, Labani SP. Childhood Cancer Incidence in India: A Review of Population-Based Cancer Registries. *Indian Pediatr* (2014) 51:218–20. doi: 10.1007/s13312-014-0377-0
3. Park SJ, Bejar R. Clonal Hematopoiesis in Cancer. *Exp Hematol* (2020) 83:105–12. doi: 10.1016/j.exphem.2020.02.001
4. Hopken UE, Rehm A. Targeting the Tumor Microenvironment of Leukemia and Lymphoma. *Trends Cancer* (2019) 5:351–64. doi: 10.1016/j.trecan.2019.05.001
5. Gonzalez H, Hagerling C, Werb Z. Roles of the Immune System in Cancer: From Tumor Initiation to Metastatic Progression. *Genes Dev* (2018) 32:1267–84. doi: 10.1101/gad.314617.118
6. Elieh Ali Komi D, Wohrl S, Bielory L. Mast Cell Biology at Molecular Level: A Comprehensive Review. *Clin Rev Allergy Immunol* (2020) 58:342–65. doi: 10.1007/s12016-019-08769-2
7. Ghably J, Saleh H, Vyas H, Peiris E, Misra N, Krishnaswamy G. Paul Ehrlich's Mastzellen: A Historical Perspective of Relevant Developments in Mast Cell Biology. *Methods Mol Biol* (2015) 1220:3–10. doi: 10.1007/978-1-4939-1568-2_1
8. Kim HS, Kawakami Y, Kasakura K, Kawakami T. Recent Advances in Mast Cell Activation and Regulation. *F1000Research* (2020) 9:F1000 Faculty Rev-196. doi: 10.12688/f1000research.22037.1
9. Ribatti D, Crivellato E. Mast Cells, Angiogenesis, and Tumour Growth. *Biochim Biophys Acta* (2012) 1822:2–8. doi: 10.1016/j.bbadis.2010.11.010
10. Nakayama S, Yokote T, Hiraoka N, Nishiwaki U, Hanafusa T, Nishimura Y, et al. Role of Mast Cells in Fibrosis of Classical Hodgkin Lymphoma. *Int J Immunopathol Pharmacol* (2016) 29:603–11. doi: 10.1177/0394632016644447
11. Molin D, Edstrom A, Glimelius I, Glimelius B, Nilsson G, Sundstrom C, et al. Mast Cell Infiltration Correlates With Poor Prognosis in Hodgkin's Lymphoma. *Br J Haematol* (2002) 119:122–4. doi: 10.1046/j.1365-2141.2002.03768.x
12. Molin D, Fischer M, Xiang Z, Larsson U, Harvima I, Venge P, et al. Mast Cells Express Functional CD30 Ligand and Are the Predominant CD30L-Positive Cells in Hodgkin's Disease. *Br J Haematol* (2001) 114:616–23. doi: 10.1046/j.1365-2141.2001.02977.x
13. Andersen MD, Kamper P, Nielsen PS, Bendix K, Riber-Hansen R, Steiniche T, et al. Tumour-Associated Mast Cells in Classical Hodgkin's Lymphoma: Correlation With Histological Subtype, Other Tumour-Infiltrating Inflammatory Cell Subsets and Outcome. *Eur J Haematol* (2016) 96:252–9. doi: 10.1111/ejh.12583
14. Franco G, Guarnotta C, Frossi B, Piccaluga PP, Boveri E, Gulino A, et al. Bone Marrow Stroma CD40 Expression Correlates With Inflammatory Mast Cell

Infiltration and Disease Progression in Splenic Marginal Zone Lymphoma. *Blood* (2014) 123:1836–49. doi: 10.1182/blood-2013-04-497271
15. Eder J, Rogojanu R, Jerney W, Erhart F, Dohnal A, Kitzwogerer M, et al. Mast Cells Are Abundant in Primary Cutaneous T-Cell Lymphomas: Results From a Computer-Aided Quantitative Immunohistological Study. *PloS One* (2016) 11:e0163661. doi: 10.1371/journal.pone.0163661
16. Rabenhorst A, Schlaak M, Heukamp LC, Forster A, Theurich S, von Bergwelt-Baildon M, et al. Mast Cells Play a Protumorigenic Role in Primary Cutaneous Lymphoma. *Blood* (2012) 120:2042–54. doi: 10.1182/blood-2012-03-415638
17. Marinaccio C, Ingravallo G, Gaudio F, Perrone T, Ruggieri S, Opinto G, et al. T Cells, Mast Cells and Microvascular Density in Diffuse Large B Cell Lymphoma. *Clin Exp Med* (2016) 16:301–6. doi: 10.1007/s10238-015-0354-5
18. Feng LL, Gao JM, Li PP, Wang X. IL-9 Contributes to Immunosuppression Mediated by Regulatory T Cells and Mast Cells in B-Cell Non-Hodgkin's Lymphoma. *J Clin Immunol* (2011) 31:1084–94. doi: 10.1007/s10875-011-9584-9
19. Fukushima N, Satoh T, Sano M, Tokunaga O. Angiogenesis and Mast Cells in non-Hodgkin's Lymphoma: A Strong Correlation in Angioimmunoblastic T-Cell Lymphoma. *Leukemia lymphoma* (2001) 42:709–20. doi: 10.3109/10428190109099333
20. Tripodo C, Gri G, Piccaluga PP, Frossi B, Guarnotta C, Piconese S, et al. Mast Cells and Th17 Cells Contribute to the Lymphoma-Associated Pro-Inflammatory Microenvironment of Angioimmunoblastic T-Cell Lymphoma. *Am J Pathol* (2010) 177:792–802. doi: 10.2353/ajpath.2010.091286
21. Xu P, Zhang C, Wang Y, Wu H, Cheng S, Fan X, et al. Increased Number of Mast Cells in the Bone Marrow of Chronic Myeloid Leukemia may Herald the Pending Myeloid Transformation—The Mast Cell Is an Indicator of Myeloid Transformation. *Trans Cancer Res* (2019) 8:2121–9. doi: 10.21037/tcr.2019.09.29
22. Pappa CA, Tsirakis G, Roussou P, Xekalou A, Goulidaki N, Konsolas I, et al. Positive Correlation Between Bone Marrow Mast Cell Density and ISS Prognostic Index in Patients With Multiple Myeloma. *Leukemia Res* (2013) 37:1628–31. doi: 10.1016/j.leukres.2013.09.012
23. Devetzoglou M, Vyzoukaki R, Kokonozaki M, Xekalou A, Pappa CA, Papadopoulou A, et al. High Density of Tryptase-Positive Mast Cells in Patients With Multiple Myeloma: Correlation With Parameters of Disease Activity. *Tumour biology: J Int Soc Oncodevelopmental Biol Med* (2015) 36:8491–7. doi: 10.1007/s13277-015-3586-9
24. Vyzoukaki R, Tsirakis G, Pappa CA, Androulakis N, Kokonozaki M, Tzardi M, et al. Correlation of Mast Cell Density With Angiogenic Cytokines in Patients With Active Multiple Myeloma. *Clin Ther* (2016) 38:297–301. doi: 10.1016/j.clinthera.2015.11.022
25. Mizuno H, Nakayama T, Miyata Y, Saito S, Nishiwaki S, Nakao N, et al. Mast Cells Promote the Growth of Hodgkin's Lymphoma Cell Tumor by Modifying the Tumor Microenvironment That Can Be Perturbed by Bortezomib. *Leukemia* (2012) 26:2269–76. doi: 10.1038/leu.2012.81
26. Fischer M, Juremalm M, Olsson N, Backlin C, Sundstrom C, Nilsson K, et al. Expression of CCL5/RANTES by Hodgkin and Reed-Sternberg Cells and Its Possible Role in the Recruitment of Mast Cells Into Lymphomatous Tissue. *Int J Cancer* (2003) 107:197–201. doi: 10.1002/ijc.11370
27. Paudel S, Mehtani D, Puri N. Mast Cells may Differentially Regulate Growth of Lymphoid Neoplasms by Opposite Modulation of Histamine Receptors. *Front Oncol* (2019) 9:1280. doi: 10.3389/fonc.2019.01280
28. Jasrotia S, Gupta R, Sharma A, Halder A, Kumar L. Cytokine Profile in Multiple Myeloma. *Cytokine* (2020) 136:155271. doi: 10.1016/j.cyto.2020.155271
29. Matthes T, Manfroi B, Zeller A, Dunand-Sauthier I, Bogen B, Huard B. Autocrine Amplification of Immature Myeloid Cells by IL-6 in Multiple Myeloma-Infiltrated Bone Marrow. *Leukemia* (2015) 29:1882–90. doi: 10.1038/leu.2015.145
30. Oldford SA, Haidl ID, Howatt MA, Leiva CA, Johnston B, Marshall JS. A Critical Role for Mast Cells and Mast Cell-Derived IL-6 in TLR2-Mediated Inhibition of Tumor Growth. *J Immunol* (2010) 185:7067–76. doi: 10.4049/jimmunol.1001137
31. Mehdawi L, Osman J, Topi G, Sjolander A. High Tumor Mast Cell Density Is Associated With Longer Survival of Colon Cancer Patients. *Acta Oncol* (2016) 55:1434–42. doi: 10.1080/0284186X.2016.1198493
32. Mao Y, Feng Q, Zheng P, Yang L, Zhu D, Chang W, et al. Low Tumor Infiltrating Mast Cell Density Confers Prognostic Benefit and Reflects Immunoactivation in Colorectal Cancer. *Int J Cancer* (2018) 143:2271–80. doi: 10.1002/ijc.31613
33. Canioni D, Deau-Fischer B, Taupin P, Ribrag V, Delarue R, Bosq J, et al. Prognostic Significance of New Immunohistochemical Markers in Refractory Classical Hodgkin Lymphoma: A Study of 59 Cases. *PloS One* (2009) 4:e6341. doi: 10.1371/journal.pone.0006341
34. Piris MA, Onaindia A, Mollejo M. Splenic Marginal Zone Lymphoma. *Best Pract Res Clin Haematol* (2017) 30:56–64. doi: 10.1016/j.beha.2016.09.005
35. Willemze R, Cerroni L, Kempf W, Berti E, Facchetti F, Swerdlow SH, et al. The 2018 Update of the WHO-EORTC Classification for Primary Cutaneous Lymphomas. *Blood* (2019) 133:1703–14. doi: 10.1182/blood-2018-11-881268
36. Lunning MA, Vose JM. Angioimmunoblastic T-Cell Lymphoma: The Many-Faced Lymphoma. *Blood* (2017) 129:1095–102. doi: 10.1182/blood-2016-09-692541
37. Iannitto E, Ferreri AJ, Minardi V, Tripodo C, Kreipe HH. Angioimmunoblastic T-Cell Lymphoma. *Crit Rev Oncol/Hematol* (2008) 68:264–71. doi: 10.1016/j.critrevonc.2008.06.012
38. Soule BP, Brown JM, Kushnir-Sukhov NM, Simone NL, Mitchell JB, Metcalfe DD. Effects of Gamma Radiation on Fcepsilonri and TLR-Mediated Mast Cell Activation. *J Immunol* (2007) 179:3276–86. doi: 10.4049/jimmunol.179.5.3276
39. Westbury CB, Freeman A, Rashid M, Pearson A, Yarnold JR, Short SC. Changes in Mast Cell Number and Stem Cell Factor Expression in Human Skin After Radiotherapy for Breast Cancer. *Radiotherapy Oncol: J Eur Soc Ther Radiol Oncol* (2014) 111:206–11. doi: 10.1016/j.radonc.2014.02.020
40. Albrecht M, Muller K, Kohn FM, Meineke V, Mayerhofer A. Ionizing Radiation Induces Degranulation of Human Mast Cells and Release of Tryptase. *Int J Radiat Biol* (2007) 83:535–41. doi: 10.1080/09553000701444657
41. Park KR, Monsky WL, Lee CG, Song CH, Kim DH, Jain RK, et al. Mast Cells Contribute to Radiation-Induced Vascular Hyperpermeability. *Radiat Res* (2016) 185:182–9. doi: 10.1667/RR14190.1
42. Somasundaram R, Connelly T, Choi R, Choi H, Samarkina A, Li L, et al. Tumor-Infiltrating Mast Cells Are Associated With Resistance to Anti-PD-1 Therapy. *Nat Commun* (2021) 12:346. doi: 10.1038/s41467-020-20600-7
43. Xie H, Li C, Dang Q, Chang LS, Li L. Infiltrating Mast Cells Increase Prostate Cancer Chemotherapy and Radiotherapy Resistances *via* Modulation of P38/P53/P21 and ATM Signals. *Oncotarget* (2016) 7:1341–53. doi: 10.18632/oncotarget.6372
44. Reddy SM, Reuben A, Barua S, Jiang H, Zhang S, Wang L, et al. Poor Response to Neoadjuvant Chemotherapy Correlates With Mast Cell Infiltration in Inflammatory Breast Cancer. *Cancer Immunol Res* (2019) 7:1025–35. doi: 10.1158/2326-6066.CIR-18-0619
45. Porcelli L, Iacobazzi RM, Di Fonte R, Serrati S, Intini A, Solimando AG, et al. Cafs and TGF-Beta Signaling Activation by Mast Cells Contribute to Resistance to Gemcitabine/Nabpaclitaxel in Pancreatic Cancer. *Cancers* (2019) 11:cancers11030330. doi: 10.3390/cancers11030330
46. Wroblewski M, Bauer R, Cubas Cordova M, Udonta F, Ben-Batalla I, Legler K, et al. Mast Cells Decrease Efficacy of Anti-Angiogenic Therapy by Secreting Matrix-Degrading Granzyme B. *Nat Commun* (2017) 8:269. doi: 10.1038/s41467-017-00327-8
47. Draghiciu O, Lubbers J, Nijman HW, Daemen T. Myeloid Derived Suppressor Cells-an Overview of Combat Strategies to Increase Immunotherapy Efficacy. *Oncoimmunology* (2015) 4:e954829. doi: 10.4161/21624011.2014.954829
48. Danelli L, Frossi B, Pucillo CE. Mast Cell/MDSC a Liaison Immunosuppressive for Tumor Microenvironment. *Oncoimmunology* (2015) 4:e1001232. doi: 10.1080/2162402X.2014.1001232
49. Jachetti E, Cancila V, Rigoni A, Bongiovanni L, Cappetti B, Belmonte B, et al. Cross-Talk Between Myeloid-Derived Suppressor Cells and Mast Cells Mediates Tumor-Specific Immunosuppression in Prostate Cancer. *Cancer Immunol Res* (2018) 6:552–65. doi: 10.1158/2326-6066.CIR-17-0385
50. Grimbaldeston MA, Chen CC, Piliponsky AM, Tsai M, Tam SY, Galli SJ. Mast Cell-Deficient W-Sash C-Kit Mutant Kit W-Sh/W-Sh Mice as a Model for Investigating Mast Cell Biology *In Vivo*. *Am J Pathol* (2005) 167:835–48. doi: 10.1016/S0002-9440(10)62055-X
51. Sacha T. Imatinib in Chronic Myeloid Leukemia: An Overview. *Mediterranean J Hematol Infect Dis* (2014) 6:e2014007. doi: 10.4084/MJHID.2014.007
52. Abbaspour Babaei M, Kamalidehghan B, Saleem M, Huri HZ, Ahmadipour F. Receptor Tyrosine Kinase (C-Kit) Inhibitors: A Potential Therapeutic Target

in Cancer Cells. *Drug Design Dev Ther* (2016) 10:2443–59. doi: 10.2147/DDDT.S89114
53. London CA, Gardner HL, Rippy S, Post G, La Perle K, Crew L, et al. KTN0158, a Humanized Anti-KIT Monoclonal Antibody, Demonstrates Biologic Activity Against Both Normal and Malignant Canine Mast Cells. *Clin Cancer Res: an Off J Am Assoc Cancer Res* (2017) 23:2565–74. doi: 10.1158/1078-0432.CCR-16-2152
54. Paez PA, Kolawole M, Taruselli MT, Ajith S, Dailey JM, Kee SA, et al. Fluvastatin Induces Apoptosis in Primary and Transformed Mast Cells. *J Pharmacol Exp Ther* (2020) 374:104–12. doi: 10.1124/jpet.119.264234
55. Gallant-Behm CL, Hildebrand KA, Hart DA. The Mast Cell Stabilizer Ketotifen Prevents Development of Excessive Skin Wound Contraction and Fibrosis in Red Duroc Pigs. *Wound Repair Regen: Off Publ Wound Healing Soc [and] Eur Tissue Repair Soc* (2008) 16:226–33. doi: 10.1111/j.1524-475X.2008.00363.x
56. Ciprandi G, Cosentino C, Milanese M, Tosca MA. Rapid Anti-Inflammatory Action of Azelastine Eyedrops for Ongoing Allergic Reactions. *Ann Allergy Asthma Immunol: Off Publ Am Coll Allergy Asthma Immunol* (2003) 90:434–8. doi: 10.1016/S1081-1206(10)61829-7
57. El-Agamy DS. Anti-Allergic Effects of Nilotinib on Mast Cell-Mediated Anaphylaxis Like Reactions. *Eur J Pharmacol* (2012) 680:115–21. doi: 10.1016/j.ejphar.2012.01.039
58. Yamaki K, Yoshino S. Tyrosine Kinase Inhibitor Sunitinib Relieves Systemic and Oral Antigen-Induced Anaphylaxes in Mice. *Allergy* (2012) 67:114–22. doi: 10.1111/j.1398-9995.2011.02717.x
59. Chang BY, Huang MM, Francesco M, Chen J, Sokolove J, Magadala P, et al. The Bruton Tyrosine Kinase Inhibitor PCI-32765 Ameliorates Autoimmune Arthritis by Inhibition of Multiple Effector Cells. *Arthritis Res Ther* (2011) 13: R115. doi: 10.1186/ar3400
60. Kim HP, Park H, Son KH, Chang HW, Kang SS. Biochemical Pharmacology of Biflavonoids: Implications for Anti-Inflammatory Action. *Arch Pharmacal Res* (2008) 31:265–73. doi: 10.1007/s12272-001-1151-3
61. Weng Z, Zhang B, Asadi S, Sismanopoulos N, Butcher A, Fu X, et al. Quercetin Is More Effective Than Cromolyn in Blocking Human Mast Cell Cytokine Release and Inhibits Contact Dermatitis and Photosensitivity in Humans. *PloS One* (2012) 7:e33805. doi: 10.1371/journal.pone.0033805
62. Lee JH, Kim JW, Ko NY, Mun SH, Her E, Kim BK, et al. Curcumin, a Constituent of Curry, Suppresses Ige-Mediated Allergic Response and Mast Cell Activation at the Level of Syk. *J Allergy Clin Immunol* (2008) 121:1225–31. doi: 10.1016/j.jaci.2007.12.1160
63. Kim NH, Jeong HJ, Kim HM. Theanine Is a Candidate Amino Acid for Pharmacological Stabilization of Mast Cells. *Amino Acids* (2012) 42:1609–18. doi: 10.1007/s00726-011-0847-9
64. Ribatti D, Ranieri G. Tryptase, a Novel Angiogenic Factor Stored in Mast Cell Granules. *Exp Cell Res* (2015) 332:157–62. doi: 10.1016/j.yexcr.2014.11.014
65. Ammendola M, Leporini C, Marech I, Gadaleta CD, Scognamillo G, Sacco R, et al. Targeting Mast Cells Tryptase in Tumor Microenvironment: A Potential Antiangiogenetic Strategy. *BioMed Res Int* (2014) 2014:154702. doi: 10.1155/2014/154702
66. Borsig L. Heparin as an Inhibitor of Cancer Progression. *Prog Mol Biol Trans Sci* (2010) 93:335–49. doi: 10.1016/S1877-1173(10)93014-7
67. Niers TM, Klerk CP, DiNisio M, Van Noorden CJ, Buller HR, Reitsma PH, et al. Mechanisms of Heparin Induced Anti-Cancer Activity in Experimental Cancer Models. *Crit Rev Oncol/Hematol* (2007) 61:195–207. doi: 10.1016/j.critrevonc.2006.07.007
68. Blaya B, Nicolau-Galmes F, Jangi SM, Ortega-Martinez I, Alonso-Tejerina E, Burgos-Bretones J, et al. Histamine and Histamine Receptor Antagonists in Cancer Biology. *Inflamm Allergy Drug Targets* (2010) 9:146–57. doi: 10.2174/187152810792231869
69. Grauers Wiktorin H, Nilsson MS, Kiffin R, Sander FE, Lenox B, Rydstrom A, et al. Histamine Targets Myeloid-Derived Suppressor Cells and Improves the Anti-Tumor Efficacy of PD-1/PD-L1 Checkpoint Blockade. *Cancer Immunol immunotherapy: CII* (2019) 68:163–74. doi: 10.1007/s00262-018-2253-6
70. Wang Y, Su H, Yan M, Zhang L, Tang J, Li Q, et al. Interleukin-33 Promotes Cell Survival *via* P38 MAPK-Mediated Interleukin-6 Gene Expression and Release in Pediatric AML. *Front Immunol* (2020) 11:595053. doi: 10.3389/fimmu.2020.595053
71. Ashrafizadeh M, Farhood B, Eleojo Musa A, Taeb S, Najafi M. Damage-Associated Molecular Patterns in Tumor Radiotherapy. *Int Immunopharmacol* (2020) 86:106761. doi: 10.1016/j.intimp.2020.106761
72. Roy A, Ganesh G, Sippola H, Bolin S, Sawesi O, Dagalv A, et al. Mast Cell Chymase Degrades the Alarmins Heat Shock Protein 70, Biglycan, HMGB1, and Interleukin-33 (IL-33) and Limits Danger-Induced Inflammation. *J Biol Chem* (2014) 289:237–50. doi: 10.1074/jbc.M112.435156
73. Ronnberg E, Ghaib A, Ceriol C, Enoksson M, Arock M, Safholm J, et al. Divergent Effects of Acute and Prolonged Interleukin 33 Exposure on Mast Cell Ige-Mediated Functions. *Front Immunol* (2019) 10:1361. doi: 10.3389/fimmu.2019.01361
74. Portales-Cervantes L, Haidl ID, Lee PW, Marshall JS. Virus-Infected Human Mast Cells Enhance Natural Killer Cell Functions. *J Innate Immun* (2017) 9:94–108. doi: 10.1159/000450576
75. St John AL, Rathore AP, Yap H, Ng ML, Metcalfe DD, Vasudevan SG, et al. Immune Surveillance by Mast Cells During Dengue Infection Promotes Natural Killer (NK) and NKT-Cell Recruitment and Viral Clearance. *Proc Natl Acad Sci USA* (2011) 108:9190–5. doi: 10.1073/pnas.1105079108
76. Burke SM, Issekutz TB, Mohan K, Lee PW, Shmulevitz M, Marshall JS. Human Mast Cell Activation With Virus-Associated Stimuli Leads to the Selective Chemotaxis of Natural Killer Cells by a CXCL8-Dependent Mechanism. *Blood* (2008) 111:5467–76. doi: 10.1182/blood-2007-10-118547
77. Romero AI, Thoren FB, Brune M, Hellstrand K. Nkp46 and NKG2D Receptor Expression in NK Cells With CD56dim and CD56bright Phenotype: Regulation by Histamine and Reactive Oxygen Species. *Br J Haematol* (2006) 132:91–8. doi: 10.1111/j.1365-2141.2005.05842.x
78. Brune M, Castaigne S, Catalano J, Gehlsen K, Ho AD, Hofmann WK, et al. Improved Leukemia-Free Survival After Postconsolidation Immunotherapy With Histamine Dihydrochloride and Interleukin-2 in Acute Myeloid Leukemia: Results of a Randomized Phase 3 Trial. *Blood* (2006) 108:88–96. doi: 10.1182/blood-2005-10-4073
79. Bodduluri SR, Mathis S, Maturu P, Krishnan E, Satpathy SR, Chilton PM, et al. Mast Cell-Dependent CD8(+) T-Cell Recruitment Mediates Immune Surveillance of Intestinal Tumors in Apc(Min/+) Mice. *Cancer Immunol Res* (2018) 6:332–47. doi: 10.1158/2326-6066.CIR-17-0424
80. Orinska Z, Bulanova E, Budagian V, Metz M, Maurer M, Bulfone-Paus S. TLR3-Induced Activation of Mast Cells Modulates CD8+ T-Cell Recruitment. *Blood* (2005) 106:978–87. doi: 10.1182/blood-2004-07-2656
81. Puri N, Roche PA. Mast Cells Possess Distinct Secretory Granule Subsets Whose Exocytosis Is Regulated by Different SNARE Isoforms. *Proc Natl Acad Sci USA* (2008) 105:2580–5. doi: 10.1073/pnas.0707854105

**Conflict of Interest:** The authors declare that the research was conducted in the absence of any commercial or financial relationships that could be construed as a potential conflict of interest.

**Publisher's Note:** All claims expressed in this article are solely those of the authors and do not necessarily represent those of their affiliated organizations, or those of the publisher, the editors and the reviewers. Any product that may be evaluated in this article, or claim that may be made by its manufacturer, is not guaranteed or endorsed by the publisher.

frontiers in Oncology

ORIGINAL RESEARCH
published: 09 November 2021
doi: 10.3389/fonc.2021.720932

# Does Ethnicity Matter in Multiple Myeloma Risk Prediction in the Era of Genomics and Novel Agents? Evidence From Real-World Data

*Akanksha Farswan[1], Anubha Gupta[1]*, Krishnamachari Sriram[2], Atul Sharma[3], Lalit Kumar[3] and Ritu Gupta[4]**

[1] Signal Processing and Biomedical Imaging Lab (SBILab), Department of Electronics and Communication, Indraprastha Institute of Information Technology-Delhi, New Delhi, India, [2] Department of Computational Biology, Indraprastha Institute of Information Technology-Delhi, New Delhi, India, [3] Department of Medical Oncology, Dr. B.R.A. IRCH, AIIMS, New Delhi, India, [4] Laboratory Oncology Unit, Dr. Bhim Rao Ambedkar Institute Rotary Cancer Hospital, All India Institute of Medical Sciences (Dr. B.R.A. IRCH, AIIMS), New Delhi, India

OPEN ACCESS

**Edited by:**
Varsha Gandhi,
University of Texas MD Anderson Cancer Center, United States

**Reviewed by:**
Stefan Knop,
Julius Maximilian University of Würzburg, Germany
Antonio Giovanni Solimando,
University of Bari Aldo Moro, Italy

***Correspondence:**
Anubha Gupta
anubha@iiitd.ac.in
Ritu Gupta
drritugupta@gmail.com;
drritu.laboncology@aiims.edu

**Specialty section:**
This article was submitted to Hematologic Malignancies, a section of the journal Frontiers in Oncology

**Received:** 05 June 2021
**Accepted:** 20 October 2021
**Published:** 09 November 2021

**Citation:**
Farswan A, Gupta A, Sriram K, Sharma A, Kumar L and Gupta R (2021) Does Ethnicity Matter in Multiple Myeloma Risk Prediction in the Era of Genomics and Novel Agents? Evidence From Real-World Data. Front. Oncol. 11:720932. doi: 10.3389/fonc.2021.720932

**Introduction:** Current risk predictors of multiple myeloma do not integrate ethnicity-specific information. However, the impact of ethnicity on disease biology cannot be overlooked. In this study, we have investigated the impact of ethnicity in multiple myeloma risk prediction. In addition, an efficient and robust artificial intelligence (AI)-enabled risk-stratification system is developed for newly diagnosed multiple myeloma (NDMM) patients that utilizes ethnicity-specific cutoffs of key prognostic parameters.

**Methods:** K-adaptive partitioning is used to propose new cutoffs of parameters for two different datasets—the MMIn (MM Indian dataset) dataset and the MMRF (Multiple Myeloma Research Foundation) dataset belonging to two different ethnicities. The Consensus-based Risk-Stratification System (CRSS) is designed using the Gaussian mixture model (GMM) and agglomerative clustering. CRSS is validated *via* Cox hazard proportional methods, Kaplan–Meier analysis, and log-rank tests on progression-free survival (PFS) and overall survival (OS). SHAP (SHapley Additive exPlanations) is utilized to establish the biological relevance of the risk prediction by CRSS.

**Results:** There is a significant variation in the key prognostic parameters of the two datasets belonging to two different ethnicities. CRSS demonstrates superior performance as compared with the R-ISS in terms of C-index and hazard ratios on both the MMIn and MMRF datasets. An online calculator has been built that can predict the risk stage of a multiple myeloma (MM) patient based on the values of parameters and ethnicity.

**Conclusion:** Our methodology discovers changes in the cutoffs with ethnicities from the established cutoffs of prognostic features. The best predictor model for both cohorts was obtained with the new ethnicity-specific cutoffs of clinical parameters. Our study also

revealed the efficacy of AI in building a deployable risk prediction system for MM. In the future, it is suggested to use the CRSS risk calculator on a large dataset as the cohort size of the present study is 25% of the cohort used in the R-ISS reported in 2015.

**Keywords: AI in cancer research, ML in cancer survival, risk stratification of multiple myeloma, GMM clustering in cancer, consensus clustering in cancer, hematological malignancy**

## INTRODUCTION

Multiple myeloma is a hematopoietic malignancy of plasma cells with an overall survival period ranging from 6 months to more than 10 years. The variability in the outcome of patients is an implication of the clinical and biological heterogeneity underlying multiple myeloma (MM). Substantial advances in tumor biology have made it possible to dissect the tumor heterogeneity present in MM, optimize patient treatment, and examine patient outcome. Multiple prognostic systems (1–5) have been described in MM that stratify patients into different risk groups. These risk groups further assist in identifying high-risk patients who may require intense therapy upfront and/or a higher monitoring frequency during the follow-up periods. The first staging system for MM was proposed in 1975 (1) followed by the development of the International Staging System (ISS) (2) in 2005 and a Revised ISS (R-ISS) (3) in 2015. The ISS utilizes serum albumin and beta2-microglobulin, while the R-ISS makes use of ISS, lactate dehydrogenase (LDH), and high-risk cytogenetic aberrations (HRCA). Currently, triplet combination therapy is the new standard of care in MM which has shifted many high-risk patients to standard-risk category, thereby justifying the need for a new risk-stratification system with the possibility of inclusion of more prognostic factors.

Although human physiological and genetic profile is known to vary across ethnic groups, the current MM risk-staging systems do not account for ethnicity-specific information that can have a huge impact on the risk score prediction. It is evident from the studies that African Americans experience two to three times higher incidence rates than Asians, Mexican-Americans, or Europeans (6). Recent studies have observed a significant variation in the overall survival of different groups belonging to distinct races/ethnicities since the introduction of novel treatment agents in MM (7–10). In a recent study, vitamin D deficiency at diagnosis was found to be a predictor of poor overall survival in MM (11). However, this was significant only for White Americans and not for African Americans even at lower cutoffs of deficiency (11). Similarly, HRCA, which is used to determine the intensity of frontline therapy, does not track with survival outcomes in African Americans (10), thereby highlighting the need for a race-specific risk-stratification system. Though ethnicity is an important prognostic factor in predicting the risk for MM (12), the variations in the clinical characteristics among the different ethnic groups have not been evaluated adequately. Therefore, it is desirable to have a staging system that includes the variations in the clinical characteristics of the patients pertaining to distinct ethnic groups. In addition, it should be based on clinical and laboratory parameters that are easily accessible in healthcare settings across the globe. Therefore, to address this concern, we first investigated the role of ethnicity in the differential clinical characteristics in the two independent cohorts of MMIn and MMRF patients with newly diagnosed multiple myeloma (NDMM) belonging to two separate ethnic groups. Furthermore, we proposed the Consensus based Risk-Stratification System (CRSS), an AI-enabled risk-stratification system, for NDMM that incorporates the ethnicity-specific cutoffs of the laboratory parameters like albumin, beta-2 microglobulin (β2M), calcium, estimated glomerular filtration rate (eGFR), hemoglobin, and age along with HRCA. The newly proposed ethnicity-aware AI-assisted CRSS method was shown to have superior performance as compared with R-ISS. In addition, we also interpreted our proposed model *via* SHapley Additive exPlanations (SHAP) (13) analysis to demonstrate the clinical significance of the risk stage predictions by CRSS. Our findings establish the significance of integrating ethnicity-specific information as well as the effectiveness of machine learning methods in devising a robust risk-staging model for MM.

## MATERIALS AND METHODS

### Datasets

A total of 1,675 entries were found in the computerized database search on June 28, 2019, with the keyword "ICD C90" registered at the Institute Rotary Cancer Centre, All India Institute of Medical Sciences (AIIMS). Patients with plasma cell dyscrasia other than MM ($n$ = 253) or who were lost to follow-up after a single visit ($n$ = 111) or before first response could be assessed ($n$ = 21) or with inadequate clinical and/or laboratory parameters ($n$ = 121) or with early deaths ($n$ = 99) were excluded. The remaining 1,070 patients of MM belonging to the Indian population, referred to as MMIn, were evaluated in this study (**Figure S1**). Out of 1,070 patients, 41 patients had one or two missing values. There are several methods to impute missing values (14–17). However, in the MMIn dataset, missing values were imputed with the median value of the parameters. An independent cohort of 900 MM patients enrolled in the Multiple Myeloma Research Foundation (MMRF) repository was also used for developing the model. Clinical and laboratory data for the MMRF dataset, belonging to the American population, are available publicly. High-risk cytogenetic information was available for 384 out of 1,070 patients in the MMIn cohort and 800 out of a total of 900 patients in the MMRF which were further used for building the staging model.

## Clinical and Laboratory Characteristics

The clinical, laboratory, and radiological data were obtained from the medical case files. The R-ISS could be assigned to a subset of patients ($n$ = 627) as described previously (18). Response outcome was estimated following the international uniform response criteria for multiple myeloma (19). Progression-free survival (PFS) was computed from the date of diagnosis till the time of progression or death. Overall survival (OS) was computed from the date of diagnosis till death due to any cause or being censored at last follow-up. Baseline clinical and laboratory features of the patients are given in **Supplementary Table S1**.

## Study Design

The complete design strategy of the consensus-based approach for developing the risk-stratification system (CRSS) is explained in this section (**Figure 1**). Data from both cohorts were separately used to develop the risk-staging models based on CRSS. Different clinical parameters were evaluated for developing the risk-staging system consisting of age, albumin, β2M, calcium, eGFR, hemoglobin, LDH, and HRCA which includes t(4;14), t(14;16), and del17. β2M and LDH levels are reflective of tumor burden and serum albumin, hemoglobin, calcium, and creatinine are reflective of the bone and renal homeostasis. eGFR was calculated from creatinine concentration using the MDRD eGFR equation (20). LDH values were brought to a common scale by multiplying each entry by 280 and dividing it by the upper limit of LDH provided for that particular entry in MMIn data. Description of the steps used in the consensus-based approach for developing the risk-staging model is given below:

*Step 1: Dividing patients into two risk groups based on established thresholds of parameters*. For each parameter, patients were initially divided into high-risk and low-risk groups using the well-established cutoffs of these parameters (21) as shown in **Table 1**. Established thresholds for albumin and β2M are derived from the ISS, and for eGFR, calcium, and hemoglobin, the thresholds are derived from the revised IMWG criteria (21).

*Step 2: Finding new thresholds of parameters via KAP*. The K-adaptive partitioning (22) (KAP) algorithm was used to find new threshold values for the parameters using complete data of MMIn ($n$ = 1,070) and MMRF ($n$ = 900). KAP was performed on the parameters of the patients yielding two threshold values for each parameter, one from PFS and the other from OS analysis. The cutoff which was close to the original value was chosen as the new cutoff for each parameter. Patients were again divided into high- and low-risk groups based on the proposed cutoffs. The proposed thresholds maximized the separation between high- and low-risk groups as compared with the established thresholds. This is evident from the lower $p$-values obtained from the log-rank test on the Kaplan–Meier curves for all the parameters. A complete list of the proposed thresholds for the MMIn and MMRF data is shown in **Table 1**.

*Step 3: Cumulative integration of the prognostic impact of the parameters*. The collective prognostic impact of the parameters was integrated into risk staging *via* creation of three different adjacency graphs using hazard ratios obtained from univariate Cox hazard analysis, $p$-values obtained from log-rank test on Kaplan–Meier curves, and ranks obtained from multivariate Cox hazard analysis.

*Step 4: Creation of the first adjacency graph*. The first adjacency graph was created using ranks obtained from the multivariate Cox hazard analysis. The parameter with the highest hazard value was given the highest rank, and the one with the lowest hazard value was given the lowest rank. The respective ranks served as the weights of each of the parameters and captured the relative impact of each parameter on the survival of patients. Next, the risk score for each patient was calculated by successive addition of the weights of all those parameters that had values (in the respective patient) greater than the cutoffs defined for the high-risk group. These patient scores were used to compute an adjacency graph of $n$ rows and $n$ columns (columns are features), where $n$ is the number of patients. Each row corresponds to one patient and each entry in the row is the absolute difference between the score of that patient with each of the patients including self.

*Step 5: Creation of the second and third adjacency graphs*. For the second adjacency graph, hazard ratio values obtained from univariate Cox hazard analysis were used. For each parameter, the highest of the two HR values obtained from PFS and OS was chosen and normalized using "minmax" scaling. The scaled HR values were assigned as the respective weights of each of the parameters representing the impact of each parameter on the survival of patients. The third adjacency graph was created using $p$-values obtained by performing a log-rank test on Kaplan–Meier curves. For each parameter, the lower of the two $p$-values obtained from PFS and OS was chosen and normalized using "minmax" scaling. The scaled $p$-values were assigned as the respective weights of each of the parameters. Furthermore, the risk score for each patient was calculated by successive addition of the weights of all those parameters that had values (in the respective patient) greater than the cutoff defined for the high-risk group. The two different patient scores obtained from univariate hazard ratios and $p$-values were further used to compute two separate adjacency graphs of $n$ rows and $n$ columns (columns are features), where $n$ is the number of patients. Each row corresponds to one patient and each entry in the row is the absolute difference between the score of that patient with each of the patients including self.

*Step 6: Gaussian mixture model (GMM) clustering on the adjacency graphs*. GMM-based clustering is an unsupervised clustering algorithm which was applied on the three adjacency graphs to obtain clustering labels.

*Step 7: Creation of a consensus graph*. The clustering outputs of the three different adjacency graphs were used to create a consensus graph (23) of size $n \times n$. The entry for the $i$th row and $j$th column in the consensus graph was determined by calculating the number of times $i$th and $j$th patients were assigned the same group. Diagonal entries were zero in this graph.

*Step 8: Hierarchical clustering on the consensus graph*. Agglomerative clustering was performed on the consensus graph to cluster the patients into three risk groups. Each

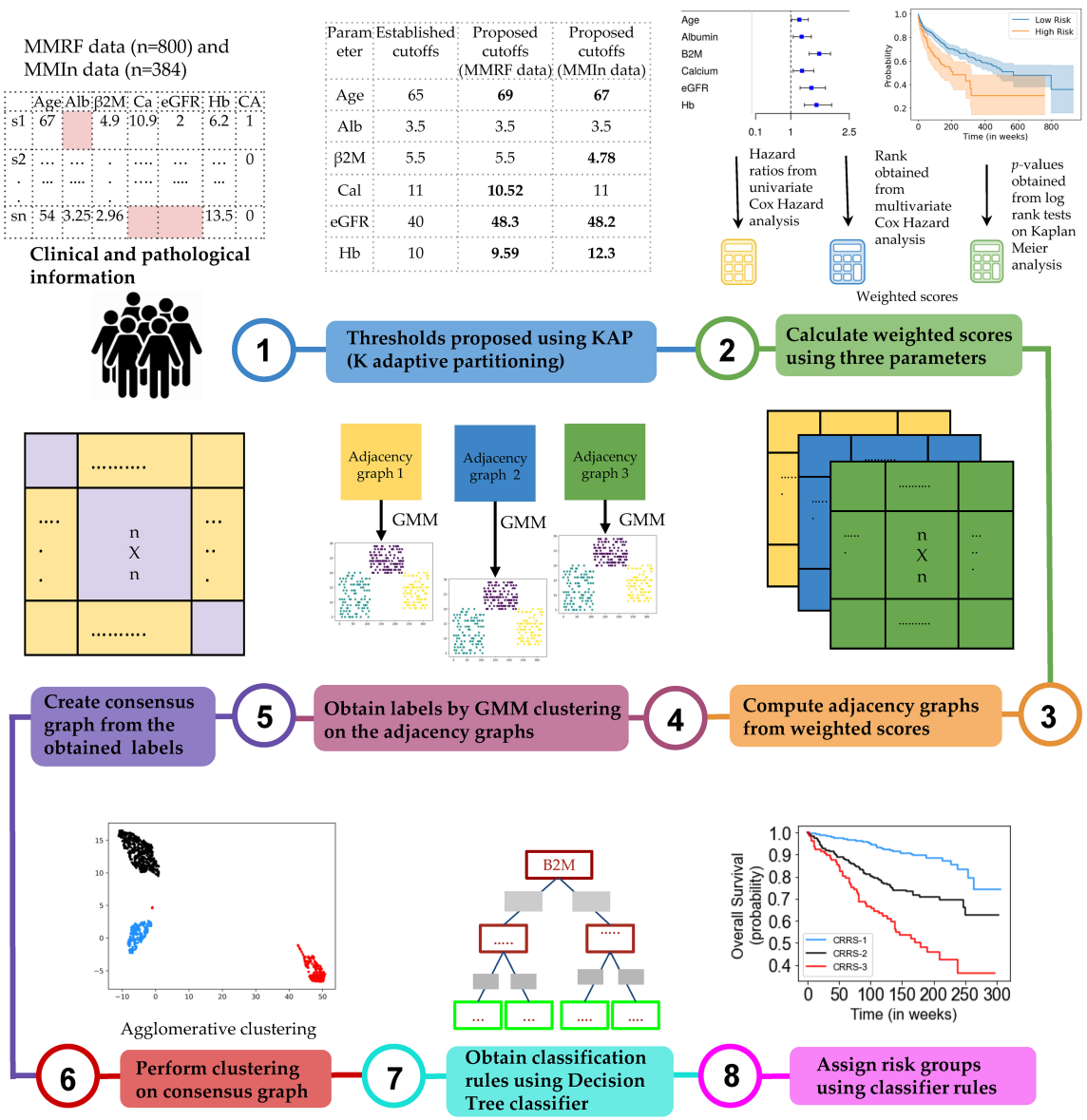


**FIGURE 1** | Workflow for the development of the Consensus-based Risk-Stratification System (CRSS) for newly diagnosed multiple myeloma patients.

cluster of patients was assigned one label: stage 1 (low risk), stage 2 (intermediate risk), or stage 3 (high risk). The rationale behind using multiple clustering was to combine the results of the clustering outputs achieved from the different adjacency graphs and ensure the stability of the final clusters deduced from agglomerative clustering.

*Step 9: Training a decision tree classifier*. The staging labels obtained from agglomerative clustering served as ground-truth labels for training the supervised decision tree classifier. The trained decision tree classifier provided the rules in terms of the parameters for the identification of risk groups, labeled as CRSS-1 (low risk), CRSS-2 (intermediate risk), and CRSS-3 (high risk) (**Figures S2, S3**).

*Step 10: Infer actual risk groups of the patients using decision tree classifier rules*. Decision tree classifier rules were then used to identify the risk stages of the patients in both cohorts. The risk stage assigned by the decision tree classifier was considered the actual risk class for each patient.

## Creation of Multiple Models on the Datasets

The CRSS method explained in **Figure 1** was used to create multiple models for the MMIn and MMRF datasets. Models A1, A2, and A3 were built for the MMIn data. Model A1 was built using established cutoffs of the parameters of albumin, β2M, LDH, and HRCA. Model A2 was built using the established

**TABLE 1** | Comparison of established and proposed cutoffs for clinical and laboratory parameters for the stratification of patients for progression-free survival (PFS) and overall survival (OS) in MMIn and MMRF using Kaplan–Meier analysis.

| Parameter | Established cutoff value | Proposed cutoff value | PFS | | OS | |
|---|---|---|---|---|---|---|
| | | | *p*-value with established cutoff | *p*-value with proposed cutoff | *p*-value with established cutoff | *p*-value with proposed cutoff |
| **MMIn (*n* = 1,070)** | | | | | | |
| Age (years) | >65 | **>67** | 0.11 | **0.012** | 5.84e-5 | **1.25e-6** |
| Albumin (g/dl) | ≤3.5 | ≤3.5 | 0.115 | 0.115 | 7.0e-4 | 7.0e-4 |
| β2M (mg/L) | ≥5.5 | **≥4.78** | **8.15e-10** | 9.32e-10 | 4.13e-10 | **4.53e-14** |
| Calcium (mg/dl) | ≥11 | ≥11 | 0.0078 | 0.0078 | 0.0037 | 0.0037 |
| eGFR (ml/min/1.73m$^2$) | ≤40 | **≤48.2** | 0.16 | **0.04** | 0.005 | **1.5e-4** |
| Hb (g/dl) | ≤10 | **≤12.3** | 0.0019 | **8.56e-5** | 0.0014 | **3.75e-7** |
| **MMRF (*n* = 900)** | | | | | | |
| Age (years) | >65 | **>69** | 3.23e-05 | **1.98e-08** | 1.06e-05 | **1.58e-09** |
| Albumin (g/dl) | ≤3.5 | ≤3.5 | 0.00017 | 0.00017 | 8.47e-07 | 8.47e-07 |
| β2M (mg/L) | ≥5.5 | ≥5.5 | 1.22e-10 | 1.22e-10 | 9.25e-13 | 9.25e-13 |
| Calcium (mg/dl) | ≥11 | **≥10.52** | 0.0077 | **1.40e-04** | 5.88e-06 | **3.49e-06** |
| eGFR (ml/min/1.73m$^2$) | ≤40 | **≤48.3** | 4.5e-05 | **4.67e-09** | 7.48e-06 | **2.48e-10** |
| Hb (g/dl) | ≤10 | **≤9.59** | 2.82e-06 | **5.69e-09** | 6.77e-06 | **5.42e-07** |

*The proposed cutoffs were found using complete data of MMIn (n = 1,070) and MMRF (n = 900). Less than or equal to cutoff reveals the increased risk in the patient. ">65" shows that a patient with age greater than 65 years is at greater risk than a patient less than 65 years. "≤3.5" shows that a patient with albumin levels less than equal to 3.5 is at a greater risk than a patient with albumin levels greater than 3.5. It holds true for other parameters also in a similar manner. Bold values of the column "proposed cutoff value" signify the change in the value of the parameters from the existing cut-offs. p-values in bold signify that p-values became more significant with the proposed changes in cutoffs.*

cutoffs of the parameters of albumin, age, calcium, eGFR, hemoglobin, β2M, and HRCA. Model A3 uses the same parameters as model A2, but with the newly proposed cutoffs of the parameters derived from the MMIn dataset. Similarly, models M1, M2, M3, and M4 were built for the MMRF data. Models M1 and M2 are equivalent to models A1 and A2, respectively. For model M3, the proposed cutoffs of parameters derived from the MMIn dataset were used for albumin, age, calcium, eGFR, hemoglobin, β2M, and HRCA. Model M4 is similar to model M3, but uses the proposed cutoffs of the parameters derived from the MMRF dataset.

# RESULTS

## Clinical and Laboratory Characteristics of Myeloma Patients

The baseline clinical and laboratory features of patients from the two cohorts were compared using unpaired Wilcoxon rank-sum test. The median values of all the parameters except albumin were found to be significantly different ($p$-value < 0.05, **Table S2**) in both cohorts thereby substantiating that the two populations are different. Novel agents (IMIDs: thalidomide or lenalidomide and/or PSI, i.e., bortezomib) either as primary or maintenance therapy were given to all the patients. Triplet therapy was rendered to 56.5% of the patients. With a median follow-up of 166 weeks (range: 14–961 weeks), 626 patients progressed (median PFS = 117 weeks) and 372 died (median OS = 166 weeks).

## Results on the MMIn Dataset (*n* = 384)

Univariate Cox analysis of the entire patient cohort ($n$ = 1,070, **Table S3**, **Figure 2**) revealed increased risk of progression and mortality for age >67 years, albumin ≤3.5, β2M ≥4.78, calcium ≥11, eGFR ≤48.2, and hemoglobin ≤12.3. Multivariate Cox hazard analysis was also performed to analyze the cumulative risk of the parameters (**Table S4**). Of the three models generated, model A3 based on ML-derived cutoffs for the prognostic parameters was the best with higher C-index and hazard ratio (**Table 2**). Using model A3, the patients were risk stratified and the largest proportion of patients were placed in CRSS-2 ($n$ = 192, 50%) followed by CRSS-1 ($n$ = 137, 35.68%) and CRSS-3 ($n$ = 55, 14.32%). KM survival analysis of CRSS groups indicated statistically significant difference in PFS between CRSS-1 and CRSS-2 groups (median PFS: 213 vs. 138 weeks; $p$ = 0.0003) and between CRSS-2 and CRSS-3 groups (median PFS: 138 vs. 100 weeks; $p$ = 0.0026) (**Figure 2**). For R-ISS, there was a statistically significant difference in PFS between R-ISS2 and R-ISS3 (median PFS: 160 vs. 105 weeks; $p$ = 0.01) but not between R-ISS1 and R-ISS2 (median PFS = 196 vs. 160 weeks; $p$ = 0.31). Furthermore, for CRSS, there was statistically significant difference in OS between CRSS-1 and CRSS-2 groups (median OS = 495 vs. 249 weeks; $p$ = 1.08e-8) as well as between CRSS-2 and CRSS-3 groups (median OS = 249 vs. 182 weeks; $p$ = 0.02). For R-ISS, there was statistical difference in OS between R-ISS2 and R-ISS3 groups (median OS = 377 vs. 168 weeks; $p$ = 1.86e-5) as well as between R-ISS1 and R-ISS2 groups (median OS = 478 vs. 377 weeks; $p$ = 0.03).

C-statistic and hazard ratios computed on CRSS surpassed the C-index and hazard ratios obtained for R-ISS with respect to both PFS and OS (**Table 2**). C-statistic for CRSS was 0.60 [Akaike information criteria (AIC) = 2,171.49, Bayesian information criteria (BIC) = 2,175.43, HR = 1.80, 95% CI = 1.46–2.21, $p$ < 5e-6] for PFS and 0.67 (AIC = 1,244.72, BIC = 1,248.67, HR = 2.43, 95% CI = 1.87–3.14, $p$ < 5e-6) for OS, while C-statistic for R-ISS was 0.57 (AIC = 2,011.14, BIC = 2,015.01, HR = 1.43, 95% CI = 1.12–1.82, $p$ = 4.18e-3) for PFS and 0.636

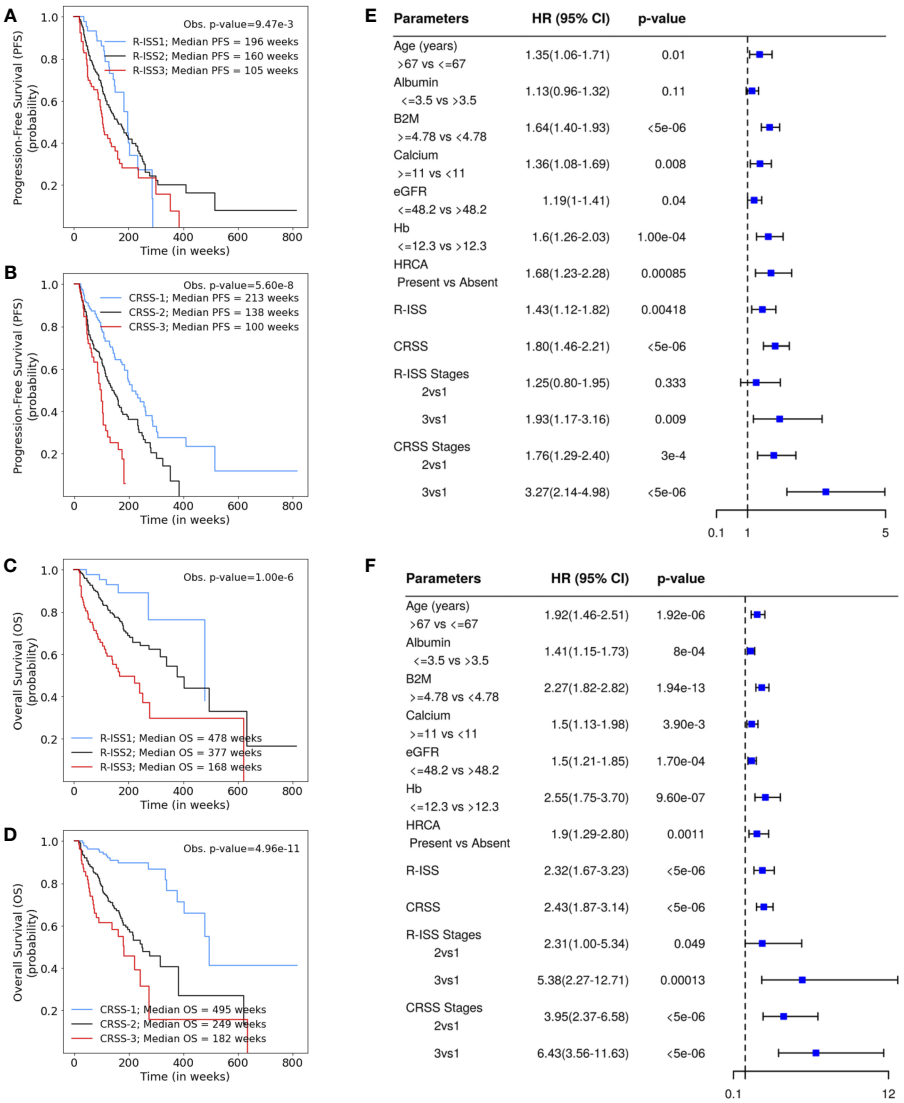


**FIGURE 2** | **(A, B)** Progression-free survival in patients with multiple myeloma (MM) from the MMIn cohort ($n$ = 1,070) stratified by the Revised International Staging System (R-ISS) ($n$ = 355) and the proposed CRSS ($n$ = 384), respectively. R-ISS1 is the low-risk stage, R-ISS2 is the intermediate-risk stage, and R-ISS3 is the high-risk stage. Median progression-free survival (PFS) for R-ISS1, R-ISS2, and R-ISS3 are 196, 160, and 105 weeks, respectively. The observed $p$-value obtained after performing a log-rank test on R-ISS is 9.47e-3. Similarly, CRSS-1 is the low-risk stage, CRSS-2 is the intermediate-risk stage, and CRSS-3 is the high-risk stage. Median PFS for CRSS-1, CRSS-2, and CRSS-3 are 213, 138, and 100 weeks, respectively. The observed $p$-value obtained after performing a log-rank test on CRSS is 5.60e-8. **(C, D)** Overall survival in patients with MM from the MMIn cohort ($n$ = 1,070) stratified by the R-ISS ($n$ = 355) and CRSS ($n$ = 384), respectively. Median overall survival (OS) for R-ISS1, R-ISS2, and R-ISS3 are 478, 337, and 168 weeks, respectively. The observed $p$-value obtained after performing a log-rank test on R-ISS is 1.00e-6. Median OS for CRSS-1, CRSS-2, and CRSS-3 are 495, 249, and 182 weeks, respectively. The observed $p$-value obtained after performing a log-rank test on CRSS is 4.96e-11. **(E, F)** Univariate Cox hazard analysis on the prognostic factors—age, albumin, beta-2 microglobulin (β2M), calcium, estimated glomerular filtration rate (eGFR), hemoglobin, and high-risk cytogenetic abnormalities (HRCA)—for PFS and OS, respectively. Hazard ratios for all the parameters except HRCA were calculated on complete data ($n$ = 1,070) for the MMIn dataset. Hazard ratio for HRCA and the risk-staging models were found using the data for which HRCA information was present ($n$ = 384 for the MMIn dataset).

(AIC = 1,132.20, BIC = 1,136.07, HR = 2.32, 95% CI = 1.67–3.23, $p$ < 5e-6) for OS.

## Results on the MMRF Dataset ($n$ = 800)

For the MMRF data, out of the four models generated, model M4 performed the best and had the highest C-index and hazard ratios as compared with the other models as well as R-ISS (**Table 2**). In the univariate Cox hazard analysis of the MMRF data, risk of progression and mortality was increased for age >69 years, β2M ≥5.5, albumin ≤3.5, hemoglobin ≤9.59, eGFR ≤48.3, and calcium ≥10.52 (**Table S3**, **Figure S4**). Multivariate Cox hazard analysis was also performed (**Table S4**). In the MMRF cohort, using the M4 model, the majority of the patients were placed in CRSS-2 ($n$ = 452, 56.5%) followed by CRSS-3 ($n$ = 174, 21.75%) and CRSS-1 ($n$ = 174, 21.75%). Results of

**TABLE 2 |** Comparison of different models devised for the risk stratification of patients in the MMIn and MMRF cohorts with the R-ISS.

| | | PFS | | | OS | | |
|---|---|---|---|---|---|---|---|
| | | **Hazard ratio** | ***p*-value** | **C-index** | **Hazard ratio** | ***p*-value** | **C-index** |
| **MMIn (*n* = 384)** | | | | | | | |
| R-ISS (*n* = 355) | | 1.42 | 0.004 | 0.57 | 2.32 | <5e-6 | 0.636 |
| | 2vs1 | 1.24 | 0.33 | | 2.31 | 0.04 | |
| | 3vs1 | 1.92 | 0.009 | | 5.37 | 0.00013 | |
| Model A1 | | 1.5 | 1.00e-5 | 0.594 | 2.03 | <5e-6 | 0.646 |
| | 2vs1 | 1.53 | 0.007 | | 2.13 | 0.0013 | |
| | 3vs1 | 2.26 | 2.00e-5 | | 4.16 | <5e-6 | |
| Model A2 | | 1.4 | 0.0001 | 0.579 | 1.74 | 1.00e-5 | 0.616 |
| | 2vs1 | 1.42 | 0.056 | | 1.9 | 0.02 | |
| | 3vs1 | 1.98 | 0.00013 | | 3.13 | 2.00e-5 | |
| Model A3 (CRSS) | | **1.8** | <5e-6 | **0.6** | **2.43** | <5e-6 | **0.67** |
| | 2vs1 | **1.76** | 3.00e-4 | | **3.95** | <5e-6 | |
| | 3vs1 | **3.27** | <5e-6 | | **6.43** | <5e-6 | |
| **MMRF (*n* = 800)** | | | | | | | |
| R-ISS (*n* = 658) | | 1.61 | 0.00001 | 0.578 | 2.26 | <5e-6 | 0.618 |
| | 2vs1 | 1.49 | 0.015 | | 1.79 | 0.03 | |
| | 3vs1 | 2.6 | 0.00001 | | 4.66 | <5e-6 | |
| Model M1 | | 1.55 | <5e-6 | 0.6 | 2.07 | <5e-6 | 0.656 |
| | 2vs1 | 1.55 | 0.00042 | | 2.06 | 0.00067 | |
| | 3vs1 | 2.4 | <5e-6 | | 4.3 | <5e-6 | |
| Model M2 | | 1.62 | <5e-6 | 0.6 | 2.36 | <5e-6 | 0.657 |
| | 2vs1 | 1.44 | 0.01 | | 2.12 | 0.0081 | |
| | 3vs1 | 2.54 | <5e-6 | | 5.22 | <5e-6 | |
| Model M3 | | 1.54 | <5e-6 | 0.604 | 2.2 | <5e-6 | 0.679 |
| | 2vs1 | 1.87 | <5e-6 | | 2.95 | <5e-6 | |
| | 3vs1 | 2.32 | <5e-6 | | 5.11 | <5e-6 | |
| Model M4 (CRSS) | | **1.79** | <5e-6 | **0.61** | **2.85** | <5e-6 | **0.676** |
| | 2vs1 | **1.76** | 8.10e-4 | | **4.1** | 3.40e-4 | |
| | 3vs1 | **3.19** | <5e-6 | | **10.61** | <5e-6 | |

*Models were built using data for which high-risk cytogenetic information (HRCA) was available (n = 384 for MMIn and n = 800 for MMRF). R-ISS information was available for only 355 out of 384 patients in the MMIn dataset and 658 out of 800 patients in the MMRF dataset. The model with the best performance was A3 and M4 (in bold).*
*Model A1: beta-2 microglobulin (β2M), albumin, LDH, and CA [del17, t(4;14), t(14;16)] at existing cutoffs. Model A2: age, β2M, albumin, calcium, estimated glomerular filtration rate (eGFR), Hb, and HRCA using existing cutoffs. Model A3: age, β2M, albumin, calcium, eGFR, Hb, and HRCA using proposed cutoffs for MMIn data. Model M1: β2M, albumin, LDH, and HRCA at existing cutoffs. Model M2: age, β2M, albumin, calcium, eGFR, Hb, and HRCA using existing cutoffs. Model M3: age, β2M, albumin, calcium, eGFR, Hb, and HRCA using proposed cutoffs for MMIn data. Model M4: age, β2M, albumin, calcium, eGFR, Hb, and HRCA using proposed cutoffs for MMRF data.*

the median PFS on CRSS groups ($p$ = 8.64e-12) and R-ISS groups ($p$ = 1.73e-5) as well as median OS on CRSS groups ($p$ = 1.08e-15) and R-ISS groups ($p$ = 6.57e-8) reveal the superior performance of the CRSS than the R-ISS (significant $p$-values; **Figure S4**).

C-statistic for CRSS in MMRF data is 0.61 (AIC = 4,126.07, BIC = 4,130.74, HR = 1.79, 95% CI = 1.52–2.12, $p$ < 5e-6) for PFS and 0.676 (AIC = 1,819.95, BIC = 1,824.62, HR = 2.85, 95% CI = 2.19–3.71, $p$ < 5e-6) for OS. C-statistic for R-ISS is 0.578 (AIC = 3,413.36, BIC = 3,416.49, HR = 1.61, 95% CI = 1.30–2.00, $p$ = 1.00e-5) for PFS and 0.618 (AIC = 1,586.78, BIC = 1,591.27, HR = 2.26, 95% CI = 1.65–3.11, $p$ < 5e-6) for OS (**Table 3**).

The 5-year OS for the MMIn ($n$ = 384) was 89.79% for CRSS-1, 47.91% for CRSS-2, and 31.36% for CRSS-3 (**Table 3**). Overall, there is a substantial difference in the percentages of the 5-year OS and median OS for different risk groups which indicate that the groups were significant. A similar stratification was achieved when the CRSS model was applied on the MMRF test dataset. The 5-year OS for MMRF data was 94.78% for CRSS-1, 65.69% for CRSS-2, and 46.91% for CRSS-3 which is quite comparable to that obtained in the MMIn data. Higher values of C-index and hazard ratios as well as lower values of partial AIC and BIC on both datasets were indicative of the superior performance of our AI-based CRSS method as compared with R-ISS.

## Statistical Analysis on the Parameters Used in CRSS

The Kruskal–Wallis test was performed to compare the median values of the parameters age, albumin, β2M, calcium, eGFR, and hemoglobin across the three risk groups for both the MMIn and MMRF datasets. There was a significant increase ($p$ < 0.05) in the values of age and β2M, while there was a significant decrease ($p$ < 0.05) in the values of albumin, eGFR, and hemoglobin as the risk of disease increased (**Figures S5, S6**) for both the MMIn and MMRF datasets. Wilcoxon rank-sum test was performed to compare the median values of the parameters between two successive risk groups and showed significant variation of parameters for both datasets.

## Model Interpretation

To ascertain the impact of individual parameters on risk stage predictions by CRSS, decision tree models built using the MMIn and MMRF datasets were analyzed using SHAP (**Figures 3**, **7**). Key

**TABLE 3 |** Prediction of progression-free survival and overall survival (in %) for CRSS and R-ISS at 1, 2, 3, 4, and 5 years in the MMIn ($n$ = 384) and MMRF datasets ($n$ = 800).

| | | MMIn data | | | | | |
|---|---|---|---|---|---|---|---|
| | | R-ISS ($n$ = 355) | | | CRSS ($n$ = 384) | | |
| | Year | 1 | 2 | 3 | 1 | 2 | 3 |
| PFS | 1 | 0.9318 | 0.8305 | 0.6967 | 0.8966 | 0.7812 | 0.7196 |
| | 2 | 0.8606 | 0.6601 | 0.5223 | 0.7709 | 0.6265 | 0.4472 |
| | 3 | 0.6404 | 0.5124 | 0.3632 | 0.6449 | 0.4729 | 0.2515 |
| | 4 | 0.3422 | 0.4179 | 0.2810 | 0.5251 | 0.3624 | 0.0587 |
| | 5 | 0.2738 | 0.2856 | 0.2342 | 0.4014 | 0.2679 | 0.0587 |
| OS | 1 | 0.9773 | 0.9387 | 0.7784 | 0.9630 | 0.8938 | 0.7976 |
| | 2 | 0.9540 | 0.8415 | 0.6393 | 0.9466 | 0.7679 | 0.6155 |
| | 3 | 0.9282 | 0.7764 | 0.5342 | 0.9098 | 0.6702 | 0.5831 |
| | 4 | 0.8895 | 0.6790 | 0.4953 | 0.8979 | 0.5691 | 0.4574 |
| | 5 | 0.8895 | 0.6422 | 0.3698 | 0.8979 | 0.4791 | 0.3136 |
| | | MMRF data | | | | | |
| | | R-ISS ($n$ = 658) | | | CRSS ($n$ = 800) | | |
| | Year | 1 | 2 | 3 | 1 | 2 | 3 |
| PFS | 1 | 0.9033 | 0.8132 | 0.6358 | 0.9325 | 0.8367 | 0.6611 |
| | 2 | 0.7957 | 0.6261 | 0.4040 | 0.8162 | 0.6734 | 0.4423 |
| | 3 | 0.6295 | 0.4862 | 0.3059 | 0.7008 | 0.5084 | 0.3129 |
| | 4 | 0.4641 | 0.3414 | 0.2781 | 0.5151 | 0.3711 | 0.2249 |
| | 5 | 0.2769 | 0.2450 | 0.2781 | 0.4121 | 0.2637 | 0.1799 |
| OS | 1 | 0.9807 | 0.9092 | 0.8559 | 0.9869 | 0.9379 | 0.8231 |
| | 2 | 0.9612 | 0.8372 | 0.6460 | 0.9689 | 0.8772 | 0.6780 |
| | 3 | 0.9286 | 0.7799 | 0.5211 | 0.9478 | 0.8217 | 0.5814 |
| | 4 | 0.8833 | 0.7461 | 0.4904 | 0.9478 | 0.7844 | 0.5293 |
| | 5 | 0.5748 | 0.7108 | 0.3678 | 0.9478 | 0.6569 | 0.4691 |

contributors of high-risk predictions in the MMIn dataset were the presence of HRCA, elevated levels of β2M, higher age, and lower levels of albumin (**Figure 3**). Furthermore, lower levels of eGFR and hemoglobin along with elevated levels of calcium also contributed to high-risk prediction in the patients. It was observed from the waterfall plots (**Figures 4**–**6**) of the randomly chosen patients in different risk stages that the order of the impact of the parameters varied in different patients within the same risk category. For the high-risk category (**Figure 6**), HRCA had the highest impact on one of the randomly chosen patients; in another patient, β2M had the highest impact in contributing to high risk, while in the third patient, age and albumin had the highest prognostic impact. This suggests that the risk assessment in MM is a cumulative function of multiple factors. An individual parameter cannot adequately capture the risk associated with MM given that other prognostic parameters could influence the outcome. Furthermore, the complex association among different parameters that encapsulates the disease risk varies according to the patients, thereby leading to a varying order of impact of parameters in the patients. Hence, the AI-based decision tree algorithms can handle such an integrated analysis. This analysis reveals that each patient is unique and multiple factors interact and impact the outcome differently in individual patients.

# DISCUSSION

The influence of ethnicities on clinical characteristics in patients belonging to distinct ethnic groups is well known, and therefore, it is of paramount interest to integrate the ethnic group-specific information in risk-staging models as it can affect the risk score prediction. The R-ISS (3) is the current standard of care for staging myeloma patients which includes a few HRCA, but molecular aberrations such as 1q gain and chromothripsis associated with adverse outcome have been overlooked (24). In fact, it includes t (4;14), which has lost significance in patients treated with triplet regimens (25). Besides, the R-ISS does not include any ethnic-specific information and, therefore, is not robust considering the large heterogeneous population of MM patients globally. An ideal risk-staging system would be based on all the known adverse prognostic factors including clinical, ethnic, and molecular aberrations. There is a tremendous heterogeneity in global healthcare systems that limit the availability of high-end molecular testing for all patients, and yet, the internet/electronic connectivity allows patients to receive medical advice from global leaders in medicine. Recently, an AI-supported risk-staging model, MRS (26), has been developed for NDMM; however, it does not include HRCA and ethnicity information. Considering the present world scenario, it is, thus, desirable to develop a simple risk-staging model that integrates ethnic-specific characteristics of the prognostic parameters that are easy to acquire in the healthcare settings worldwide.

## Risk-Staging Models and Their Performance as Compared With the R-ISS

In contrast to the R-ISS which utilizes four parameters, seven parameters were taken into consideration for designing the

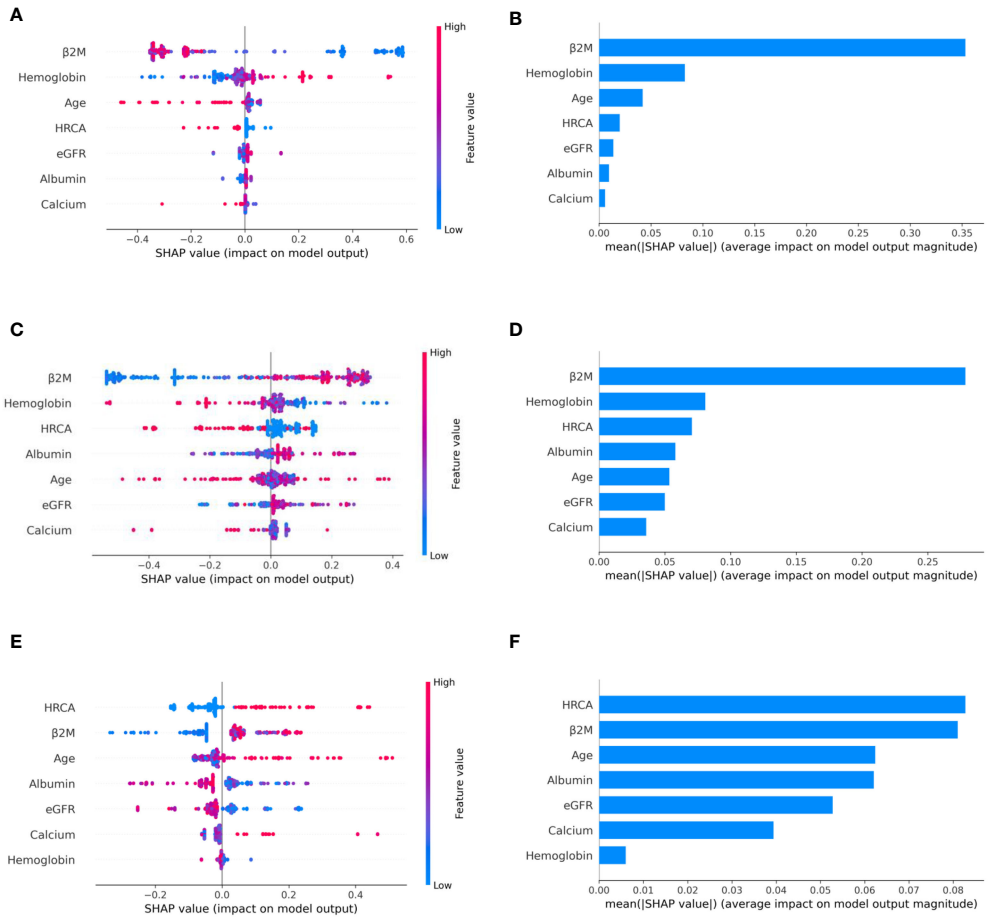


**FIGURE 3** | Model interpretation using SHAP (SHapley Additive exPlanations). SHAP summary plots for different risk stages inferred from MMIn data showing the relative impact of different parameters (top to bottom) contributing to a particular risk stage prediction. **(A, B)** CRSS-1: Normal levels of β2M and hemoglobin are the key contributors to the low-risk stage prediction. Furthermore, high values of age on the left side of the summary plot are pushing the model away from the low-risk prediction and are indicative of either intermediate or high risk. Overall, β2M has the highest impact and calcium has the lowest impact on the low-risk stage prediction. **(C, D)** CRSS-2: β2M and hemoglobin are the key contributors to the intermediate-risk stage. Elevated levels of β2M with lower levels of hemoglobin are indicative of intermediate risk. **(E, F)** CRSS-3: Presence of HRCA is contributing the most to the high-risk stage. Elevated values of β2M and calcium and lower levels of albumin, hemoglobin, and eGFR are contributing toward the high-risk stage prediction.

CRSS. It was observed that the cutoff values for these parameters derived using KAP vary in the two cohorts, one of which belongs to Indian and the other belongs to the American population. For the Indian data, there was a change in the cutoff values for β2M, age, eGFR, and hemoglobin, while there was no change in the cutoff value for calcium and albumin as shown in **Table 1**. For the MMRF data, there was a change in cutoff values for calcium, eGFR, hemoglobin, and age, while the cutoff values for albumin and β2M remain unchanged. The median age of onset of MM in the Indian population is almost a decade early as compared with the population in the USA (27, 28). This supported our assertion of choosing different cutoffs of age for MMIn from the MMRF dataset.

Various models were built on the different combinations of the parameters using both the established and proposed cutoffs for the two datasets. The best staging model for both datasets was obtained when the proposed cutoffs for the respective cohorts were used. When the ML-derived cutoffs were used for the parameters age, eGFR, hemoglobin, and β2M in the A3 model, performance was enhanced significantly in terms of high C-index and hazard ratios as compared with the R-ISS. A similar observation was noticed in the M4 model which utilized ML-derived cutoffs obtained for the MMRF dataset and achieved the best performance among all the models with a significant improvement in the C-index as well as hazard ratios as compared with the R-ISS. Overall, A3 and M4 were the best staging models for the MMIn and MMRF data, respectively. The improvement in the performance of the model verified our hypothesis that the cutoffs of the different parameters vary with different ethnicities.

The plausibility of the proposed model was further substantiated by performing significance testing. The Kruskal–Wallis test showed statistically significant variations ($p < 0.05$) in

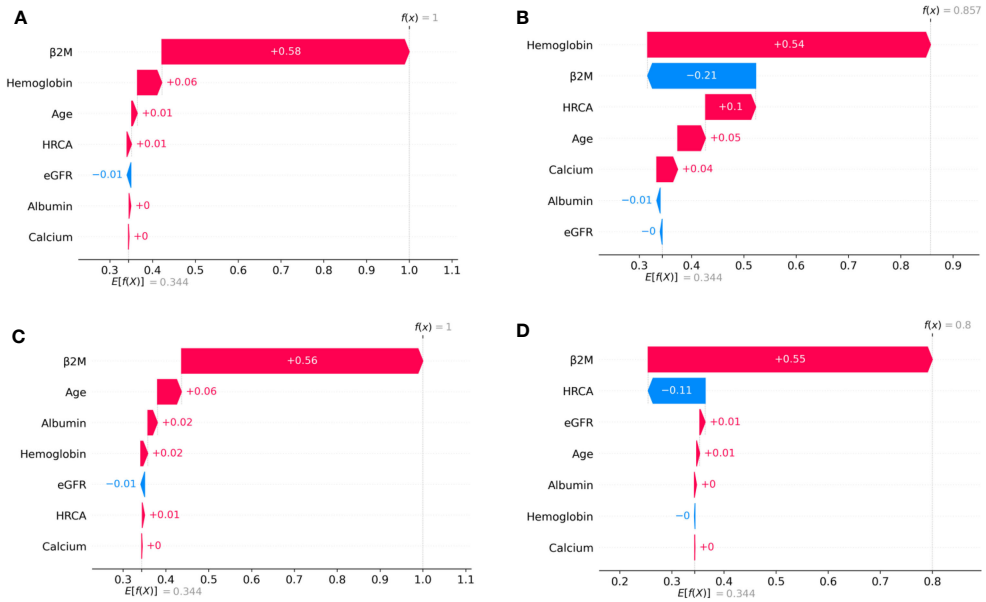


**FIGURE 4** | SHAP waterfall plots for the randomly chosen four patients in low-risk stage (CRSS-1) from the MMIn dataset. The pink color shows the positive impact of the feature, while the blue color shows the negative impact of the feature. Features with a positive impact contributed to the class of low-risk stage prediction, while features with a negative impact contributed to class opposite to low risk. β2M, hemoglobin, age, and HRCA have the highest overall impact on low-risk stage prediction in the MMIn dataset. However, this ranking itself differs from patient to patient as can be seen in **(A–D)**. **(A)** β2M has the highest impact followed by hemoglobin, age, and HRCA. **(B)** Hemoglobin has the highest impact followed by β2M and age. **(C, D)** β2M has the highest impact followed by age and HRCA.

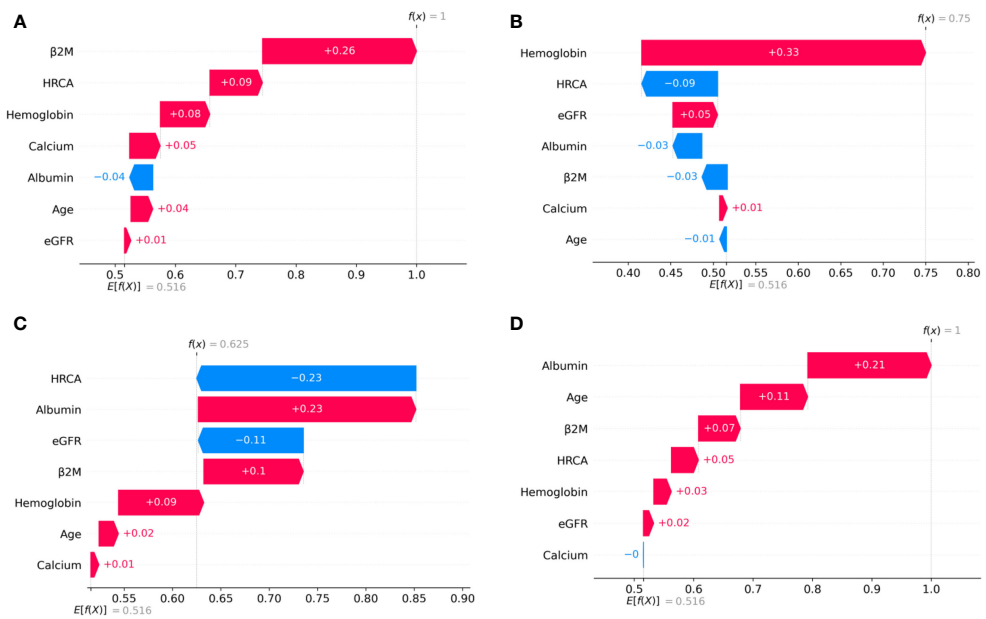


**FIGURE 5** | SHAP waterfall plots for the randomly chosen four patients in the intermediate-risk stage (CRSS-2) from the MMIn dataset. The pink color shows the positive impact of the feature, while the blue color shows the negative impact of the feature. Features with a positive impact contributed to the class of intermediate-risk stage prediction, while features with a negative impact contributed to the class opposite to intermediate risk. β2M, hemoglobin, HRCA, and albumin have the highest overall impact on the intermediate-risk stage prediction in the MMIn dataset. However, the ranking of the features itself differs from patient to patient as can be seen in **(A–D)**. **(A)** β2M has the highest impact followed by HRCA. **(B)** Hemoglobin has the highest impact followed by HRCA. **(C)** HRCA has the highest impact followed by albumin. **(D)** Albumin has the highest impact followed by age.

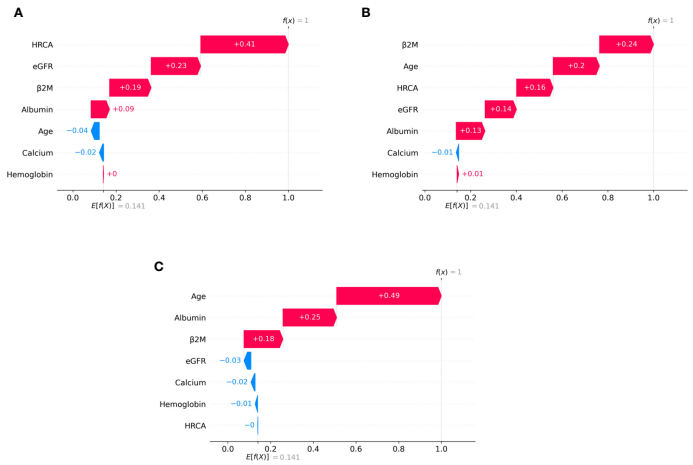


**FIGURE 6** | SHAP waterfall plots for randomly chosen patients in high-risk stage (CRSS-3) from the MMIn dataset. The pink color shows the positive impact of the feature, while the blue color shows the negative impact of the feature. Features with a positive impact contributed to the class of high-risk stage prediction, while features with a negative impact contributed to class opposite to highest risk. HRCA, β2M, age, and albumin have the highest overall impact on high-risk stage prediction. However, this ranking differs from patient to patient as can be seen in **(A–C)**. **(A)** HRCA has the highest impact. **(B)** β2M has the highest impact. **(C, D)** Age and albumin have the highest impact.

the median values of the parameters age, albumin, β2M, eGFR, and hemoglobin across the three risk groups (**Figures S4, S5**) for both datasets. Furthermore, the Wilcoxon rank-sum test revealed statistically significant variations ($p < 0.05$) in the median values of the parameters between two successive risk groups (CRSS-1 and CRSS-2; CRSS-2 and CRSS-3). Furthermore, CRSS for the MMIn and MMRF datasets were interpreted using SHAP (13) to establish the clinical relevance of the risk stages predicted by the CRSS. For the MMIn data, elevated levels of β2M and calcium with lower levels of eGFR and hemoglobin contributed to high risk, whereas in the MMRF data, elevated levels of β2M and lower levels of hemoglobin, eGFR, and albumin contributed to high risk in myeloma patients. These findings are in accordance with the observations mostly identified in high-risk MM patients. Additionally, it was observed that the order of impact of hemoglobin was higher in low-risk stage prediction in the MMIn dataset as compared with the MMRF dataset, while the order of impact of hemoglobin was higher in high-risk stage prediction in the MMRF dataset as compared with the MMIn dataset (**Figures 3**, **7**). The difference in the rankings can be attributed to the varying ethnicities and further confirmed our claim of using ethnicity-aware risk-staging models for MM. In the present study, we have used the MMIn and MMRF cohorts belonging to Indian and American ethnicities, respectively, for building CRSS models. Results on both cohorts have strengthened our claim that the robustness of the staging model is amplified by inclusion of ethnicity-specific cutoffs of the prognostic factors as well as by utilizing AI techniques.

The classification rules were obtained using a decision tree classifier on the classification output of the best performing models in both MMIn and MMRF data. Overall classification accuracy was 94.79% and 98% for the MMIn and MMRF data, respectively. Final risk stages were evaluated using the classification rules in both datasets. Furthermore, it is evident from the UMAP plots that both the MMIn and MMRF data were not visible as three separate risk groups initially in the absence of CRSS risk labels (**Figures S3A, C, E**). With the addition of these risk labels with every patient sample, the subjects could be seen to be grouped separately (where a group corresponds to one risk label) in the UMAP plot (**Figures S3B, D**). This demonstrates the ability of the CRSS model in identifying the risk groups correctly from the non-separable data. To further validate our model, we found risk stages in 123 prospective subjects of MMIn data that were not used to build the CRSS model. UMAP plots (**Figure S3F**) suggest that the prospective subjects got correctly aligned to their respective risk stages inferred *via* CRSS.

For the MMIn data, β2M was in the highest level of hierarchy in the classification rules followed by hemoglobin and HRCA (**Figure S2A**). For the MMRF data, the prognostic factor in the highest level of hierarchy was β2M followed by albumin and Hb (**Figure S2B**). The cutoff values for β2M, albumin, and Hb were 5.2, 3.55, and 9.64. The cutoffs for β2M and albumin were not changed, but the cutoff value proposed for Hb was 9.59, which was close to the observed value in the classification rules. This observation further justified our choice of using new cutoffs for the risk-staging model.

## Conclusion

In this work, we examined the impact of ethnicity-based cutoffs of laboratory parameters derived using the ML algorithm on risk prediction in Indian and American patients with MM. We trained different risk-staging models for both the MMRF and MMIn datasets. The best predictor model was obtained when ethnicity-specific cutoffs of the clinical parameters were utilized. Furthermore, we presented a new reliable and robust AI-enabled risk-staging system, namely, CRSS, which utilizes easily acquirable

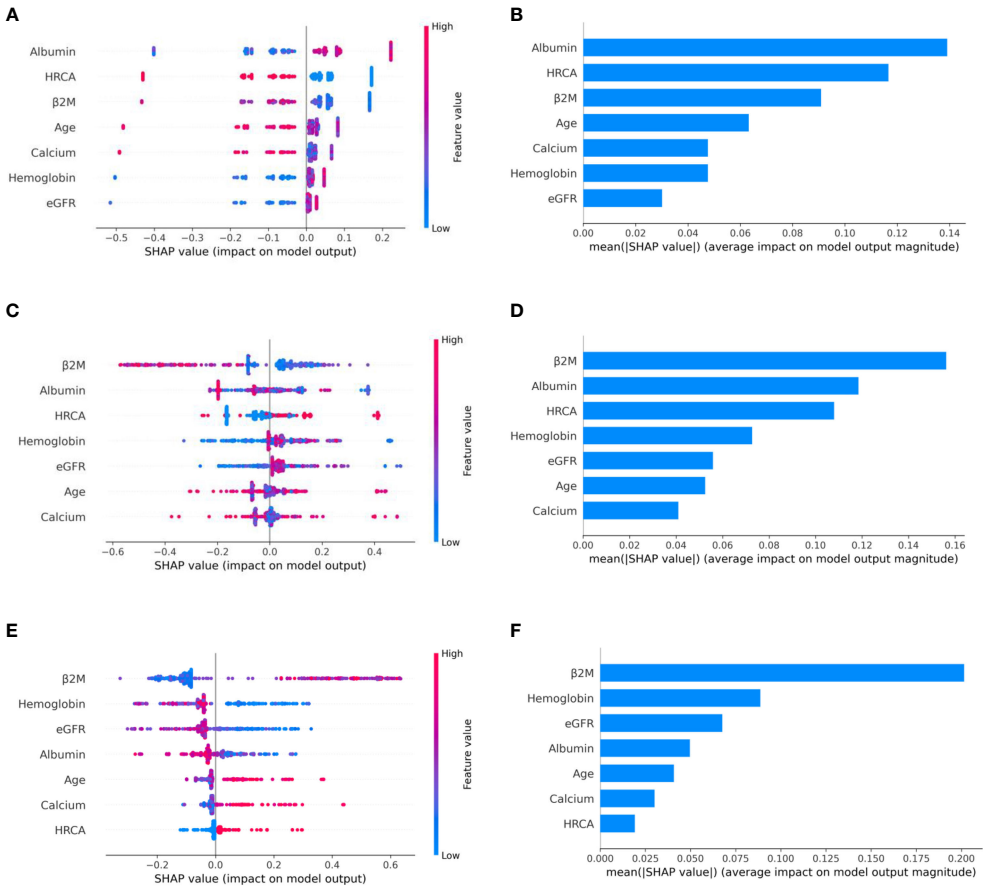


**FIGURE 7** | Model interpretation using SHAP. SHAP summary plots for different risk stages inferred in MMRF data showing the impact of different parameters used in the model. **(A, B)** CRSS-1: albumin, HRCA, and β2M have the highest impact on the low-risk stage. Normal levels of albumin, absence of HRCA, and lower values of β2M are contributing to low risk (CRSS-1) in myeloma patients. **(C, D)** CRSS-2: β2M, albumin, and HRCA are the key contributors to the intermediate-risk stage. **(E, F)** CRSS-3: β2M and hemoglobin have the highest impact on the high-risk stage. Elevated levels of β2M and lower values of hemoglobin are contributing toward the high-risk stage in the patient. Lower values of albumin and eGFR are further promoting high-risk stage prediction.

laboratory and clinical parameters, i.e., age, albumin, β2M, calcium, eGFR, and hemoglobin along with HRCA (**Table S5**). Risk stratification achieved by AI-assisted CRSS is able to better separate the patients into different risk groups as compared with the R-ISS. High concordance-index and hazard ratios reveal the superior performance of the CRSS as compared with the R-ISS.

Furthermore, the clinical and biological significance of the decision tree classifier rules for risk stage prediction in MM patients was deduced *via* SHAP analysis on both datasets. The successful evaluation of our proposed staging system on both datasets establishes the utility of the proposed ethnicity-aware staging system for NDMM patients, treated largely with novel agents or a combination thereof, in a real-world scenario. Our study also highlights the importance of application of AI in building CRSS, thereby enhancing the prediction of survival outcome and separability of risk stages in NDMM patients. We have also developed a web platform-based AI-assisted ethnicity-aware MM risk-staging calculator.

## Limitations and Future Work

The CRSS has been built on a smaller set of NDMM patients as compared with the R-ISS (3) study. In the future, the CRSS model may be tested on larger datasets with varying ethnic groups as the cohort size of the present study is 25% of the cohort used in the R-ISS reported in 2015. As the CRSS calculator becomes available online, data could be generated by independent groups for further validation in real-world scenarios.

## DATA AVAILABILITY STATEMENT

The original contributions presented in the study are included in the article/**Supplementary Material**. Further inquiries can be directed to the corresponding authors. CRSS calculator can be found at: http://sbilab.iiitd.edu.in/pub_files/CRRScalculator_edit.html.

## ETHICS STATEMENT

The studies involving human participants were reviewed and approved by IEC, AIIMS. The patients/participants provided their written informed consent to participate in this study.

## AUTHOR CONTRIBUTIONS

AF: methodology, software, formal analysis, investigation, validation, and writing—original draft preparation. AG: methodology, investigation, validation, writing—original draft preparation, resources, project management, and supervision. KS: formal analysis, validation, and supervision. LK: resources. AS: resources. RG: conceptualization, investigation, validation, resources, writing—original draft preparation, project management, and supervision. All the authors had full access to the final version of the report. All authors contributed to the article and approved the submitted version.

## FUNDING

This work was supported by grants from the Department of Biotechnology, Govt. of India (Grant: BT/MED/30/SP11006/2015), and the Department of Science and Technology, Govt. of India (Grant: DST/ICPS/CPS-Individual/2018/279(G)). The funding bodies had no role in study design, data collection, data analysis, data interpretation, or writing of the report.

## ACKNOWLEDGMENTS

AF would like to thank the University Grants Commission, Govt. of India, for the UGC-Senior Research Fellowship. The authors acknowledge the MMRF and dbGaP (Project #18964) for providing the dataset. These data were generated as part of the Multiple Myeloma Research Foundation Personalized Medicine Initiative. The authors would also like to thank the Centre of Excellence in Healthcare, IIIT-Delhi for the support in their research.

## SUPPLEMENTARY MATERIAL

The Supplementary Material for this article can be found online at: https://www.frontiersin.org/articles/10.3389/fonc.2021.720932/full#supplementary-material

## REFERENCES

1. Durie BG, Salmon SE. A Clinical Staging System for Multiple Myeloma Correlation of Measured Myeloma Cell Mass With Presenting Clinical Features, Response to Treatment, and Survival. *Cancer* (1975) 36(3):842–54. doi: 10.1002/1097-0142(197509)36:3<842::AID-CNCR2820360303>3.0.CO;2-U
2. Greipp PR, SanMiguel J, Durie BG, Crowley JJ, Barlogie B, Boccadoro M, et al. International Staging System for Multiple Myeloma. *J Clin Oncol* (2005) 23:3412–20. doi: 10.1200/JCO.2005.04.242
3. Palumbo A, Avet-Loiseau H, Oliva S, Lokhorst HM, Goldschmidt H, Rosinol L, et al. Revised International Staging System for Multiple Myeloma: A Report From International Myeloma Working Group. *J Clin Oncol* (2015) 33 (26):2863. doi: 10.1200/JCO.2015.61.2267
4. Rago A, Grammatico S, Za T, Levi A, Mecarocci S, Siniscalchi A, et al. Prognostic Factors Associated With Progression of Smoldering Multiple Myeloma to Symptomatic Form. *Cancer* (2012) 118(22):5544–9. doi: 10.1002/cncr.27657
5. Schinke M, Ihorst G, Duyster J, Wäsch R, Schumacher M, Engelhardt M. Risk of Disease Recurrence and Survival in Patients With Multiple Myeloma: A German Study Group Analysis Using a Conditional Survival Approach With Long-Term Follow-Up of 815 Patients. *Cancer* (2020) 126(15):3504–15. doi: 10.1002/cncr.32978
6. Howlader N, Noone AM, Krapcho M, Miller D, Bishop K, Kosary CL, et al. *SEER Cancer Statistics Review, 1975–2014*. (2017), based on November 2016 SEER data submission.
7. Ailawadhi S, Aldoss IT, Yang D, Razavi P, Cozen W, Sher T, et al. Outcome Disparities in Multiple Myeloma: A SEER-Based Comparative Analysis of Ethnic Subgroups. *Br J Haematol* (2012) 158(1):91–8. doi: 10.1111/j.1365-2141.2012.09124.x
8. Waxman AJ, Mink PJ, Devesa SS, Anderson WF, Weiss BM, Kristinsson SY, et al. Racial Disparities in Incidence and Outcome in Multiple Myeloma: A Population-Based Study. *Blood* (2010) 116(25):5501–6. doi: 10.1182/blood-2010-07-298760
9. Costa LJ, Brill IK, Omel J, Godby K, Kumar SK, Brown EE. Recent Trends in Multiple Myeloma Incidence and Survival by Age, Race, and Ethnicity in the United States. *Blood Adv* (2017) 1(4):282–7. doi: 10.1182/bloodadvances.2016002493
10. Derman BA, Jasielec J, Langerman SS, Zhang W, Jakubowiak AJ, Chiu BC. Racial Differences in Treatment and Outcomes in Multiple Myeloma: A Multiple Myeloma Research Foundation Analysis. *Blood Cancer J* (2020) 10 (8):1–7. doi: 10.1038/s41408-020-00347-6
11. Yellapragada SV, Fillmore NR, Frolov A, Zhou Y, Dev P, Yameen H, et al. Vitamin D Deficiency Predicts for Poor Overall Survival in White But Not African American Patients With Multiple Myeloma. *Blood Adv* (2020) 4 (8):1643. doi: 10.1182/bloodadvances.2019001411
12. Alexander DD, Mink PJ, Adami HO, Cole P, Mandel JS, Oken MM, et al. Multiple Myeloma: A Review of the Epidemiologic Literature. *Int J Cancer* (2007) 120(S12):40–61. doi: 10.1002/ijc.22718
13. Lundberg SM, Lee S-I. A Unified Approach to Interpreting Model Predictions. In: *Proceedings of the 31st International Conference on Neural Information Processing Systems (Nips'17)*. Red Hook, NY, USA: Curran Associates Inc. (2017). p. 4768–77.
14. Farswan A, Gupta A. TV-DCT: Method to Impute Gene Expression Data Using DCT Based Sparsity and Total Variation Denoising, in: *InICASSP 2019-2019 IEEE International Conference on Acoustics, Speech and Signal Processing (ICASSP)*, 2019 May 12. pp. 1244–8, IEEE.
15. Gehlot S, Farswan A, Gupta A, Gupta R. CT-NNBI: Method to Impute Gene Expression Data Using DCT Based Sparsity and Nuclear Norm Constraint With Split Bregman Iteration, in: *In2019 IEEE 16th International Symposium on Biomedical Imaging (ISBI 2019)*, 2019 Apr 8. pp. 1315–8, IEEE.
16. Farswan A, Gupta A, Gupta R, Kaur G. Imputation of Gene Expression Data in Blood Cancer and Its Significance in Inferring Biological Pathways. *Front Oncol* (2020) 9:1442. doi: 10.3389/fonc.2019.01442
17. Montealegre JR, Zhou R, Amirian ES, Scheurer ME. Uncovering Nativity Disparities in Cancer Patterns: Multiple Imputation Strategy to Handle Missing Nativity Data in the Surveillance, Epidemiology, and End Results Data File. *Cancer* (2014) 120(8):1203–11. doi: 10.1002/cncr.28533
18. Gupta R, Kaur G, Kumar L, Rani L, Mathur N, Sharma A, et al. Nucleic Acid Based Risk Assessment and Staging for Clinical Practice in Multiple Myeloma. *Ann Hematol* (2018) 97(12):2447–54. doi: 10.1007/s00277-018-3457-8

19. Kumar S, Paiva B, Anderson KC, Durie B, Landgren O, Moreau P, et al. International Myeloma Working Group Consensus Criteria for Response and Minimal Residual Disease Assessment in Multiple Myeloma. *Lancet Oncol* (2016) 17:e328–46. doi: 10.1016/S1470-2045(16)30206-6
20. Florkowski CM, Chew-Harris JS. Methods of Estimating GFR–different Equations Including CKD-EPI. *Clin Biochem Rev* (2011) 32(2):75.
21. Rajkumar SV. Multiple Myeloma: 2016 Update on Diagnosis, Risk-Stratification, and Management. *Am J Hematol* (2016) 91(7):719–34. doi: 10.1002/ajh.24402
22. Eo SH, Kang HJ, Hong SM, Cho H. K-Adaptive Partitioning for Survival Data, With an Application to Cancer Staging. (2013). arXiv preprint arXiv:1306.4615.
23. Monti S, Tamayo P, Mesirov J, Golub T. Consensus Clustering: A Resampling-Based Method for Class Discovery and Visualization of Gene Expression Microarray Data. *Mach Learn* (2003) 52(1-2):91–118. doi: 10.1023/A:1023949509487
24. Kaur G, Gupta R, Mathur N, Rani L, Kumar L, Sharma A, et al. Clinical Impact of Chromothriptic Complex Chromosomal Rearrangements in Newly Diagnosed Multiple Myeloma. *Leukemia Res* (2019) 76:58–64. doi: 10.1016/j.leukres.2018.12.005
25. Avet-Loiseau H, Leleu X, Roussel M, Moreau P, Guerin-Charbonnel C, Caillot D, et al. Bortezomib Plus Dexamethasone Induction Improves Outcome of Patients With T (4; 14) Myeloma But Not Outcome of Patients With Del (17p). *J Clin Oncol* (2010) 28(30):4630–4. doi: 10.1200/JCO.2010.28.3945
26. Farswan A, Gupta A, Gupta R, Hazra S, Khan S, Kumar L, et al. AI-Supported Modified Risk Staging for Multiple Myeloma Cancer Useful in Real-World Scenario. *Trans Oncol* (2021) 14(9):101157. doi: 10.1016/j.tranon.2021.101157
27. Unnikrishnan A, Khan AM, Narayan P, Norkin M. Striking Age Differences of Multiple Myeloma (MM) Diagnosis in Patients of Indian and Pakistani Descent in the United States Compared to Native Countries. *J Clin Oncol* (2017) 35:e13070. doi: 10.1200/JCO.2017.35.15_suppl.e13070
28. Konatam AM, Sadashivudu G. Age of Onset of Multiple Myeloma: A Paradigm Shift in Indian Patients. *Indian J Appl Res* (2016) 6:3.

**Conflict of Interest:** The authors declare that the research was conducted in the absence of any commercial or financial relationships that could be construed as a potential conflict of interest.

frontiers in Oncology

ORIGINAL RESEARCH
published: 01 December 2021
doi: 10.3389/fonc.2021.766888

# Preclinical Evaluation of a Novel Dual Targeting PI3Kδ/BRD4 Inhibitor, SF2535, in B-Cell Acute Lymphoblastic Leukemia

*Yongsheng Ruan[1,2†], Hye Na Kim[1†], Heather A. Ogana[1], Zesheng Wan[1], Samantha Hurwitz[1], Cydney Nichols[1], Nour Abdel-Azim[1], Ariana Coba[1], Seyoung Seo[1], Yong-Hwee Eddie Loh[3], Eun Ji Gang[1], Hisham Abdel-Azim[1], Chih-Lin Hsieh[4], Michael R. Lieber[5], Chintan Parekh[1], Dhananjaya Pal[6], Deepa Bhojwani[1], Donald L. Durden[6,7] and Yong-Mi Kim[1*]*

[1] Department of Pediatrics, Division of Hematology, Oncology, Blood and Marrow Transplantation, Children's Hospital Los Angeles, Norris Comprehensive Cancer Center, University of Southern California Keck School of Medicine, Los Angeles, CA, United States, [2] Department of Pediatrics, Nanfang Hospital, Southern Medical University, Guangzhou, China, [3] University of Southern California (USC) Libraries Bioinformatics Services, University of Southern California, Los Angeles, CA, United States, [4] University of Southern California (USC) Department of Urology, University of Southern California (USC) Norris Comprehensive Cancer Center, Los Angeles, CA, United States, [5] University of Southern California (USC) Department of Pathology, University of Southern California (USC) Norris Comprehensive Cancer Center, Los Angeles, CA, United States, [6] Department of Pediatrics, University of California San Diego, San Diego, CA, United States, [7] SignalRx Pharmaceuticals Inc., Omaha, NE, United States

The PI3K/Akt pathway—and in particular PI3Kδ—is known for its role in drug resistant B-cell acute lymphoblastic leukemia (B-ALL) and it is often upregulated in refractory or relapsed B-ALL. Myc proteins are transcription factors responsible for transcribing pro-proliferative genes and c-Myc is often overexpressed in cancers. The chromatin regulator BRD4 is required for expression of c-Myc in hematologic malignancies including B-ALL. Previously, combination of BRD4 and PI3K inhibition with SF2523 was shown to successfully decrease Myc expression. However, the underlying mechanism and effect of dual inhibition of PI3Kδ/BRD4 in B-ALL remains unknown. To study this, we utilized SF2535, a novel small molecule dual inhibitor which can specifically target the PI3Kδ isoform and BRD4. We treated primary B-ALL cells with various concentrations of SF2535 and studied its effect on specific pharmacological on-target mechanisms such as apoptosis, cell cycle, cell proliferation, and adhesion molecules expression using *in vitro* and *in vivo* models. SF2535 significantly downregulates both c-Myc mRNA and protein expression through inhibition of BRD4 at the c-Myc promoter site and decreases p-AKT expression through inhibition of the PI3Kδ/AKT pathway. SF2535 induced apoptosis in B-ALL by downregulation of BCL-2 and increased cleavage of caspase-3, caspase-7, and PARP. Moreover, SF2535 induced cell cycle arrest and decreased cell counts in B-ALL. Interestingly, SF2535 decreased the mean fluorescence intensity (MFI) of integrin α4, α5, α6, and β1 while increasing MFI of CXCR4, indicating that SF2535 may work through inside-out signaling of integrins. Taken together, our data provide a rationale for the clinical evaluation of targeting PI3Kδ/BRD4 in refractory or relapsed B-ALL using SF2535.

**Keywords: PI3Kδ, p-AKT, BRD4, c-Myc, acute lymphoblastic leukemia, SF2535**

OPEN ACCESS

***Edited by:***
*Gurvinder Kaur, All India Institute of Medical Sciences, India*

***Reviewed by:***
*Srimoyee Mukherjee, Tufts University School of Medicine, United States*
*Deepshi Thakral, All India Institute of Medical Sciences, India*

***Correspondence:**
*Yong-Mi Kim*
*ymkim@chla.usc.edu*

*†These authors have contributed equally to this work*

***Specialty section:***
*This article was submitted to Hematologic Malignancies, a section of the journal Frontiers in Oncology*

***Received:*** *30 August 2021*
***Accepted:*** *11 November 2021*
***Published:*** *01 December 2021*

***Citation:***
*Ruan Y, Kim HN, Ogana HA, Wan Z, Hurwitz S, Nichols C, Abdel-Azim N, Coba A, Seo S, Loh Y-HE, Gang EJ, Abdel-Azim H, Hsieh C-L, Lieber MR, Parekh C, Pal D, Bhojwani D, Durden DL and Kim Y-M (2021) Preclinical Evaluation of a Novel Dual Targeting PI3Kδ/BRD4 Inhibitor, SF2535, in B-Cell Acute Lymphoblastic Leukemia. Front. Oncol. 11:766888. doi: 10.3389/fonc.2021.766888*

## INTRODUCTION

Despite a high five-year survival rate, relapsed and refractory B-cell acute lymphoblastic leukemia (B-ALL) remains a problem in children (1) the and prognosis for adult B-ALL patients is poor (2). During treatment, leukemia cells interact with the bone marrow (BM) microenvironment and obtain a survival benefit, known as cell adhesion-mediated drug resistance (CAM-DR) (3). This drug resistance in B-ALL can be achieved by increased pro-survival intracellular signaling as a result of adhesion to the BM microenvironment. The PI3K-AKT pathway has been identified as one of the most significant pro-survival pathways in CAM-DR and leukemia cell-BM stromal cell contact has been shown to upregulate phosphorylated AKT in B-ALL (4). Despite great interest in inhibition of the AKT pathway *via* targeting PI3K isoforms in leukemia, a clinically available drug for B-ALL treatment remains elusive (4–6).

In addition, PI3K inhibition facilitates degradation of the transcription factor MYC through the GSK-3β-dependent MYC phosphorylation pathway (7). Emerging reports have indicated oncogenic protein c-Myc plays a critical role in survival, proliferation, and drug resistance in both B and T-ALL (8–11). However, direct targeting of Myc has been a challenge due to its "undruggable" protein structure (12). Currently, targeting c-Myc transcription by interfering with chromatin-dependent signal transduction to RNA polymerase by BRD4 inhibition has shown great promise (12, 13). BRD4 is a member of the bromodomain and extraterminal domain (BET) family of proteins which binds to acetylated lysine residues at promoter and enhancer regions, including regions for the *MYC* gene (14). BRD4 has been proposed to be a critical chromatin regulator that maintains disease progression in acute myeloid leukemia (AML) (15). As a result, suppression of BRD4 with shRNA or JQ1, a bromodomain inhibitor, caused anti-leukemic effects *in vitro* and *in vivo*. An increasing number of studies show promising results of BET protein inhibition with preclinical inhibitors, such as JQ1 in AML cell lines, *ex vivo* patient samples, or mouse models (16, 17). BET inhibition also been shown to be efficient against primary childhood B-ALL by decreasing c-Myc protein stability, suppressing progression at DNA replication forks, and sensitizing primary B-ALL towards dexamethasone *in vitro* and *in vivo* (18). There are few BET inhibitors that have been used in clinical trials, including OTX015 (MK-8628), an analog of JQ1, in a Phase 1 trial for AML (19). In this dose-escalation study, three patients achieved complete remission and two additional patients had partial blast clearance (19). Previous studies have shown that concomitant inhibition of PI3K and BRD4 by SF2523 blocks MYC expression and activation, promotes MYC degradation, and markedly inhibits neuroblastoma cell growth and metastasis (20). Taken together, PI3K and BRD4 inhibition cause downregulation of c-Myc owing to promotion of c-Myc degradation and attenuation of c-Myc transcription. Therefore, it is a rationale for synthesis of a dual targeting PI3K and BRD4 inhibitor (21, 22).

Herein, we evaluated SF2535, a novel small molecule inhibitor of PI3Kδ and BRD4, in B-ALL. We have reported the chemical structures of SF2535, which is a derivative of SF2523 (20). Both SF2535 and SF2523 were found from a discovery of the 5-morpholino-7H-thieno[3,2-b]pyran-7-one (TP-scaffold) system, which was the foundation of a new compound class of potential PI3K inhibitors with improved potency. As BRD4 bromodomains (BDs) are targets of TP-scaffold inhibitors, both SF2535 and SF2523 bind to BRD4 BD1 to a similar extent according to displacement and NMR titration experiments (20). Unlike SF2523, which is a highly selective and potent inhibitor of PI3K, particularly of the PI3Kα isoform, SF2535 specifically targets PI3Kδ. Since the PI3Kδ isoform is expressed selectively in hematopoietic cells and PI3Kδ signaling is active in many B-cell leukemias and lymphomas (23), we chose B-ALL as the disease model for the preclinical evaluation of SF2535.

## MATERIALS AND METHODS

### Patient Samples and Cell Culture

Bone marrow samples were obtained from B-ALL patients after informed signed consent from patients in compliance with the Institutional Review Board regulations of Children's Hospital Los Angeles. Primary B-ALL blasts from bone marrow aspirates were isolated by Ficoll (GE Healthcare) gradient centrifugation and co-cultured with irradiated OP9 stroma cells (ATCC) in MEM-alpha supplemented with 20% fetal bovine serum (FBS, Invitrogen), 100U/ml penicillin and 100μg/ml streptomycin at 37°C and 5% $CO_2$. Patient sample information is listed in **Table S1**.

### Starvation and Activation Assay for Detection of Phosphorylated-Akt$^{Ser473}$

B-ALL cells were serum-deprived by washing twice with Dulbecco's Phosphate-Buffered Saline (DPBS, Invitrogen) and cultured in MEM-alpha media at 37°C and 5% $CO_2$ overnight. Following another wash with DPBS, B-ALL cells were treated with vehicle control DMSO or SF2535 for 30 minutes. Subsequently, FBS was added to a final concentration of 20% to all cells except for the no-activation control groups. Whole cell lysates were isolated after 1 hour for Western blot analysis for phosphorylated-Akt$^{Ser473}$ (p-AKT$^{S473}$) detection.

### Western Blot

B-ALL cells were harvested and lysed in M-PER buffer (Invitrogen) containing 1% protease inhibitor cocktail (VWR). Protein concentration was determined by Bradford protein assay. Proteins were separated by 4-12% Bis-Tris protein gels (Invitrogen) and transferred to PVDF membranes (Invitrogen). The antibodies (Abs) used are listed in **Table S2**.

### Chromatin Immuno-Precipitation (ChIP)

Cells were treated with DMSO or SF2535 5μM for 18 hours and were then harvested and processed using ChIP kit according to the manufacturer instructions (Abcam). In brief, the cells were fixed with 1.1% Formaldehyde, quenched by 10% glycine, and lysed. The lysates were sonicated in order to shear DNA to form DNA fragments with optimal size of 200-1000bp. A portion of

the diluted chromatin was set aside for the INPUT. Diluted chromatins were incubated with anti-BRD4 (1:50, CST), anti-histone H3 (4μg, Abcam) as positive control, or no antibody as negative control overnight with rotation at 4°C. The antibody binding beads were added and washed according to the manufacturer's instructions. The samples were treated with DNA-purifying slurry and Proteinase K to purify DNA. Samples were subjected to qPCR using the c-MYC promoter primers (F: 5'-GAGCAGCAGAGAAAGGGAGA-3', R: 5'-CAGCCGAGCACTCTAGCTCT-3'). Fold enrichment was analyzed as described previously described (24).

## RNA Extraction and qPCR

Cells were treated with DMSO or 5μM SF2535 for 6 hours. Total RNA was extracted using the Qiagen RNeasy kit (Qiagen) and cDNA was produced by the SuperScript III First-Strand Synthesis System (Invitrogen). cDNA was amplified by specific c-Myc primers (F 5'-CTTCTCTCCGTCCTCGGATTCT-3'; R 5'-GAAGGTGATCCAGACTCTGACCTT-3') and GAPDH primers (F 5'-GTTGCCATCAATGACCCCTTCATTG-3'; R 5'-GCTTCACCACCTTCTTGATGTCATC-3') with PowerUp SYBR Green Master Mix (Applied Biosystems) using a ABI 7900HT qPCR machine. Relative expression levels of c-Myc were normalized to GAPDH expression and calculated as described previously (24).

## Apoptosis Analysis With Annexin V and DAPI Staining

Following 24 hours or 72 hours treatment of DMSO or SF2535, B-ALL cells were resuspended in 1X Annexin V binding buffer (Becton Dickinson) at a concentration of $1\times10^6$ cells per mL. 2.5μl Annexin V PE (BioLegend) and 2.5μl DAPI (50μg/mL, Invitrogen) were added to 100μl of the cell suspension. After 15 min incubation at room temperature in the dark, B-ALL cells were analyzed by flow cytometry using BD FACS Canto II.

## Cell Cycle Analysis

B-ALL cells were treated with DMSO or SF2535 (0.2μM 1μM, or 5μM) for 24 hours. Subsequently, cells were stained with CytoPhase™ Violet (BioLegend) at 5μM and incubated for 90 minutes at 37°C and 5% $CO_2$ and analyzed on a BD FACSCanto II flow cytometer. Furthermore, BrdU incorporation assay (Phase-Flow™ BrdU cell proliferation kit FITC-conjugated, BioLegend) according to the protocol of the manufacturer was performed as confirmation of the results. In brief, BrdU solution was added to cell suspension at 0.5μL/mL. Following 1.5-hour incubation, B-ALL cells were harvested and washed. Buffer A was added for 20 minutes at 4°C to fix cells. Then after cell permeabilization and repeat fixation of cells, cells were treated with DNAse and incubated 1 hour at 37°C. Lastly, 5μL of anti-BrdU antibody was added to each tube for 15 minutes at room temperature in the dark. Cells were resuspended with PBS containing DAPI (1μg/mL) prior to acquiring on a flow cytometer.

## Cell Proliferation Assay

$1\times10^6$ B-ALL cells were seeded per condition in triplicates on irradiated OP9 stromal cells as previously described (25). B-ALL cells were treated with DMSO or SF2535 (0.2μM 1μM, or 5μM) for 24 hours and 72 hours. Cell numbers were counted by Trypan blue exclusion on a hemocytometer under an inverted phase-contrast microscope.

## Flow Cytometry

B-ALL cells were treated with the indicated concentration of SF2535 for 24h. Subsequently, B-ALL cells were resuspended in 100μl PBS containing FACS antibodies or the respective isotype controls (information can be found in **Table S3**). Following incubation at 4°C for 30 min, B-ALL cells were washed by 1ml PBS and resuspended in PBS containing DAPI (1μg/mL) then analyzed with a BD FACSCanto II flow cytometer. Flow cytometry data was analyzed with FlowJo 7.0 software (FlowJo LLC).

## Cell Adhesion Assay

$2.5\times10^4$/well irradiated OP9 cells were seeded onto a tissue culture 96-well plates and cultured overnight. Simultaneously, B-ALL cells were treated with different concentrations of SF2535 or DMSO for 24 hours. Then live B-ALL cells were harvested, washed once with DPBS, and resuspended at the final concentration of $0.2\times10^6$/200μL with culture medium. B-ALL cells were dispended onto an irradiated OP9 96-well plate with 200 μL in each well and allowed to adhere for 2 hours at 37°C. Non-adhering cells were removed and remaining cells on OP9 were gently washed with 100 μL of DPBS. Adherent cells and supernatant cells were counted by Trypan blue exclusion on a hemocytometer.

## Animal Studies

Primary relapsed B-ALL cells (LAX56) were intravenously injected into NOD.Cg-*Prkdc*$^{scid}$ *Il2rg*$^{tm1Wjl}$/SzJ (NSG, The Jackson Laboratory) mice ($1\times10^6$cells/mouse). After 3 weeks of engraftment, SF2535 (30 mg/kg, dissolved in 20% dimethylacetamide (DMA) and 80% Captisol (20% w/v in water for 2mg/ml)) (n=6) or vehicle (n=6) was administered once by intraperitoneal (i.p.) injection. After 24 hours, mice were sacrificed and bone marrow, spleen, and peripheral blood were harvested, and red blood cells were lysed by RBC lysis buffer (Invitrogen). The animal study was performed in compliance with a research protocol approved by the Institutional Animal Care and Use Committee (IACUC), the Saban Research Institute of Children's Hospital Los Angeles.

## Data Analysis and Statistics

All statistical analyses were performed using GraphPad Prism 5. The mean was chosen as a center value for all graphs. 95% confidence interval (95% CI), a standard deviation of the mean was used as measures of spread as indicated in figure legends and the *Results* section. Statistical analysis was performed using paired Student's t-test or one-way ANOVA followed by Tukey's multiple comparison tests for statistical analyses as appropriate. A p-value of $<0.05$ was considered statistically significant.

## Treatment of Normal B Cells With SF2535

$0.5\text{x}10^6$ of immortalized EBV-transformed normal B cell lines 3301015 and 5680001 (kind gift from Dr. Hsieh and Dr. Lieber)

were treated with 5μM of SF2535 in 1mL of R10 medium in a 24-well tissue culture plate. After 24hours, cells were harvested and washed with DPBS. Washed cells were stained with 7AAD and Annexin V in Annexin V staining buffer. Viability of cells was assessed by measuring the percentage of 7AAD/Annexin V double negative population.

# RESULTS

## PI3Kδ and BRD4 Expression in B-ALL

Expression of PI3Kδ and BRD4 was determined in fifteen primary B-ALL and three B-ALL cell lines representing various cytogenetics (**Table S1**). Most of the primary B-ALL and cell lines expressed similar levels of PI3Kδ despite their difference in cytogenetics, while BRD4 levels were variable (**Figure 1A**). In order to choose primary B-ALL patient samples for further analysis, we made selections based on their diagnosis status (relapsed or refractory), expression of both PI3Kδ (**Figure S1A**) and BRD4 (**Figure S1B**) based on quantitative densitometric analysis, and inclusion of a wide range of karyotypes including *BCR-ABL1*+ status. Based on these factors we selected LAX56, LAX7R, and TXL3 for subsequent studies.

## SF2535 Downregulates c-Myc and p-AKT in B-ALL

To determine the effective concentration of SF2535 in primary B-ALL cases, we treated three primary B-ALL (LAX56, LAX7R, and TXL3) cells with increasing concentrations of SF2535 for 48 hours. SF2535 dose-dependently induced apoptosis in all B-ALL cells, and the calculated $EC_{50}$ values of SF2535 were 2.4μM (95% CI, 1.990μM - 2.935μM), 1.5μM (95% CI, 1.389μM - 1.633μM), and 3.2 μM (95% CI, 2.718μM – 3.670μM) in LAX56, LAX7R and TXL3, respectively (**Figure S2**). Based on these values, three different doses of SF2535, 0.2μM, 1μM, and 5μM, were chosen for subsequent studies. As c-Myc transcription is mediated by BRD4 binding to the promoter region (12), we evaluated the specific effect of SF2535 on BRD4 binding on the c-Myc promoter by chromatin immunoprecipitation (ChIP). In all three cases, SF2535 decreased BRD4 binding to the c-Myc promoter site compared to DMSO (LAX56 P<0.0001, LAX7R P<0.0001, TXL3 P<0.0001) (**Figure 1B**). Subsequently, mRNA transcript levels of c-Myc expression were significantly decreased upon SF2535 treatment in all three cases (LAX56 P=0.0020, LAX7R P=0.0002, TXL3 P=0.0009) (**Figure 1C**). Finally, SF2535 prominently downregulated c-Myc protein expression in a dose-dependent manner, which was determined by Western blot (**Figure 1D**, **Figure S3A**). Decrease in c-Myc protein expression could be restored by the proteasome inhibitor MG132, which shows c-Myc degradation in B-ALL occurs through the ubiquitin-proteasome pathway (26) (**Figure 1E**, **Figure S3B**). SF2535 also decreased phosphorylated AKT in LAX56, LAX7R and TXL3, demonstrating the on-target effect of SF2535 on PI3Kδ. Following serum starvation of leukemia cells, B-ALL cells were treated with DMSO (vehicle control) or 0.2μM, 1μM, or 5μM of SF2535 for 30 minutes followed by 1 hour serum-induced activation. Levels of p-$AKT^{S473}$ decreased in a dose-dependent manner from SF2535 in LAX56, LAX7R, and TXL3 B-ALL cells (**Figure 1F**, **Figures S3C, D**).

## SF2535 Induces Apoptosis in B-ALL Cells Through Changes in the Intrinsic Apoptotic Pathway

To determine the apoptotic effect of SF2535 in primary B-ALL, LAX56, LAX7R, and TXL3 cells were treated with DMSO or 0.2μM, 1μM, or 5μM SF2535 for 24 hours and 72 hours (**Figure 2**). The percentages of apoptotic cells were significantly increased after 24 hours with 5μM SF2535 compared to DMSO control for LAX56 (51.48 ± 4.51% vs 31.28 ± 4.94%, P<0.0001), LAX7R (53.86 ± 14.02% vs 19.98 ± 8.51%, P<0.0001), and TXL3 (39.51 ± 10.49% vs 20.90 ± 4.05%, P<0.0001) (**Figures 2A–C**), and were also significantly increased after 72 hours of treatment (**Figures 2D–F**) in four independent experiments performed. We further analyzed whether SF2535 affects components of the intrinsic apoptotic pathway, including caspase-3, caspase-7, PARP and the anti-apoptotic component BCL-2. 5μM SF2535 significantly increased cleaved PARP, caspase-3, and caspase-7 in LAX56, LAX7R, and TXL3. Moreover, SF2535 5μM markedly decreased BCL-2 after 72 hours in both LAX7R and TXL3, yet not in LAX56 (**Figures 2G–I**).

## SF2535 Causes Cell Cycle Changes and Suppresses Cell Counts in B-ALL

In order to determine if the decrease in proliferation was due to cell cycle arrest, we performed cell cycle analysis in SF2535-treated B-ALL cells. LAX56, LAX7R and TXL3 cells were treated with DMSO control or with 0.2μM, 1μM or 5μM of SF2535. After 24 hours, percentage of cells in G0+G1 phase increased while the percentage of cells in S phase decreased in all SF2535-treated groups except for TXL3 treated with 0.2μM of SF2535 (**Figure 3**). In LAX56 cells (**Figure 3A**), 0.2μM, 1μM and 5μM SF2535 when compared to DMSO prolonged G0+G1 phase (P=0.278, P=0.006, P<0.001, respectively) and arrested S phase (P=0.044, P=0.011, P<0.001, respectively). Similarly, significant prolonged G0+G1 phase was found in LAX7R (**Figure 3B**) and TXL3 (**Figure 3C**). The summarized results of mean and standard deviation of two independent triplicate experiments and representative flow cytometry figures are depicted in **Figure S4**. In addition, BrdU incorporation assays were performed, and similar results were shown (**Figure S5**). According to the apoptotic effect and S phase cell cycle arrest of SF2535, we performed cell count assays to assess the potential effects on proliferation by SF2535 in B-ALL cells. We treated B-ALL cells with DMSO or 0.2μM, 1μM, or 5μM SF2535 for 24 and 72 hours. Both 1μM and 5μM SF2535 significantly inhibited cell proliferation after 72 hours of treatment of LAX56 (**Figure 3D**), LAX7R (**Figure 3E**), and TXL3 (**Figure 3F**). For instance, at 72 hours, 1μM and 5μM of SF2535 reduced the number of viable cells compared to $(2.74 \pm 0.33) \times 10^6$ in DMSO to $(1.49 \pm 0.49) \times 10^6$in SF2535 1μM (P<0.0001) and $(0.29 \pm 0.17) \times 10^6$ in SF2535 5μM (P<0.0001), in LAX56.

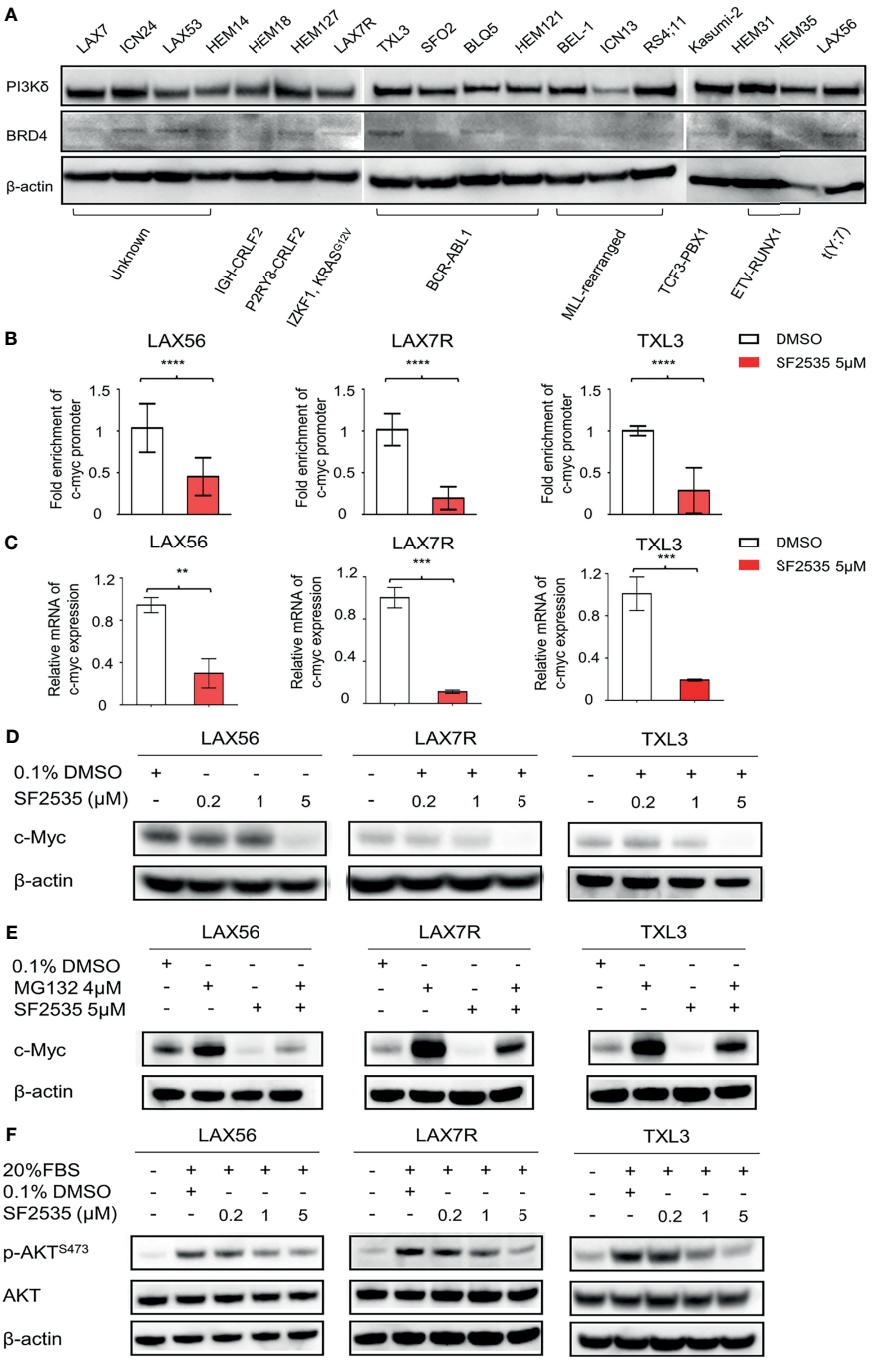


**FIGURE 1** | SF2535 downregulates c-Myc and p-AKT. **(A)** PI3Kδ and BRD4 expression in whole cell lysates in B-ALL. **(B)** Primary B-ALL LAX56, LAX7R and TXL3 cells were treated with SF2535 at 5μM. After 18 hours, the cells were harvested for BRD4 ChIP analysis which was performed at the c-Myc promoter site. Data were combined from three independent experiments per leukemia. Data was analyzed by paired Student's t-test, where ****P<0.0001 vs. ctrl (DMSO). **(C)** qPCR data showing the effect of SF2535 on c-Myc expression in B-ALL cells. Experiment was performed in triplicate. Data was analyzed by Student's t test, where **P<0.01, ***P<0.001 vs. ctrl (DMSO). **(D)** LAX56, LAX7R and TXL3 cells were treated with 0.1% DMSO or SF2535 (0.2μM, 1μM, or 5μM) for 48 hours. c-Myc expression of B-ALL cells was analyzed by Western blot. **(E)** LAX56, LAX7R, and TXL3 cells were pre-treated with either 0.1%DMSO control or proteasome inhibitor MG132 (4μM) for 45 min and subsequently treated with SF2535 at 5μM for 6 hours. c-Myc expression was analyzed by Western blot. **(F)** LAX56, LAX7R and TXL3 cells were cultured in MEM-α without serum overnight. Subsequently, cells were treated with 0.1% DMSO control, SF2535 (0.2μM, 1μM, 5μM) for 30 mins. Cells were activated with 20% FBS for 1 hour. Western blots of p-AKT$^{S473}$ and AKT are shown. β-actin was used as internal control for equal protein loading for Western blots **(D–F)**. One of two independent experiments per leukemia was performed for **(D–F)**.

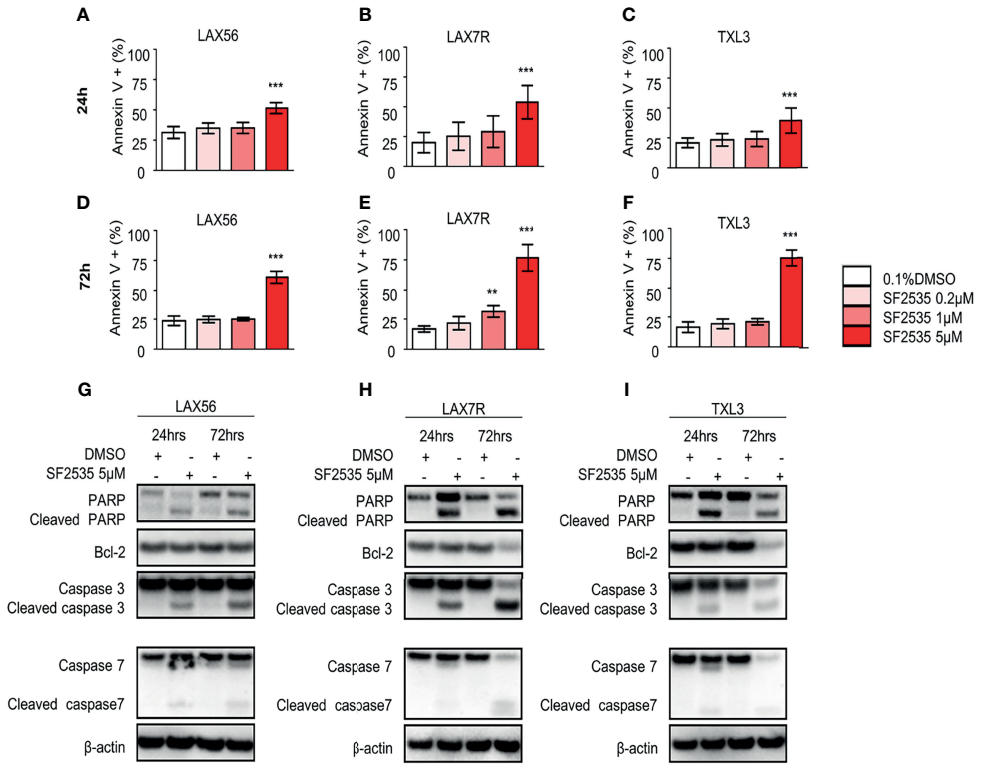


**FIGURE 2** | SF2535 induces apoptotic effects in B-ALL cells. LAX56, LAX7R and TXL3 B-ALL cells were cultured in presence of 0.1% DMSO (white bars) or SF2535 (0.2μM, 1μM, or 5μM) (in red bars) for 24 **(A–C)** and 72 hours **(D–F)** and apoptosis was assessed by percent of Annexin V$^+$ cells by flow cytometry. Data are pooled from four independent experiments performed in triplicates. P-values are calculated using one-way ANOVA test and Tukey's multiple comparison test. **P<0.01, ***P<0.001 compared to the DMSO group. LAX56, LAX7R and TXL3 B-ALL cells were cultured in presence of 0.1% or SF2535 5μM for 24 and 72 hours and proteins were isolated for Western blot analysis **(G–I)**. β-actin was used as loading control. One of two experiments is shown.

## SF2535 Decreases Surface Integrin Expression

Our previous studies have shown that cell adhesion-mediated drug resistance (CAM-DR) plays a crucial role in relapsed and refractory B-ALL (27, 28). Previously, we have shown inhibition of PI3Kδ with idelalisib in B-ALL inhibited homing of cells into the bone marrow (29). Decrease in homing may be due to the inability of cells to adhere to surrounding microenvironment upon PI3Kδ inhibition. In order to determine if blockade of PI3Kδ affects expression level of surface adhesion in B-ALL cells, we assessed integrin α4, α5, α6, β1, and CXCR4 expression in SF2535 treated B-ALL. LAX56, LAX7R and TXL3 were treated with DMSO control or with 0.2μM, 1μM or 5μM of SF2535. After 24 hours, cells were stained with anti-integrin α4, α5, α6, β1, and CXCR4 antibodies and their mean fluorescence intensity (MFI) was assessed by flow cytometry. To exclude dead cells which can interfere with flow cytometry data analysis, viable cells were strictly gated and a representative gating strategy of 5μM SF2535 treated LAX56 cells is shown in **Figure S6A**. As a result, histograms of integrin α4, α5, α6, β1, and CXCR4 showed relatively small changes in expression levels of integrin subunits and CXCR4 between DMSO and SF2535-treated groups (**Figures 4A–C**). Moreover, MFI of integrin α4, α5, α6, and β1 significantly decreased in SF2535 treated groups while MFI of CXCR4 increased in LAX56, LAX7R and TXL3 after SF2535 treatment (**Figures 4D–R**, **S6**). This result shows dual inhibition of PI3Kδ and BRD4 decreases integrin expression on the cell surface that is important for adhesion of leukemia cells to the microenvironment. However, SF2535 hardly decreased percentages of integrin α4, α5, and β1 expression (**Figures S6E–S**) and cells may compensate for the loss of integrin subunits by expressing other surface molecules implicated in adhesion, such as CXCR4. In order to further evaluate the physiological and biological relevance of integrin expression effect, we performed cell adhesion assays. Firstly, B-ALL cells were plated at $0.2 \times 10^6$/200μL onto 96 well tissue culture plates seeded with or without irradiated OP9 stromal cells, which has multiple integrin ligands (25, 27), B-ALL cells were allowed to adhere for 4 hours. Subsequently, cells were treated with increasing SF2535 doses and cultured overnight. More de-adhered B-ALL cells were found in SF2535 treatment groups, whereas SF2535 induced more dead cells compared to DMSO vehicle control (**Figure S7**). Since SF2535 induces apoptosis of B-ALL, we pre-treated B-ALL with SF2535 for 24 hours and harvested live cells. Harvested cells were washed and plated at $0.2 \times 10^6$/200μL onto 96 well tissue culture plates seeded

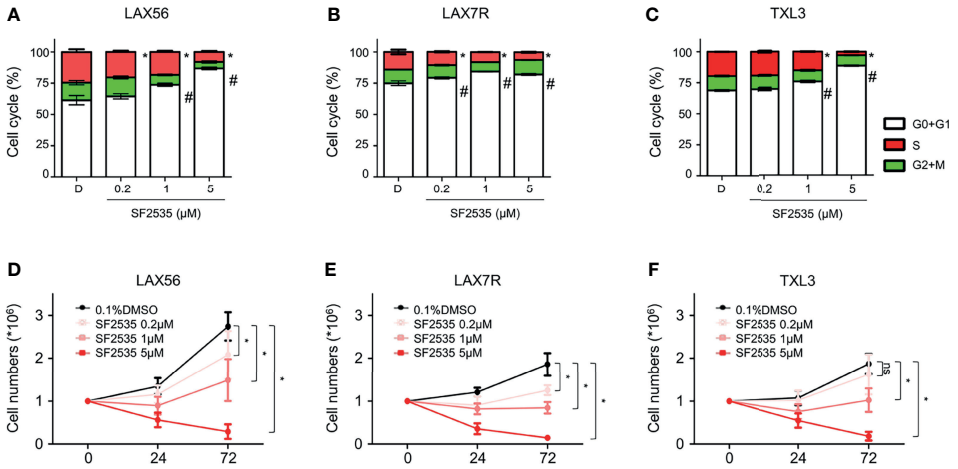


**FIGURE 3** | SF2535 prolongs G0+G1 phase arrest and attenuates S phase. **(A)** LAX56, **(B)** LAX7R and **(C)** TXL3 B-ALL cells were treatment with DMSO or SF2535 (0.2μM, 1 μM, or 5μM) for 24 hours. Cell cycle was assessed *via* flow cytometry after 24 hours of treatment. White bars indicate G0+G1 Phase. Green bars indicate G2+M Phase. Red bars indicate the S Phase. P-value *<0.05: Comparing S phase compared to DMSO S phase. P-value #<0.05: Comparing G0+G1 phase to DMSO G0+G1 phase. The results are representative of two independent triplicate experiments. To determine the effect of SF2535 on proliferation and cell numbers, LAX56 **(D)**, LAX7R **(E)** and TXL3 **(F)** B-ALL cells were treated with DMSO or SF2535 (0.2μM, 1μM, or 5μM) for 24 and 72 hours. Numbers of live cells were counted by Trypan blue exclusion on a hemocytometer. Data of three independent triplicate experiments in triplicates are combined. P-value *<0.05 compared to DMSO; ns, not significant.

with irradiated OP9 stromal cells for 2 hours allowing B-ALL cells to adhere. We observed that 5μM SF2535 significantly inhibited adhesion of the three B-ALL cells to stromal cells (**Figure 5**).

## SF2535 Decreases Peripheral Leukemic Burden in Mouse Model

We evaluated *in vivo* efficacy of the drug in a leukemia-engrafted mouse model. In order to determine the *in vivo* effects of SF2535, NSG mice were first intravenously injected with $1\times10^6$ LAX56 cells per mouse. After 3 weeks of engraftment, the mice were treated either with the vehicle control (n=6) or SF2535 (30mg/kg, n=6) (**Figure S8A**). SF2535 was administered once to the mice and the early effects of the drug on B-ALL cells were evaluated. After 24 hours post-injection of SF2535, the mice were sacrificed and bone marrow (BM), spleen cells (SPC), and peripheral blood (PB) were collected and analyzed for human $CD45^+CD19^+$ expression *via* flow cytometry (**Figures S8B–D**). Leukemia burden, shown as percentage of human $CD45^+CD19^+$, in PB was significantly decreased in SF2535-treated mice (P=0.0202) (**Figure S8D**) yet there was no decrease of human leukemia in BM or SPC (**Figures S8B, C**). This result shows the dose and timing of SF2535 administration is sufficient to decrease leukemia burden in the peripheral blood. Effect of SF2535 on normal mature B-cells.

Finally, we tested SF2535 toxicity in two immortalized normal B cell lines, 3301015 and 5680001. At 24hours post-treatment, SF2535 decreased viability of 3301015 cells compared to control treated cells (71.6 ± 2.5%; N=3 vs 63.6 ± 0.3%; N=3) (P=0.03) while viability of 5680001 cells was not affected by SF2535. (**Figure S9**).

# DISCUSSION

PI3K has been targeted by copanlisib and duvelisib which were approved by the FDA for use in CLL and follicular lymphoma (30, 31). It has been demonstrated that PI3K also plays a crucial role in ALL (4, 29). Our findings show that PI3K is broadly expressed in B-ALL and the key downstream signal p-AKT $^{S473}$ is markedly downregulated by dual inhibition of PI3Kδ-BRD4 by SF2535 (**Figure 1F**). In addition, it is well established that c-Myc plays a major role in mature B-ALL and Burkitt lymphoma (32, 33), however, there are few studies that explore the role of c-Myc in other types of B-ALL. Ott et al. reported that BET bromodomain inhibition using JQ1 targets both c-Myc and IL7R in high-risk *CRLF2*-rerranged and other B-ALL (34). Moreover, oncogenic Myc is also a difficult target for cancer therapy, and alternative approaches have been taken to indirectly target Myc by blocking pathway events upstream of c-Myc (12). Our previous study showed feasibility of targeting Myc with a dual-activity PI3K-BRD4 inhibitor (20). In our present study, we have demonstrated that c-Myc is expressed in B-ALL, and c-Myc was markedly downregulated by inhibition of its promoter site by SF2535 (**Figures 1B–D**). SF2535 also led to a decrease in p-AKT$^{S473}$ levels upon inhibition of PI3Kδ. Our data show that SF2535 led to downregulation of both p-AKT and c-Myc in B-ALL. However, as BRD4 expression is highly variable in samples (**Figure 1A**, **S1B**), it would be appropriate to determine the BRD4 expression before SF2535 treatment.

Inhibition of c-Myc has been shown to result in apoptosis in T-ALL (34, 35). Our data also indicate that dual inhibition of PI3Kδ and BRD4 results in apoptosis or primary B-ALL cells using SF2535 (**Figures 2A–F**). Furthermore, we demonstrated that SF2535-induced apoptosis occurs through the intrinsic pathway *via*

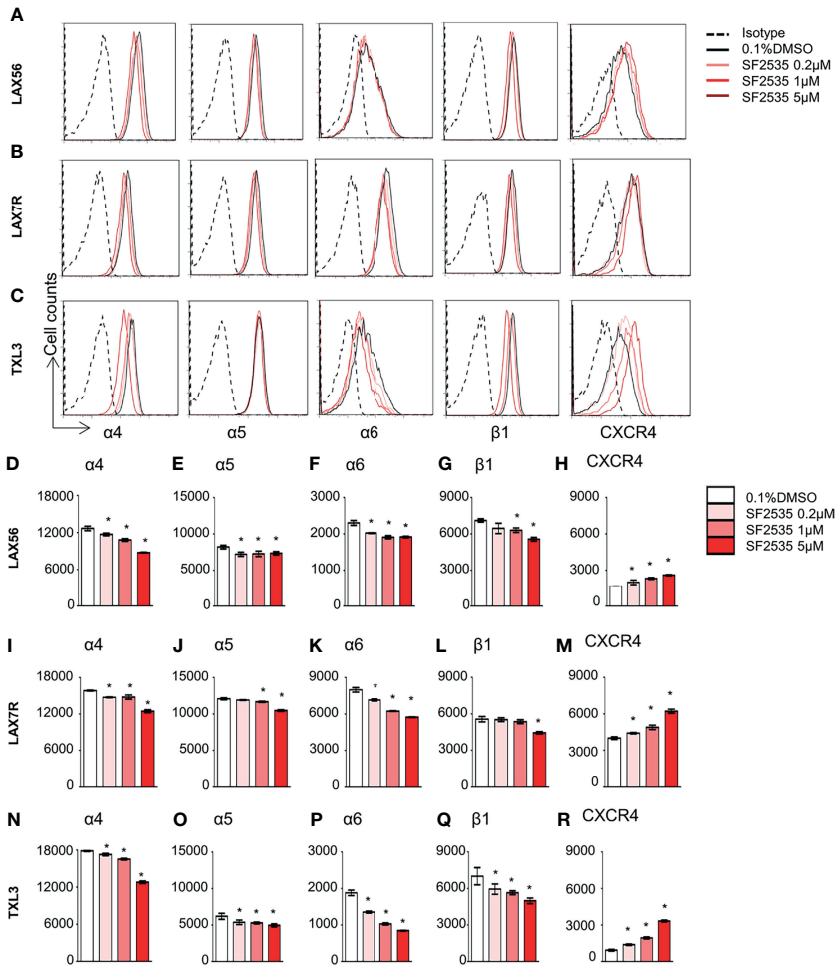


**FIGURE 4** | SF2535 affects adhesion molecules. Representative histograms for integrin α4, α5, α6, β1, and CXCR4 expression for **(A)** LAX56, **(B)** LAX7R and **(C)** TXL3 cells were treated with 0.1% DMSO (in white bars) or SF2535 (0.2μM, 1μM, 5μM in gradient red bars) for 24 hours. **(D–R)** Mean fluorescence intensity (MFI) of integrin α4, α5, α6, β1, and CXCR4 were shown on indicated y-axis in **(D–H)** LAX56, **(I–M)** LAX7R and **(N–R)** TXL3 B-ALL cells. P-value *<0.05 compared to DMSO control. One representative experiment out of at least two independent experiments is shown.

increasing cleavage of PARP, caspase-3 and caspase-7 and decreasing BCL-2 (36) (**Figures 2G–I**). Inhibition of PI3Kδ and BRD4 not only induced apoptosis, but also caused cell cycle arrest and decreased proliferation (**Figure 3**). A potential mechanism is that BET bromodomain inhibition affects key regulators of the cell cycle such as cyclin D1 expression (20).

Recently, we have suggested that BRD4 regulates the immunosuppressive myeloid tumor microenvironment which can be blocked by PI3K/BRD4 inhibitors using SF2523 (24). The bone marrow environment has been shown to promote CAM-DR in ALL (37). Our previous studies have identified the integrin α4 and α6 as an adhesion molecule that plays a critical role in B-ALL through CAM-DR (25, 27). Our results indicate dual inhibitors of PI3Kδ and BRD4 using SF2535 affected the expression of adhesion molecules including integrin α4, α5, α6, β1, while CXCR4 was increased (**Figure 4**). This finding suggests a relationship between integrins and PI3Kδ through outside-in signaling (28) and would warrant further mechanistic studies. It has been shown that integrin α6 and β1 are regulated by the c-Myc oncogene in colorectal cancer cells (38, 39) and a murine hematopoietic cell line (40). Yao et al. recently showed that use of a PI3Kδ inhibitor resulted in a significant reduction of leukemia metastasis to the central nervous system due to decreased integrin α6 expression despite minimally decreased bone marrow disease burden (41). It is possible that CXCR4 expression compensates for the downregulation of integrins, which requires further investigation. Although dual inhibitors of PI3K and BRD4 has been investigated in some solid tumors (20, 24), the current study is the first study to evaluate SF2535 in B-ALL. The bioavailability of SF2535 and its route of penetration and clearance remained unknown. Our preliminary *in vivo* results show that dual inhibition of PI3Kδ and BRD4 led to a reduction of leukemia cell numbers in the peripheral blood of leukemia bearing mice. Mice tolerated 10mg/kg SF2535 for continuous treatment up to 4 weeks, yet the low dosage of SF2535 was not effective enough to prolong the survival of leukemia engrafted mice, while higher doses 30 mg/kg were not

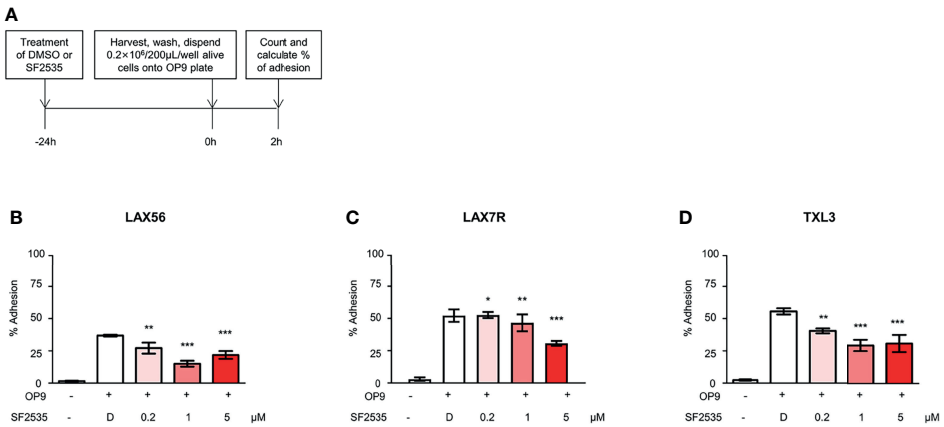


**FIGURE 5** | SF2535 moderately inhibits B-ALL adhesion to OP-9 cells. **(A)** Schema of adhesion assays. **(B)** LAX56, **(C)** LAX7R, and **(D)** TXL3 cells were treated with DMSO **(D)** or SF2535 for 24 hours. After harvest and wash, $0.2\times10^6$ alive cells per well were placed on pre-seeded OP9 cells plate for 2 hours. Adhesion and supernatant cells were counted by Trypan Blue exclusion. Percentage (%) of alive adhesion cells were presented. Experiments were performed in triplicates. *P < 0.05, **P < 0.01, ***P < 0.001 compared to DMSO group.

well tolerated in mice (data not shown). We have shown in a small study that SF2535 may decrease viability of mature B-cells to a small but statistically significant extent. These results indicate that SF2535 may induce toxicity in normal B cells, which requires further follow-up studies.

Taken together, these results reveal that SF2535 efficaciously induces apoptosis through downregulating c-Myc and p-AKT pathways in primary B-ALL providing a rationale for further preclinical evaluation of PI3Kδ and BRD4 inhibition in B-ALL.

## DATA AVAILABILITY STATEMENT

The original contributions presented in the study are included in the article/**Supplementary Material**. Further inquiries can be directed to the corresponding author.

## ETHICS STATEMENT

The animal study was reviewed and approved by IACUC CHLA. Written informed consent was obtained from the minor(s)' legal guardian/next of kin for the publication of any potentially identifiable images or data included in this article.

## AUTHOR CONTRIBUTIONS

Conceptualization of the study: DB, DD, and Y-MK. YR, HK, and Y-MK designed the research. YR, HK, HO, SH, EG, ZW, CN, NA-A, AC, Y-HL, CP, HA-A, DP, and SS performed the research, analyzed and interpreted the data. C-LH and ML contributed valuable material, technical expertise and interpreted the data. YR, HK, and Y-MK wrote the initial draft of the manuscript. All authors contributed to the article and approved the submitted version.

## FUNDING

This work was supported in part by the National Institutes of Health (R01 CA172896 to Y-MK and CA215656 to DD).

## ACKNOWLEDGMENTS

We thank the Animal Facility for outstanding animal husbandry and the Flow Cytometry Core of the Saban Research Institute and the USC Molecular Genomics Core for their exceptional help. We thank the USC Libraries Bioinformatics Service for assisting with data analysis. The bioinformatics software and computing resources used in the analysis are funded by the USC Office of Research and the Norris Medical Library.

## SUPPLEMENTARY MATERIAL

The Supplementary Material for this article can be found online at: https://www.frontiersin.org/articles/10.3389/fonc.2021.766888/full#supplementary-material

## REFERENCES

1. Hunger SP, Mullighan CG. Acute Lymphoblastic Leukemia in Children. *N Engl J Med* (2015) 373(16):1541–52. doi: 10.1056/NEJMra1400972

2. Gokbuget N, Dombret H, Ribera JM, Fielding AK, Advani A, Bassan R, et al. International Reference Analysis of Outcomes in Adults With B-Precursor Ph-Negative Relapsed/Refractory Acute Lymphoblastic Leukemia. *Haematologica* (2016) 101(12):1524–33. doi: 10.3324/haematol.2016.144311

3. Sison EAR, Kurre P, Kim YM. Understanding the Bone Marrow Microenvironment in Hematologic Malignancies: A Focus on Chemokine, Integrin, and Extracellular Vesicle Signaling. *Pediatr Hematol Oncol* (2017) 34(6-7):365–78. doi: 10.1080/08880018.2017.1395938
4. Sanchez VE, Nichols C, Kim HN, Gang EJ, Kim YM. Targeting PI3K Signaling in Acute Lymphoblastic Leukemia. *Int J Mol Sci* (2019) 20(2):412. doi: 10.3390/ijms20020412
5. Kienle DL, Stilgenbauer S. Approved and Emerging PI3K Inhibitors for the Treatment of Chronic Lymphocytic Leukemia and Non-Hodgkin Lymphoma. *Expert Opin Pharmacother* (2020) 21(8):917–929. doi: 10.1080/14656566.2020.1737010
6. Hewett YG, Uprety D, Shah BK. Idelalisib- A PI3Kdelta Targeting Agent for B-Cell Malignancies. *J Oncol Pharm Pract* (2016) 22(2):284–8. doi: 10.1177/1078155215572933
7. Dey N, Leyland-Jones B, De P. MYC-Xing it Up With PIK3CA Mutation and Resistance to PI3K Inhibitors: Summit of Two Giants in Breast Cancers. *Am J Cancer Res* (2015) 5(1):1–19.
8. Follini E, Marchesini M, Roti G. Strategies to Overcome Resistance Mechanisms in T-Cell Acute Lymphoblastic Leukemia. *Int J Mol Sci* (2019) 20(12):3021. doi: 10.3390/ijms20123021
9. Reyes-Garau D, Ribeiro ML, Roue G. Pharmacological Targeting of BET Bromodomain Proteins in Acute Myeloid Leukemia and Malignant Lymphomas: From Molecular Characterization to Clinical Applications. *Cancers* (2019) 11(10):1483. doi: 10.3390/cancers11101483
10. Swaminathan S, Hansen AS, Heftdal LD, Dhanasekaran R, Deutzmann A, Fernandez WDM, et al. MYC Functions as a Switch for Natural Killer Cell-Mediated Immune Surveillance of Lymphoid Malignancies. *Nat Commun* (2020) 11(1):2860. doi: 10.1038/s41467-020-16447-7
11. Weng AP, Millholland JM, Yashiro-Ohtani Y, Arcangeli ML, Lau A, Wai C, et al. C-Myc Is an Important Direct Target of Notch1 in T-Cell Acute Lymphoblastic Leukemia/Lymphoma. *Genes Dev* (2006) 20(15):2096–109. doi: 10.1101/gad.1450406
12. Chen H, Liu H, Qing G. Targeting Oncogenic Myc as a Strategy for Cancer Treatment. *Signal Transduct Target Ther* (2018) 3:5. doi: 10.1038/s41392-018-0008-7
13. Delmore JE, Issa GC, Lemieux ME, Rahl PB, Shi J, Jacobs HM, et al. BET Bromodomain Inhibition as a Therapeutic Strategy to Target C-Myc. *Cell* (2011) 146(6):904–17. doi: 10.1016/j.cell.2011.08.017
14. Filippakopoulos P, Qi J, Picaud S, Shen Y, Smith WB, Fedorov O, et al. Selective Inhibition of BET Bromodomains. *Nature* (2010) 468(7327):1067–73. doi: 10.1038/nature09504
15. Zuber J, Shi J, Wang E, Rappaport AR, Herrmann H, Sison EA, et al. RNAi Screen Identifies Brd4 as a Therapeutic Target in Acute Myeloid Leukaemia. *Nature* (2011) 478(7370):524–8. doi: 10.1038/nature10334
16. Wingelhofer B, Somervaille TCP. Emerging Epigenetic Therapeutic Targets in Acute Myeloid Leukemia. *Front Oncol* (2019) 9:850. doi: 10.3389/fonc.2019.00850
17. Braun T, Gardin C. Investigational BET Bromodomain Protein Inhibitors in Early Stage Clinical Trials for Acute Myelogenous Leukemia (AML). *Expert Opin Invest Drugs* (2017) 26(7):803–11. doi: 10.1080/13543784.2017.1335711
18. Da Costa D, Agathanggelou A, Perry T, Weston V, Petermann E, Zlatanou A, et al. BET Inhibition as a Single or Combined Therapeutic Approach in Primary Paediatric B-Precursor Acute Lymphoblastic Leukaemia. *Blood Cancer J* (2013) 3:e126. doi: 10.1038/bcj.2013.24
19. Berthon C, Raffoux E, Thomas X, Vey N, Gomez-Roca C, Yee K, et al. Bromodomain Inhibitor OTX015 in Patients With Acute Leukaemia: A Dose-Escalation, Phase 1 Study. *Lancet Haematol* (2016) 3(4):e186–95. doi: 10.1016/S2352-3026(15)00247-1
20. Andrews FH, Singh AR, Joshi S, Smith CA, Morales GA, Garlich JR, et al. Dual-Activity PI3K-BRD4 Inhibitor for the Orthogonal Inhibition of MYC to Block Tumor Growth and Metastasis. *Proc Natl Acad Sci USA* (2017) 114(7):E1072–E80. doi: 10.1073/pnas.1613091114
21. Stratikopoulos EE, Dendy M, Szabolcs M, Khaykin AJ, Lefebvre C, Zhou MM, et al. Kinase and BET Inhibitors Together Clamp Inhibition of PI3K Signaling and Overcome Resistance to Therapy. *Cancer Cell* (2015) 27(6):837–51. doi: 10.1016/j.ccell.2015.05.006
22. Vann KR, Pal D, Morales GA, Burgoyne AM, Durden DL, Kutateladze TG. Design of Thienopyranone-Based BET Inhibitors That Bind Multiple Synthetic Lethality Targets. *Sci Rep* (2020) 10(1):12027. doi: 10.1038/s41598-020-68964-6
23. Zirlik K, Veelken H. Idelalisib. *Recent Results Cancer Res Fortschr Krebsforsch Progres Rech Cancer* (2018) 212:243–64. doi: 10.1007/978-3-319-91439-8_12
24. Joshi S, Singh AR, Liu KX, Pham TV, Zulcic M, Skola D, et al. SF2523: Dual PI3K/BRD4 Inhibitor Blocks Tumor Immunosuppression and Promotes Adaptive Immune Responses in Cancer. *Mol Cancer Ther* (2019) 18(6):1036–44. doi: 10.1158/1535-7163.MCT-18-1206
25. Gang EJ, Kim HN, Hsieh YT, Ruan Y, Ogana HA, Lee S, et al. Integrin Alpha6 Mediates the Drug Resistance of Acute Lymphoblastic B-Cell Leukemia. *Blood* (2020) 136(2):210–23. doi: 10.1182/blood.2019001417
26. Farrell AS, Sears RC. MYC Degradation. *Cold Spring Harbor Perspect Med* (2014) 4(3). doi: 10.1101/cshperspect.a014365
27. Hsieh YT, Gang EJ, Geng H, Park E, Huantes S, Chudziak D, et al. Integrin Alpha4 Blockade Sensitizes Drug Resistant Pre-B Acute Lymphoblastic Leukemia to Chemotherapy. *Blood* (2013) 121(10):1814–8. doi: 10.1182/blood-2012-01-406272
28. Shishido S, Bonig H, Kim YM. Role of Integrin Alpha4 in Drug Resistance of Leukemia. *Front Oncol* (2014) 4:99. doi: 10.3389/fonc.2014.00099
29. Adam E, Kim HN, Gang EJ, Schnair C, Lee S, Lee S, et al. The PI3Kdelta Inhibitor Idelalisib Inhibits Homing in an *In Vitro* and *In Vivo* Model of B ALL. *Cancers (Basel)* (2017) 9(9):121. doi: 10.3390/cancers9090121
30. Flinn IW, Miller CB, Ardeshna KM, Tetreault S, Assouline SE, Mayer J, et al. DYNAMO: A Phase II Study of Duvelisib (IPI-145) in Patients With Refractory Indolent Non-Hodgkin Lymphoma. *J Clin Oncol* (2019) 37(11):912–22. doi: 10.1200/JCO.18.00915
31. Flinn IW, Hillmen P, Montillo M, Nagy Z, Illes A, Etienne G, et al. The Phase 3 DUO Trial: Duvelisib vs Ofatumumab in Relapsed and Refractory CLL/SLL. *Blood* (2018) 132(23):2446–55. doi: 10.1182/blood-2018-05-850461
32. Zhang C, Amos Burke GA. Pediatric Precursor B-Cell Acute Lymphoblastic Leukemia With MYC 8q24 Translocation - How to Treat? *Leuk Lymphoma* (2018) 59(8):1807–13. doi: 10.1080/10428194.2017.1387914
33. Molyneux EM, Rochford R, Griffin B, Newton R, Jackson G, Menon G, et al. Burkitt's Lymphoma. *Lancet* (2012) 379(9822):1234–44. doi: 10.1016/S0140-6736(11)61177-X
34. Ott CJ, Kopp N, Bird L, Paranal RM, Qi J, Bowman T, et al. BET Bromodomain Inhibition Targets Both C-Myc and IL7R in High-Risk Acute Lymphoblastic Leukemia. *Blood* (2012) 120(14):2843–52. doi: 10.1182/blood-2012-02-413021
35. Roderick JE, Tesell J, Shultz LD, Brehm MA, Greiner DL, Harris MH, et al. C-Myc Inhibition Prevents Leukemia Initiation in Mice and Impairs the Growth of Relapsed and Induction Failure Pediatric T-ALL Cells. *Blood* (2014) 123(7):1040–50. doi: 10.1182/blood-2013-08-522698
36. Carneiro BA, El-Deiry WS. Targeting Apoptosis in Cancer Therapy. *Nat Rev Clin Oncol* (2020) 17(7):395–417. doi: 10.1038/s41571-020-0341-y
37. Hazlehurst LA, Dalton WS. Mechanisms Associated With Cell Adhesion Mediated Drug Resistance (CAM-DR) in Hematopoietic Malignancies. *Cancer Metastasis Rev* (2001) 20(1-2):43–50. doi: 10.1023/a:1013156407224
38. Boudjadi S, Carrier JC, Groulx JF, Beaulieu JF. Integrin Alpha1beta1 Expression Is Controlled by C-MYC in Colorectal Cancer Cells. *Oncogene* (2016) 35(13):1671–8. doi: 10.1038/onc.2015.231
39. Groulx JF, Boudjadi S, Beaulieu JF. MYC Regulates Alpha6 Integrin Subunit Expression and Splicing Under Its Pro-Proliferative ITGA6A Form in Colorectal Cancer Cells. *Cancers* (2018) 10(2):42. doi: 10.3390/cancers10020042
40. Fujimoto H, Tanaka Y, Liu ZJ, Yagita H, Okumura K, Kosugi A, et al. Down-Regulation of Alpha6 Integrin, an Anti-Oncogene Product, by Functional Cooperation of H-Ras and C-Myc. *Genes Cells: Devoted Mol Cell Mech* (2001) 6(4):337–43. doi: 10.1046/j.1365-2443.2001.00428.x
41. Yao H, Price TT, Cantelli G, Ngo B, Warner MJ, Olivere L, et al. Leukaemia Hijacks a Neural Mechanism to Invade the Central Nervous System. *Nature* (2018) 560(7716):55–60. doi: 10.1038/s41586-018-0342-5


**Conflict of Interest:** DD has ownership interest (including stock, patents, etc.) in and is a consultant/advisory board member of SignalRx Pharmaceuticals Inc.

The remaining authors declare that the research was conducted in the absence of any commercial or financial relationships that could be construed as a potential conflict of interest.

**Publisher's Note:** All claims expressed in this article are solely those of the authors and do not necessarily represent those of their affiliated organizations, or those of

the publisher, the editors and the reviewers. Any product that may be evaluated in this article, or claim that may be made by its manufacturer, is not guaranteed or endorsed by the publisher.

# Advantages of publishing in Frontiers

**OPEN ACCESS**
Articles are free to read for greatest visibility and readership

**FAST PUBLICATION**
Around 90 days from submission to decision

**HIGH QUALITY PEER-REVIEW**
Rigorous, collaborative, and constructive peer-review

**TRANSPARENT PEER-REVIEW**
Editors and reviewers acknowledged by name on published articles

**Frontiers**
Avenue du Tribunal-Fédéral 34
1005 Lausanne | Switzerland

**Visit us:** www.frontiersin.org
**Contact us:** frontiersin.org/about/contact

**REPRODUCIBILITY OF RESEARCH**
Support open data and methods to enhance research reproducibility

**DIGITAL PUBLISHING**
Articles designed for optimal readership across devices

**FOLLOW US**
@frontiersin

**IMPACT METRICS**
Advanced article metrics track visibility across digital media

**EXTENSIVE PROMOTION**
Marketing and promotion of impactful research

**LOOP RESEARCH NETWORK**
Our network increases your article's readership